MACROCYCLIC COMPOUNDS AND THEIR USE AS ELECTROCATALYSTS FOR THE ELECTROCHEMICAL REDUCTION OF CARBON DIOXIDE

Caroline Smith

A Thesis Submitted for the Degree of PhD
at the
University of St Andrews

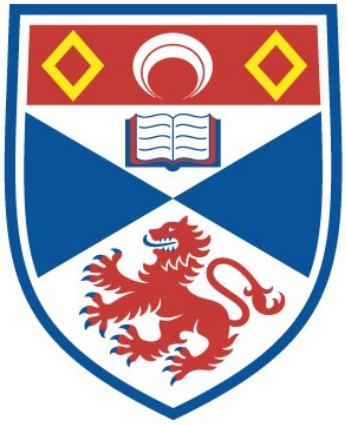

1995

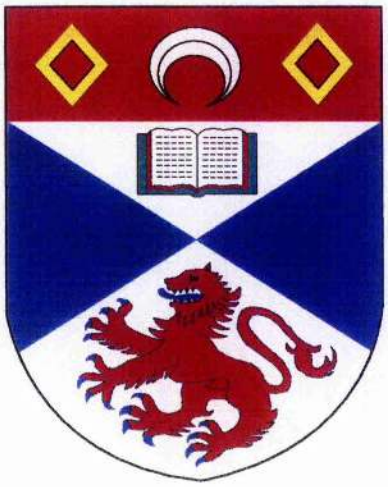

Macrocyclic Complexes and their Use as Electrocatalysts for the Electrochemical Reduction of Carbon Dioxide

A thesis presented by Caroline Smith, *B.Sc.*, to the University of St. Andrews in application for the degree of Doctor of Philosophy.

February 1995

Declarations

I, Caroline I. Smith, hereby certify that this thesis has been composed by myself, that it is a record of my work and it has not been accepted in partial or complete fulfilment of any other degree or professional qualification

Signed _____ Date 7.2.95

I was admitted to the Faculty of Science of the University of St. Andrews under Ordinance General No. 12 on the 1st of October 1991 and as a candidate for the degree of Ph.D. on the 1st of October 1992.

Signed _____ Date 7.2.95

We hereby certify that the candidate has fulfilled the conditions of the Resolution and Regulations appropriate to the Degree of Ph.D.

Signature of Date 7/2/95

Supervisors Date 7/2/95

Declaration

In submitting this thesis to the University of St. Andrews, I understand that I am giving permission for it to be made available for its use in accordance with the regulations of the University library for the time being in force, subject to any copyright vested in the work not being affected thereby. I also understand that the title and abstract will be published, and that a copy of the work may also be made and supplied to any *bona fide* library or research worker.

To Mum

and Dad

Contents

Chapter Three

A Study of the Mechanism of the Electrochemical Reduction of CO_2 by Rotating Disc Studies on $[Ni(cyclam)]^{2+}$

Chapter Four

A Study of the Adsorption of $[Ni(cyclam)]^{2+}$

Chapter Five

A Survey of a Variety of Tetradentate Macrocycle and Chelate Complexes Carbon Dioxide Reduction

Chapter Six

New Catalysts for the Reduction of Carbon Dioxide

Acknowledgements

I would like to express my sincere gratitude to Prof. Robert W. Hay and Dr. Joe A. Crayston whose tireless enthusiasm and expert guidance has been an invaluable aid to me and my research during my Ph.D. at St. Andrews.

Thanks are due to Prof. Neil F. Curtis for helpful hints in the art of making macrocycles. Dr. Philip Mallon for proof-reading this thesis and persuading me to stick with it when everything was against me. Mrs Lynn Christie for running and analysing the a.c. impedance results. The technical staff at the Chemistry Department in St. Andrews, most notably Jim Bews (computing), Bobby Cathcart and Jim Rennie (Mechanical Workshop), Colin Smith (glass-blowing), John Smith (for supplying copper gauze and membrane), Melanja Smith (NMR), and Sylvia Smith (elemental analysis).

I am indebted to the ESPRC (formerly SERC) for financial support throughout my course and the Departmental Travel Fund and the European Science Foundation for supporting conference travel.

I would especially like to thank my mum and dad for all the help and support during my time at University.

List of Abbreviations

bipy	2,2'-bipyridine
CoA	Coenzyme A
CoM	Coenzyme M
CV	Cyclic Voltammetry
diphos	1,2-bis(diphenylphosphino)ethane
DME	Dropping Mercury Electrode
DMF	Dimethyl Formamide
DMSO	Dimethyl Sulphoxide
EDTA	Ethylenediaminetetraacetic acid
EPR	Electron Paramagnetic Resonance
EXAFS	Extended X-Ray Absorption Fine Structure
FAD	Flavin Adenine Dinucleotide
GC	Gas Chromatography
GC	Glassy Carbon
GtC	gigatonnes, expressed as carbon
HMDE	Hanging Mercury Drop Electrode
HPLC	High Performance Liquid Chromatography
IR	Infra-red
MCD	Magnetic Circular Dichroism
MeCN	Acetonitrile
NAD	Nicotinamide Adenine Dinucleotide
NMR	Nuclear Magnetic Resonance
ppm	parts per million
RDE	Rotating Disc Electrode
r.p.m.	Revolutions per minute
RRDE	Rotating Ring-Disc Electrode
SCE	Saturated Calomel Electrode

$TBAPF_6$	Tetrabutylammonium Hexafluorophosphate
TBAT	Tetrabutylammonium Tetrafluoroborate
UV-Vis	Ultra Violet - Visible Spectrum
Z	Impedance

Abstract

The environmental problem of carbon dioxide pollution has caused considerable interest over recent years. Much work has concentrated on catalysts for the reduction of carbon dioxide. There are two main methods for the reduction, electrochemical and photochemical reduction. There are several catalysts reported in the literature but the most selective and efficient one for the electrochemical reduction of carbon dioxide to carbon monoxide is nickel(II) 1,4,8,11-tetraazacyclodecane perchlorate (more commonly known as $[Ni(cyclam)]^{2+}(ClO_4)_2$).

In order to understand how this catalysis occurs the complex was investigated using a variety of electrodes and solvents in order to determine the best system for catalysis to occur. The best system is an aqueous solution of the complex with sodium perchlorate as the supporting electrolyte and with a mercury working electrode.

The effect of macrocycle ring size was investigated using [n]aneN_4 complexes, n = 13 - 16. The highest current produced under carbon dioxide was for the n = 14 ring. Subsequent complexes investigated have a [14]-membered backbone. The other important effect in the macrocyclic structure is the nature of the conformation of the complex. Cyclam itself exists as five conformations, three of which are readily accessible. The other conformations do not reduce carbon dioxide to the same extent as the original $[Ni(cyclam)]^{2+}$. The origin of this difference was shown to be related to the extent of adsorption of each conformer. Also, if the chelate sequence of the cyclam is changed from cyclam to isocyclam the catalytic efficiency is lowered but the potential at which the reduction occurs is more positive.

Rotating disc electrochemistry was attempted in order to find a method for comparing the catalytic efficiency of different complexes. A mercury plated copper electrode was used but unfortunately the mercury deteriorated and left behind bare copper. Copper itself showed current plateaux for reduction under carbon dioxide; these current plateaux varied linearly with (rotation rate)$^{1/2}$. On closer examination the current plateaux were due to the Ni(II/I) reduction and not carbon dioxide reduction.

The adsorption of the catalyst onto the mercury is important as it is this adsorbed species that is catalytically active. To determine the nature of the catalytic species various electrochemical techniques such as chronocoulometry and a.c. impedance were employed to measure the extent of the adsorption. Chronocoulometry showed that adsorption occurred on the mercury, but adsorption onto the copper surface was inhibited in the presence of carbon dioxide. A.C. impedance spectroscopy showed that adsorption occurred at -1.20 V which is considerably more positive than the redox potential of the complex.

A variety of unsaturated macrocycles were also investigated for catalytic behaviour. As the unsaturated macrocycles have lower redox potentials than the corresponding saturated macrocycle, the result should be that the potential for the reduction becomes more positive. However with these macrocycles no reduction of carbon dioxide is observed under the same conditions as $[Ni(cyclam)]^{2+}$.

A series of new catalysts has been identified. These complexes have the ability to reduce carbon dioxide at more positive potentials with a greater current efficiency, than $[Ni(cyclam)]^{2+}$. The new catalysts are based on a [14]aneN_6 backbone. The extra nitrogen atoms appear to stabilise the intermediate hydrogen bonded Ni^{I}-CO_2 adduct.

"Might I suggest that, from this moment on, the rest of this discourse is conducted by those with brains larger than a grape?"

Kryten

(Red Dwarf VI)

"There's an old human saying, "If you're going to talk garbage, expect pain.""

A. J. Rimmer

(Red Dwarf VI)

Chapter One

A. The Biochemistry of Nickel

1.0 Introduction

For many years nickel was thought to be an essential trace element but only in recent years has its functions been identified. The first nickel protein to be identified was urease[1], 49 years after Sumner first isolated and crystallised the enzyme[2]. It has a widespread occurrence and its specific requirement for nickel explains many of the effects in plants suffering from a nickel deficiency. Many bacteria, including hydrogen bacteria, methanogens and acetogens, were found to have a high demand for nickel as a trace element. This requirement for nickel was not recognised for a long time because the nickel dissolved from the stainless steel culture apparatus was sufficient[3].

The requirement for nickel was explained when the enzyme hydrogenase was found to contain nickel using EPR spectroscopy. The characteristic EPR spectrum of nickel(III) was observed by Lancaster in the membranes of methanogenic bacteria[4]. This was confirmed by growing the cells on the ^{61}Ni ($I = {}^{3}/_{2}$) isotope and observing the hyperfine splitting of the spectrum into four lines. Similar spectra have also been observed in sulphate-reducing bacteria[5], photosynthetic bacteria[6] and hydrogen-oxidising bacteria[7]. Hydrogenases are enzymes that catalyse the production or consumption of hydrogen gas. Not all of the hydrogenases found to date contain nickel, and even in some that do contain nickel no EPR signal is observed[8].

In methanogenic bacteria nickel is also used in a second process, where there is a series of complex steps leading to the release of methane gas[9]. The enzyme involved is methyl-coenzyme M reductase which contains a cofactor F_{430}, which has a nickel porphinoid complex. The methanogens belong to an unusual group of bacteria described as Archaebacteria which are thought to be ancient[10]. Like acetogens they are strict anaerobes. Although they are now restricted in habitat, these organisms,

with the nickel metabolism and related cobalamins, may have played an important part in the early phases of evolution.

A third nickel containing enzyme is found in some strictly anaerobic bacteria and involves the oxidation of carbon monoxide to carbon dioxide, and also in the formation of acetyl-coenzyme A from carbon monoxide. This reaction was first reported in 1932 by Fischer[11] where it was found to occur in sewage sludge. It has the trivial name of carbon monoxide dehydrogenase. The principal function of this enzyme is to synthesise acetyl-coenzyme A and is the major enzyme of acetogenic bacteria, which have a novel pathway for the fixation of carbon dioxide[12], and is also found in methanogens.

1.1 Urease

Urease was the first enzyme shown to contain nickel and was first isolated from jack beans by Sumner[2]. It catalyses the hydrolysis of urea to ammonia and carbon dioxide via the intermediate formation of a carbamate ion:-

$$(NH_2)_2CO + H_2O \longrightarrow CO_2 + 2NH_3 \qquad (1.1)$$

The protein has a multimeric structure with a relative molecular mass of 590,000 Da. Analysis of the protein showed that there were 12 nickel atoms per molecule[1]. There are six subunits in the protein and binding studies shows two nickel atoms per active site and binding of one substrate molecule[1]. When the metal was removed by treating with EDTA at pH 3.7, the optical absorption and enzymic activity correlated with the nickel content[1]. This, along with the enzyme's sensitivity to chelating agents, shows that nickel is essential to the enzyme's activity[1].

1.1.1 Spectroscopic Properties

The nickel in urease is nonmagnetic and appears to be in the Ni(II) oxidation state. The UV-visible spectrum in the presence of the competitive inhibitor

mercaptoethanol shows absorption peaks at 324, 380 and 420 nm which are assigned as sulphur-nickel charge transfer transitions. The nickel is in an octahedral site, although in carboxypeptidase the nickel is co-ordinated to one cysteine sulphur, two histidine imidazoles and the carboxylate of a glutamate residue.

EXAFS studies on urease are similar to those of nickel benzimidazole complexes[13], which is consistent with the nickel being co-ordinated to histidine nitrogen and oxygen ligands in the enzyme. The EXAFS spectrum obtained is probably the average of the two binding sites.

1.1.2 Mechanism of Catalysis

The mechanism for urease catalysis is based on the studies of reactions with poor substrates such as formamide, acetamide and N-methylurea[14]. These studies suggest that the two nickel ions are both in the active site, one for binding urea and the other for binding an hydroxide ion, which acts as an efficient nucleophile. The nickel ions would have to be within 0.6 nm of each other but this is unconfirmed spectroscopically. This reaction is analogous with the peptide hydrolysis by carboxypeptidase[15] in which a hydroxide ion is bound to the zinc (see Figure 1.1).

1.2 Hydrogenase

1.2.1 Types of Hydrogenase

In contrast to urease, the nickel in other bacterial enzymes appears to have a redox function and to take up the oxidation states of Ni(I) and Ni(III).

The nickel hydrogenases are now some of the most studied nickel proteins, although the interest in these has only arisen in the last few years, and there is evidence that the nickel is involved in the catalytic cycle. Hydrogenase is not just one but a class of enzymes. They may be distinguished in function as they can produce or consume hydrogen in reactions with a range of physiological electron acceptors or donors. They can also be distinguished from each other by their molecular and catalytic properties:-

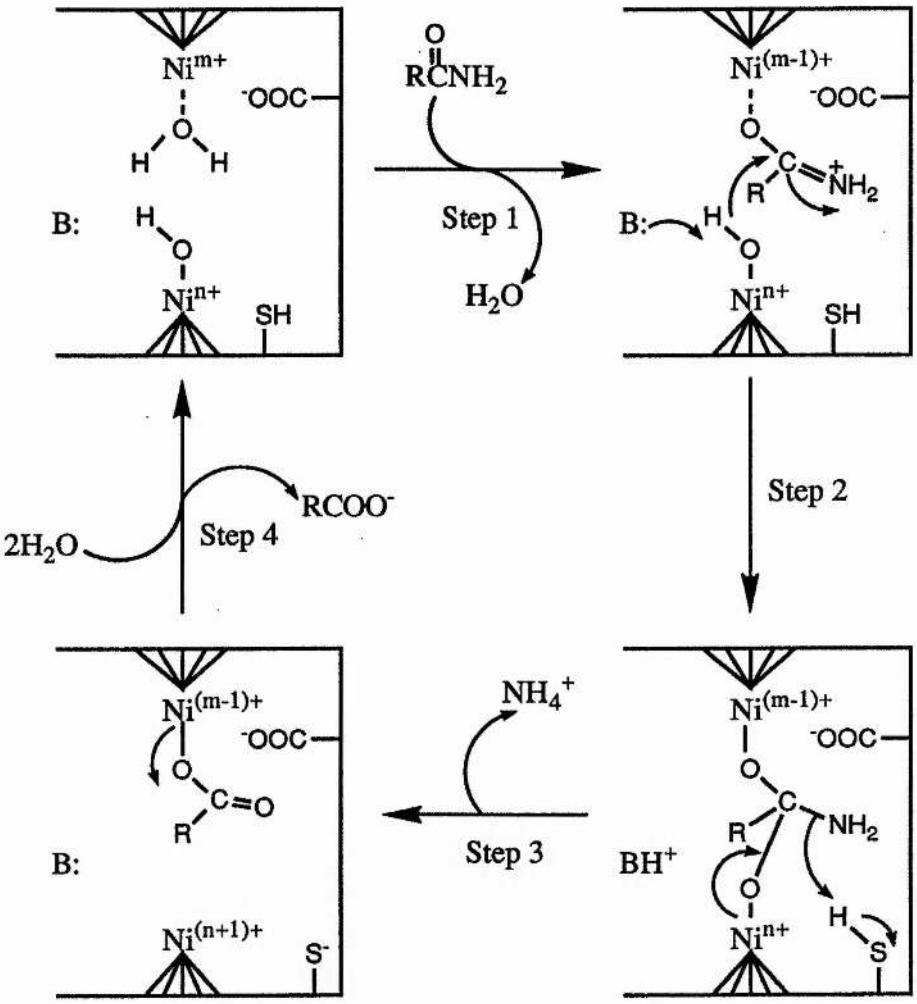

Figure 1.1

Proposed Reaction Cycle for Urease.

For Urea R = $-NH_2$

Step 1:- Urea is activated towards nucleophilic attack by oxygen co-ordination to a nickel ion; the $=N^+H_2$ is stabilised by interaction with a protein carboxylate.

Step 2:- Nucleophilic attack by an hydroxide ion co-ordinated to the second nickel, to form a tetrahedral intermediate.

Step 3:- Breakdown of the tetrahedral intermediate to form a co-ordinated carbamate ion.

Step 4:- Hydrolysis releases carbamate ion, the initial product of urease on urea.

i) The type of iron-sulphur clusters and other groups such as flavin or selenium that are present.

ii) The types of EPR signals due to nickel.

iii) The sensitivity to oxygen deactivation and also in some cases slow, reductive reactivation.

iv) The different ratio of products in hydrogen isotope-exchange assays.

With all the hydrogenases there is a common pattern of protein composition. They consist of two protein subunits which have relative molecular masses of approximately 60, 000 and 30,000 Da[8], with some evidence indicating that the nickel is in the larger subunit. Some of the more complex hydrogenases contain other subunits concerned with the reduction of specific electron acceptors.

1.2.2 EPR Spectroscopic Properties of Nickel

The co-ordination and oxidation states of nickel in hydrogenase are difficult to determine because the iron-sulphur clusters obscure the optical spectra and also as the commonest oxidation state of nickel (*i.e.* Ni(II)) is EPR silent. Some hydrogenases however are not EPR silent and are the best indicators as to the function of the nickel.

The general belief is that the EPR detectable signal in oxidised hydrogenase is low spin Ni(III) which is d^7. When the enzyme is reduced the EPR signal disappears which is consistent with a Ni(II) oxidation state.

The EPR spectra of *D. gigas* hydrogenase shows a prominent signal with g values of 2.32, 2.21 and 2.01, termed Ni-A, and also a minor signal in the oxidised hydrogenase termed Ni-B. When certain hydrogenases[16] are progressively reduced by hydrogen, the EPR spectra show three stages:- firstly the Ni-A and Ni-B signals disappear; followed by a new signal appearing (termed Ni-C) and finally this disappears. The Ni-C signal represents an intermediate oxidation state since it can be restored by flushing away excess hydrogen with argon.

1.2.3 Midpoint Redox Potentials

The reduction potentials of various EPR detectable nickel species in hydrogenase are all less than -0.242 V versus SCE. This contrasts with synthetic complexes with amino acids where the oxidation of Ni(II) to Ni(III) occurs at much higher potentials (-241.2 to -240.8 mV) and reorganisation of the complex occurs.

There are various factors that could stabilise the Ni(III) state and hence lower the potential of Ni(II)/(III). One common method is to use sulphur as a ligand. It is well known that for a transition metal centre with a particular ligand arrangement, a protein environment can change the midpoint potential over a range of several hundred millivolts by means of electrostatic and other effects. A confined binding site is another way to lower the potential but this is difficult to achieve in the flexible environment of a protein.

The opposite problem occurs if Ni(I) is involved in the reaction cycle, since the Ni(II)/Ni(I) couple is generally more negative by about 1 V than the Ni(II)/Ni(III). In some hydrogenases the enzyme undergoes a slow change in conformation during the conversion to the active species, where the alleged Ni(I) EPR signal appears, and so the altered conformation may stabilise the Ni(I) state. The Ni(I) state is stabilised relative to the Ni(II) state by ligands favouring tetrahedral co-ordination.

1.2.4 Co-ordination State of Nickel

In hydrogenases where the nickel is EPR detectable, the similarity of the spectra suggests that the nickel environment is conserved. Although there is a wide variety of catalytic activity and specificity among the hydrogenases, there may only be a few different types of nickel centres.

At present there is no evidence to suggest whether the nickel is co-ordinated directly to the protein, as in copper and iron-sulphur proteins, or to an organic cofactor, as in the molybdenum hydroxylases and hemoproteins.

a) X-Ray Absorption Spectroscopy

X-Ray absorption edge spectra and EXAFS studies can determine the co-ordination geometry of the nickel sites. Nickel K-edge X-ray absorption can be used but there are very few model compounds to compare the nickel oxidation state with.

b) Hyperfine Interactions

All assignments of nickel in EPR spectra have been made by using the isotope ^{61}Ni and identifying the splitting pattern.

The EPR spectra of oxidised hydrogenases do not show any significant hyperfine splitting by ^{14}N, which shows that there is no significant delocalization onto the nitrogen ligands. There is also no change in the linewidth when D_2O is used instead of H_2O.

c) Electron Spin-Echo Spectroscopy

This technique suggests that there is an indirect co-ordination of the nickel to nitrogen.

d) Magnetic Circular Dichroism (MCD)

The technique is used to observe optical transitions due to paramagnetic species. Ni(III) has been observed against a background of iron-sulphur cluster absorption in some hydrogenases. Spectra of *M. thermoautotrophicum* hydrogenase at low temperatures yields MCD bands in the regions of 300 - 460 and 530 - 670 nm and have been assigned as nickel d-d transitions and sulphur to nickel charge transfer bands.

1.2.5 Derivatives of Nickel

Altered forms of nickel hydrogenases have been observed under conditions in which substitution is expected at the hydrogen-binding site. They have been interpreted as species containing hydrogen, hydride or carbon monoxide. These are

relevant to the mechanism of hydrogen production and how the inhibition by carbon monoxide occurs. These species have only been observed by EPR spectroscopy at present.

a) Reactions with Hydrogen

The Ni-C EPR signal is observed in some nickel hydrogenases under hydrogen. This nickel species is photosensitive and irradiation by visible or near-UV light at cryogenic temperatures produces a new EPR signal. The photochemical reaction is reversed at temperatures above 200 K[16].

Raman spectroscopy has been used to study nickel protoporphyrins and showed that the photochemical behaviour of nickel sites is complex and dependent on the protein environment. Nickel in porphyrin complexes favours a four or six co-ordinate structure and in nickel-substituted human haemoglobin one type of binding site takes up a four-co-ordinate geometry and the other site (like the heme binding site in myoglobin) is forced into a five-co-ordinate geometry. After laser excitation, the four-co-ordinate sites undergo photoassociation with a fifth ligand, as in protoporphyrin complexes[17]. In contrast, the five co-ordinate sites undergo photodissociation and, unlike iron porphyrins, the recombination of nickel and the ligand is very rapid.

b) Reactions with Carbon Monoxide

Carbon monoxide is an inhibitor of most nickel hydrogenases with the exception of the soluble hydrogenases of hydrogen bacteria. The inhibition is competitive with hydrogen showing that the two molecules bind to the same site. EPR studies of the Ni-A signal, indicate that in the oxidised hydrogenase the Ni(III) is unreactive to carbon monoxide[18]. So it is probably the Ni(II) or Ni(I) that binds the carbon monoxide. Reaction of reduced hydrogenase with carbon monoxide produces both EPR silent and detectable states, which may be different carbonyl species.

c) Interactions with Oxygen

Oxygen inhibits some hydrogenases and completely destroys others, in particular some iron hydrogenases. In the hydrogenases that survive exposure to oxygen, the active site is unreactive to hydrogen and carbon monoxide under oxidising conditions. It is thought that there is a protective mechanism for organisms which may encounter oxygen *in vivo*, so the active site becomes inaccessible to all gases.

1.2.6 Interactions of Nickel with Iron-Sulphur Centres

All the hydrogenases isolated to date are iron-sulphur proteins and the activity is associated with the [4Fe-4S] cluster as well as the nickel. In some hydrogenases the nickel and iron-sulphur cluster are undetectable by EPR suggesting a strong anti-ferromagnetic coupling. These two groups may act together to transfer two electrons to the hydrogen.

1.2.7 Catalytic Properties

a) Activity States of Nickel-Containing Hydrogenases

The characteristic EPR signal due to Ni(III) is observed in some hydrogenases but not in all[8]. The signal is due to an oxidised form of the enzyme not directly involved in the catalysis and is supported by studies of the enzyme activity in response to oxidising and reducing agents. One well studied case is that of *D. gigas* hydrogenase[19], although when all oxygen is removed, a reductant is required to reduce the oxidised form to a state where it can react with hydrogen.

The enzymatic activity, whether measured by hydrogen production, consumption or isotope exchange, is variable depending on the history of the sample[20,21]. They may not show their full activity until subjected to some form of reactivation which varies among the hydrogenases. The *D. gigas* hydrogenase, when studied under various reactivating conditions, showed that the enzyme could be obtained in different forms with different activity and since they can all be fully

reactivated, this shows that there is more than one type of inactive oxidised enzyme[19,22]. The simplest theory is that there are two:- one which is rapidly activated by reduction during the assay and the second which is activated slowly by strong reductants. These have been termed the *ready* and *unready* states respectively. Using the interpretation of Berlier *et al* [20], the unready state is associated with a tightly bound oxygen, but alternatively the two states might be different protein conformations[19].

b) Mechanism of Catalysis

The behaviour of EPR detectable nickel and iron-sulphur clusters in hydrogenase during redox experiments suggests several possible reaction schemes. The Ni-C species is particularly important since its potentials for appearance and disappearance during reduction are comparable with the H^+/H_2 potential, at the low partial pressures of hydrogen encountered by these organisms. The potentials are also pH dependent, which is consistent with hydrogen production. Also, the low-temperature photochemical reaction of the Ni-C species shows a strong kinetic isotope effect with the ^2H.

The hypothetical reaction mechanism is shown in Figure 1.2, and is consistent with the redox and pH dependence of the EPR detectable nickel species. Hydrogen is known to undergo heterolytic cleavage and it is proposed that this is an intramolecular reaction, leading to the formation of a Ni(II) hydride and a protonated base in the enzyme (Step 1). The Ni-C species is thus thought to be a protonated Ni(I) species. An alternative suggestion for this state is a dihydrogen complex, $Ni(III).H_2$. These can only be separated by kinetic measurements.

1.2.8 Other Functions of Nickel in Hydrogenases

The soluble hydrogenase from the hydrogen-oxidising bacterium *N. opaca* is one of the class that contain flavin and use NAD as the electron acceptor[23]. The protein has four dissimilar subunits and contains approximately four atoms of nickel,

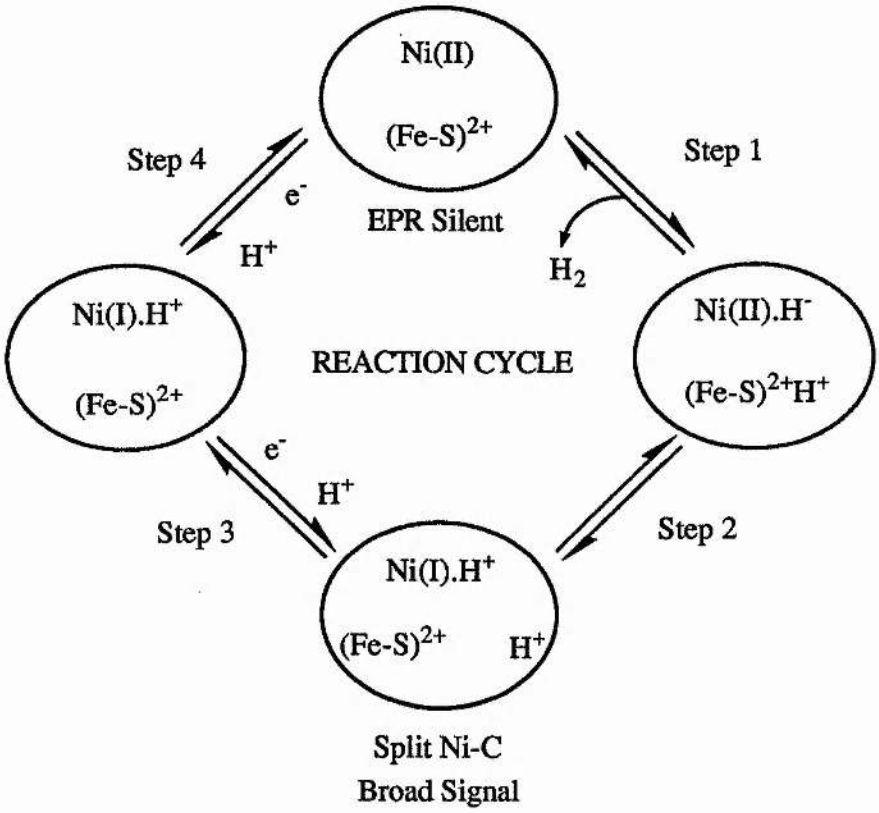

Figure 1.2

Hypothetical Reaction Cycle for *D. Gigas* Hydrogenase.

This reaction scheme is based on the EPR and redox properties of the nickel. Only the nickel centre and one [4Fe-4S] cluster are shown.

Step 1:- Enzyme, in the activated conformation and Ni(II) oxidation state causes heterolytic cleavage of H_2.

Step 2:- Intramolecular electron transfer to the iron-sulphur cluster producing a protonated Ni(I) site.

Step 3:- Reoxidation of the iron-sulphur cluster and release of a proton.

Step 4:- Reoxidation of Ni and release of the other proton.

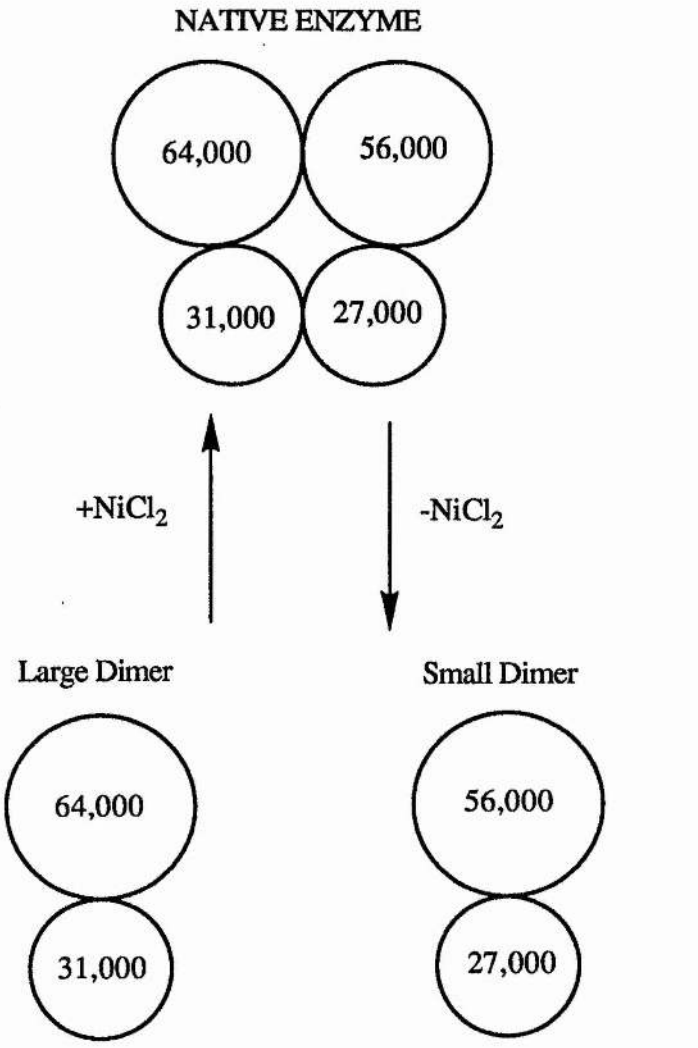

Figure 1.3

Dissociation and reassociation of soluble, NAD-linked hydrogenase from *Nocardia opaca* . "Diaphorase" refers to NADPH-acceptor reductase activity.

one FMN, three [Fe-4S] clusters, one [2Fe-2S] cluster and up to one [3Fe-xS] cluster.

Two of the nickel atoms were easily removed by dialysis which differs from the nickel in other hydrogenases[23]. The enzyme would only catalyse electron transfer from hydrogen to NAD if cations were added, Ni^{2+} being the most effective[23]. In the absence of cations the enzyme could be separated as two dimers (Figure 1.3). One of the subunits contained two tightly bound nickel atoms and one [4Fe-4S] cluster and had hydrogen-acceptor reductase activity. The other subunit contained flavin and iron-sulphur clusters and had NADH-acceptor reductase activity. So in *N. opaca* hydrogenase, which so far is unique, the nickel has two functions:- in catalysis and in keeping the protein structure.

1.3 Methyl-Coenzyme M Reductase

1.3.1 Factor 430

F_{430} is a yellow water soluble compound and was first extracted from boiled cells of methanogenic bacteria and its isolation was first reported by Gunsalus and Wolfe[24]. The cofactor has a Soret band in the visible region at 430 nm. Functionally F_{430} is the prosthetic group of the methylreductase system and is also found in the free state in cell extracts.

The presence of nickel in F_{430} was shown by Diekert *et al*[25] and Whitman and Wolfe[26]. It has a tetrapyrrole structure (Figure 1.4) and the structure of the cofactor in the cell is probably the penta acid. It is a tetrahydro derivative of a porphinoid which is related to the corrins, for which the term "corphin" was coined by Pfaltz *et al*[27]. The specificity of this macrocycle for nickel is due to the six-membered ring which introduces a slight pucker into the planar structure. An EXAFS study of the nickel environment of the isolated F_{430} indicated two nitrogens at 0.191 - 0.192 and two at 0.210 - 0.214 nm[28]. This is consistent with nickel in a square-planar co-ordination to a puckered corphin structure. In the intact protein, protein component C of methyl-CoM reductase, the absorption-edge spectra are indicative of nickel with a co-

ordination number greater than four, probably octahedral.

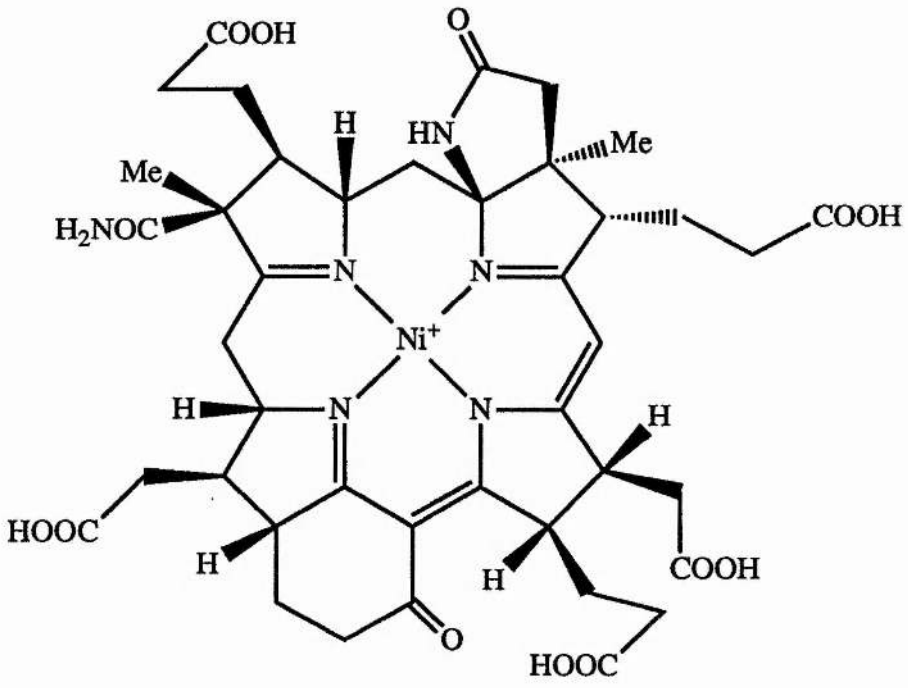

Figure 1.4

The Structure of Factor 430M.

1.3.2 EPR Spectra

Albracht *et al*[29] have observed an EPR spectrum from whole cells of *M. thermoautotrophicum* which appears to arise from protein bound F_{430}. The same type of spectrum was also observed in purified methyl-CoM reductase[30]. The paramagnetic species from whole cells was only partially reduced by treatment with hydrogen and unaffected by carbon monoxide. Gel filtration on this shows it to be part of a soluble protein[29]. The spectrum was broadened by substitution with ^{61}Ni and showed hyperfine splitting which could be simulated as interaction with four equivalent nitrogen atoms, corresponding to the four nitrogens of a tetrapyrrole. The lineshape of the spectrum is consistent with nickel in a tetragonally distorted octahedral ligand field. This confirms the assignment as a nickel species bound in a planar tetrapyrrole structure. It is not possible to determine the oxidation state of the nickel, although the observation that it was observed in isolated factor F_{430} treated

with dithionite suggests that it is Ni(I).

1.3.3 Function

F_{430} is required for the activity of the methyl reductase system, which catalyses the reduction of the methyl group of methyl-CoM *i.e.* 2-(methylthio)ethanesulfonate to methane:

$$CH_3\text{-}S\text{-}CH_2\text{-}CH_2\text{-}SO_3^- + H_2 \longrightarrow CH_4 + HS\text{-}CH_2\text{-}CH_2\text{-}SO_3^- \quad (1.2)$$

This is a complex process, involving the deazaflavin reducing hydrogenase and other proteins, provisionally named factors A-2, A-3 and C[9]. The system requires initial activation by ATP before the reaction can proceed[26]. Component C consists of two of each of three protein subunits of 68, 45 and 38.5 kDa and contains two molecules of F_{430} per molecule, as well as stoichiometric amounts of coenzyme M. F_{430} appears to be tightly, but noncovalently, bound to the enzyme.

The exact role of the nickel in F_{430} in methane formation is not clear at present. Analogy with the cobalamins and the observation of an EPR detectable reduced state might suggest that it is involved in either methyl-group transfer, reduction or both.

1.4 Carbon Monoxide Dehydrogenase

1.4.1 Catalytic Properties

This enzyme catalyses the interconversion of carbon monoxide to carbon dioxide using suitable electron acceptors and donors. The reaction occurs via an enzyme-bound one-carbon intermediate:-

$$CO \longrightarrow [C_1] \longrightarrow CO_2 + 2e^- + 2H^+ \quad (1.3)$$

The enzyme was first isolated from *C. thermoaceticum, Clostridium formicoaceticum*

and *Clostridium pasteurianum* by Diekert and Thauer[31]. They showed that the synthesis of the enzyme required nickel. The enzyme is present in large amounts in acetogenic bacteria and is involved in an unusual pathway for the fixation of carbon dioxide with the formation of acetate[32,33]. In the acetogens this reaction is involved both in the production of energy, giving acetate as a waste product and in the biosynthesis of cell components starting from acetate. The enzyme is also present in methanogenic bacteria where it is used in the biosynthetic metabolism[12].

Carbon monoxide dehydrogenase has a high molecular weight and values ranging from 150,000 to 460,000 have been reported[32]. The analysis of the enzyme derived from *C. thermoaceticum* had a composition of two nickel, one zinc, eleven iron and fourteen sulphur atoms per dimeric enzyme and a relative molecular mass of 150,000 Da[34].

1.4.2 Spectroscopy

The low temperature EPR spectrum of carbon monoxide dehydrogenase in the reduced state is complex with *g* values of 2.04, 1.94 and 1.90 and 2.01, 1.86 and 1.75, which is probably two [4Fe-4S] clusters. The clusters are oxidised by carbon dioxide and reduced by carbon monoxide.

The EPR spectrum under non-reducing conditions has *g* values of 2.21, 2.11 and 2.02 and is attributed to Ni(III)[35]. Due to the low intensity of the spectrum it is not established as to whether this is an active state of the enzyme.

Two more relevant spectra were observed in the reduced enzyme after treatment with carbon monoxide. Recent simulations show that the spectra are consistent with a complex of one nickel and three iron atoms, analogous to a [4Fe-4S] cluster in which one iron is substituted by a nickel[36].

B. Carbon Dioxide - Atmospheric Pollution

1.5 The Global Behaviour of Man-Made Carbon Dioxide

1.5.1 Atmospheric Measurements and Man-Made Inputs

a) Atmospheric Measurements

The earliest attempted measurements of carbon dioxide in the atmosphere were over 200 years ago, although Thorpe's results in 1867 was the first believable study[37]. Those measurements and the ones made up until the 1950's are suspect for a number of reasons including unrepresentative sampling, contamination and poor analytical methods. Recently all the earlier data has been evaluated and although there is a lot of scatter, a value of 290 ppm is assumed to be representative of the carbon dioxide concentration in the atmosphere prior to the large scale industrialisation. This value is not generally accepted and it is unfortunate when modelling the increase in the carbon dioxide concentration in the last century.

In spite of the scatter, there is some evidence for an increase in atmospheric carbon dioxide in the first half of this century. Reliable evidence for this is provided by accurate measurements made over the last twenty years at several locations.[38] A striking feature of these results is that there is a general agreement between the yearly average measurements made at widely spaced locations, thus establishing that the increase in atmospheric carbon dioxide is a global event. This uniformity is due to the residence time of carbon dioxide in the atmosphere being about seven years, so no matter how and where a carbon dioxide molecule enters or leaves the system, it is well mixed within the atmospheric reservoir by the wind systems.

b) Man-Made Inputs

A major source of man-made carbon dioxide for the atmosphere is the combustion of fossil fuel. The contribution from this source for the period from 1860 was estimated by Keeling in 1973[39], based on United Nations data on the amounts of

different types of fuel burned and knowledge of the quantity of carbon dioxide produced from the combustion of unit amounts of each fuel type. In 1973 and 1974, Rotty revised the calculations to include an additional source since 1950 from the flaring of natural gas and the small contribution from the manufacture of cement[40]. Since then the calculations have been updated regularly.

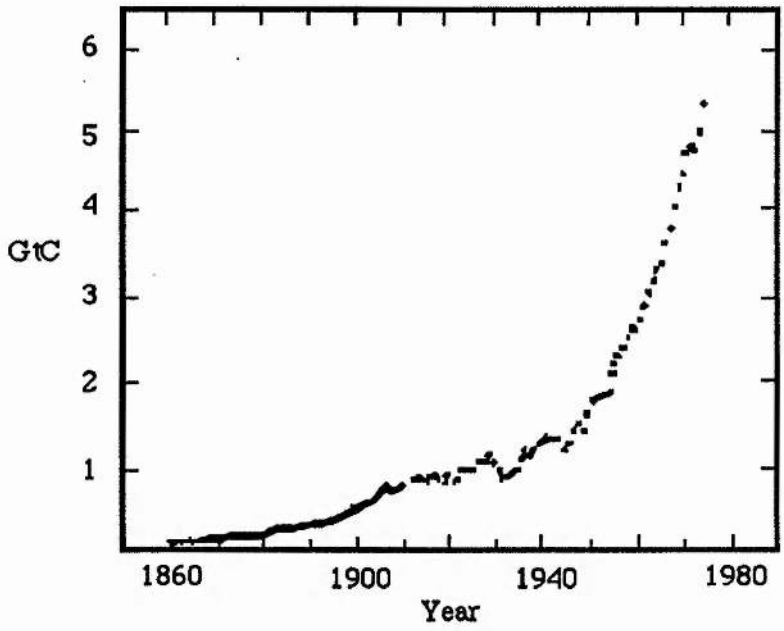

Figure 1.5

Annual Production of CO_2 from fossil fuels and cement 1860-1977.

Data from C. D. Keeling, *Tellus*, 1973, **25**, 174-198.

The results show the expected sharply rising trend of carbon dioxide with time (Figure 1.5). However, when the emissions are plotted on a logarithmic scale it is apparent that the rate of increase in carbon dioxide injected into the atmosphere has, with well defined and explicable exceptions, been constant. The exceptions correspond to the two World Wars and the "Great Depression" of the 1930's. These apart, the rate of increase has been close to 4.3 % per year from 1860 to the early 1970's. If the periods of lesser fuel usage are included then the average annual increase in the 118 years from 1860 to 1978 has been 3.5 % with total emissions during this time being 155 GtC.

1.5.2 Uptake of Carbon Dioxide by the Oceans

At present, estimation of the magnitude of the oceanic sink for man-made carbon dioxide is generally done by the use of models. The models involve three stages:-

i) estimation of the equilibrium capacity of seawater to take up excess atmospheric carbon dioxide,

ii) quantification of the rate at which such excess carbon dioxide can cross the air-sea interface into the surface oceans,

iii) assessment of the rate at which surface waters mix with deeper layers.

a) The Equilibrium Capacity of Seawater to Absorb Carbon Dioxide

The following equations describe the uptake of carbon dioxide by pure water:-

$$CO_2(g) \overset{H_2O}{\rightleftharpoons} CO_2(aq) \qquad (1.4)$$

$$CO_2(aq) + H_2O(l) \rightleftharpoons H_2CO_3(aq) \qquad (1.5)$$

$$H_2CO_3(aq) \rightleftharpoons H^+(aq) + HCO_3^-(aq) \qquad (1.6)$$

$$HCO_3^-(aq) \rightleftharpoons H^+(aq) + CO_3^-(aq) \qquad (1.7)$$

Equation (1.4) and its associated equilibrium constant quantify the ratio of carbon dioxide molecules in the liquid to those in the gas phase. Similar expressions exist for the dissolution of all gases and for many gases (*e.g.* O_2, N_2, CO, CH_4, N_2O) this is all that is required since they do not react chemically with water. For carbon dioxide and other gases which react with water additional equations are required. For CO_2, $H_2CO_3(aq)$ is formed which although a weak acid can dissociate producing bicarbonate and carbonate ions with the release of H^+ ions.

Seawater is, of course, not pure water and contains substantial amounts of

dissolved salts. Most of the material is neutral electrolyte which alters the equilibrium constants, although the effect is not that large. More important is the amount of bicarbonate and carbonate ions derived from the weathering of non-neutral salts.

b) Exchange of Carbon Dioxide Across the Air-Sea Interface

Near the ocean surface the water is generally well mixed by the action of wind, waves and tides; the depth of this upper layer being an average of about 75 m. It is separated from the deep oceans by a region approximately 1 km thick, where the water temperature decreases rapidly with depth (known as the thermocline). The temperature gradient in the thermocline region makes it stably stratified and hence an important barrier to the downward transfer of the excess carbon dioxide taken up by the upper mixed layer. Since the surface layer is well mixed, in carbon dioxide uptake models it is generally treated as being homogeneous with the rate at which it responds to a change in the atmospheric partial pressure of carbon dioxide, determined by the rate at which the gas can cross the air-sea interface.

c) Oceanic Mixing

It has been shown that since the surface layer is such a small volume it is not an important sink for excess carbon dioxide. The total uptake by the oceans depends on the extent to which these surface waters can mix with the thermocline and the deep ocean layers underneath, containing about 15 and 50 times as much carbon, respectively, as the surface layer.

Generally the oceans are stably stratified and only when exceptionally dense water is formed at the surface, following cooling or salinity increase due to ice formation, can sinking to appreciable depths occur. The Norwegian and Greenland Seas and around Antarctica are the principal regions where these processes are effective in producing deep ocean water. This sinking is balanced by slow, upward motion of deep water in other regions of the ocean.

1.5.3 Heterogeneous Processes which might Increase Oceanic Uptake of Carbon Dioxide

a) Biological Uptake

Marine plants are thought to fix about 25 GtC each year, however, since the figure of 25 GtC per year represents gross fixation as recycling of carbon dioxide is rapid on a timescale of weeks. The quantity of fixed carbon escaping from the upper mixed layer into the deeper water is of the order of 10 % of the gross fixation rate and, after oxidation at depth, the amount sedimented out of the system is probably only about 10 % of this (*i.e.* 0.25 GtC per year).

The productivity of marine plankton appears to be nutrient rather than carbon dioxide limited. Since man's activities have increased the input of plant nutrient elements (particularly phosphorus and nitrogen) into the oceans, then enhanced production and subsequent sedimentation might contribute a valid route for uptake of additional carbon dioxide by the marine environment. Only phytoplankton producing carbohydrate (or other forms of organic carbon) according to the classical photosynthetic reaction (Equation (1.8)) constitute a potential sink for excess carbon dioxide.

$$6CO_2(g) + 6H_2O(l) \xrightarrow[\substack{\text{Nutrients}\\ \text{Chlorophyll}}]{h\nu} C_6H_{12}O_6(s) + 6O_2(g) \qquad (1.8)$$

b) Reaction with Marine Minerals

Another way in which oceans could take up more carbon dioxide is by reaction with the appropriate mineral phases, either in bottom sediments or suspended in the water column. Water containing dissolved carbon dioxide reacting with solid calcium carbonate producing calcium and bicarbonate ions, is an example how such a reaction could occur. This is, of course, the same reaction which takes place on land when water containing carbon dioxide reacts with calcium carbonate in the weathering of calcitic minerals, a reaction which provides some of the natural alkalinity of

seawater by inflow of $Ca^{2+}(aq)$, $HCO_3^-(aq)$ and $CO_3^{2-}(aq)$ from rivers.

1.5.4 The Terrestrial Biosphere and Atmospheric Carbon Dioxide

There is a possibility that land vegetation may also play a role in longer term changes in atmospheric carbon dioxide levels. There are two ways in which this could occur. Firstly, since plants abstract carbon dioxide from the air and convert it into fixed carbon in the process of photosynthesis, will increased levels of atmospheric carbon dioxide lead to an increase in photosynthetic fixation of carbon dioxide? Long term storage of this additional plant material in trees and soils could then constitute a valid sink for excess atmospheric carbon dioxide. In contrast, the second possibility is that the cutting of virgin forests and other changes to existing vegetation and soils may have created an additional source of atmospheric carbon dioxide. This would operate by the processes of respiration/decomposition and burning, mobilising carbon dioxide, formerly sequestered in the biosphere as fixed carbon. These two effects work in opposition with respect to their roles in altering levels of carbon dioxide in the atmosphere.

1.6 Climatic Consequences of Increased Carbon Dioxide Concentrations

1.6.1 The Greenhouse Effect

There is little doubt, that in the absence of other climatic perturbations, an increase in atmospheric carbon dioxide concentrations will give rise to globally averaged warming of the lower atmosphere. The degree of warming for a given increase in the carbon dioxide concentration is, however, difficult to predict. The warming, which is likely to vary geographically, could ultimately be larger than any rise in temperature experienced in the past 10,000 years. Associated with the warming are likely to be corresponding changes in the distribution of rainfall and the patterns of the atmospheric circulation.

Although the possibility of a carbon dioxide-induced climatic change was first

studied quantitatively by Callendar in 1938[41], much of the research on the likely magnitude of the change has been done in the last twenty years with the aid of numerical models of climate[42]. The direct effects on the Earth's radiation budget of larger carbon dioxide concentrations (the "greenhouse" effect) and the subsequent feedback processes triggered by the initial changes in the climate system must be modelled. However, even the most sophisticated models lack realistic representations of many of the physical and dynamic processes involved, and their simulations can, at present, only serve as a guide to the way in which the climate may change.

1.6.2 Clues from the Past

a) Warm World Scenarios Based on Historical Analogues

Numerical models of climate are unable to predict the likely regional variations in climate change induced by increasing carbon dioxide concentrations. In order to obtain an idea of the possible magnitude of such changes, several studies have been made on climatic data from periods when the climate was generally warmer than at present[43]. Since the causes of the previously warm periods may have been factors other than increased carbon dioxide, these results are indicators of the scale of change which could occur, not geographical predictions of future climatic change. However, it is possible that similar regional climatic changes could result from very different global climatic change mechanisms. Some tentative support for this view is found in the model of Manabe and Wetherald[42], which responds very similarly to two different climatic forcings:- one a doubling of carbon dioxide, the other an increase of 2 % in the solar constant[42].

b) Past Atmospheric Carbon Dioxide Concentration Deduced from Ice Cores

Reconstruction of the atmospheric carbon dioxide content in previous centuries can be determined by analysis of air trapped in natural ice. Relating past carbon dioxide levels to the then prevailing climate should provide valuable information on the interaction between carbon dioxide and climate, although cause and

effect relationships may be difficult to deduce.

An estimate of the atmospheric carbon dioxide concentration over the past 40,000 years, deduced by Neftel *et al* in 1982[44], from ice samples from Greenland and Antarctica is shown in Figure 1.6. This is in good agreement with that of Delmas *et al* [45], based on two different Antarctic cores. The minimum concentrations of about 200 ppmv coincide with the peak of the glaciation between 15,000 and 20,000 years ago, with an increase occurring during the climatic recovery towards the warm, hypsithermal period some 8000 years ago.

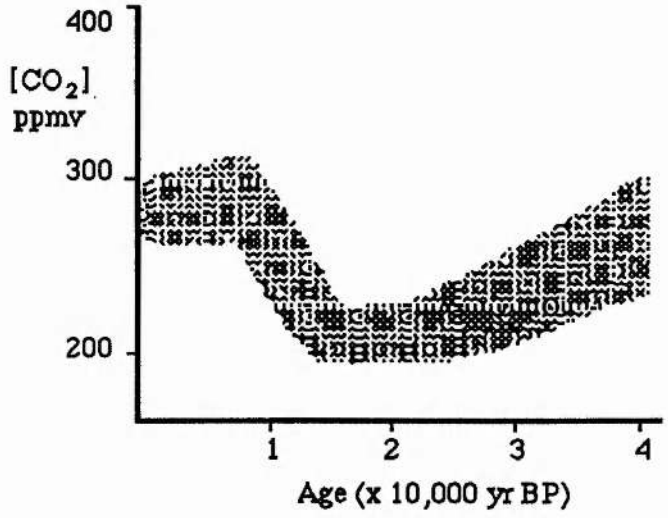

Figure 1.6

Range of Atmospheric CO_2 During the Past 40, 000 Years

Estimated from Ice Core Analysis.

Data from Neftel *et al* ; *Nature*, 1982, **295**, 220-223.

It is possible to ascribe the climatic warming to the increasing levels of carbon dioxide, but it is not clear if the carbon dioxide increase preceded or lagged behind the temperature change. The global mean temperature increase over this period is estimated to have been well over 2 K, which, on the basis of climate model results, is considerably more than would be expected from an increase in the carbon dioxide concentration of around 30-40 % suggested by ice core results. However the removal of a greater extent of ice could have led to a much stronger ice-albedo feedback than

would occur today, and consequently a larger warming for a given carbon dioxide increase could have resulted.

1.7. Implications of Increased Carbon Dioxide Levels on the Use of Energy in the Future

1.7.1 Introduction

Most studies[46] seem to indicate that a doubling of carbon dioxide concentrations in the atmosphere will lead to a mean temperature increase in the lower troposphere of 2-3°C. A man-made shift in climate of this magnitude would be significant since one would have to go back at least 10,000 years in order to find changes of this size occurring naturally. This leads to a number of important questions which concern industry, including:-

i) What would be the direct effect of such a climatic shift on energy demand?

ii) What is the timescale of the increase in atmospheric carbon dioxide?

iii) When will it be known with reasonable certainty if the Earth's surface is to experience a significant carbon dioxide-induced warming?

iv) Are there any technological solutions which might be used to reduce (or halt) the rate of atmospheric carbon dioxide increase?

v) What role should individual nations and their energy industries play in research into the carbon dioxide/climate issue nationally and internationally?

1.7.2 The Direct Effect of Climate Change on Energy Demand

The way in which a carbon dioxide-induced climatic change would influence energy demand would vary across the globe, due to the regional character of the climatic change and to the different patterns of energy use. In the following case the figures relate to the UK and assume mean global warming.

a) Electricity

The sensitivity of present electricity demand to temperature, averaged out over the whole year, is about 1 % per °C, *i.e.* if the temperature is 1°C lower than average

then the electricity demand increases by 1 %. Yearly averaging covers up seasonal variations in sensitivity which are greatest in spring and autumn (2 % per °C), very small in summer and almost the average in winter. So it would seem that even a 3°C warming of the climate would lead to less than a 5 % decrease in electricity demand, even assuming society does not adapt, *e.g.* installing air-conditioning.

b) Oil and Gas

The supply position of the UK oil and gas industry is more sensitive to the effect of temperature than the electricity industry. The temperature sensitivity of oil supplies in winter is between 4 % (fuel oil) and 5 % (gas oil) per °C temperature change. British Gas estimates a typical sensitivity of 4 % per °C.

The higher sensitivities of oil and gas compared with electricity is because the former is used for space heating more and so demand is more susceptible to outside temperature.

1.7.3 The Timescale of Atmospheric Carbon Dioxide Increase

In order to calculate the timescale of a future increase in atmospheric carbon dioxide, it is necessary to make several assumptions, all of which are questionable, so the following predictions are uncertain. It is assumed that the atmospheric carbon dioxide concentration was 339 ppm in 1982, and in future the mix of fossil fuel burned will be the same. Another uncertainty is the proportion of the carbon dioxide emitted remaining in the atmosphere.

Calculations using the above information indicate that, unless fossil fuel growth rates are significantly below 2 % per year, then sometime in the mid to latter part of the next century atmospheric carbon dioxide will stand at double its pre-industrial value. A shift away from fossil fuel to energy sources which are not carbon dioxide producers (*e.g.* nuclear and renewable) would allow a growth in energy output but with a lesser carbon dioxide penalty, *i.e.* the date at which carbon dioxide reaches a given level will be delayed.

1.7.4 When Will it be Certain that a Carbon Dioxide-Induced Climatic Change Will Occur?

Since there are many uncertainties in model predictions for the climatic impact of increased atmospheric carbon dioxide, the reality of the calculated temperature increase is unlikely to gain widespread acceptance until it is shown to be actually occurring.

A doubling of atmospheric carbon dioxide is predicted to produce a tropospheric temperature increase of 2-3°C which would be easily recognised. However, up to the present the carbon dioxide increase has only been 15-25 % for which the corresponding temperature rise is about 0.2-0.3°C. This is difficult to see against the natural variability of the climate. If the carbon dioxide-climate models are accurate, then sometime between now and a point in the next century, the atmospheric carbon dioxide level will double and so the warming will be apparent.

The conclusion is that by the turn of the century it should be possible, in principal, to verify or reject by observation the climate model predictions.

1.7.5 Technological Options for Reducing the Rate of Increase in Atmospheric Carbon Dioxide

Various possible measures exist which would allow energy production and use in the future with a lesser penalty in terms of carbon dioxide emission than has occurred in the past. Some of these options are:-

i) More efficient use of existing energy sources, *e.g.* decreasing fuel consumption of cars, better insulation of buildings *etc.*

ii) Change to fuels which produce low or zero amounts of carbon dioxide. All the renewable sources of energy (wind, waves, solar, hydro) are essentially carbon dioxide-free.

iii) Planting trees.

iv) Remove carbon dioxide from emissions coming from fixed sources.

Chapter One References

1. N. E. Dixon, C. Gazzola, R. L.Blakely and B. Zerner, *J. Am. Chem. Soc.*, 1975, **97**, 4131
2. J. B. Sumner, *J. Biol. Chem.*, 1926, **69**, 435
3. R. K. Thauer, G. Diekert and P. Schonheit, *Trends Biochem. Sci.*, 1980, **11**, 304
4. J. R. Lancaster Jr., *FEBS Lett.*, 1980, **115**, 285
5. R. Cammack, D. Patil, R. Aguirre and E. C. Hatchikian, *FEBS Lett.*, 1982, **142**, 289
6. S. P. J. Albracht, M. L. Kalkman and E. C. Slater, *Biochem. Biophys. Acta.*, 1983, **724**, 309
7. K. Schneider, D. S. Patil and R. Cammack, *Biochem. Biophys. Acta.*, 1983, **748**, 353
8. R. Cammack, V. M. Fernandez and K. Schneider, *Biochemie.*, 1986, **68**, 85
9. R. S. Wolfe, *Trends Biochem. Sci.*, 1985, **16**, 305
10. C. R. Woese, L. J. Magrum and G. E. Fox, *J. Mol. Evol.*, 1978, **11**, 245
11. F. Fischer, R. Lieske and K. Winzer, *Biochem. Z.*, 1935, **245**, 2
12. G. Fuchs, *FEMS Microbiol. Rev.*, 1986, **39**, 181
13. S. S. Hasnain and B. Piggott, *Biochem. Biophys. Res. Commun.*, 1983, **112**, 279
14. N. E. Dixon, P. W. Riddles, C. Gazzola, R.L. Blakeley and B. Zerner, *Can. J. Biochem.*, 1980, **58**, 1335
15. M. J. Kendrick, M. T. May, M. J. Plishka and K. D. Robinson, In "Metals in Biological Systems", p142-149, Ellis Horwood, Chichester, 1992
16. J. W. Van der Zwaan, S. P. J. Albracht, R. D. Fontijn and E. C. Slater, *FEBS Lett.*, 1985, **179**, 271
17. E. W. Findsen, K. Alston, J. A. Shelnutt and M. R. Ondria, J. *Am. Chem. Soc.*, 1986, **108**, 4009

18. (a) R. Cammack, D. S. Patil, E. C. Hatchikian and V. M. Fernandez, *Biochim. Biophys. Acta.*, 1987, **872**, 98

(b) J. W. Van der Zwaan, S. P. J. Albracht, R. D. Fontijn and Y. B. M. Roelofs, *Biochim. Biophys. Acta.*, 1986, **872**, 208

19. V. M. Fernandez, E. C. Hatchikian and R. Cammack, *Biochem. Biophys. Acta.*, 1985, **832**, 69

20. Y. M. Berlier, G. Fauque, P. A. Lespinat and J. LeGall, *FEBS Lett.*, 1982, **140**, 185

21. T. Lissolo, S. Pulvin and D. Thomas, *J. Biol. Chem.*, 1984, **259**, 11725

22. V. M. Fernandez, E. C. Hatchikian, D. S. Patil and R. Cammack, *Biochem. Biophys. Acta.*, 1986, **883**, 145

23. K. Schneider, H. G. Schlegel and K. Jochim, *Eur. J. Biochem.*, 1984, **138**, 533

24. R. P. Gunsalus and R. S. Wolfe, *FEMS Microbiol. Lett.*, 1978, **3**, 191

25. G. Diekert, B. Klee and R. K. Thauer, *Arch. Microbiol.*, 1980, **124**, 103

26. W. B. Whitman and R. S. Wolfe, *Biochem. Biophys. Res. Commun.* , 1980, **92**, 1196

27. A. Pfalz, B. Jaun, A. Fassler, A. Eschenmoser, R. Jaenchen, H. H. Gilles, G. Diekert and R. K. Thauer, *Helv. Chim. Acta.*, 1982, **65**, 828

28. (a) R. A. Scott, P. L. Hartzell, R. S. Wolfe, J. LeGall and S. P. Cramer, In "Frontiers in Bioinorganic Chemistry" (A. V. Xavier, ed.), p20 VCH Publ., Weinheim, FRG, 1985

(b) G. P. Diakun, B. Piggot, H. J. Tinto, D. A. Fuchs and R. K. Thauer, *Biochem. J.*, 1985, **232**, 281

29. S. P. J. Albracht, D. Ankel-fuchs, J. W. Van der Zwaan, R. D. Fontijn and R. K. Thauer, *Biochem. Biophys. Acta.*, 1986, **870**, 50

30. R. P. Hausinger, W. H. Orme-Johnson and C. Walsh, *Biochemistry*, 1984, **23**, 801

31. G. Diekert and R. K. Thauer, *J. Bacteriol*, 1978, **136**, 597

32. J. G. Zeikus, R. Kerby and J. A. Krzycki, *Science*, 1985, **227**, 1167

33. A. Hemming and K. H. Blotevogel, *Trends Biochem. Sci.*, 1985, **16**, 198

34. S. G. Ragsdale, J. E. Clark, L. G. Ljungadahl, L. L. Lundie and Drake, *J. Biol. Chem.*, 1983, **258**, 2364

35. S. W. Ragsdale, L. G. Ljungdahl and D. V. derVartanian, *Biochem. Biophys. Res. Commun.*, 1983, **115**, 658

36. S. W. Ragsdale, H. G. Wood, T. A. Morton, L. G. Ljungdahl and D. V. der Vartanian, In "The Bioinorganic Chemistry of Nickel", (J. R. Lancaster Jr., ed.) VCH Publ., Deerfield Beach, Florida, 1988

37. T. E. Thorpe, *Quaterly Journal of the Chem. Society of London*, 1867, **20**, 189-199

38. W. W. Kellogg, Climatic Change, (J. Gribbin, ed.), Cambridge Univ. Press, 1978, 205-227

39. C. D. Keeling, *Tellus*, 1973, **25**, 174-198

40. R. M. Rotty, *Tellus*, 1973, **25**, 508-517

41. G. S. Callendar, *Quaterly Journal of the Royal Meteorological Society*, 1958, **64**, 223-240

42. S. Manabe and R. T. Wetherald, *Journal of the Atmospheric Sciences*, 1980, **37**, 99-18

43. (a) W. W. Kellogg, *Effects of Human Activities on Global Climate*, WMO Tech Note No. 156, WMO No. 486, Geneva

(b) J. Williams, *Climatic Change*, 1980, **2**, 249-266

(c) T. M. L. Wigley, P. D. Jones and P. M. Kelly, *Nature*, 1980, **283**, 17-21

44. A. Neftel, H. Oeschger, J. Schwander, B. Stauffer and R. Zumbrunn, *Nature*, 1982, **295**, 220

45. R. J. Delmas, J-M. Ascencio and M. Legrand, *Nature*, 1980, **284**, 155-157

46. (a) T. M. L. Wigley, Uranium and Nuclear Energy, 1981, Butterworth, 291-322

(b) W. W. Kellogg and R. Schware, Climate Change and Society, Westview

Press, Boulder Colorado, 1981, 178 pp

Chapter Two

A Study of the Reduction of CO_2 by $[Ni(cyclam)]^{2+}$

2.0 Introduction

Since Fischer and Eisenberg[1] first discovered that macrocyclic complexes of nickel and cobalt electrocatalytically reduced carbon dioxide there has been a great deal of interest in this area. They reported that at least five tetraazamacrocyclic complexes (two cobalt and three nickel) catalytically reduced carbon dioxide to either carbon monoxide or a 2:1 mixture of carbon monoxide and hydrogen. The process was shown to be catalytic: when no complex was in the solution no carbon monoxide was detected by GC, even at potentials as low as -1.6 V versus SCE. Without carbon dioxide only hydrogen was detected as the product. A protic source is also needed for the catalysis to occur as when the complexes were electrolysed in dry DMSO in the presence of carbon dioxide no carbon monoxide was detected. The mechanism is unclear but a metal hydride is proposed as an intermediate. The reaction would then proceed via the direct attack of carbon dioxide on this metal hydride rather than co-ordination at the metal centre.

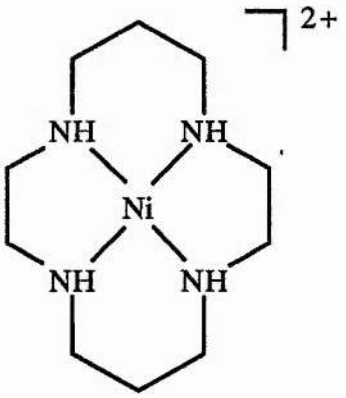

Figure 2.1

The structure of 1,4,8,11-tetra-azacyclotetradecane nickel(II), commonly called nickel cyclam.

Sauvage *et al* [2] reported an extremely selective electrocatalyst for the reduction of carbon dioxide to carbon monoxide (with very little hydrogen) even in pure water. This catalyst was 1,4,8,11-tetra-azacyclodecane nickel(II) chloride $[Ni(cyclam)]^{2+}$ (Figure 2.1). This process had a turnover frequency of 32 h^{-1} at -1.05 V[2] with the catalyst being quantitatively recycled. The Faradaic yields were almost quantitative which confirmed the high selectivity of the process considering the different concentrations in the solution; $[CO_2] < 0.1$ M and $[H_2O] \approx 55$ M. Cyclic voltammetry was used to determine whether catalysis was occurring. They found[2] that in water the reversibility of the couple was lost but there was an increase in the cathodic peak. In acetonitrile the reversibility was lost but there was no increase in the cathodic current. Also of note was that in dilute potassium nitrate the reversibility of the couple is lost under argon and so the $[Ni(cyclam)]^{2+}$ is also an electrocatalyst for the reduction of nitrate to ammonium ions. The reason why cyclam is such a selective catalyst is proposed to be due to the macrocyclic structure which makes the reduced complex resistant to decomplexation. Another factor is that the metal centre is readily accessible for reaction with carbon dioxide.

Sauvage *et al* [3] have proposed a mechanism based on a detailed study on the reaction of carbon dioxide with $[Ni(cyclam)]^{2+}$ (Figure 2.2). The initial step is the reduction of the Ni(II) complex, with the Ni(I) species being strongly adsorbed onto the mercury surface. The latter species could either interact with a proton to form a hydride or react with carbon dioxide. Formation of the hydride is unlikely since no hydrogen is detected in the reaction.

Since $[Ni(cyclam)]^{2+}$ was such an effective catalyst the obvious compound to examine as an electrocatalyst would be the bis$[Ni(cyclam)]^{4+}$ complex, which has two cyclam units joined up head to tail. This allows the possibility of coupling between two carbon dioxide molecules to form C_2 products which are useful starting materials. However, it was shown[4] that although the binuclear complex was an electrocatalyst for carbon dioxide reduction no coupling products were found. It was not as selective as the mononuclear complex but was found to be an effective catalyst for the reduction

of water.

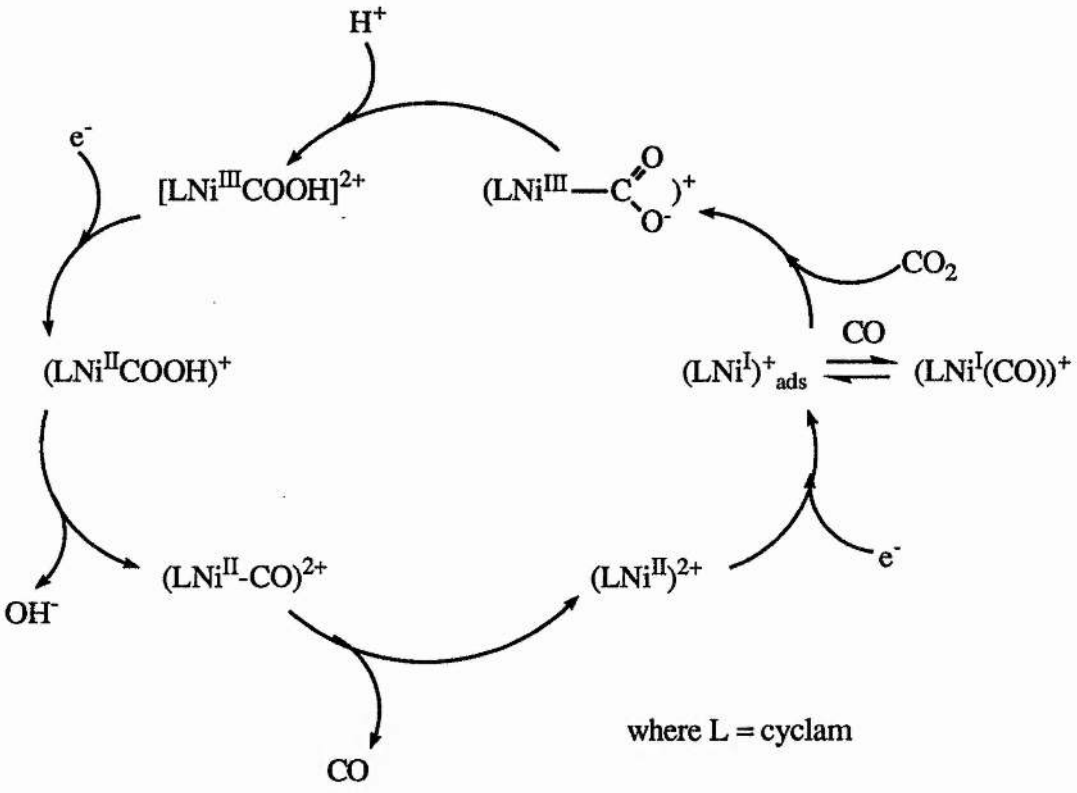

Figure 2.2

Proposed mechanistic cycle for the electrocatalytic reduction of CO_2 into CO by $Ni(cyclam)^{2+}$ in water.

The study of the mechanism for nickel cyclam has become an active area in recent years. Fujihira *et al* [5] used various electrochemical techniques to determine the mechanism. The main methods used were cyclic voltammetry, polarography and electrocapillarity in aqueous solutions with and without the catalyst and under nitrogen, carbon monoxide and carbon dioxide.

Under carbon monoxide a new peak appeared at -0.6 V which is assigned to the CO co-ordinating to the Ni(I)-cyclam generated in solution. Under carbon dioxide a large cathodic current is observed both on GC and Hg-Au electrodes although the current density is much lower on GC. An anodic peak is also observed at -0.7 V which is similar to that seen under carbon monoxide; this peak confirms the

assignment that carbon monoxide is the main product on both electrode surfaces.

A study of the dependence of the current density on the logarithmic concentration of Ni(II)-cyclam produces an adsorption isotherm-like plot. This behaviour is indicative of the adsorbed species on the electrode being the catalytic species, *i.e.* the adsorbed Ni(I)-cyclam rather than the Ni(I)-cyclam in the aqueous bulk.

Electrocapillarity experiments show that without the catalyst present there is no appreciable adsorption of carbon monoxide onto the mercury surface. However when the catalyst is present under nitrogen both the Ni(II) and Ni(I) cyclam complexes can adsorb onto the electrode. Under carbon monoxide the co-ordination of CO to the electrogenerated Ni(I)-cyclam in solution diminishes the amount of adsorbed catalyst. The $[LNi^{I}(CO)]$ does not adsorb onto the electrode so desorption of the catalyst occurs.

A polarography study[5] shows that the abrupt decrease in the catalytic current in the CV was not caused by depletion of the carbon dioxide but a decrease in the catalytic activity of the mercury surface with Ni(I)-cyclam$_{ad}$.

Fujihira has also been interested in the effect of N-alkylation of nickel cyclam on the catalysis[6]. The electrocatalytic reduction of carbon dioxide occurred by the electrocatalytic mechanism and not by the surface EC mechanism as previously believed[5]. The effect of alkylation was to reduce the cathodic current produced under carbon dioxide. The best of the alkylated complexes studied was the N-monomethylated complex due to the similarity of this complex with $[Ni(cyclam)]^{2+}$.

The behaviour of $[Ni(cyclam)]^{+}$ at mercury electrodes has been studied in great detail recently.[7] The complexes $[Ni(cyclam)]^{2+}$, $[Ni(cyclam)]^{+}$ are adsorbed onto the mercury surface at potentials negative of -0.6 V, confirming the work of Fujihira *et al*[5]. Double-potential chronocoulometric experiments, especially the reverse potential steps, reveal the presence in solution near the electrode of an activated form of the complex, $[Ni(cyclam^{*})]^{2+}$, which is generated by the oxidative desorption of $[Ni(cyclam)]^{+}_{ads}$. This form is more readily re-reduced to $[Ni(cyclam)]^{+}_{ads}$ than the

stable form obtained when the salt is dissolved. It is proposed that this complex has an unusual ligand conformation which only lasts for a few seconds. A strong interaction of the complex with the mercury surface is required in order for the reductive adsorption to proceed at potentials greater than -0.6 V, and presumably requires a ligand conformation which facilitates binding between the metal centre and the mercury surface. The reduction of Ni(II) to Ni(I) may encourage the binding by forcing the Ni(I) out of the plane to some extent. The adsorbed complex would bind carbon dioxide as a ligand, reaching almost octahedral co-ordination.

The studies are in basic agreement with those of Sauvage[3] although there are a few minor differences which are shown in Figure 2.3. The electrocatalyst is the adsorbed $[Ni(cyclam)]^+$ with the reconfigured ligand and forms the CO_2 adduct on the electrode surface which is then reduced to CO.

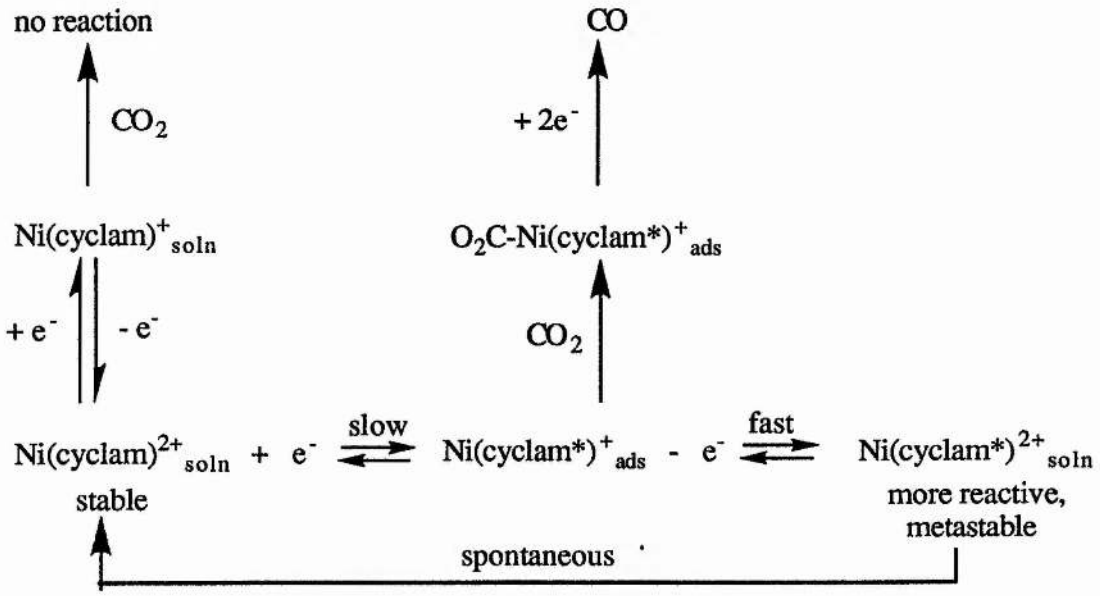

Figure 2.3

Reaction scheme showing the reductive adsorption of $[Ni(cyclam)]^{2+}$, the oxidative desorption of $[Ni(cyclam)]^+_{ads}$ and their possible connection with the catalytic reduction of CO_2 at mercury electrodes in solutions of $[Ni(cyclam)]^{2+}$.

It has been suggested[5] that the small anodic peak at -0.1 V was assigned to

$[Hg(cyclam)]^{2+}$ caused by the decomplexation of the nickel from the cyclam ligand. However recent work[7,8] has proved that the nickel does not decomplex under these conditions. Also the free cyclam has a characteristic wave[8] which is not observed in these cases.

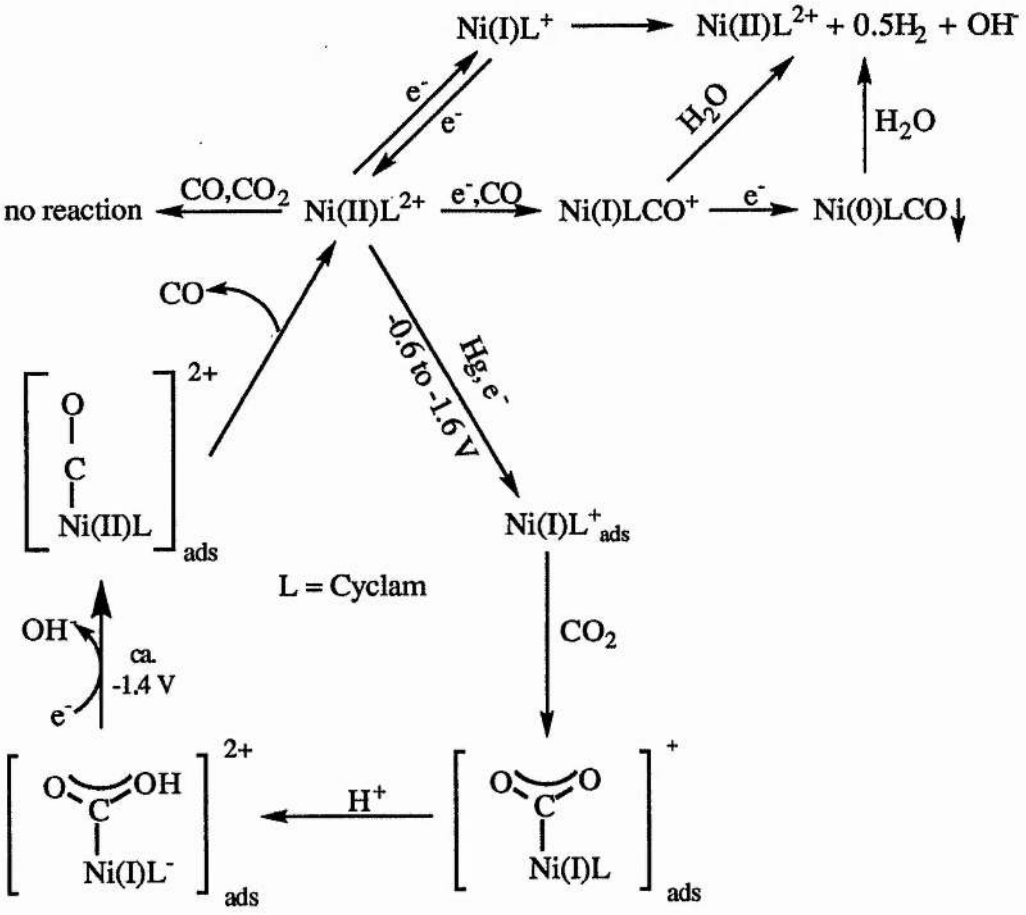

Figure 2.4

Reaction scheme summarising the electrochemical behaviour of $[Ni(cyclam)]^{2+/+/0}$ in the presence and absence of CO or CO_2.

Recent work[9] has concentrated on the mechanistic scheme and finding out how this catalysis occurs. This work is in agreement with previous studies[3,5] although there is no evidence of decomplexation. One main feature which occurs is the presence of an insoluble grey precipitate which is oxidised at -0.15 V. The precipitate leads to the passivation of the electrode surface which explains the sharp

decrease in the cathodic wave after CO_2 has been reduced. The Ni(0) complex can either interfere with the adsorption of the catalyst or the co-ordination of the CO_2 to the adsorbed catalyst. The scheme proposed is shown in Figure 2.4.

Theoretical calculations were undertaken to determine whether carbon dioxide could co-ordinate to the Ni(I) complex.[10] The complexes $Ni^{I}F(NH_3)_4(CO_2)$ (1), $[Ni^{I}(NH_3)_4(CO_2)]^+$ (2) and $[Ni^{II}F(NH_3)_4(CO_2)]^+$ (3) were investigated by the ab inito MO/SD-CI method. These complexes can be thought of as intermediates in the electrocatalytic reduction of carbon dioxide with Ni(cyclam)Cl_2 where $(NH_3)_4$ and F are models of cyclam and Cl. The CO_2 can form a stable η^1-CO_2 complex, with $Ni^{I}F(NH_3)_4$ but not with $[Ni^{I}(NH_3)_4]^+$ or $[Ni^{II}F(NH_3)_4]^+$. The F^- ligand pushes up the d_z2 orbital energy and neutralises the positive charge of Ni(I), allowing a strong $Ni \rightarrow CO_2$ charge transfer and stabilising CO_2 co-ordination. Also the charge neutralisation by F^- co-ordination decreases the charge-dipole repulsion between the distorted CO_2 and Ni(I). On the other hand, (2) does not have the F^- ligand, and (3) is a positively charged Ni(II) complex. As a result, (1) forms a stable η^1-CO_2 complex unlike (2) and (3). This greater charge transfer in (1) increases the negative charge on the oxygen atom which promotes protonation of the co-ordinated CO_2 as proposed in Sauvage's mechanism.[3]

Further studies[11] indicate that the binding energy of CO to the molecule $[Ni^{II}F(CO)(NH_3)_4]^+$ is very small (42 $kJmol^{-1}$). This implies that the CO molecule readily dissociates from the Ni^{II} centre and the catalytic cycle starts again. These results suggest possible improvement in the efficiency of the electrochemical reduction of carbon dioxide: 1) the presence of an anionic ligand such as Cl^- or an anode adsorbing metal complex to stabilise the η^1-CO_2 co-ordination; 2) use of a protic solvent to encourage protonation; and 3) the use of an appropriate buffer to prevent the OH^- by-product from suppressing protonation of co-ordinated CO_2.

A recent advance in the study of electrocatalysts for carbon dioxide is the development of Differential Electrochemical Mass Spectroscopy (DEMS).[12] In modern electrochemistry, in-situ spectroscopic analysis of intermediates and products

is a valuable tool for determining the course of an electrochemical reaction. The EMS technique (*i.e.* electrochemical mass spectroscopy which was developed initially by Bruckenstein *et al.*[13]) combines mass spectroscopy and electrochemical techniques. The technique involves a stationary gas permeable Au electrode sputtered onto a water repellent membrane in a rotational flow produced by a rotating rod.[14] This gives the same relation between the limiting diffusion current and the rotation speed as for the conventional rotating disc electrode (Equation 2.1). Indeed the equation

$$i_d = 0.422nFAc^*D^{2/3}\nu^{-1/6}\omega^{1/2} \qquad (2.1)$$

holds except for the numerical coefficient which was calculated to be 0.63 with respect to 1 mM $K_3[Fe(CN)_6]$. This technique has the advantage of being more sensitive than conventional GC methods to carbon monoxide present in minute amounts in another gas such as hydrogen.

Apart from $[Ni(cyclam)]^{2+}$ itself a variety of other catalysts have been reported to reduce carbon dioxide and have been the subject of recent reviews.[15] Several groups have explored the use of nickel,[16] cobalt,[17] rhenium,[18] ruthenium,[19] rhodium, iridium and osmium complexes[20] of bipy-type ligands in the electroreduction of carbon dioxide.

The complex $Re(bipy)(CO)_3Cl$ is used in the photochemical systems of carbon dioxide reduction for generating carbon monoxide in the presence of an organic electron donor.[18(a)] This complex yields carbon monoxide at -1.50 V vs SCE in 9:1 DMF/H_2O with a 98 % faradaic yield under certain conditions.

Other rhodium, ruthenium and iridium complexes have been proposed as catalysts for the electrochemical reduction of carbon dioxide to carbon monoxide or formate, in anhydrous acetonitrile and with $TBA^+PF_6^-$ as the supporting electrolyte.[20] Cyclic voltammetry under carbon dioxide showed that the current intensity increases in the potential range -1.20 V to -1.70 V vs SCE. Product analysis on the electrolysis of *cis*-$Rh(bipy)_2(CF_3SO_3)_2^+$ under carbon dioxide showed tri-n-butylamine and 1-

butene in addition to formate and hydrogen as the products. This indicates that the supporting electrolyte is partially consumed in the course of the reaction.

Phosphine complexes are used extensively in homogeneous catalysis (*e.g.* hydrogenation, hydroformylation and hydrosilylation of olefins) but have not been widely investigated for carbon dioxide reduction.

$Rh(diphos)_2Cl$ in anhydrous acetonitrile[21] at -1.55 V vs Ag wire produces formate with a faradaic yield of 22-42 % depending on the electrolysis time. Acetonitrile is the proton source necessary for the formation of formate, as small amounts of $CN\text{-}CH_2\text{-}COO^-$ have been detected.

Iron-sulphur complexes, $[Fe_4S_4(SR)_4]^{2-}$, have also been found to reduce carbon dioxide at -2.0 V vs SCE in DMF.[22] Formate was found as the favoured product over that of oxalate or carbon monoxide due to the tetranuclear cluster. As the potential applied is so negative the proton required in the reaction is provided by the tetraalkylammonium salt used as the supporting electrolyte. Mixed clusters (Mo-Fe-S or W-Fe-S) were also tested but under the electrolysis conditions applied (-2.0 V vs SCE) the cluster structures were rapidly destroyed.

As well as the electrochemical reduction of carbon dioxide there has been interest in the photochemical reduction of carbon dioxide.[23] In the catalytic reduction of carbon dioxide by a molecular species, the initial step is the reduction of the molecular catalyst prior to the electron transfer to the carbon dioxide. The above discussion concentrates on cases where the cathode is the electron source, the electron being either transferred at the interface between the electrode and the molecular catalyst in solution or being injected into a surface film containing the electrocatalyst. Another approach is to provide the electrons for the system via an intermediate photochemically generated reductant. The reducing species can be obtained either by direct adsorption of light leading to a strongly reducing excited state or by quenching of the excited state of a photoactive species by an electron donor, followed by formation of the reduced state of the catalyst.

Owing to its exceptional photoredox properties, the complex $Ru(bipy)_3^{2+}$ has

been widely employed in a large variety of systems related to light energy conversion to chemical[24] or electrochemical[25] energy. It has also been used for photochemically reducing carbon dioxide to carbon monoxide[26] or formate.[27] When $Ru(bipy)_3^{2+}$ is associated with a complex of cobalt(II) or $[Ni(cyclam)]^{2+}$ and an irreversibly consumed electron donor (tertiary amine) or ascorbic acid, carbon dioxide is converted to carbon monoxide and hydrogen under visible light irradiation.[17,28]

2.1 Cyclic Voltammetry

2.1.1 Introduction

Cyclic voltammetry and other potential sweep techniques have developed rapidly over the last couple of decades; equally important are the mathematical descriptions which allow kinetic parameters to be determined. Usually cyclic voltammetry (CV) is used when studying the system for the first time but there are better techniques for determining precise kinetic data.

The potential-time waveform used in sweep measurements is shown in Figure 2.5. The simplest of these is linear sweep voltammetry and involves sweeping the electrode potential between the limits E_1 and E_2 at a known sweep rate, ν, before stopping the potential sweep. A more useful technique is cyclic voltammetry. Here the waveform is the same initially but when the potential E_2 is reached the sweep is reversed. When the potential E_1 is again reached a variety of things can happen. The sweep can be stopped, reversed again or continued to another value E_3. In both these techniques the current is recorded as a function of the applied potential. Scan rates vary from a few mVs^{-1} to a few hundred Vs^{-1}. High values of scan rates however lead to complications. Double layer charging causes large background currents, $i_{dl} = \nu D_{dl}$ where C_{dl} is the double layer capacity. The higher currents produced at higher scan rates cause greater iR_u voltage drops tending to distortion of the response (R_u = uncompensated resistance). Recently microelectrodes have been used at fast scan rates to reduce charging currents and the effect of uncompensated resistance.

In a typical qualitative study, voltammograms are recorded over a wide range

of scan rates and for various values of E_1, E_2 and E_3. There will usually be several peaks and from the behaviour of these peaks as the potential limits and scan rates are changed and also the difference between the first and subsequent scans can determine how and what processes are occurring. Also from the dependence of the peak height on scan rate the role of adsorption, diffusion and coupled homogenous chemical reactions can be identified.

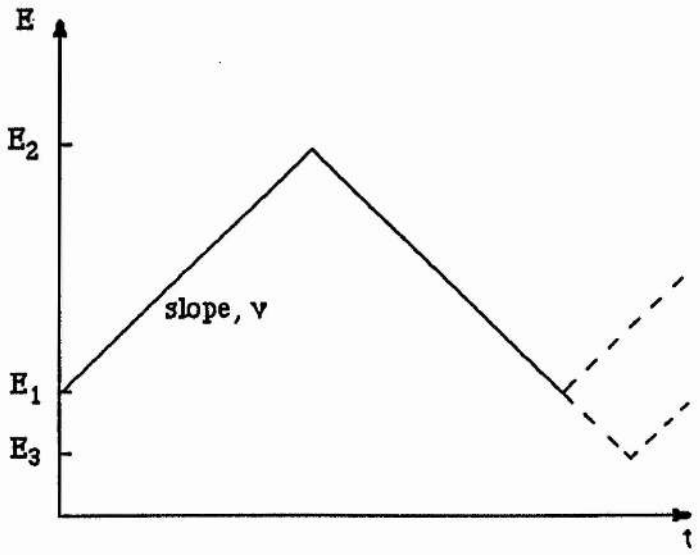

Figure 2.5

Potential-time profiles for sweep voltammetry.

2.1.2 Reversible Reactions

Consider a simple reversible reaction

$$O + ne^- \rightleftharpoons R \qquad (2.2)$$

where only O is initially present in solution. If a slow linear potential sweep is applied to such a system the voltammogram recorded will compare to a steady state I vs E curve. But as the scan rate is increased a peak of increasing height develops (as shown in Figure 2.6). The reason why this effect occurs is because of the concentration profile of O as a function of the potential.

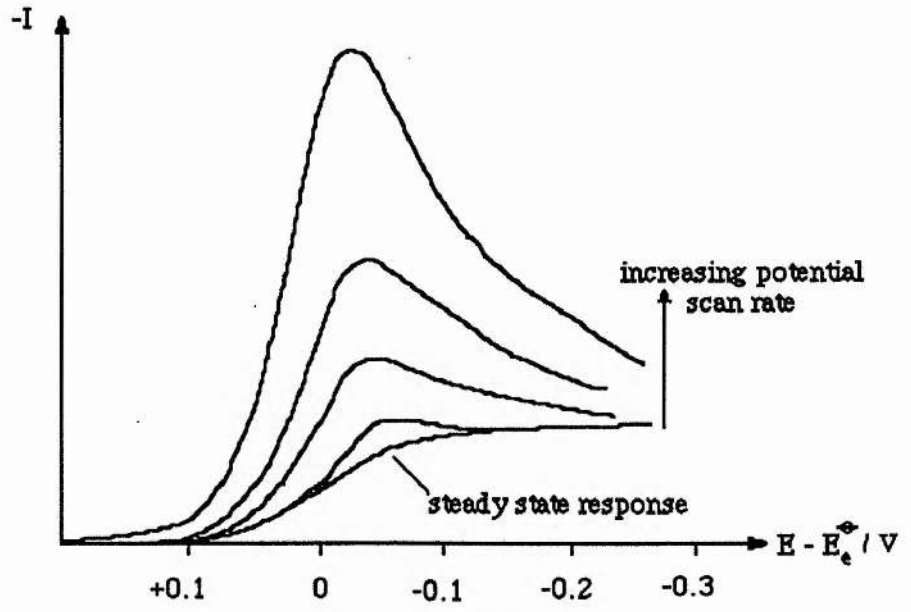

Figure 2.6

A series of linear sweep voltammograms for the reaction

$O + e^- \rightarrow R$, at several potential scan rates.

Under steady state conditions the concentrations above a certain distance from the electrode are maintained uniform by natural convection. The region next to the electrode (the Nernst diffusion layer) however has linear concentration gradients. The ratio of c_O^σ/c_R^σ is, for a reversible reaction, given by the Nernst equation,

$$E = E_e^\ominus + \frac{2.3RT}{nF} \log \frac{c_O^\sigma}{c_R^\sigma} \qquad (2.3)$$

and so as the potential goes more negative the surface concentration of the reactant must decrease. The concentration gradient increases and so the current increases. This continues until the surface concentration approaches zero and so the steady state concentration profile cannot change further and the current reaches a plateau. If the scan rate is increased there is insufficient time for the diffusion layer to return to the equilibrium state. The diffusion layer does not extend far into solution and the concentration profiles are as seen in Figure 2.7. As soon as a potential where O is

reduced is reached then the surface concentration of O decreases from the bulk value to satisfy the Nernst equation so a concentration gradient is set up (Figure 2.7 (a)). As a result a current which is proportional to the value of the gradient at the electrode flows in the external circuit. Once the gradient is set up it does not remain constant as

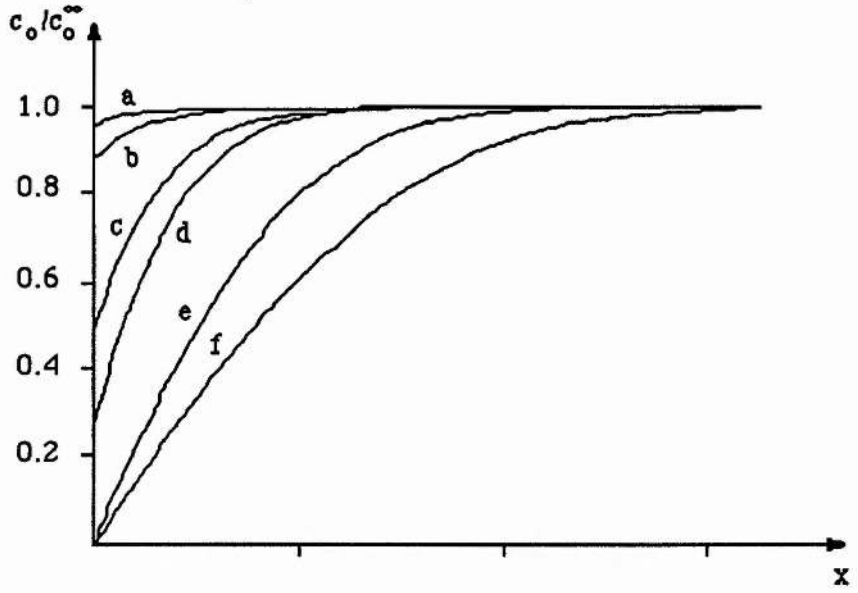

Figure 2.7

Concentration-distance profiles for the electroactive species, O, in the reaction $O + e^- \rightarrow R$ during a linear potential sweep experiment. The curves correspond to the potentials a) $E_e^\ominus$+90 mV, b) $E_e^\ominus$+50 mV, c) $E_e^\ominus$, d) $E_e^\ominus$ -28 mV, e) $E_e^\ominus$ -128 mV, f) $E_e^\ominus$ -280 mV.

diffusion causes it to decrease. The electrode potential is still changing and so the surface concentration of O is further decreased (b) and (c) until it reaches zero (d). At any given potential the concentration is greater than the steady state and so the current is larger. Once $(c_O)_{x=0}$ reaches zero the concentration gradient starts to decrease, due to the relaxation effect (e) and (f) and hence the current flowing must also decrease. The overall effect is the peak current-potential curve shown in Figure 2.6.

When the potential sweep is reversed the current follows the forward sweep for slow rates (pseudo steady state) but not for faster scan rates. Here when the sweep

is reversed there is a significant concentration of R at the electrode and R is still formed on the reverse sweep until the potential reaches $E_e^{\ominus}$. However, as the potential approaches $E_e^{\ominus}$ the R present near the electrode begins to be reoxidised back to O (for the surface concentrations to satisfy the Nernst equation) and a reverse current flows. Since the electrode potential is changing then the surface concentration of R eventually reaches zero. With similar arguments that are applied to the forward sweep, the current on the reverse sweep will also show a peaked response but of opposite sign. A typical cyclic voltammogram is shown in Figure 2.8. Of note is that the charge associated with the anodic process is low compared to the forward reduction process. The reason for this is that during most of the reaction there is a concentration difference driving R away from the electrode. Most of the product R diffuses into the bulk solution and cannot be reoxidised on the time scale of a cyclic voltammetry experiment.

It is possible to determine the exact form of the cyclic voltammogram mathematically by solution of Fick's second law with the appropriate initial and boundary conditions. The solution shows that the peak current density is proportional to the concentration of the electroactive species and also to the square root of the scan rate and diffusion coefficient.

Experimentally a plot of current versus potential for various scan rates is plotted and to test the reversibility of the system a plot of I_p as a function of $v^{1/2}$ is both linear and passes through the origin. If this is the case there are other tests to be applied:

1. $\Delta Ep = \Delta E_p^a - \Delta E_p^c = 59/n$ mV.
2. $|E_p - E_{p/2}| = 59/n$ mV.
3. $|I_p^a/I_p^c| = 1$.
4. $I_p \alpha v^{1/2}$.
5. E_p is independent of $v^{1/2}$.
6. at potentials beyond E_p, $I^{-2} \alpha t$.

If one or more of these conditions is not satisfied then the electron transfer is not

reversible on the time scale of the experiment and the process is more complicated than originally thought.

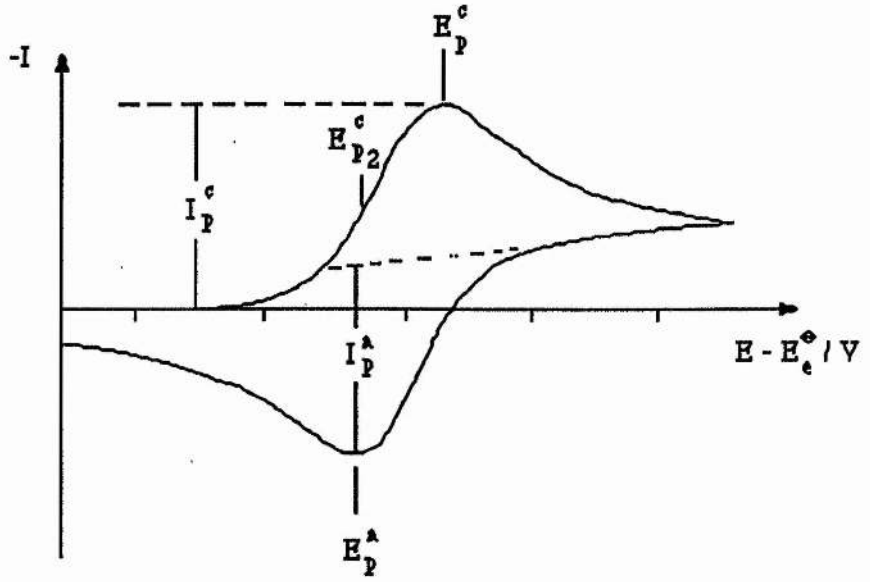

Figure 2.8

Cyclic voltammogram for a reversible process, $O + e^- \rightarrow R$.

Initially only O present in solution.

A reversible cyclic voltammogram can only be observed when both O and R are stable and the kinetics of electron transfer are fast, so that at all potentials and potential scan rates the electron transfer process on the surface is in equilibrium and so the surface concentrations follow the Nernst equation.

2.1.3 Irreversible Systems

In the case of the reversible system the rates of electron transfer at all potentials are greater than the rate of mass transport and so the Nernst equilibrium is maintained at the electrode surface. However when the rate of electron transfer is not fast enough to maintain this equilibrium then the shape of the cyclic voltammogram changes. At low potential scans the rate of electron transfer is greater than mass transport and a reversible cyclic voltammogram is recorded. As the scan rate is increased, however, the rate of mass transport increases and becomes comparable to

the rate of electron transfer. The most noticeable effect is to increase the peak separation. Also the peak current density is proportional to the concentration and the square root of the scan rate. The peak is smaller in comparison to a reversible one under the same conditions the reason for this is related to the shape of the peak. As the peak for the irreversible system is more drawn out, the surface concentration of O changes more slowly with potential, and at the instant when the surface concentration effectively reaches zero, the concentration profile for O is less steep and the flux to the surface lower.

The most notable feature of a cyclic voltammogram of a totally irreversible system is the total absence of the reverse peak. However this does not always mean that the process is an irreversible electron transfer. Other tests have to be applied to the system and these are:

1. no reverse peak.
2. $I_p^c \alpha \nu^{1/2}$.
3. E_p^c shifts $-30/\alpha_c n_\alpha$ mV for each decade increase in ν.
4. $|E_p - E_{p/2}| = 48/\alpha_c n_\alpha$ mV.

It is quite common for a process that is reversible at low scan rates to become irreversible at high scan rates after having passed through a region known as quasi-reversible at intermediate values. This transition from reversibility occurs when the relative rate of the electron transfer with that to mass transport is insufficient to maintain the Nernstian equilibrium at the electrode surface. In a quasi-reversible region both the forward and back reactions make a contribution to the observed current, and the region is generally recognised to have the following boundaries.

$$0.3\nu^{1/2} \geq k \geq 2\text{x}10^{-5}\nu^{1/2} \text{ cms}^{-1} \qquad (2.4)$$

This change from reversible, to quasi-reversible and finally irreversible behaviour can readily be seen from a plot of I_p as a function of $\nu^{1/2}$. The tests for a quasi-reversible system are:

1. $|I_p|$ increases with $\nu^{1/2}$ but is not proportional to it.

2. $|I_p^a/I_p^c| = 1$ provided $\alpha_c = \alpha_a = 0.5$.

3. ΔE_p is greater than 59/n mV and increases with increasing ν.

4. E_p^c shifts negatively with increasing ν.

2.1.4 Coupled Homogeneous Reactions

(a) The CE Mechanism

This mechanism can be represented in the following way:

$$Y \underset{K_{-1}}{\overset{K_1}{\rightleftharpoons}} O \qquad (2.5)$$

followed by

$$O + ne^- \rightleftharpoons R \qquad (2.2)$$

Typical examples of this system are the reduction of weak acids and the reduction of formaldehyde in aqueous solution, where it is present in both an electroactive form and an inactive hydrated form.

Consider the case where the electron transfer is reversible and where the chemical step is very slow, the current is therefore purely kinetically controlled and there are no peaks on the cyclic voltammogram. Instead a simple steady state type wave is obtained and the chemical rate constants are obtained from the limiting current form

$$i_L = -nFc_Y^{\infty}D^{1/2}K(k_1 + k_{-1}) \qquad (2.6)$$

provided the value of the equilibrium constant, K is known.

If the chemical reaction is very fast the cyclic voltammogram will be the same

as that for a simple diffusion controlled electron transfer. Under intermediate conditions the surface concentration of the reducible species O, and hence the current will be partially controlled by the kinetics of equation (2.5) and so the shape of the cyclic voltammogram, particularly the forward peak will be different from the reversible situation. The tests for this mechanism are:

1. $I_p^c/v^{1/2}$ decreases as v increases.

2. $|I_p^a/I_p^c|$ increases with v and is always ≥ unity.

(b) The EC Reaction

The EC scheme is a common mechanism in organic electrochemistry and is described in equations (2.2) and (2.7).

$$O + ne^- \rightleftharpoons R \qquad (2.2)$$

$$R \underset{K_{-1}}{\overset{K_1}{\rightleftharpoons}} Y \qquad (2.7)$$

The cyclic voltammogram obtained depends on the relative rates of the two steps. The simplest case is when electron transfer is totally reversible: the presence of the chemical reaction has no effect on the cyclic voltammogram obtained and so kinetic data can be derived for the chemical reaction. This situation gives the same properties as for an irreversible system. Similar properties also occur when the electron transfer step is relatively fast, if the rate constant for the chemical reaction is very large.

The effect of a following chemical reaction is greatest on the reverse sweep where R is reoxidised. If the chemical reaction is fast, R is rapidly removed from the region near the electrode. Then at low scan rates no reverse peak is observed but by decreasing the experimental time scale, *i.e.* increasing the scan rate, a reverse peak can become apparent. In the region where there is no reverse peak, known as the pure kinetic zone, it can be shown that the effect of the chemical reaction is to shift the

cathodic peak positive of the E_p^c value for the reversible electron transfer. This is because the coupled chemical reaction reduces the concentration of R at the surface from the value it would have had for a simple electron transfer reaction. The electrode reaction therefore has to work harder to maintain Nernstian equilibrium at the surface. However, the peak is shifted back 30/n mV (at 25°C) in a negative direction for each tenfold increase in v, provided the chemical reaction is first order in the intermediate produced at the electrode surface. Eventually as the scan rate is increased the reverse peak begins to appear and the rate of change of E_p with scan rate decreases. The ratio of the anodic and cathodic peaks increases with scan rate until reversible behaviour occurs. It is from the region where the reverse peak is obtained, but the ratio $|I_p^a/I_p^c|$ is less than one, that kinetic data can be obtained.

The diagnostic tests for this mechanism are:

1. $|I_p^a/I_p^c|$ is less than one but tends to unity as v is increased.
2. $I_p^c/v^{1/2}$ decreases slightly with increasing v.
3. E_p^c is positive of the value for the reversible case.
4. E_p^c shifts negatively with increasing n, and in the pure kinetic region shifts by 30/n mV per 10 fold increase in n (19/n mV for a second order reaction).

(c) The Catalytic Mechanism

This is a following chemical reaction mechanism where the reactant is regenerated chemically. The analysis under second order conditions is difficult and so it is usual to arrange that $c_x^\infty >> c_o^\infty$. The concentration of X is essentially unchanged throughout the experiment, and so the chemical reaction can be treated as pseudo first order.

$$O + ne^- \rightleftharpoons R \qquad (2.8)$$

$$R + X \xrightarrow{k} O + Y \qquad (2.9)$$

Under pseudo first order conditions, and where k is small or v large, the chemical reaction has no effect and so simple reversible behaviour is seen. For larger values of k, or as the value of n is decreased, more reactant R is generated and therefore $|I_p^c|$ values are higher than predicted by the Randles-Sevcik equation (equation (2.10)). The $|I_p^c/v^{1/2}|$ values decrease with decreasing scan rate and so the peak becomes less pronounced. In the limiting case the peak disappears altogether and is replaced by a scan rate independent plateau.

The current density of the plateau is given by

$$I_L = -nFc_o^{\infty}(Dkc_x^{\infty})^{1/2} \qquad (2.10)$$

and k values can readily be obtained from the experimental value of i_L and equation (2.10). In certain instances the plateau current is not easily measured so an alternative method is used which involves comparing the value of the ratio of peak currents in the presence and absence of X with tabulated data.

The general diagnostic tests for this mechanism are:

1. $|I_p^c|/v^{1/2}$ decreases with increasing v.
2. I_p^c may reach a limiting value at low scan rates.
3. $|I_p^c|$ values are greater than predicted by Randles-Sevcik equation.
4. $|I_p^a/I_p^c| << 1$.

This mechanism is usually easily identified as it is the only one in which the $|I_p^c/v^{1/2}|$ value increases so markedly on decreasing the scan rate.

(d) The ECE Mechanism

$$O + n_1e^- \rightleftharpoons R \qquad (2.11)$$

$$R \xrightarrow{k} O' \qquad (2.12)$$

$$O' + n_2e^- \rightleftharpoons R' \qquad (2.13)$$

This is another type of following reaction where the initial reaction product reacts chemically to yield a species O' which is further reduced. This scheme is common in the multi-electron transfer processes in organic electrochemistry.

The behaviour of an ECE system is best seen by plotting $|I_p^c/v^{1/2}|$ for peak I due to equation (2.11) on the first scan as a function of v. At low scan rates the mass transport is slow, and so a peak current corresponding to an irreversible two electron process is observed, but at high scan rates only the reversible one electron process is found. The value of k can be obtained by the analysis of the $|I_p^c/v^{1/2}|$ vs log n plots;

$$I_p^c/v^{1/2} = -\pi^{1/2}Fc_o^{\infty}(\frac{DnF}{RT})^{1/2}\{n_1\chi c_o^{\infty} + n_2\varphi c_o^{\infty}\} \qquad (2.14)$$

where χ and φ values are available in tabulated form as functions of (kRT/nFv). By curve fitting experimental $I_p^c/v^{1/2}$ data to equation (2.14) the value of k is determined.

The diagnostic tests for the ece mechanism are:

1. $I_p^c/v^{1/2}$ varies with scan rate but may reach limiting values at high and low scan rates.

$|I_p^c/v^{1/2}|$ (low v) > $|I_p^c/v^{1/2}|$ (high v)

2. $|I_p^a/I_p^c|$ increases with scan rate and tends to one at a high scan rate.

2.1.5 Surface Processes

The previous discussion has assumed that all the reactants and products are freely soluble in solution and that surface processes, such as phase formation and removal, and product or reactant adsorption do not need to be considered. If the peaks on a cyclic voltammogram are not similar to those discussed earlier then surface processes will be involved.

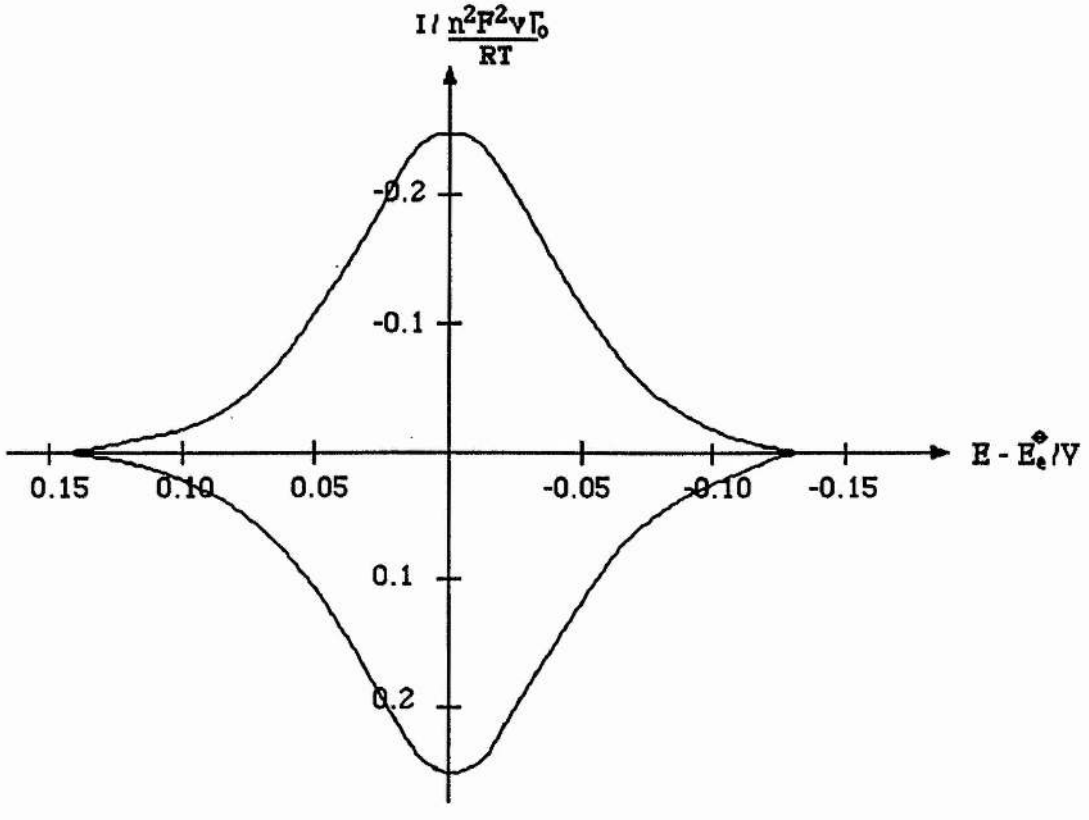

Figure 2.9

Theoretical cyclic voltammogram for the reduction of adsorbed O and reoxidation of the product where (a) the free energies of adsorption of O and R are equal and (b) adsorption follows a Langmuir isotherm.

(a) Adsorption

The simplest case involving adsorption is when only the adsorbed forms of O and R are electroactive in the potential range being investigated. The most common way for this situation to arise is that the reduction potential of adsorbed O is shifted to a potential well positive of that of the dissolved O. This system is reasonably straight forward so that the effects of mass transport are ignored. If the electron transfer is reversible then a cyclic voltammogram similar to that shown in Figure 2.9 will be obtained. The major differences when compared to a voltammogram for a reaction in which both reactant and product are in solution is that the peaks are sharp and symmetrical , the current rising from essentially zero to a peak value then falling again to zero, and there is little or no peak separation. Also the charges associated with

anodic and cathodic processes are equal. The symmetrical nature of the peak arises from the fixed amount of reactant - only O on the surface at the start of the scan can be reduced. The actual value of I_p, E_p and the peak width all depend on the type of adsorption isotherm involved and the relative strengths of adsorption of O and R. For the case where adsorption is described by a Langmuir isotherm it can be shown that $E_p^a = E_p^c$, and the peak current density is given by equation (2.15).

$$|I_p^c| = \frac{n^2F^2\Gamma_o}{4RT}\nu \qquad (2.15)$$

where Γ_o is the surface excess of O before the start of the scan, *i.e.* the peak current is proportional to the scan rate, ν, and not to the square root. The area under the cathodic peak, Q, corresponds to the charge associated with the reduction of the adsorbed layer of O and this enables the surface excess of O to be determined by equation (2.16).

$$\Gamma_o = |\frac{Q}{nF}| \qquad (2.16)$$

For non-Nernstian systems the shape of the cyclic voltammogram changes. For the irreversible case the forward peak stops being symmetric and there is no reverse peak. For a quasi-reversible system there is a reversible peak but both peaks are asymmetric and the peak potentials are not coincident.

A similar type of discussion can be applied to the system where the reactant has been attached to the electrode by chemical means. These electrodes, known as chemically modified electrodes have been the subject of recent attention for their possible use in catalysis. They have similar behaviour to the adsorption systems (as the number of reactant sites on the surface is fixed) and their cyclic voltammetric behaviour is analysed in a similar way.

The above discussion has assumed that only the adsorbed species are electroactive; the more general situation where both adsorbed and solution species are

electroactive is described by the following equations:

$$O_{soln} \rightleftharpoons O_{ads} \tag{2.17}$$

$$O + ne^- \rightleftharpoons R \tag{2.18}$$

$$R_{soln} \rightleftharpoons R_{ads} \tag{2.19}$$

Figure 2.10 (a) and (b) show voltammograms corresponding to strong reactant and strong product adsorption respectively for a process where the electron transfer is reversible. The symmetrically shaped peaks correspond to the reaction of the adsorbed species, whilst the conventionally shaped ones are due to the solution species. Strong reactant adsorption gives rise to a post-peak while strong product adsorption gives a pre-peak (an adsorbed reactant is stabilised with respect to the electrode reaction and therefore reacts less readily, whereas product adsorption favours reaction). The scan rate dependence of pre- or post-peaks and the solution peaks are rather different; whereas the former increases in height proportional to the scan rate the latter only increases with $\nu^{1/2}$. In addition, the concentration dependence of the two types are different, the solution peaks vary linearly with concentration while the adsorption peak will increase but reach a limiting value corresponding to complete surface coverage. A classic example of strong product adsorption is the reduction of protons at a platinum electrode.

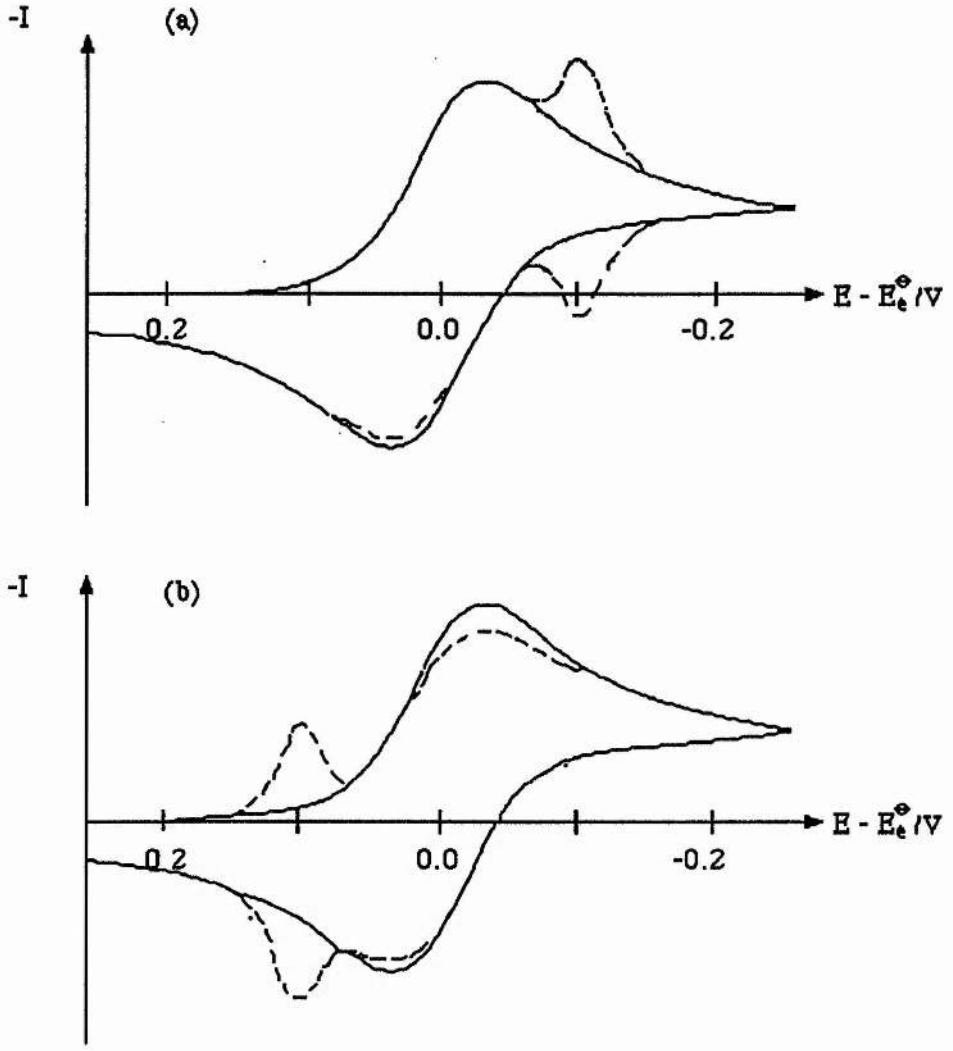

Figure 2.10

Theoretical cyclic voltammograms for the reduction of O when (a) O is strongly adsorbed, (b) R is strongly adsorbed. The dashed lines indicate the response with adsorption, and the solid line that for a simple reversible process without adsorption.

The separation between the adsorption and solution peaks is indicative of the relative strength of adsorption, and when the strength reduces the relative separation decreases. Hence for weakly adsorbed species the two peaks are not discernible and a distorted cyclic voltammogram (as shown in Figure 2.11) is obtained. In the case of weak reactant adsorption the forward peak will be higher than the simplest reversible system, and the reverse peak is also enhanced but not as much. For weak product adsorption the situation is reversed; the height of the forward peak hardly changes

from the reversible system although it shifts to positive potentials with increasing scan rate, whereas the reverse peak is significantly enhanced.

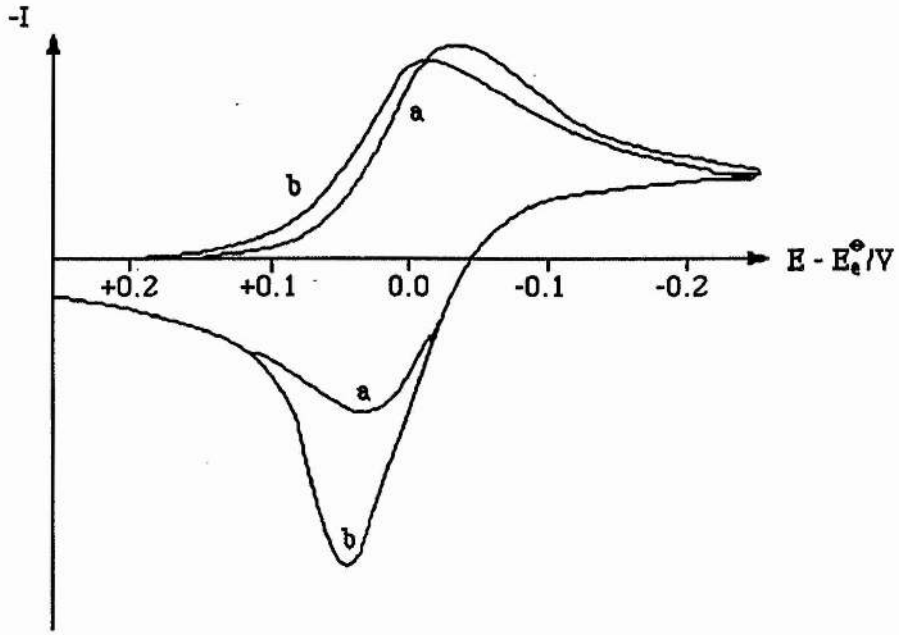

Figure 2.11

The effect of weak product adsorption is shown in curve (b). Curve (a) is again the response for a simple reversible system.

The behaviour of systems where the electron transfer is either irreversible or quasi-reversible is similar to the above and is discussed elsewhere.

(b) Deposition Processes

Figure 2.12 shows a typical cyclic voltammogram encountered in studies of deposition of metals, or other phases from dilute solutions onto a foreign substrate, *e.g.* Hg on carbon. The forward deposition peak is very similar to a process only involving a solution soluble species with the leading edge being slightly steeper. The major changes are on the reverse scan - the current crosses the forward scan, whilst the reverse peak is sharp and symmetrical. This feature is due to the reacting material being deposited on the electrode and so does not need to diffuse in order to react. It is therefore like an adsorbed species. The area under the reverse peak, a stripping peak,

corresponds to the amount of material deposited on the electrode.

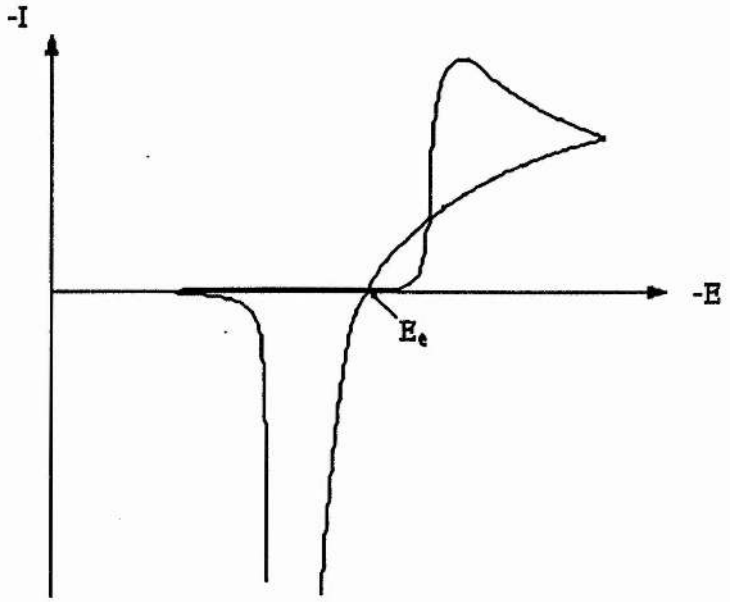

Figure 2.12

Schematic cyclic voltammogram for a metal deposition reaction exhibiting a nucleation overpotential.

The best way to explain the cross-over is to consider a specific example, Pb on carbon. Before the growth of lead on the carbon can occur there is formation of thermodynamically stable nuclei on the surface. The formation of such nuclei requires a more negative potential than that required to reduce the Pb^{2+} cations and leads to a nucleation overpotential, *i.e.* the potential has to be more negative to deposit Pb on carbon than on Pb itself. So on the forward scan a potential much more negative than the equilibrium potential for the Pb/Pb^{2+} couple in the test solution is needed for the deposition to occur. On the reverse scan, however, the deposition occurs at a lead surface and so continues until the equilibrium potential is reached. The second cross-over on the cyclic voltammogram is the equilibrium potential (for fast M/M^{n+} couples), and the difference in potential between this point and the potential where deposition begins on the forward scan is the nucleation overpotential. The nucleation potential on the first scan is greater than on the second and subsequent scans, also

different methods of surface preparation results in different values of overpotential.

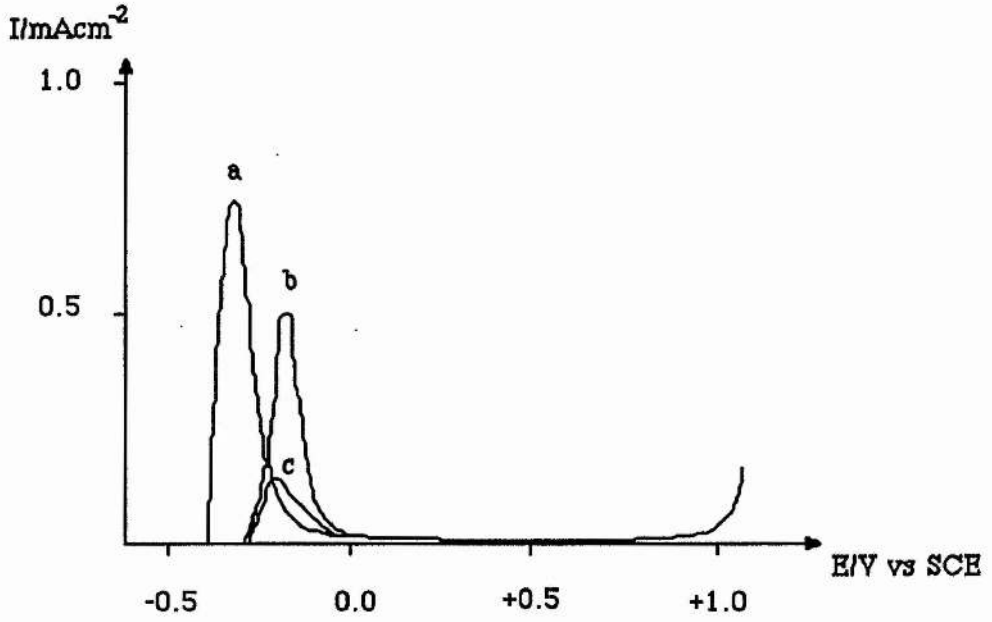

Figure 2.13

Linear potential sweeps for various steels in H_2SO_4 (2 mol dm^{-3}) at a scan rate of 3 mVs^{-1}. The steels are (a) 304, (b) 800, (c) 316 L.[29]

(c) Passivation

Passivating layers are particularly important since they are responsible for the stability of many metals and alloys in common use. An insoluble film of metal salt, or oxide, is formed on the electrode by a reaction such as equation (2.20)

$$M + X^- \longrightarrow MX + e^- \qquad (2.20)$$

and this layer protects the metal and prevents further dissolution. Figure 2.13 shows typical voltammograms for passivation. The current rises as the film grows on the surface then falls off rapidly as the surface passivates. Sometimes, depending on the chemical reversibility of the system, this layer may or may not be removed when the scan is reversed.

2.2 Electrochemistry of $[Ni(cyclam)]^{2+}$

2.2.1 The Electrochemistry of Nickel Cyclam in Various Solvents

A complete study of the mechanism for carbon dioxide reduction was undertaken but in order to find how this occurs the behaviour of the complex under argon has to be understood before the catalytic behaviour sets in. The best solvent for the catalysis on a particular electrode was investigated. Since it had been reported[3] that the catalysis occurred on mercury the systems looked at were a platinum and a hanging mercury drop working electrode (HMDE). The results obtained are summarised in Tables 2.1 and 2.2. With the platinum working electrode it is possible to observe both the Ni(II/I) and the Ni(III/II) redox couples in organic solvents, as shown in a typical CV (Figure 2.14). However, in a mixed solvent system (9:1 $MeCN/H_2O$) and in aqueous solutions the reduction wave is masked by hydrogen evolution. When carbon dioxide is bubbled into the solution the reversibility of the Ni(II/I) redox couple is lost but the current for the cathodic peak stays the same. There is no effect on the Ni(III/II) redox couple under carbon dioxide as the Ni(II) and Ni(III) have no part in the catalytic cycle as proposed by Sauvage and Anson[4,8,9] where Ni(I) is the active species.

			Reaction with CO_2		
Solvent	Ni(II/I) (V)	Ni(III/II) (V)	i_{pa}	Δi_{pc}	E_{pc}
MeCN	-1.45 (100)	+0.81 (60)	0	no change	-1.50 V
DMF	-1.43 (140)	+0.81 (60)	0	no change	-1.56 V
9:1 $MeCN/H_2O$	not seen	+0.74 (70)	-	-	-
water	not seen	+0.77 (180)	-	-	-

Table 2.1

The effect of various solvents on the electrochemistry of a 5 mM $[Ni(cyclam)]^{2+}$ solution using a Pt working electrode. The figures in brackets denote the peak separation in mV.

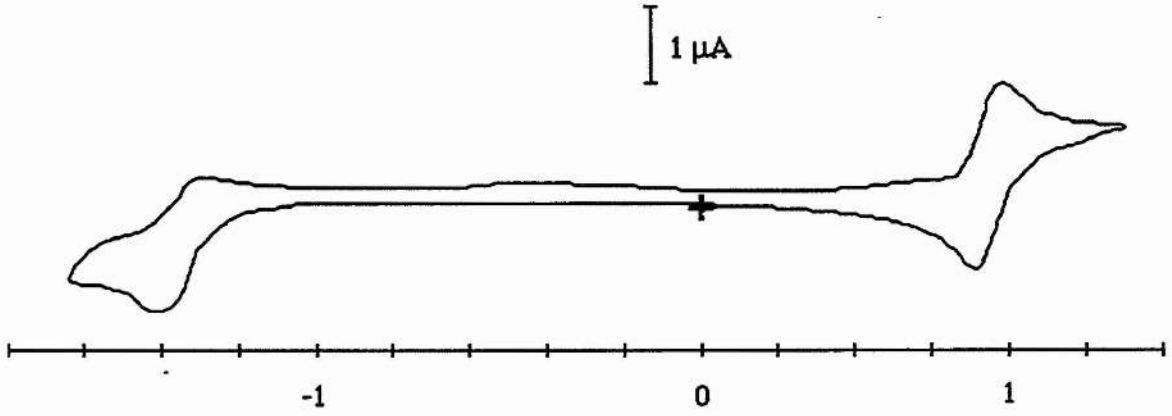

Figure 2.14

A typical cyclic voltammogram of $[Ni(cyclam)]^{2+}$ in MeCN + 0.1 M TBAT with a Pt/Pt/SCE electrode system.

The next step was to look at the different solvents using the HMDE. Here it is only possible to investigate the Ni(II/I) redox couple since the mercury oxidises above 0 V vs SCE. The Ni(II/I) is observed in all solvents although the peak separation varies and in most cases does not approach the ideal 59 mV value (see Section 2.1.2). The actual kinetics of the electron transfer in organic solvents is slow while in aqueous or mixed solvents the system is almost Nernstian. When carbon dioxide is bubbled into the solution there is a change in the behaviour of the Ni(II/I) redox couple. The current associated with the reduction increases and the reversibility is lost. The most obvious feature in the catalytic current is that the peak potential shifts to more positive potentials in protic solvents. This observation is supported by other work, and reflects the need for protons in the reduction. Although catalysis is observed in MeCN (an aprotic solvent), this is possibly due to trace amounts of water allowing a small amount of catalysis at a highly negative potential - quite close to that for carbon dioxide reduction at a bare mercury electrode. With a limiting amount of protons (in 9:1 MeCN/H_2O) then there is a higher current associated with the reduction and the potential shifts more positive. The best and lowest potential for carbon dioxide occurs in water, where the reduction occurs at -1.40 V, a potential lower than the reduction potential for the Ni(II/I).

		Reaction with CO_2		
Solvent	Ni(II/I) (V)	i_{pa}	Δi_{pc}	E_{pc}
MeCN	-1.46 (280)	0	98 μA	-2.15 V
DMF	-1.40 (i)		no catalysis	
9:1 MeCN/H_2O	-1.45 (100)	0	125 μA	-1.70 V
water	-1.56 (120)	0	200 μA	-1.40 V

Table 2.2

The effect of various solvents on the electrochemistry of a 5 mM $[Ni(cyclam)]^{2+}$ solution using a HMDE working electrode. The figures in brackets denote the peak separation in mV.

2.2.2 The Electrochemistry of Nickel Cyclam with Various Electrodes

The next stage in the investigation is to look at the electrode system and how the particular surface affects the catalysis. In acetonitrile there is no catalysis except on the mercury electrode (Table 2.3), and catalysis occurs at a high overpotential[30] (-2.15 V) which is almost the same value as that for the reduction of CO_2 to $CO_2^{\bullet-}$ at a bare mercury electrode with no catalysis (-2.21 V).

			Reaction with CO_2		
Electrode	Ni(II/I) (V)	Ni(III/II) (V)	i_{pa}	Δi_{pc}	E_{pc}
Pt	-1.45 (100)	+0.81 (60)	0	no change	-1.50 V
GC	-1.35 (180)	+1.13 (180)	0	no change	-1.40 V
HMDE	-1.46 (280)	-	0	98 μA	-2.15 V

Table 2.3

The effect of various electrodes on the electrochemistry of a 5 mM $[Ni(cyclam)]^{2+}$ solution in MeCN containing 0.1 M TBAT. The figures in brackets denote the peak separation in mV.

However in a mixed solvent system (9:1 MeCN/H_2O), see Table 2.4, then the catalyst has protons to aid the reduction. With platinum and glassy carbon working electrodes the redox couple for the Ni(III/II) oxidation is observed but the Ni(II/I) is only observed on GC under argon. On reaction with carbon dioxide there is no effect on the Ni(III/II) wave, but the reversibility of the Ni(II/I) is lost without any increase in the current of the cathodic peak. This indicates an EC rather than an EC catalytic reaction (Section 2.1.4).

The major difference occurs when the GC electrode is electroplated with a thin layer of mercury,[31] giving the complex a mercury surface to bind to. The Ni(II/I) redox couple is observed at -1.44 V (ΔEp = 80 mV) which is a typical Nernstian couple (Section 2.1.2). When this system reacts with carbon dioxide a large catalytic current of 270 μA is observed at -2.04 V. This is a higher current than for the

mercury (125 μA at -1.70 V) but the electrode has serious problems with surface corrosion and a subsequent loss of mercury overlayer, causing this value for the catalytic current to be irreproducible.

			Reaction with CO_2		
Electrode	Ni(II/I) (V)	Ni(III/II) (V)	i_{pa}	Δi_{pc}	E_{pc}
Pt	not seen	+0.74 (70)	0	no change	-
GC	-1.50 (100)	+0.78 (180)	0	no change	-1.55 V
GC/Hg	-1.44 (80)	-	0	270 μA	-2.04 V
HMDE	-1.45 (100)	-	0	125 μA	-1.70 V

Table 2.4

The effect of various electrodes on the electrochemistry of 5 mM $[Ni(cyclam)]^{2+}$ in an 9:1 $MeCN/H_2O$ solution containing 0.1 M TBAT. The figures in brackets denote the peak separation in mV.

			Reaction with CO_2		
Electrode	Ni(II/I) (V)	Ni(III/II) (V)	i_{pa}	Δi_{pc}	E_{pc}
Pt	not seen	+0.77 (180)		no effect	
GC	not seen	+0.76 (80)	0	260 μA	-1.52 V
GC/Hg	-1.33 (60)	-	0	240 μA	-1.38 V
Cu	not seen	-	0	400 μA	-1.40 V
Au/Hg	-1.54 (120)	-		no effect	
HMDE	-1.56 (120)	-	0	200 μA	-1.40 V

Table 2.5

The effect of various electrodes on the electrochemistry of $[Ni(cyclam)]^{2+}$ in an aqueous solution containing 0.1 M $NaClO_4$.

Another problem associated with the electrode is that with other known

catalysts the electrode did not show activity for the reduction of carbon dioxide so this electrode was rejected as a means of screening different macrocyclic complexes for catalytic activity.

In an entirely aqueous system (see Table 2.5) a platinum electrode does not show any reduction couple because of the hydrogen evolution process, although the nickel(II) oxidation is observed and is consistent with previous work.[32]

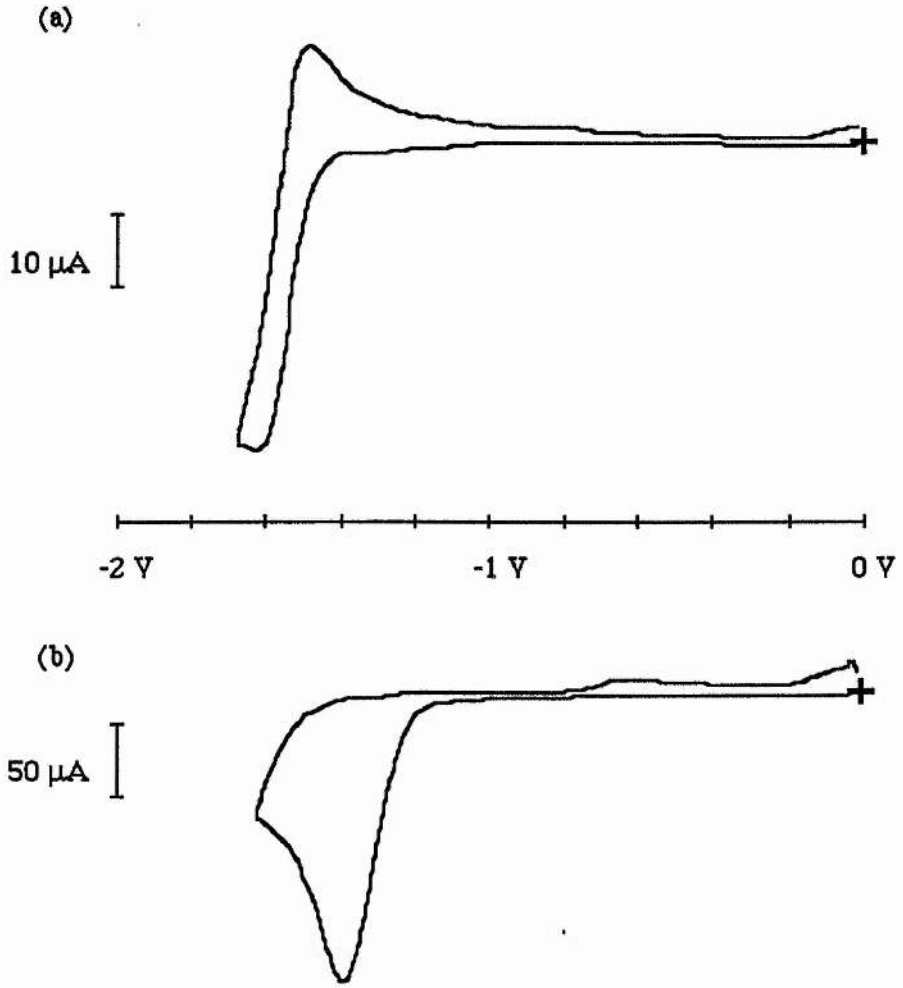

Figure 2.15

A typical cyclic voltammogram of $[Ni(cyclam)]^{2+}$ in water with an HMDE + 0.1 M $NaClO_4$ (a) under argon and (b) under carbon dioxide.

With the glassy carbon electrode similar behaviour is observed to that of platinum and carbon dioxide produced a catalytic current but tended to lose activity

very quickly. A copper electrode was also tried to observe the effect of carbon dioxide reduction on the surface. Under argon no redox couple for the Ni(II/I) reduction is seen because of the hydrogen evolution reaction. However, in the presence of carbon dioxide a catalytic current of 0.4 mA (area = 0.071 cm^2) is observed at -1.40 V. This is definitely due to the $[Ni(cyclam)]^{2+}$ because when the $[Ni(cyclam)]^{2+}$ is absent there is no current at the potential under investigation. The background current under argon is also negligible at this potential, this will be discussed later. The same Ni(II/I) reduction potential was observed using a GC/Hg film electrode but when carbon dioxide is allowed to react with the $[Ni(cyclam)]^{+}$ a current of 240 μA is observed at -1.38 V. This is a higher value than for the hanging mercury drop system (a typical cyclic voltammogram is shown in Figure 2.15) but not if the values of current densities are compared (0.197 compared to 14.388 $mAcm^{-2}$). Another electrode tested in the aqueous system was a gold electrode plated with mercury.[33] A Ni(II/I) wave was visible at this electrode but when carbon dioxide was allowed into the cell there was no change in the voltammogram.

Redox Mediator	Effect on CV under N_2	Effect on CV under CO_2
4,4'-bipyridyl	no $Ni^{II/I}$ redox couple	-1.04 V and -0.44 V
imidazole	no $Ni^{II/I}$ redox couple	no change
pyridine	no $Ni^{II/I}$ redox couple	no change
methyl viologen	-0.66 V (80) and -0.98 V (80) but no $Ni^{II/I}$ redox couple	no change

Table 2.6

The effect of redox mediators on $[Ni(cyclam)]^{2+}$ with a Au/Hg film electrode in an aqueous solution containing 0.1 M $NaClO_4$.

Since there appeared to be a problem with observing the Ni(II/I) redox couple in aqueous solution, the use of a redox mediator to aid the electron transfer from the

electrode to the Ni(II) centre was explored. Some common redox mediators are imidazole, 4,4'-bipyridyl and methyl viologen. The redox mediators should increase the reversibility of the nickel reduction couple. An Au/Hg electrode was used to present the nickel complex with a mercury surface to allow the catalysis to occur and also because on this electrode the effect of hydrogen evolution is greatest. The results are summarised in Table 2.6. The effect of adding the redox mediators has no effect on the CV under nitrogen. When carbon dioxide is bubbled through the solution in the main there is no effect on the CV. Only with 4,4'-bipyridyl do new peaks appear at -1.04 V and -0.44 V. However there is no catalytic current for the reduction of carbon dioxide.

To determine the nature of the peaks at -1.04 V and -0.44 V inorganic ions such as formate, carbonate, bicarbonate and oxalate were tested in the presence of $[Ni(cyclam)]^{2+}$ and the redox mediator. The results are summarised in Table 2.7. From the electrochemistry of nickel cyclam in the presence of the redox mediator 4,4'-bipyridyl it is possible to determine that the presence of the new peaks are due to formate in the solution. However it is impossible to assign the anodic peak present in the catalytic cycle (-0.15 V) under carbon dioxide. It has been proposed that this is the $[Ni(cyclam)]^{2+}$.CO complex losing carbon monoxide and rejoining the catalytic cycle.

Inorganic Ion Added	Redox Mediator	Effect on CV
Sodium Formate	4,4'-bipyridyl	-1.23 V (260) -0.58 V
Sodium Carbonate	4,4'-bipyridyl	-1.22 V (200) -1.12 V
Sodium Bicarbonate	4,4'-bipyridyl	-1.16 V (160)
Ammonium Oxalate	4,4'-bipyridyl	-1.11 V (140)

Table 2.7

The effect of inorganic ions on the electrochemistry of $[Ni(cyclam)]^{2+}$ with a Au/Hg film electrode in an aqueous solution containing the inorganic ion.

Since Ni(I) is proposed as an intermediate in the catalytic cycle of carbon dioxide reduction by nickel cyclam as shown in Figure 2.3, the environment of the Ni(I) was thought to be important. In order to test this theory simple nickel compounds were tested for activity towards carbon dioxide reduction. The results are summarised in Table 2.8. It is not possible to detect the Ni(II/I) redox couple and under carbon dioxide there is no sign of a catalytic wave. Since no catalytic wave is observed in the presence of carbon dioxide then the environment around the nickel centre is important. Given that the macrocycle is an important part of the catalyst, in a subsequent investigation we look into the effect of the macrocyclic structure on the catalytic cycle.

Complex	Solvent	Electrode	CV under N_2	CV under CO_2
$Ni(BF_4)_2$	pH 6 phosphate buffer	GC/Hg	no $Ni^{II/I}$ redox couple	increase in H_2 evolution
$Ni(ClO_4)_2$	water	GC/Hg	no $Ni^{II/I}$ redox couple	decrease in H_2 evolution
$Ni(ClO_4)_2$	water	HMDE	no $Ni^{II/I}$ redox couple	increase in H_2 evolution

Table 2.8

The effect of Ni(I) on the reduction of carbon dioxide.

2.2.3 The Effect of Concentration on the Catalysis of Carbon Dioxide

Since the cyclam does effect carbon dioxide reduction on a mercury electrode, the actual mechanism by which this catalysis occurs has to be investigated. The first step is to look at the effect of both the $[Ni(cyclam)]^{2+}$ catalyst and the carbon dioxide concentration on the catalysis.

A 25 ml solution of the $[Ni(cyclam)]^{2+}$ is treated with carbon dioxide and the catalytic current recorded (Table 2.9). A plot of catalytic current versus the nickel concentration in mM gives a logarithmic dependence. This is indicative of adsorption

[Ni] (mM)	log [Ni]	Catalytic Current (μA)	Voltage (V)
0.9997	-1.3×10^{-4}	145	-1.80
1.7730	0.2487	175	-1.50
3.2940	0.5177	210	-1.56
6.5872	0.8187	228	-1.46
8.234	0.9156	240	-1.44
10.036	1.002	255	-1.48

Table 2.9

Results of catalytic current as a function of nickel concentration in an aqueous solution containing 0.1 M $NaClO_4$.

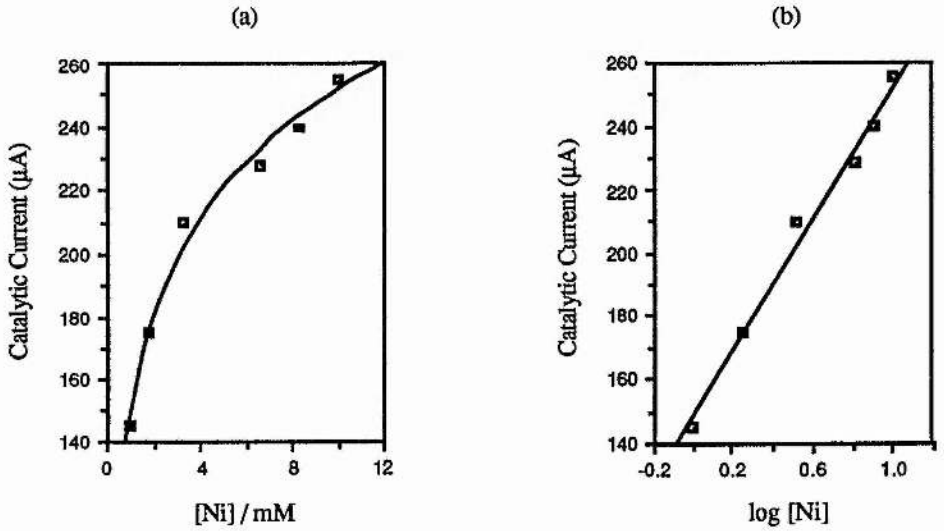

Figure 2.16

Plots of current versus concentration (a) [Ni] and (b) log [Ni].

of the complex onto the electrode. Surface sites are taken up by the complex so the catalytic current levels off. The graphs are shown in Figure 2.16 and show that there is clearly a linear dependence on log [Ni]. Another important fact of notice is that as the concentration of the complex increases the overpotential of the reduction decreases until a value closer to the thermodynamic potential of the reduction of carbon dioxide

to carbon monoxide is obtained, rather than the one electron reduction to the radical anion on a bare electrode.

The effect of bubbling time on the actual catalytic current was also investigated since bubbling for long periods of time gave higher currents. A standard 5 mM solution was treated with carbon dioxide and the current recorded as a function of time. The results are summarised in Table 2.10. As can be seen the catalytic current increases with time and the peak potential for the reduction of carbon dioxide decreases and hence the reduction becomes more favourable. However, the reduction potential does reach a limiting value with time which suggests an equilibrium situation where the reduction potential only reaches -1.40 V with this particular complex.

Time (minutes)	Catalytic Current (μA)	E_{pc} (V)
20	54	-1.50
40	92	-1.70
60	146	-1.48
80	210	-1.42
120	220	-1.44

Table 2.10

Results of catalytic current as a function of time in an aqueous solution of 5 mM $[Ni(cyclam)]^{2+}$ + 0.1 M $NaClO_4$.

As shown in Figure 2.17 the current tails off with time so in order to get an idea of how the different complexes behave with respect to $[Ni(cyclam)]^{2+}$ a standard time of 20 minutes is used to allow the carbon dioxide to react with the Ni^{I} electrogenerated in solution.

The next stage is to look into the effect of carbon dioxide concentration on the catalytic current. The same solution was used as in the previous set of concentration studies. Carbon dioxide was mixed with argon to give different ratios of carbon dioxide in the solution. The results are shown in Table 2.11.

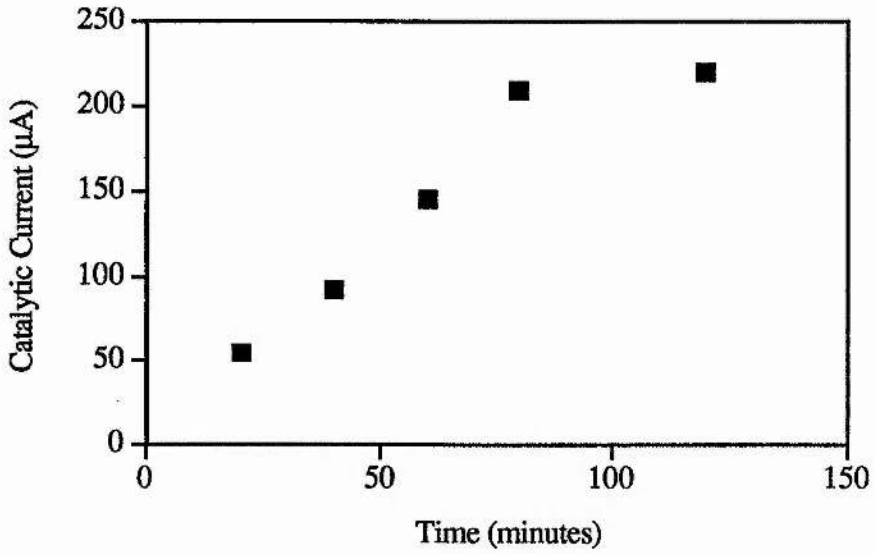

Figure 2.17

Plot of current as a function of time.

$[CO_2]$ /mM	Catalytic Current (μA)	$[CO_2]$ /mM	Catalytic Current (μA)
0.716	16	6.6	110
1.41	30.5	13.2	125
2.06	46	19.8	145
2.69	53	26.4	165
3.88	66	33	167

Table 2.11

Results of catalytic current as a function of carbon dioxide concentration.

If these results are plotted then a logarithmic relationship is obtained for $[CO_2]$ dependence (Figure 2.18).

This logarithmic dependence is also indicative of the adsorption of the carbon dioxide molecule onto the electrode. The carbon dioxide binds to the Ni(I) that has already adsorbed to the electrode as shown by the pre-wave at -1.30 V.

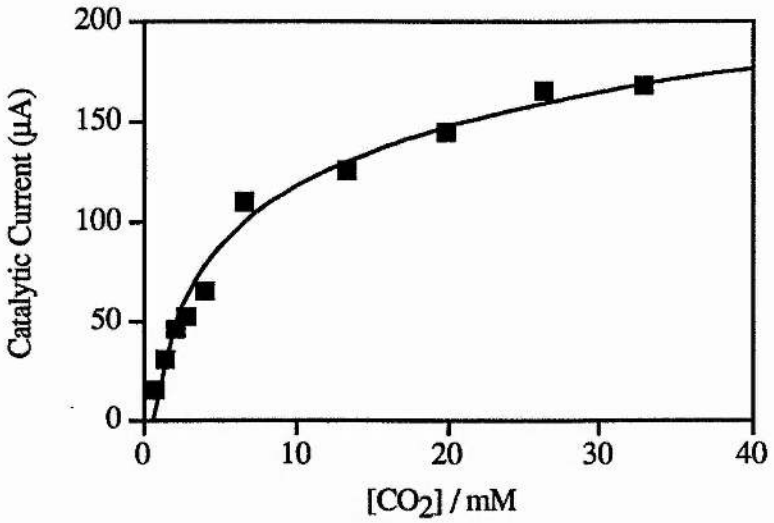

Figure 2.18

Plot of current as a function of carbon dioxide concentration.

2.2.4 The Effect of pH on the Catalysis of Carbon Dioxide

A preliminary investigation into the effect of pH on the catalytic current indicated that there was a dramatic variance as the pH changes. To test this particular aspect a 1 mM solution of nickel cyclam was made up to the pH as shown and each solution tested for catalytic behaviour. The results are summarised in Table 2.12 and the graph is shown in Figure 2.19.

Solution	pH	Catalytic Current (μA)
0.1 M $HClO_4$	1	none
buffer	4	190
0.1 M $NaClO_4$	7	200
buffer	9	185
0.1 M NaOH	13	38

Table 2.12

Results of catalytic current as a function of pH.

It is obvious that at low and high pH values the activity of the complex falls off. This effect is due to the protonation and deprotonation of the N-H groups in various pH solutions (the pK_a values for the ligand are 11.05, 10.31, and the next two are < 2)[34]. There is no effect of pH on the catalytic current in the normal pH range used when investigating the complex as the complex exists in the diprotonated form across the pH 4 -10 range. This means that the solution does not need to be buffered when testing for catalytic activity.

This pH investigation is in disagreement with that proposed by Sauvage[3] who obtained a linear dependence on pH in a similar range (4 - 9) although he also noted the drop in activity at extreme values.

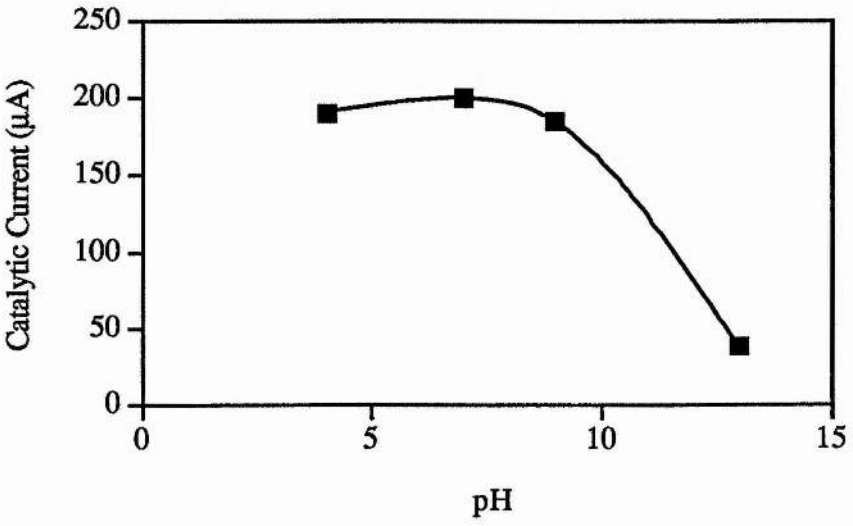

Figure 2.19

A plot of catalytic current as a function of pH.

2.2.5 The Effect of Magnesium Ions on the Catalytic Reduction of Carbon Dioxide

Mg^{2+} (a known Lewis acid catalyst) is thought to complex to the co-ordinated carbon dioxide and hence facilitate the reduction and cleavage of the carbon-oxygen bond.[35] The addition of magnesium perchlorate to 25 ml of a 5 mM solution of nickel(cyclam) perchlorate in water with 0.1 M sodium perchlorate as supporting

μL of Mg^{2+} Added	moles of Mg^{2+}/mol dm^{-3}	Current Produced Under CO_2
0	0	200
5	2.50×10^{-7}	240
10	5.00×10^{-7}	250
15	7.50×10^{-7}	265
20	1.00×10^{-6}	250
25	1.25×10^{-6}	290
30	1.50×10^{-6}	230
35	1.75×10^{-6}	225
40	2.00×10^{-6}	260
45	2.25×10^{-6}	360
50	2.5×10^{-6}	300

Table 2.13

The effect of Mg^{2+} ions on the catalytic current.

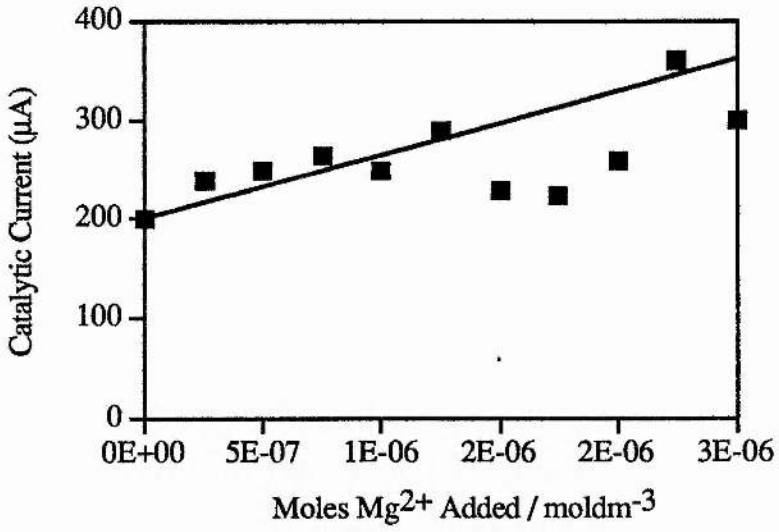

Figure 2.20

Plot of catalytic current as a function of moles of Mg^{2+} added.

electrolyte at room temperature under an atmosphere of pure carbon dioxide results in

an increase in the current from 200 μA to 500 μA.

This effect was investigated further by the controlled addition of the ions giving the results which are summarised in Table 2.13. A plot of the current produced against the moles of magnesium added is shown in Figure 2.20. This set of experiments suggest that the addition of Mg^{2+} has an initial positive effect on the catalysis, but further addition may interfere with the process. For a Hg drop size of 1.39 mm^2 only ~3 pmol of Mg^{2+} would be required to cover all of the catalytic sites, but presumably more is required since there is a dynamic equilibrium between Mg^{2+}(ads) and Mg^{2+}(soln). On reflection it may not be surprising that variable results are observed since the catalyst is confined to the surface and the negatively polarised mercury surface may directly interact with the Mg^{2+} ions in preference to the adsorbed nickel catalyst.

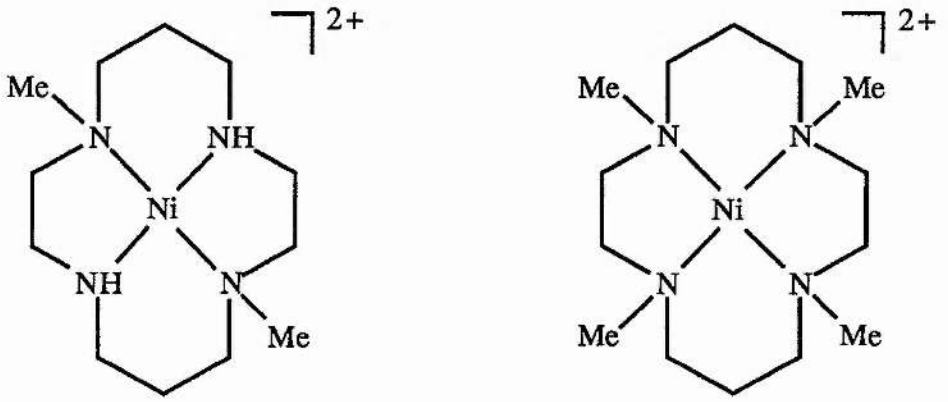

$[Ni(Me_2cyclam)]^{2+}$ $[Ni(Me_4cyclam)]^{2+}$

Figure 2.21

Structures of the N-alkylated cyclams.

2.3 The Effect of N-alkylation on Carbon Dioxide Reduction

Since a hydrogen-bonded complex is proposed as an intermediate in the catalytic cycle then to test this particular aspect different complexes with varying degrees of alkylation were tested for their catalytic activity. The complexes tested in addition to cyclam are shown in Figure 2.21 and the results are summarised in Table

2.14.

As the degree of N-alkylation is increased the value of the $E_{1/2}$'s for both the Ni(II/I) reduction and the Ni(II/III) oxidation tend to more positive values. To find a better catalyst we require a lower potential for the reduction of carbon dioxide as well as a large current. The alkylation of the nitrogen atoms satisfies the requirement for the redox potential but does not increase the current produced under carbon dioxide.

					Reaction with CO_2		
Complex	Solvent	Electrode	Ni(II/III)/V	Ni(II/I)/V	i_{pa}	i_{pc}	E_{pc}
[14]aneN_4	MeCN	Pt	+0.81 (60)	-1.45 (100)	-	-	-
	water	HMDE	-	-1.59 (180)	0	122 μA	-1.48 V
Me_2[14]aneN_4	MeCN	Pt	+0.88 (120)	-1.35 (60)	-	-	-
	water	Au/Hg	-	-1.33 (60)	-	-	-
	water	HMDE	-	-1.49 (180)	0	40 μA	-1.76 V
Me_4[14]aneN_4	MeCN	Pt	+1.62 (200)	-0.83 (140)	-	-	-
	water	HMDE	-	-1.03 (140)	0	70 μA	-1.54 V

Table 2.14

The effect of N-alkylation on catalytic activity.

As can be seen from the above table the alkylation of the nitrogen atoms reduces the catalytic current and the peak potential for the reduction tends to more negative values. This effect is due to the lack of hydrogen bonding that occurs when the carbon dioxide binds to the Ni(I) centre. This mechanism was first proposed by Sauvage and subsequent papers have agreed with this point.[3,7,9]

2.4 A Comparison of the Ring Size and the Effect on Carbon Dioxide Reduction

The nickel complexes of [n]aneN$_4$ macrocycles (n = 13 - 16, Figure 2.22) were tested for their catalytic activity towards carbon dioxide reduction and the results are summarised in Table 2.15. From the table it is clear that the $E_{1/2}$ for the Ni(III/II) process follows the order 13<14<15<16. This order relates to the energy of the redox orbital on the nickel ion. Consider the molecular orbital diagram (Figure 2.23) for a square planar d^8 metal ion, then as the ligand field increases the d_{z^2} energy increases so it is easier to remove an electron from the orbital. The ligand field interaction is largest for the smallest ring macrocycle because the nitrogen atoms are forced in closer to the metal, the so called "elastic band" effect.[36]

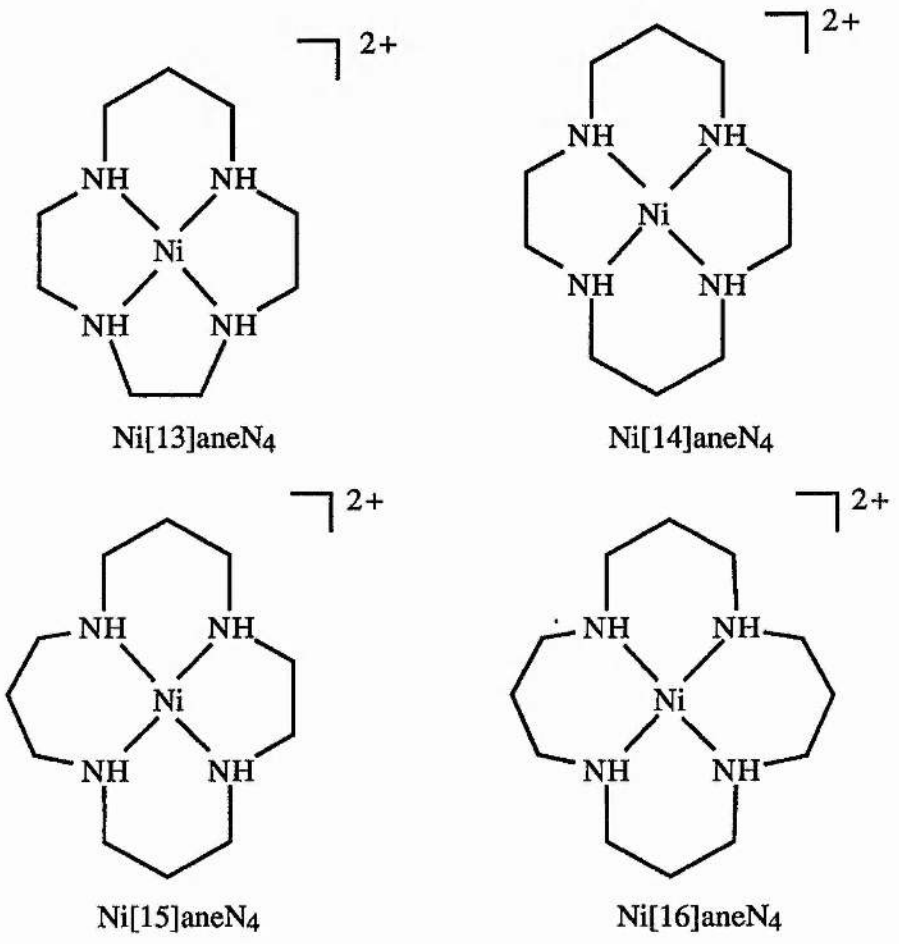

Figure 2.22

Structures of the $(Ni[n]aneN_4)^{2+}$ Macrocycles (n = 13-16).

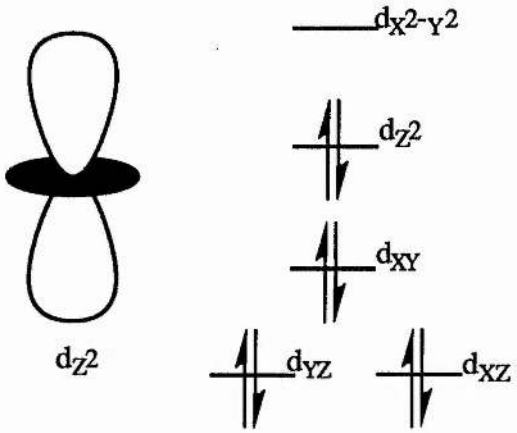

Figure 2.23

Molecular orbital diagram for a square-planar complex.

					Reaction with CO_2		
Complex	Solvent	Electrode	Ni(II/I) (V)	Ni(III/II) (V)	i_{pa}	i_{pc} (μA)	E_{pc} (V)
[13]	9:1	GC	not seen	+0.76 (120)		-	
	9:1	HMDE	-1.84 (i)	-	0	11	-1.6
[14]	MeCN	Pt	-1.45 (100)	+0.81 (60)		-	
	9:1	HMDE	-1.45 (100)	-	0	125	-1.7
	water	HMDE	-1.56 (120)	-	0	200	-1.4
[15]	MeCN	Pt	not seen	+1.23 (60)		-	
	MeCN	HMDE	-1.75 (140)	-		-	
	9:1	HMDE	-1.40 (160)	-	0	44	-1.7
[16]	MeCN	Pt	not seen	+1.47 (60)		-	
	9:1	HMDE	-1.44 (i)	-	0	41	-1.72

Table 2.15

Electrochemistry of Ni[n]aneN$_4$ Macrocycles for n = 13-16.

The figures in brackets denote the peak separation in mV.

It is a curious feature that the Ni(II/I) voltammetric waves for the [13]-, [15]-

and [16]aneN_4 complexes are only observed with the mercury electrode. No wave is observed when using solid electrodes (Au, GC, Pt) even in dry acetonitrile which is in disagreement with previous work[37] where waves were obtained in potassium nitrate solution. As the ring size increases we see a corresponding decrease in the redox potential. This is in agreement with previous work[32] which suggests that as you increase the ring size the reduction becomes easier, since the Ni(I) ion is larger and should fit more closely into the cavity. The exception to this trend is the (Ni[13]aneN_4)$^{2+}$ which has a higher redox potential than expected because of the size of the ring being an exact fit for the Ni(II) ion.

Comparing the catalytic activities of the various macrocycles by plotting the catalytic current against ring size (Figure 2.24) shows a maximum at a [14]-membered ring. It should be possible therefore to look at other series of macrocycles and see the same trend. For further investigation only [14]-membered complexes will be looked at, both for ease of synthesis and this effect on the catalytic activity.

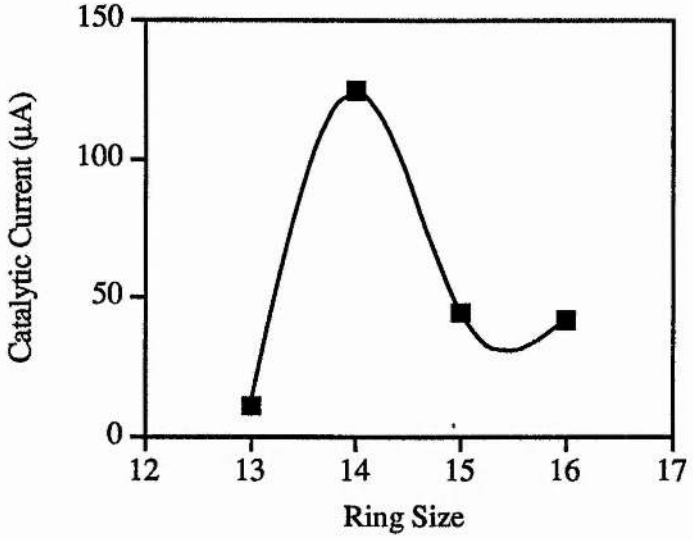

Figure 2.24

Plot of catalytic current as a function of ring size.

Under carbon dioxide all of the complexes show a pre-wave on the catalytic sweep (~-1.3 to -1.5 V) which corresponds to the complex being adsorbed onto the

electrode surface[3], or as other authors have recently suggested, to the reorientation of adsorbed complex.[7] In the experiment if the sweep is immediately reversed after the pre-wave is observed then the peak does not become reversible. The potential of the pre-wave corresponds to the redox potential of the Ni(II/I) reduction.

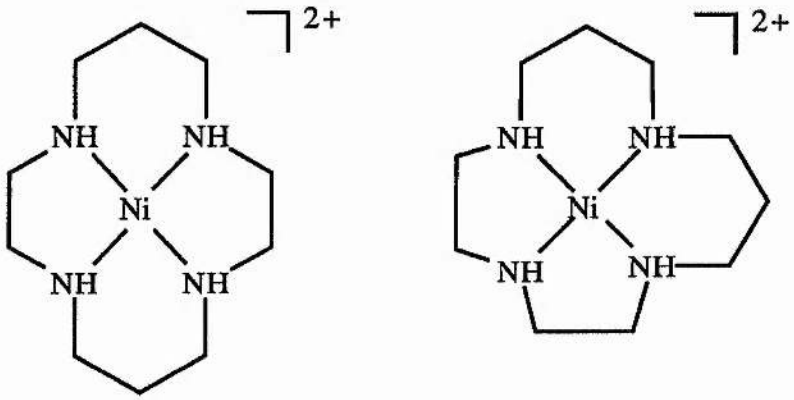

Figure 2.25

Structures of $[Ni(cyclam)]^{2+}$ and $[Ni(isocyclam)]^{2+}$.

2.5 Investigation of Isomers of $[Ni(cyclam)]^{2+}$ as Catalysts for Carbon Dioxide Reduction

The comparison of $[Ni(cyclam)]^{2+}$ with $[Ni(isocyclam)]^{2+}$ (structures shown in Figure 2.25) is the next important stage in the investigation. A 1 mM aqueous solution of the complex in 0.1 M $NaClO_4$ was used. $[Ni(isocyclam)]^{2+}$ shows a reversible one-electron redox couple at -1.45 V vs SCE whose peak current i_{pc} has a linear dependence on (scan rate)$^{1/2}$ (see Table 2.16). This value is close to that reported by Fabbrizzi *et al* [38] using MeCN as solvent (-1.628 V vs Ag/Ag^+). The more anodic potential that we have measured is clearly affected by the different solvent and reference electrode combination and may also be related to the CV being recorded in aqueous media in which the yellow planar form exists in greater concentration than the blue $[NiL(S)_2]^{2+}$ form. When carbon dioxide was bubbled through the solution for 20 minutes and then the CV recorded, an increase in the cathodic current (i_{pc}) from 2 μA to 26 μA was observed, accompanied by a shift in E_p^c

from -1.52 V to -1.32 V in comparison to that under argon. Although the current produced by $[Ni(isocyclam)]^{2+}$ is less than that of cyclam, $E_p^c(CO_2)$ is reduced by 160 mV. If carbon dioxide bubbles through the solution for a longer period of time then the current does not alter but the E_p^c is further shifted to -1.26 V.

The $[Ni(isocyclam)]^{2+}$ has a 5,5,6,6 chelate sequence of rings compared to the 5,6,5,6 sequence of $[Ni(cyclam)]^{2+}$. The changing of the chelate sequence, while not altering the cavity size, reduces the current produced under an carbon dioxide atmosphere but reduces E_p^c(cat). This changing of the chelate sequence alters the conformation of the nitrogen atoms and the stereochemistry of the N-hydrogen atoms. In general other catalysts reported and others we have studied in Chapter Six tend to have a lower current but the reduction occurs at more negative voltages.

			Reaction with CO_2		
Complex	Ni(III/II) (V)	Ni(II/I) (V)	i_{pa}	i_{pc}	E_{pc}
$[Ni(isocyclam)]^{2+}$	-1.45 (140)	+0.85 (100)	0	26 μA	-1.32 V
$[Ni(cyclam)]^{2+}$	-1.59 (180)	+0.81 (60)	0	122 μA	-1.48 V

Table 2.16

A comparison of $[Ni(cyclam)]^{2+}$ with $[Ni(isocyclam)]^{2+}$ in an aqueous solution containing 0.1 M $NaClO_4$. The Ni(II/I) recorded on an HMDE electrode and the Ni(III/II) recorded on a Pt electrode. The figures in brackets denote the peak separation in mV.

For low-spin nickel(II) tetramine complexes the energy of the *d-d* band is a measure of the energy of the equatorial Ni-N interactions. The λ_{max} for the planar $[Ni(isocyclam)]^{2+}$ (466 nm, 21,460 cm^{-1}) occurs at 1000 cm^{-1} lower in frequency than for $[Ni(cyclam)]^{2+}$ (22,470 cm^{-1}), establishing that the asymmetric macrocycle exerts weaker metal donor atom interactions than its more symmetrical isomer.[39] This weaker interaction enables the reduction to proceed at more positive potentials.

2.6 Investigation of the Conformations of Nickel Cyclam as Catalysts for Carbon Dioxide Reduction

Cyclam can exist as various conformations[40] with different configurations of the N-H bond, ranging from the four methyl groups pointing upwards from the ring as found in tetramethylcyclam complexes, to the two-up-two-down hydrogen atom conformation found in the *trans* cyclam complexes. The structure of these complexes are shown in Figure 2.26, since it has been reported both by Sauvage and Fujihira[3,6]

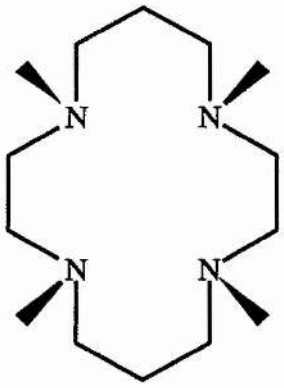

RSRS I
Found in TMC complexes

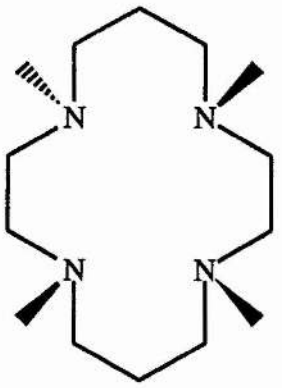

RSSS II

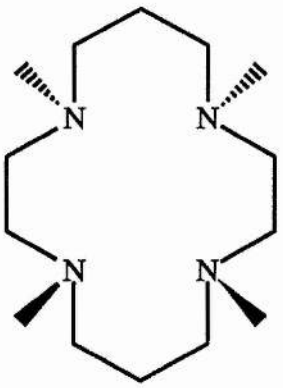

RSSR III
Stable *trans* -complexes (non labile)

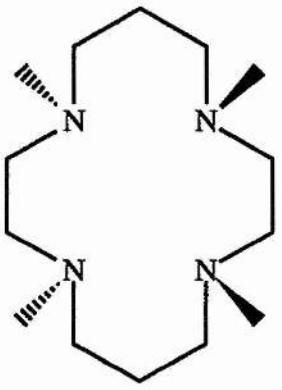

RRSS IV

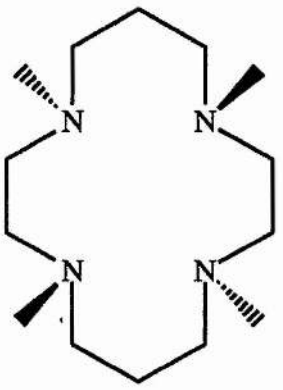

RRRR (SSSS) V
Found in folded *cis*-complexes and labile *trans* -complexes

Figure 2.26

Conformations of [14]aneN_4 Macrocycles.

that the conformation of the N-H bond is important because it interacts with the carbon dioxide molecule to stabilise the formation of the intermediate Ni^{I}-CO_2 complex. To test this theory we looked at the conformations I, III and V. The conformation I (RSRS) has the four nitrogens lying above the plane of the cyclam ring and is found in $[Ni(TMC)]^{2+}$. The conformation III is found in $[Ni(cyclam)]^{2+}$ prepared in the normal way by reacting nickel perchlorate with 1,4,8,11-tetraazacyclodecane. This complex has an RSSR conformation of nitrogens and is the stable form found in extremely stable complexes. The conformation V is found in folded *cis* complexes and in labile *trans* complexes. The *cis* -cyclam is converted into the square planar RRRR form by dissolving up the complex in 0.1 M perchloric acid and leaving for several days. The reaction proceeds as shown in Figure 2.27. The *trans* V isomer is stable in pH 1-4 but in higher pH solutions the conformation converts into the more stable RSSR form.[41] This conversion is rapid but it is possible to observe the electrochemistry of both complexes at an intermediate pH before the conversion is complete.

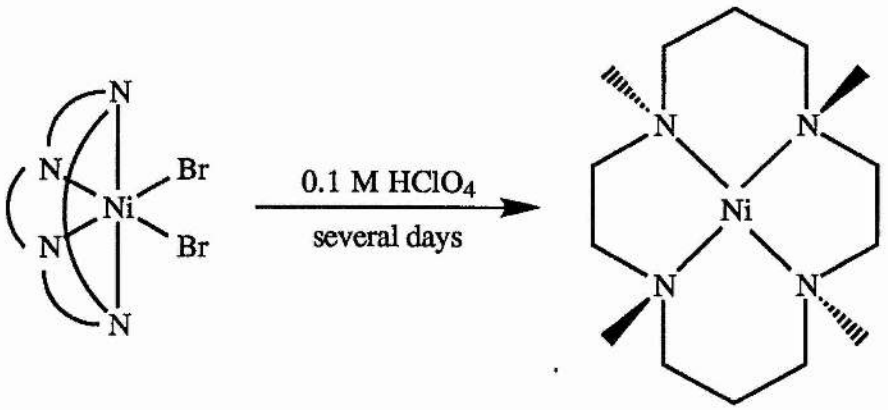

cis -cyclam Br_2
blue

square planar
yellow

Figure 2.27

Conversion of the *cis* -cyclam to the square planar form.

Anson *et al* [7] reported that the adsorption of $[Ni(cyclam)]^{2+}$ occurred at potentials more positive than the redox potential of the isomer in solution and also that

the desorption occurred with a change in the conformation of the complex. This reaction was supposed to occur rapidly on the time scale of an electrochemical experiment. Investigations were carried out on an easily accessible isomer of the trans V in order to determine whether this isomerization occurred.

The complexes investigated in addition to the usual, trans-III cyclam were $[Ni(TMC)]^{2+}$ and the RRRR trans-V conformation of $[Ni(cyclam)]^{2+}$ made by the reaction scheme shown in Figure 2.27. The trans-V isomer was run in 0.1 M $HClO_4$ with a platinum electrode to determine the redox potential of the conformer before testing the catalytic behaviour. The results are shown in Table 2.17. The redox potential of the trans-V isomer is shifted more positive than the trans-III by 200 mV. This shift is caused by a lower crystal field stabilisation energy (CFSE) than for the trans-III conformation which is the thermodynamically stable isomer. The complex does not catalyse carbon dioxide reduction in acidic conditions so the pH of the solution was increased to ca pH 4.5 by the addition of NaOH. At this pH the peak is still not well defined with only an irreversible wave at -1.50 V (since the complex is

			Reaction with CO_2		
Conformation	Ni(II/I) (V)	Ni(III/II) (V)	i_{pa}	Δi_{pc}	E_{pc}
trans-III	-1.56 (120)	+0.74 (70)	0	200 μA	-1.40 V
trans-V	-1.20 (160)	+0.92 (80)	-	-	-
I (RSRS) $[Ni(TMC)]^{2+}$	-1.03 (140)	+1.62 (200)	0	70 μA	-1.54 V
cis-cyclam-Br_2	-1.48 (480)		-	-	-

Table 2.17

A comparison of the behaviour of different conformations of $[Ni(cyclam)]^{2+}$.

The figures in brackets denote the peak separation in mV.

undergoing isomerization at this pH the peaks are indistinguishable). However, when carbon dioxide is bubbled into the solution there is a catalytic current of 82 μA at

-1.50 V with a pre-wave at -1.32 V. When the pH is further increased to 12 two waves are observed at -1.2 V (ΔEp = 160 mV) and -1.63 V (ΔEp = 140 mV), the first wave is due to the RRRR conformer while the second wave is the RSSR conformer

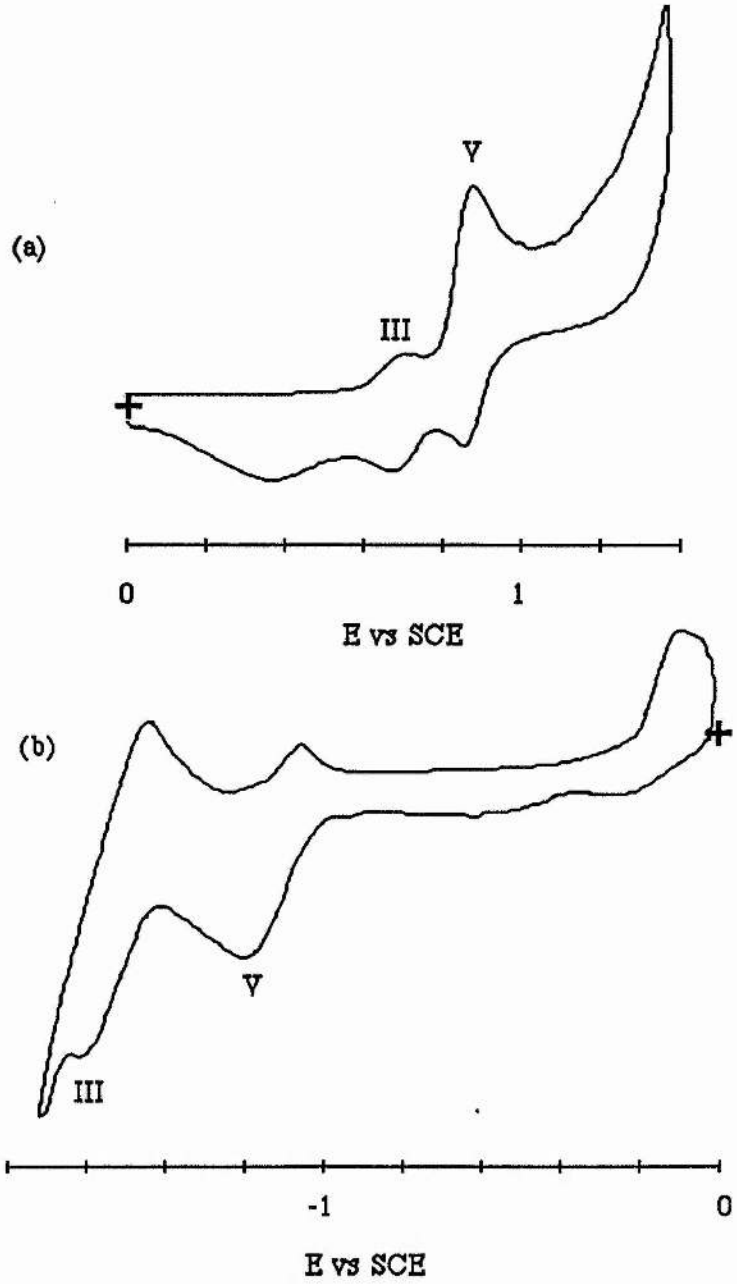

Figure 2.28

A typical cyclic voltammogram of RRRR cyclam with the RSSR also present with (a) Pt and (b) an HMDE working electrode system in pH 12 solution

(see Figure 2.28). When carbon dioxide is bubbled into the solution a current of 38 μA is observed at -1.4 V. When argon is allowed back into the cell only the peak at -1.63 V indicative of the $[Ni(cyclam)]^{2+}$ trans-III complex is observed. Since no catalysis occurs at pH 1 but some is seen at higher pH values then this catalysis occurs from the RSRS conformation after isomerization has occurred. The original *cis* -cyclam-Br_2 was also tested for catalytic activity. On an HMDE the peak is at -1.48 V (ΔE_p = 480 mV) and when carbon dioxide is allowed to bubble through the solution there is no evidence of catalysis and the redox couple is also lost. When argon is bubbled through the solution the redox couple is restored to -1.46 V (ΔE_p = 80 mV).

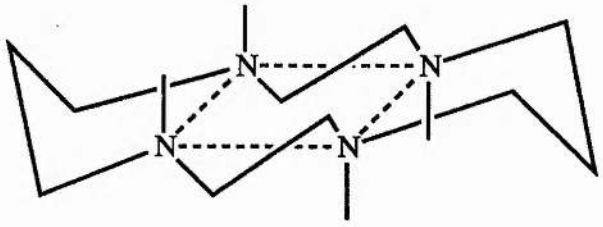

Trans III

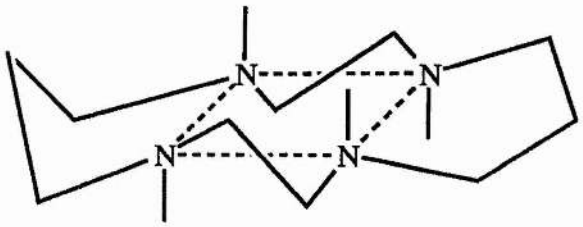

Trans V

Figure 2.29

Conformations of $[Ni(cyclam)]^{2+}$

The *cis* -cyclamBr_2 does not catalyse the reduction of carbon dioxide because there is no free site on the nickel centre for co-ordination to occur. The catalysis occurs at the surface of the mercury with an adsorbed nickel species, this complex probably does not adsorb, but if adsorption did occur there is no possibility of co-ordination of the carbon dioxide molecule onto the complex so there can be no

electron transfer from the Ni^{I} to the CO_2. When the bromine atoms are replaced and the rearrangement of the macrocyclic structure occurs to give a square planar nickel centre this complex can co-ordinate CO_2 but still does not facilitate the electrochemical reduction. The difference in the conformation is shown in Figure 2.29 where the RSRS is a chair compared to the boat of the RRRR.[42]

$[Ni(TMC)]^{2+}$ with the RSRS conformation has an Ni(II/I) redox potential at -1.03 V (ΔEp = 140 mV) while under carbon dioxide a current of 70 μA is observed at -1.54 V. This conformation has all the methyl groups sitting above the plane of the ring. Although the redox potential is much higher, the nature of the methyl groups is important. If the complex can adsorb onto the mercury surface there are two possibilities for the lack of activity. These are either: 1) the methyl groups interact with the mercury surface instead of the Ni centre and hence electron transfer from the electrode to the Ni(II) is inhibited; or 2) the Ni(II) binds to the mercury surface and the methyl groups point down from the surface and block the interaction of the carbon dioxide with the Ni(I).

2.7 Bulk Electrolysis of $[Ni(cyclam)]^{2+}$

To determine the products formed in the reaction a bulk electrolysis cell was designed[43] (Figure 2.30) to allow a mercury pool as the working electrode. There was a sampling valve to allow the removal of samples by a gas syringe in order that the product of the reaction could be determined by gas chromatography using either a 5 A molecular sieves or a carbosieves column. The molecular sieves column detects carbon monoxide, hydrogen, oxygen and methane but not carbon dioxide as this is adsorbed onto the column. Using the carbosieves column it is therefore possible to detect the carbon dioxide as well. However the quantities of carbon monoxide produced were so minute that it was impossible to determine any product by this method.

However, carbon monoxide adsorbs onto platinum[44] at +1.0 V vs SCE. By placing a platinum foil electrode into the bulk electrolysis solution which is connected

to the second electrode circuit on the potentiostat, then it is possible to see the characteristic peak of carbon monoxide (Figure 2.31). This method can therefore be used as a screening process for carbon monoxide formation in the reduction.

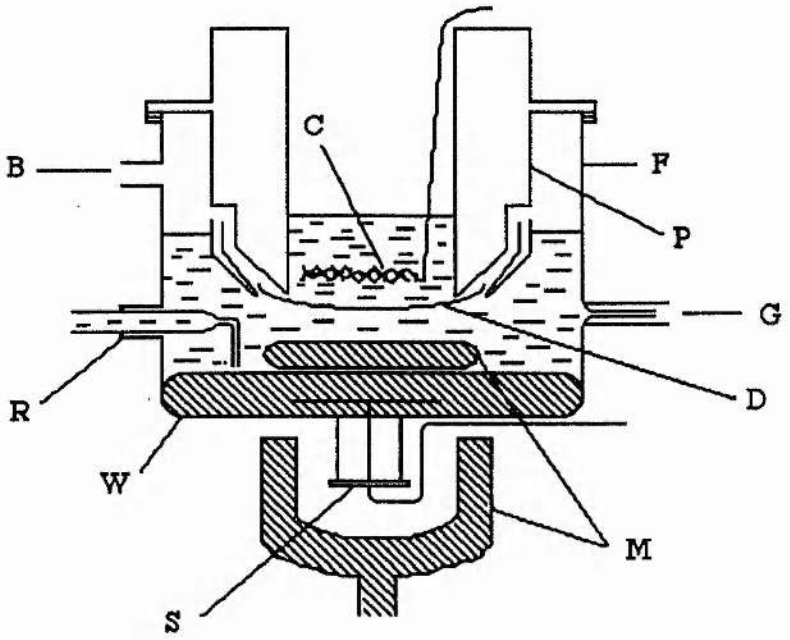

Figure 2.30

Design for the bulk electrolysis cell.

B-to gas bubbler, C-counter electrode, D-flexible diaphragm, F-glass-flange cell body, G-gas inlet, M-magnetic stirrer and follower, P-PTFE counter-electrode compartment, R-reference-electrode probe, S-silicone rubber septum and W-mercury-pool working electrode (Area = 44 cm^2)

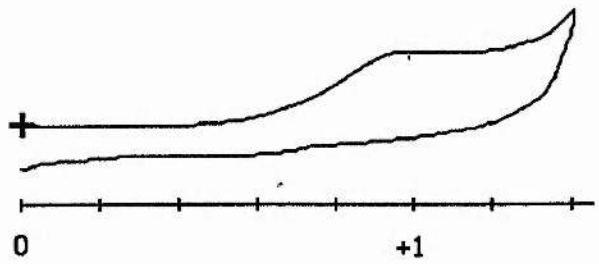

Figure 2.31

Bulk electrolysis of a 5 mM solution of $[Ni(cyclam)]^{2+}$ showing the adsorption of CO onto Pt

2.8 Conclusions

The best system for determining catalytic behaviour is to use a mercury electrode either in water preferably or in 9:1 MeCN/H_2O if the complex is insoluble in water. The addition of a known Lewis acid increases the current produced under carbon dioxide. Alkylation of the nitrogen atoms decreases the catalytic activity, as does changing the ring size. The only conformation of cyclam that is selective appears to be the trans-III complex which also has a free site for carbon dioxide co-ordination.

2.9 Experimental Section

Infra-red spectra were recorded as KBr discs on a Perkin Elmer 1710 Infra-red Fourier Transform Spectrometer.

NMR spectra were recorded using a Varian Gemini-200 Spectrometer (200 MHz) and a Bruker AM300 NMR Spectrometer (300 MHz).

Mass spectra were recorded using an AEI MS902 Spectrometer.

Conductivities of 10^{-3} moldm^{-3} solutions of the complexes in acetonitrile were measured at 25°C using a PT1-18 digital conductivity meter and dip-type cell with platinised electrodes.

Magnetic susceptibility measurements were made on a Johnson-Matthey magnetic susceptibility balance.

Electronic spectra were recorded on a Philips PU8720 scanning spectrometer and a Perkin-Elmer Lamda 5 spectrometer against a background of pure solvent.

Elemental analyses were carried out in house at St. Andrews by Mrs Sylvia Smith.

Melting points were determined using a Gallenkamp melting point apparatus.

Cyclic voltammetry was carried out with a Pine Instruments RDE 4 (EG & G, Wokingham, UK) potentiostat with a Graphtec XY Recorder WX2300. The CV's were obtained in high performance liquid chromatography grade (hplc) acetonitrile or dimethylformamide with 0.1 M tetrabutylammonium perchlorate or tetrabutylammonium tetrafluoroborate as supporting electrolyte or in aqueous solutions with 0.1 M sodium perchlorate as supporting electrolyte. The working electrode was either mercury (Metrohm Hanging Mercury Drop Electrode, HMDE with drop surface area 1.39 mm^2), platinum, glassy carbon, glassy carbon-mercury amalgam, copper or a gold-mercury amalgam; the counter electrode was platinum wire and the reference electrode was a SCE. After fabrication solid electrodes were polished firstly with successively finer grades of wet/dry paper (#120, 240, 600, 800). Thereafter polishing with diamond paste (Engis) of grade 6, 1 and 0.25 μm was carried out, with 5 minutes sonication in distilled water between grades. Alternatively,

grades alumina 3, 1 and 0.5 μm (Buehler) were used instead of the diamond paste. If necessary, during an experiment the electrode was repolished at the finest grade of alumina. Bulk electrolysis of a solution was carried out using a mercury working electrode, a platinum counter electrode and a SCE as the reference electrode. The membrane used in the cell was a 05-1005K-115 cloth obtained from Mr. John Smith.

Carbon dioxide/argon mixtures were prepared by adjusting the flow rates of each gas. Catalytic currents were measured by subtracting the current in the absence of carbon dioxide (presumed to be the hydrogen evolution or the Ni(II/I) couple) from the peak height of the catalytic wave in the presence of carbon dioxide.

Preparation of Ni(II) 1,4,8,11-tetra-aza-cyclotetradecane perchlorate.[45]

0.5 g (2.5 mmoles) of 1,4,8,11-tetra-azacyclotetradecane was dissolved in the minimum amount of methanol and 0.9 g (2.5 mmoles) of nickel perchlorate hydrate in methanol were mixed together. The resulting solution was left in the fridge overnight to crystallise.

Yield = 1.05 g

I.R. Data:- ν(C-H) = 2860 cm^{-1}, ν(N-H) = 3200 cm^{-1}, $\nu(ClO_4^-)$ = 1100 cm^{-1}, $\nu(ClO_4^-)$ = 640 cm^{-1}

Microanalysis:- Calculated for $NiC_{10}H_{24}N_4Cl_2O_8$

C 26.23 % H 5.28 % N 12.24 %

Found: C 27.67 % H 5.19 % N 12.36 %

λ_{max} = 451 nm

Preparation of Ni(II) 1,8-dimethyl-1,4,8,11-tetra-aza-cyclotetradecane perchlorate.[45]

1.14 g (5 mmoles) of 1,8,-dimethyl-1,4,8,11-tetra-azacyclotetradecane was dissolved in ethanol and 1.93 g (5 mmoles) of nickel perchlorate hydrate dissolved in methanol were added together. The resulting solution was left in the fridge overnight to crystallise.

Yield = 0.15 g

I.R. Data:- ν(C-H) = 2956 cm^{-1}, ν(N-H) = 3391 cm^{-1}, $\nu(ClO_4^-)$ = 1103 cm^{-1}, $\nu(ClO_4^-)$ = 636 cm^{-1}

Microanalysis:- Calculated for $NiC_{12}H_{28}N_4Cl_2O_8.C_2H_6O$

C 31.61 % H 6.44 % N 10.53 %

Found: C 34.66 % H 6.98 % N 11.49 %

λ_{max} = 458 nm

Preparation of Ni(II) 1,4,8,11-tetramethyl-1,4,8,11-tetra-aza-cyclotetradecane perchlorate.[46]

0.64 g (2.5 mmoles) of 1,4,8,11-tetramethyl-1,4,8,11-tetra-azacyclotetradecane was dissolved up in the minimum amount of methanol and 0.9 g (2.5 mmoles) of nickel perchlorate hydrate in methanol were added together. The resulting red solution was left in the fridge overnight to crystallise out.

Yield = 1.15 g

I.R. Data:- ν(C-H) = 2898 cm^{-1}, ν(N-H) = 3545 cm^{-1}, $\nu(ClO_4^-)$ = 1108 cm^{-1}, $\nu(ClO_4^-)$ = 639 cm^{-1}

Microanalysis:- Calculated for $NiC_{14}H_{32}N_4Cl_2O_8.H_2O$

C 31.61 % H 6.44 % N 10.53 %

Found: C 31.68 % H 5.77 % N 9.72 %

λ_{max} = 394 nm, 505 nm and 650 nm

Preparation of Ni(II) 1,4,8,12-tetra-aza-cyclopentadecane perchlorate.[47]

0.5 g (2.25 mmoles) of 1,4,8,12-tetra-azacyclopentadecane was dissolved in the minimum amount of methanol and 0.82 g (2.25 mmoles) of nickel perchlorate hydrate in methanol were added together. The resulting yellow solution was left in the fridge overnight to crystallise.

Yield = 0.5 g

I.R. Data:- ν(C-H) = 3250 cm^{-1}, ν(N-H) = 2900 cm^{-1}, $\nu(ClO_4^-)$ = 1103 cm^{-1}, $\nu(ClO_4^-)$ = 630 cm^{-1}

Microanalysis:- Calculated for $NiC_{11}H_{26}N_4Cl_2O_8.H_2O$

C 26.96 % H 5.75 % N 11.43 %

Found: C 27.89 % H 5.32 % N 11.80 %

λ_{max} = 449 nm

Preparation of other nickel complexes.

The rest of the complexes used in this chapter were obtained from Professor R. W. Hay.

Chapter Two References

1. B. Fischer and R. Eisenberg, *J. Am. Chem. Soc.*, 1980, **102**, 7363
2. M. Beley, J. P. Collin, R. Ruppert and J. P. Sauvage, *J. Chem. Soc. Chem. Comm.*, 1984, 1315
3. M. Beley, J. P. Collin, R. Ruppert and J. P. Sauvage, *J. Am. Chem. Soc.*, 1986, **108**, 7461
4. J. P. Collin, A. Jouaiti and J. P. Sauvage, *Inorg. Chem.*, 1988, **27**, 1986
5. M. Fujihira, Y. Hirata and K. Suga, *J. Electroanal. Chem.*, 1990, **292**, 199
6. M. Fujihira, Y. Nakamura, Y. Hirata, U. Akiba and K. Suga, *Denki Kagaku*, 1991, **59**, 532
7. G. B. Balazs and F. C. Anson, *J. Electroanal. Chem.*, 1992, **322**, 325
8. G. B. Balazs and F. C. Anson, *J. Electroanal. Chem.*, 1992, **335**, 75
9. G. B. Balazs and F. C. Anson, *J. Electroanal. Chem.*, 1993, **361**, 149
10. S. Sakaki, *J. Am. Chem. Soc.*, 1990, **112**, 7813
11. S. Sakaki, *J. Am. Chem. Soc.*, 1992, **114**, 2055
12. M. Fujihira and T. Noguchi, *Chem. Lett.*, 1992, 2043
13. S. Bruckenstein and R. R. Gadde, *J. Am. Chem. Soc.*, 1971, **93**, 5941
14. S. Hamada, M. Itoh, H. Matsuda and J. Yamada, *J. Electroanal. Chem.*, 1978, **91**, 107
15. (a) J. P. Collin and J. P. Sauvage, *Coord. Chem. Rev.*, 1989, **93**, 245
    (b) B. P. Sullivan, K. Krist and H. E. Guard, "Electrochemical and Electrocatalytic Reactions of Carbon Dioxide", Elsevier, Amsterdam, 1993
16. S. Daniele, P. Ugo, G. Bontempelli and M. Florani, *J. Electroanal. Chem.*, 1987, **219**, 259
17. F. R. Keene, C. Creutz and N. Sutin, *Coord. Chem. Rev.*, 1985, **64**, 247
18. (a) J. Hawecker, J. M. Lehn and R. Ziessel, *J. Chem. Soc. Chem. Comm.*, 1983, 536
    (b) J. Hawecker, J. M. Lehn and R. Ziessel, *J. Chem. Soc. Chem. Comm.*,

1984, 328

(c) J. Hawecker, J. M. Lehn and R. Ziessel, *Helv. Chim. Acta.*, 1986, **69**, 1990

(d) B. P. Sullivan and T. J. Meyer, *J. Chem. Soc. Chem. Comm.*, 1984, 1244

(e) B. P. Sullivan , C. M. Bolinger, D. Conrad, W. J. Vining and T. J. Meyer, *J. Chem. Soc. Chem. Comm.*, 1985, 1414

(f) B. P. Sullivan and T. J. Meyer, *Organometallics*, 1986, **5**, 1500

(g) M. R. M. Bruce, E. Megehee, B. P. Sullivan, H. Thorp, T. R. O'Toole, A. Downart and T. J. Meyer, *Organometallics.*, 1988, **7**, 238

19. (a) H. Ishida, K. Tanaka and T. Tanaka, *Chem. Lett.*, 1985, 405

(b) H. Ishida, H. Tanaka, K. Tanaka and T. Tanaka, *J. Chem. Soc. Chem. Comm.*, 1987, 131

(c) H. Ishida, K. Tanaka and T. Tanaka, *Organometallics*, 1987, **6**, 181

20. C. M. Bolinger, B. P. Sullivan , D. Conrad, J. A. Gilbert, N. Story and T. J. Meyer, *J. Chem. Soc. Chem. Comm.*, 1985, 796

21. S. Slater and J. H. Wagenknecht, *J. Am. Chem. Soc.*, 1984, **106**, 5367

22. Y. Matsumoto, Y. Uchida, M. Hidai, M. Tesuka, T. Yajima and A. Tsuchiya, *J. Am. Chem. Soc.*, 1982, **104**, 6834

23. (a) E. Fujita, B. S. Brunschwig, T. Ogata and S. Yanagida, *Coord. Chem. Rev.*, 1994, **132**, 195

(b) J. O'M Bockris and J. C. Wass, *Mater. Chem. and Phys.*, 1989, **22**, 249

(c) C. A. Craig, L. O. Spreer, J. W. Otvos and M. Calvin, *J. Phys. Chem.*, 1990, **94**, 7957

(d) D. A. Morgenstern, R. E. Wittrig, P. E. Fanwick and C. P. Kubiak, *J. Am. Chem. Soc.*, 1993, **115**, 6470

(e) W. Leitner, *Angew. Chem. Int. Ed. Engl.*, 1994, **33**, 173

24. (a) J. R. Bolton (Ed.), "Solar Power and Fuels", Academic Press, New York, 1977

(b) J. S. Connolly (Ed.), "Solar Energy Photochemical Conversion and Storage", Academic Press, New York, 1981

25. M. S. Wrighton, *Pure Appl. Chem.*, 1985, **57**, 57

26. J. M. Lehn and R. Ziessel, *Proc. Natl. Acad. Sci. USA*, 1982, **79**, 701

27. (a) N. Kitamura and S. Tazuke, *Chem. Lett.*, 1983, 1109

(b) J. Hawecker, J. M. Lehn and R. Ziessel, *J. Chem. Soc. Chem. Comm.*, 1985, 56

28. (a) R. Ziessel, J. Hawecker and J. M. Lehn, *Helv. Chim. Acta.*, 1986, **69**, 1065

(b) J. L. Grant, K. Goswami, L. O. Spreer, J. W. Otvos and M. Calvin, *J. Chem. Soc. Dalton Trans.*, 1987, 2105

29. Southampton Electrochemistry Group, "Instrumental Methods in Electrochemistry", Ellis Horwood, Chichester, 1985

30. The thermodynamic potential for the $2e^-$ reduction of CO_2 to CO is -0.79 V vs SCE.

31. P. J. Daly, D. J. Page and R. G. Compton, *Anal. Chem.*, 1983, **55**, 1191

32. F. V. Lovecchio, E. S. Gore and D. H. Busch, *J. Am. Chem. Soc.*, 1974, **96**, 3109

33. (a) M. Fujihira, Y. Hirata and K. Suga, *J. Electroanal. Chem.*, 1990, **292**, 199

(b) B.A.S. (Bioanalytical Systems Inc.), West Lafayette, Indiana, Technical Reference Manual

34. M. M. Hassan, Ph.D. Thesis, St. Andrews, 1992

35. M. Hammouche, D. Lexa, M. Momenteau and J. M. Saveant, *J. Am. Chem. Soc.*, 1991, **113**, 8455

36. D. H. Busch, *Acc. Chem. Res.*, 1978, **11**, 392

37. G. M. Melson, "Co-ordination Chemistry of Macrocyclic Compounds", Plenum, New York, 1979, Pg. 410

38. L. Sabatini and L. Fabbrizzi, *Inorg. Chem.*, 1979, **18**, 438

39. R. W. Hay, B. Kinsman and C. I. Smith, *Polyhedron*, in press

40. (a) B. Bosnich, C. K. Poon and M. L. Tobe, *Inorg. Chem.*, 1965, **4**, 1102

(b) G. M. Melson, "Co-ordination Chemistry of Macrocyclic Compounds", Plenum, New York, 1979, Pg. 222

41. (a) L. Fabbrizzi, *Inorg. Chem.*, 1977, **16**, 2667

(b) L. Sabatini and L. Fabbrizzi, *Inorg. Chem.*, 1979, **18**, 438

(c) E. J. Billo, *Inorg. Chem.*, 1981, **20**, 4019

(d) E. J. Billo, *Inorg. Chem.*, 1984, **23**, 236

42. K. R. Adam, M. Antolovich, L. G. Brigden and L. F. Lindoy, *J. Am. Chem. Soc.*, 1991, **113**, 3346

43. A. Weissberger and B. W. Rossiter, "Techniques of Chemistry Volume I, Physical Methods of Chemistry", Wiley, New York, Pg. 79

44. (a) H. Huang, C. Fierro, D. Scherson and E. B. Yeager, *Langmuir*, 1991, 1154

(b) B. Z. Nikolic, H. Huang, D. Gervasio, A. Lin, C. Fierro, R. R. Adzic and E. B. Yeager, *J. Electroanal. Chem.*, 1990, **295**, 415

45. E. K. Barefield, F. Wagner, A. W. Herlinger and A. R. Dahl, *Inorg. Syn.*, 1976, **16**, 220

46. (a) E. K. Barefield and F. Wagner, *Inorg. Chem.*, 1973, **12**, 2435

(b) M. J. D'Aniello Jr., M. T. Mocella, F. Wagner, E. K. Barefield and I. C. Paul, *J. Am. Chem. Soc.*, 1975, **97**, 192

(c) L. F. Lindoy, "The Chemistry of Macrocyclic Ligand Complexes", Cambridge University Press, Cambridge, Pg. 16

47. (a) E. K. Barefield, F. Wagner, A. W. Herlinger and A. R. Dahl, *Inorg. Syn.*, 1976, **16**, 222, substituting 202 g (1 mole) of 1,3-dibromopropane for the dibromoethane.

(b) E. K. Barefield and G. Freeman, *Inorg. Syn.*, 19, **20**, 108

(c) R. W. Hay and M. T. H. Tarafder, *J. Chem. Soc. Dalton Trans.*, 1991, 823

Chapter Three

A Study of the Mechanism of the Electrochemical Reduction of CO_2 by Rotating Disc Studies on $[Ni(cyclam)]^{2+}$

3.0 Introduction

Convection is the transport of species because of external mechanical forces. In an electrochemical system this can arise from the movement of the electrode (as the expanding Hg surface in an dropping mercury electrode (DME) or by the rotation/vibration of the electrode), agitation of the solution (gas, stirrer or ultrasound) or flowing the solution past the electrode surface. In these cases a complete description of the convection requires the solution of a three dimensional hydrodynamic problem to give in, for example, Cartesian co-ordinates the components of the velocity of the solution in the directions x, y and z *i.e.* V_x, V_y and V_z. Convection is only effective in bringing about changes in concentration where there is already a concentration gradient; then the change in concentration of any species due to convection is given by equation (3.1)

$$-\frac{\partial c}{\partial t} = V_x \frac{\partial c}{\partial x} + V_x \frac{\partial c}{\partial y} + V_x \frac{\partial c}{\partial z} \qquad (3.1)$$

and this change is superimposed on that due to diffusion. Hence, the total change in concentration with time is given by

$$\frac{\partial c}{\partial t} = D\left[\frac{\partial^2 c}{\partial x^2} + \frac{\partial^2 c}{\partial y^2} + \frac{\partial^2 c}{\partial z^2}\right] - \left[V_x \frac{\partial c}{\partial x} + V_y \frac{\partial c}{\partial y} + V_z \frac{\partial c}{\partial z}\right] \qquad (3.2)$$

In electrochemistry the concentration gradients always occur in the boundary layer close to the electrode surface. When convection is present in a system, it is an important form of mass transport, and current densities 3-100 times greater than the

steady state diffusion limited value are common.

In a study of the mechanism and kinetics of electrode reactions, an important element in the design of an experiment is to provide a mass transport regime where the transport of species to and form the electrode surface may be controlled and varied in a known way. Methods involving convective diffusion are excellent for establishing a defined and reproducible mass transport regime. However to obtain quantitative information from an experiment the convective diffusion regime in the cell must be described exactly, and the resulting equations solvable; then the consequences of changes in the role of convection may be predicted and used for comparison with experimental data. In fact, few convective diffusion systems are able to be solved exactly; rotating or vibrating wire electrodes are examples where the mass transport is well defined and reproducible but not calculable. On the other hand, the rotating ring disc electrode, the DME and flow through a channel between parallel or concentric tube electrodes, are cases where exact equations have been obtained.

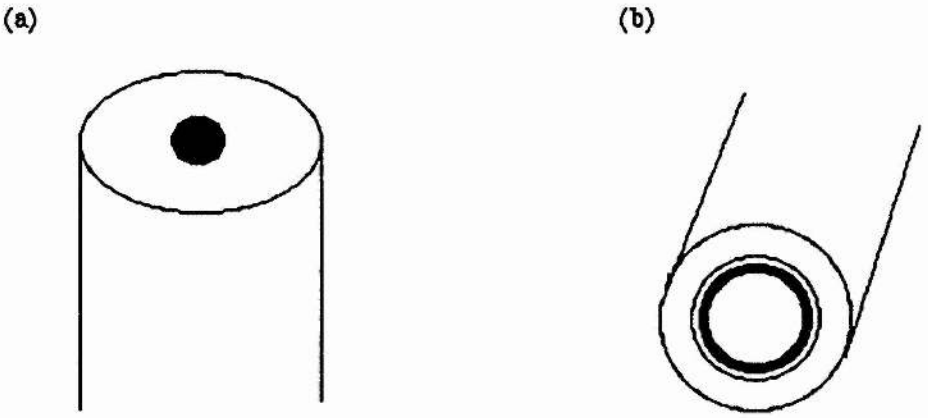

Figure 3.1

Schematic diagrams of (a) a rotating disc electrode, (b) a rotating ring-disc electrode.

The rotating disc and rotating ring disc electrodes are now the most popular systems for kinetic and mechanistic studies; in particular the rotating disc electrode, which combines an ease of construction and use with the ability to control and vary the rate of mass transport over a very wide range. Rotating disc and ring disc

electrodes are shown in Figure 3.1. In the former, a disc of the electrode material is surrounded by a non-conducting sheath (usually polyethylene, PTFE or epoxy resin) constructed so that the faces of the electrode and the sheath are flush and only the face of the disc electrode is exposed to the electrolyte solution; the electrode is rotated perpendicular to the face of the disc. In the ring-disc system, a similar disc is separated from a concentric ring electrode by a thin non-conducting gap.

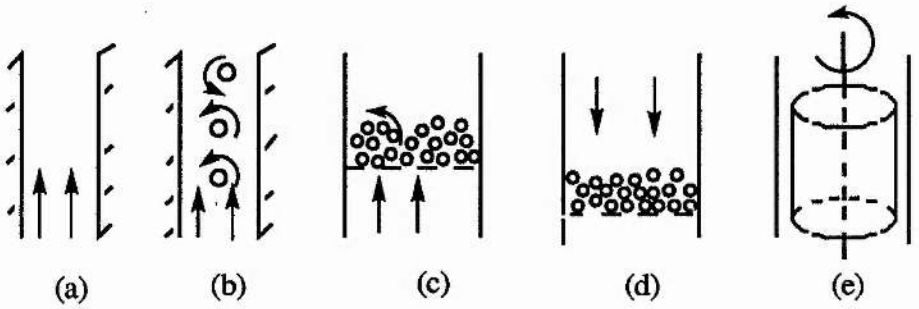

Figure 3.2

Convective diffusion regimes commonly found in industrial cells, (a) flow through channel formed by two parallel electrodes (or by one electrode and a membrane), (b) flow through such a channel but containing a turbulence promoter (*e.g.* a set of non-conducting bars or a net), (c) fluidised bed electrode, (d) packed bed electrode, (e) rotating cylinder electrode within a concentric tube.

In an industrial environment, quite different convective diffusion regimes are employed and some of the common examples are shown in Figure 3.2. The most common one is where the electrolyte solution flows through a channel between two parallel electrodes or an electrode and a separator (case (a)) or where turbulence promoters are in the channel (case (b)). These introduce eddies into the flow, increasing mixing and the rate of mass transfer. In bed electrodes (case (c) and (d)) the particles perform the dual role of electrode and turbulence promoters. The last example (case (e)) is the rotating cylinder electrode.

3.1 Hydrodynamics of the Rotating Disc System

When a disc electrode surrounded by a non-conducting sheath is rotated in a large volume of solution (*i.e.* the cell walls do not interfere with the flow pattern), a well defined flow pattern distribution is established. This is shown in Figure 3.3, where it can be seen that the electrode system acts as a pump, pulling the solution vertically upwards towards the disc and then throwing it outwards.

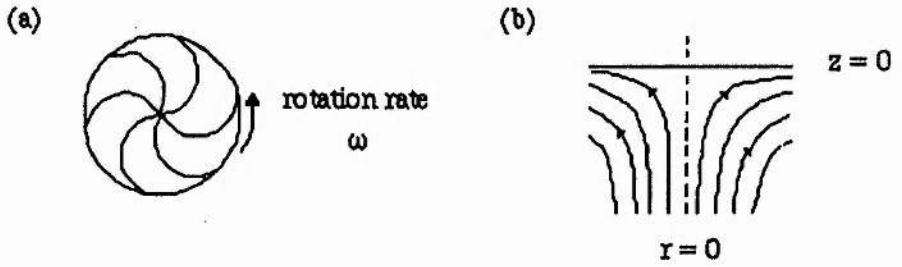

Figure 3.3

Flow patterns created by the rotating disc electrode (a) solution flow close to the electrode surface, viewed from below, (b) view from the side showing how the solution is pumped towards the disc, then thrown outwards.

3.2 The Rotating Disc Electrode

The applications of the rotating disc electrode (RDE) to the study of the mechanism and kinetics of electrode reactions will be discussed in sections dealing with total mass transfer, reversible electron transfer, totally irreversible processes, quasi-reversible electron transfer and coupled chemical reactions. However in general, two types of experiment are important. In the first, the shape of the I vs E curve at a single rotation rate is analysed, here the RDE is being used essentially to provide a highly controlled mass transport regime. In the second, the current density, at one or a series of potentials, is investigated as a function of rotation rate. If the RDE is to be used to isolate pure kinetic data from situations where in unstirred solution the steady state current is partially mass transfer controlled, it is a general principle that the current is measured as a function of rotation rate and the data is extrapolated to conditions where the rate of mass transport is infinite, *i.e.* $\omega = \infty$.

3.2.1 Experimental Factors

The RDE has considerable practical advantages over techniques such as cyclic voltammetry, potential sweep or a.c. methods. The rate of mass transport to the electrode may be varied over a substantial range and in a controlled way without resorting to a rapid change in the electrode potential which inevitably leads to the measured current having a contribution from charging the double layer. Since in most experiments with the RDE only (pseudo) steady state currents are measured, the recorded current may be unequivocally equated with the faradaic current.

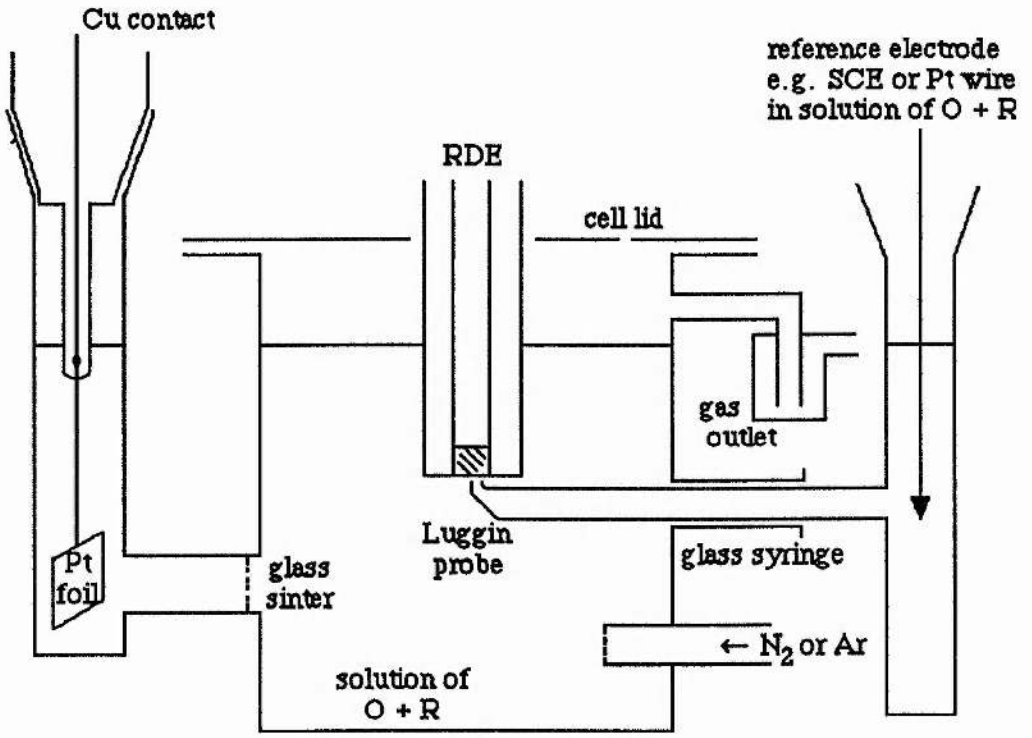

Figure 3.4

Cell used for rotating disc electrode experiments.

There has been much discussion of the design of the cell for RDE experiments. For example, much is made of any eccentricity of the rotation, and it was also held that the non-conducting sheath should be bell shaped. Furthermore, from the theoretical viewpoint, the radius of the sheath should be much larger than that of the active disc, and the cell walls should be well away from the RDE.

Fortunately in practice these factors are seldom important at least over the common range of rotation rates, $10 < \omega < 1000\ s^{-1}$ or $100 < \frac{60\omega}{2\pi} < 10{,}000$ r.p.m.. Indeed Figure 3.4 shows a widely used cell design, and it is also found that the Luggin capillary, apparently in the main flow pattern is not a problem. For large currents (mA) the iR_u drop must be minimised and so the R_u is minimised by using the Luggin capillary. Hence overall it can be said that the design of the RDE and cell is not critical.

The problems which do arise in experiments with the RDE are most commonly associated with leakage of solution into any gap between the active disc material and the insulating sheath, and with noise introduced by poor or dirty electrical contacts. Now the shaft of the RDE is normally linked directly to the motor drive and the electrical contact made either with a high quality carbon brush contact (Ag/C material) or by a wire dipping into a circular trough of mercury around the shaft.

3.2.2 Mass Transport Control

For potentials where the surface concentration of the electroactive species is zero, the equation relating the limiting current density (for an oxidation) and the rotation rate is given by equation (3.3),

$$i_L = 0.62nFAD^{2/3}\nu^{-1/6}c^{\infty}\omega^{1/2} \qquad (3.3)$$

where i_L is the limiting current, n is the number of electrons, F is Faradays constant, A is the electrode area in cm^2, D is the diffusion coefficient in cm^2s^{-1}, ν is the solution viscosity, c is the bulk concentration in $moldm^{-3}$ and ω is the rotation rate in s^{-1}. This expression is known as the Levich equation, and it provides an excellent test that the current is entirely mass transport controlled: a plot of I vs $\omega^{1/2}$ should be linear and pass through the origin, and the slope of such a plot may be used to estimate the diffusion coefficient for the electroactive species. Except when a chemical reaction limits the current density, the Levich equation will describe the rotation rate

dependence of the anodic and cathodic limiting currents at high positive and high negative overpotentials respectively.

3.2.3 Reversible Electron Transfer

If the standard rate constant for the reaction

$$O + ne^- \rightleftharpoons R \tag{3.4}$$

is large, the I-E response, at all rotation rates, will appear reversible. At high positive or negative overpotentials, the current density will be given by the Levich equation, but even in the potential range where the current is a strong function of potential (*i.e.* around the reversible potential), a plot of I vs $\omega^{1/2}$ will be linear. The slope of the plot will, however, be less than predicted by the Levich equation since the surface concentration of electroactive species will not be zero.

The complete I-E response can also be found by substituting into the Nernst equation:

$$E = E_e^{\ominus} + \frac{2.3RT}{nF} \log \frac{c_O^{\sigma}}{c_R^{\sigma}} \tag{3.5}$$

the ratio of the surface concentrations, $c_O^{\sigma}/c_R^{\sigma}$ found by manipulation of the following equations resulting from a Nernst diffusion layer model

$$I_L^C = -nFk_m c_O^{\infty} \tag{3.6}$$

$$I_L^A = -nFk_m c_R^{\infty} \tag{3.7}$$

where I_L^C and I_L^A are the cathodic and anodic limiting current densities respectively (if the solution contains only O or only R, one of these limiting current densities will, of

course, be zero) and the equations for the current density at any potential, *i.e.*

$$I = -nFkm(c_O^{\infty} - c_O^{\sigma}) \tag{3.8}$$

$$I = nFk_m(c_R^{\infty} - c_R^{\sigma}) \tag{3.9}$$

The equation which results is

$$E = E_e^{\ominus} + \frac{2.3RT}{nF} \log \frac{I - I_L^C}{I - I_L^A} \tag{3.10}$$

where for the purpose of analysis of the data, $E_e^{\ominus} \approx E_{1/2}$. Equation (3.10) should permit the I-E data for all rotation rates and potentials to be collapsed onto a single line.

3.2.4 Irreversible Electrode Reactions

In the case of an irreversible electrode process

$$O + ne^- \xrightarrow{\vec{k}} R \tag{3.11}$$

the back reaction is ignored (*i.e.* $\overleftarrow{k} = 0$). The I-E curve at an RDE for such a reaction has the familiar sigmoidal shape and with respect to the dependence of current density on rotation rate, the curve can be broken into three different areas.

(i) In the limiting current region, the current density depends only on the rate of mass transport, and i_L is proportional to $\omega^{1/2}$.

(ii) At very low current density, the current density is totally determined by the kinetics of electron transfer, and the rate of mass transport will not affect the current density. Hence I is independent of ω.

(iii) In the intermediate zone of mixed control, the current density is partially mass

transport controlled, and I must therefore vary with ω. But a plot of I vs $\omega^{1/2}$ is non-linear.

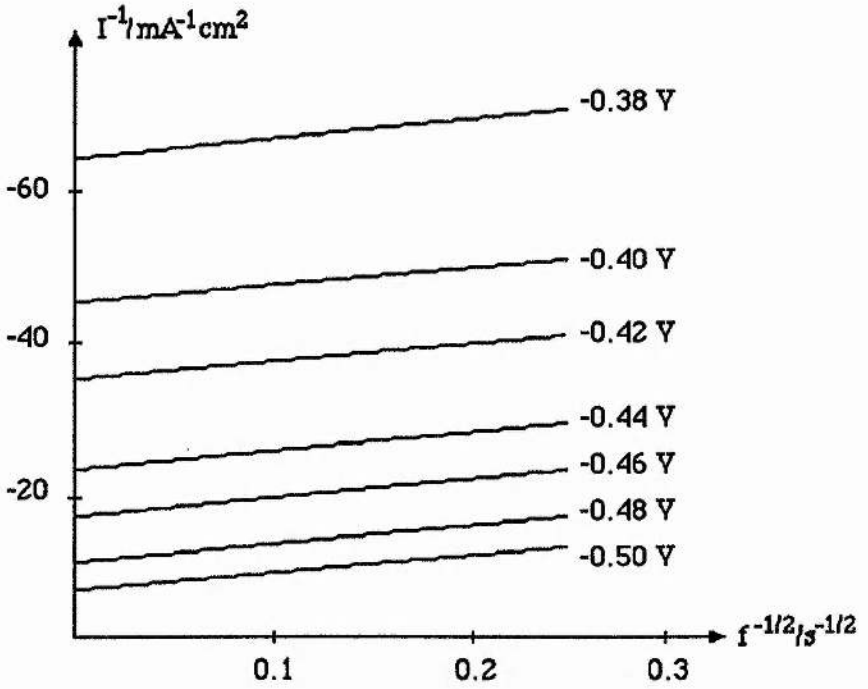

Figure 3.5

I^{-1} versus $f^{1/2}$ plots as a function of potential for a rotating brass electrode in aerated seawater (note $\omega = 2\pi f$).[1] Potentials quoted vs the normal calomel electrode.

The approach to obtain $\vec{k}$ in the intermediate zone is to measure I as a function of ω and then to extrapolate the current density to $\omega = \infty$. Clearly

$$I_{\omega\to\infty} = -nF\vec{k}c_O^{\infty} \tag{3.12}$$

The procedure for extrapolation of the I-ω data to $\omega = \infty$ results in the required equation

$$-\frac{1}{I} = \frac{1}{nF\vec{k}c_O^{\infty}} + \frac{1.61\nu^{1/6}}{nFc_O^{\infty}D^{2/3}}\frac{1}{\omega^{1/2}} \tag{3.13}$$

and so a plot of $|I|^{-1}$ vs $\omega^{-1/2}$ should be linear, and the intercept used to calculate $\vec{k}$. Also the slopes of these plots $\frac{d|I|^{-1}}{d\omega^{-1/2}}$ should be independent of potential, while the intercepts (because of $\vec{k}$) vary strongly with potential. Indeed $\log\vec{k}$ vs E is a form of Tafel plot and should therefore be linear. Figure 3.5 shows a set of I^{-1} vs $\omega^{-1/2}$ plots constructed from data for the reduction of oxygen on an aluminium brass.[1]

The Nernst diffusion layer approach can also be used to obtain the equation for the complete I-E response. The result is

$$\log\frac{I_L^c}{I-I_L^c} = \text{const.} + \log c_O^\infty - \frac{\alpha_C nF}{2.3RT}E \qquad (3.14)$$

for a reduction and

$$\log\frac{I_L^a}{I_L^a-I} = \text{const} + \log c_R^\infty - \frac{\alpha_A nF}{2.3RT}E \qquad (3.15)$$

for an oxidation.

These equations may be used to put I-E data from several rotation rates and a series of bulk concentrations onto a single linear plot. Figure 3.6 shows data from several rotation rates for the reduction of oxygen at gold[2] in 0.1 mol dm^{-3} NaOH, the slope of the graph is $(120\ mV)^{-1}$, confirming that only $1e^-$ is transferred before and during the rate determining step.

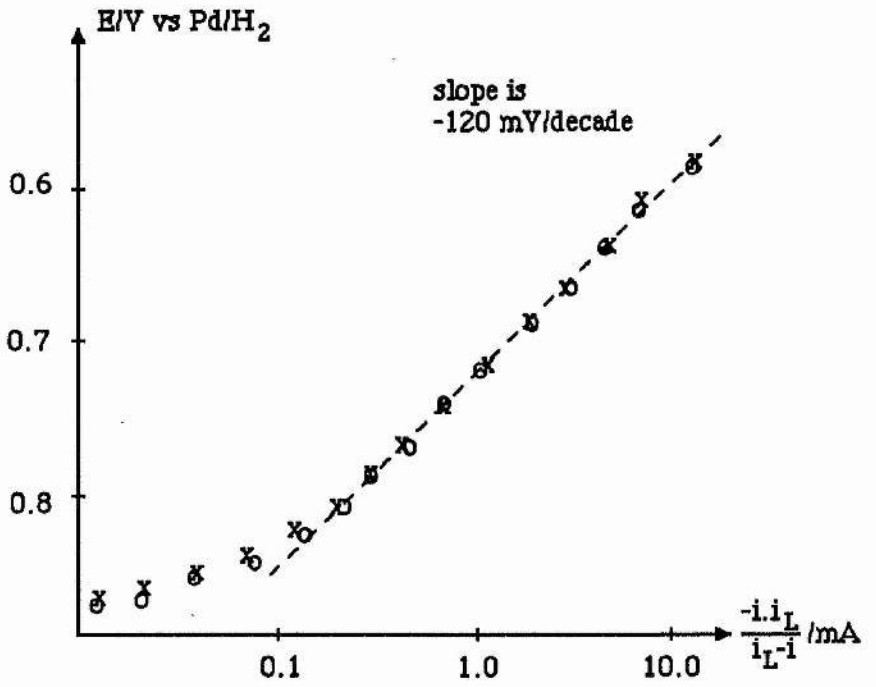

Figure 3.6

Test of equation (3.15) using data for the reduction of oxygen at gold in NaOH (0.1 mol dm^{-3}).[2] o 6400 r.p.m. x 1600 r.p.m.

3.2.5 Quasi-reversible Electron Transfer

In this case, both the forward and back electron transfer processes must be considered. Initially systems

$$O + ne^- \underset{k}{\overset{\vec{k}}{\rightleftharpoons}} R \qquad (3.16)$$

where both halves of the redox couple are solution-free species will be considered. The I-E curve will have the three zones (i) - (iii) described in section 3.2.4, and to develop a procedure for isolating the kinetic data from the mixed region, the Nernst diffusion layer concept is used again. The equations based on equating the fluxes at the disc surface can be written as

$$k_m(c_O^\infty - c_O^\sigma) = -k_m(c_R^\infty - c_R^\sigma) \qquad (3.17)$$

and

$$I = -nFk_m(c_O^{\infty} - c_O^{\sigma}) \tag{3.18}$$

and the current is given by

$$I = nF(\overleftarrow{k}c_R^{\sigma} - \overrightarrow{k}c_O^{\sigma}) \tag{3.19}$$

Combining these equations gives

$$\frac{1}{I} = \frac{1}{nF\overleftarrow{k}c_R^{\infty} - \overrightarrow{k}c_O^{\infty}} + \frac{\overleftarrow{k} + \overrightarrow{k}}{nFk_m(\overleftarrow{k}c_R^{\infty} - \overrightarrow{k}c_O^{\infty})} \tag{3.20}$$

To determine the equation for the dependence of I on ω, $k_m = \frac{D}{\delta}$ and that δ is given by equation (3.21)

$$\delta = \frac{1.61\nu^{1/6}D^{1/3}}{\omega^{1/2}} \tag{3.21}$$

Then

$$\frac{1}{I} = \frac{1}{nF\overleftarrow{k}c_R^{\infty} - \overrightarrow{k}c_O^{\infty}} + \frac{1.61(\overleftarrow{k} + \overrightarrow{k})\nu^{1/6}}{nF(\overleftarrow{k}c_R^{\infty} - \overrightarrow{k}c_O^{\infty})D^{2/3}} \frac{1}{\omega^{1/2}} \tag{3.22}$$

This equation again suggests that the I-ω data in the potential region of mixed control should be treated by plotting $|I|^{-1}$ vs $\omega^{-1/2}$ and both $\overleftarrow{k}$ and $\overrightarrow{k}$ can be found using the slope and intercept of the plot. In fact only at potentials close to the reversible potential, say $\frac{-2.3RT}{2\alpha_C nF} < \eta < \frac{2.3RT}{2\alpha_C nF}$, is it really necessary to consider both the forward and back reaction. Outside this range, the analysis can be simplified, *e.g.* for cathodic

overpotentials $h < \frac{-2.3RT}{2\alpha_C nF}$, $\vec{k} c_O^{\infty} \gg \overleftarrow{k} c_R^{\infty}$ and $\vec{k} \gg \overleftarrow{k}$, and equation (3.22) becomes

$$-\frac{1}{I} = \frac{1}{nF\vec{k}c_O^{\infty}} + \frac{1.61\nu^{1/6}}{nFc_O^{\infty}D^{2/3}}\frac{1}{\omega^{1/2}} \qquad (3.23)$$

and the kinetic constant can be obtained directly from the intercept.

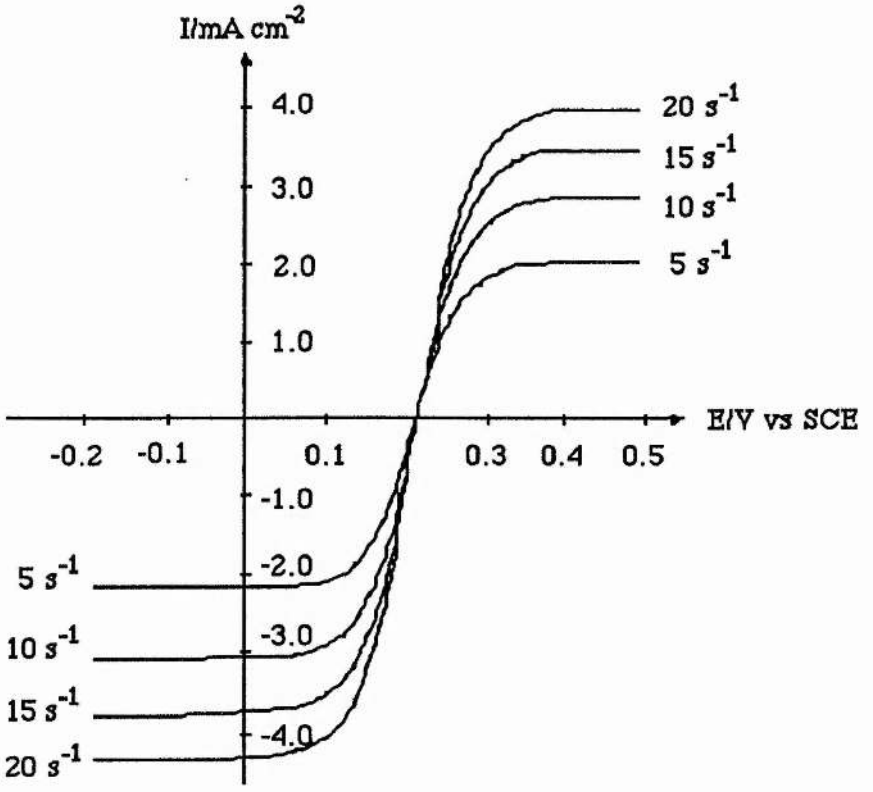

Figure 3.7

Experimental data for the study of $Fe(CN)_6^{4-}/Fe(CN)_6^{3-}$ couple in KCl (0.5 mol dm^{-3}). $c_O^{\infty} = c_R^{\infty} = 10$ mmol dm^{-3}. Au electrode[3] I-E curves as function of rotation rates.

Figure 3.7 and Figure 3.8 shows experimental data for the $Fe(CN)_6^{4-}/Fe(CN)_6^{3-}$ couple.[3] Figure 3.7 shows the I-E curves at a series of rotation rates of a gold disc electrode,[3] and the three zones (with respect to ω) are clearly seen. At the two extremes of potential, the limiting current plateaux are clearly observed, and it can be

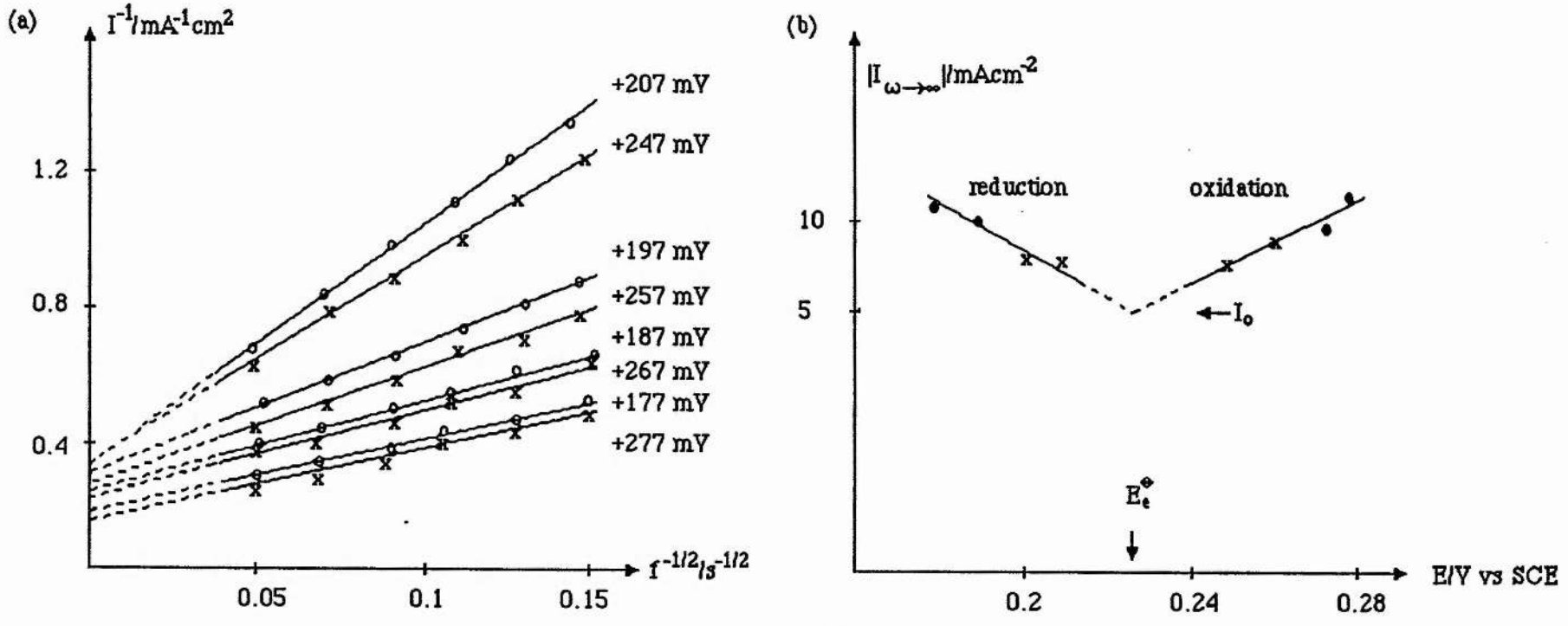

Figure 3.8

Experimental data for the study of $Fe(CN)_6^{4-}/Fe(CN)_6^{3-}$ couple in KCl (0.5 mol dm^{-3}). $c_O^\infty = c_R^\infty = 10$ mmol dm^{-3}. Au electrode (a) I-E curves as function of rotation rates. (a) I^{-1} vs $f^{-1/2}$ plots ($\omega = 2\pi f$) at a series of potentials. o reduction, x oxidation. (b) Tafel analysis of kinetic currents, *i.e.* the log of the inverse of the intercepts of (a) vs potential. • uncorrected data. x data corrected for the back reaction.

seen that $I_L \propto \omega^{1/2}$. Also, at I = 0 the I-E curves at all ω converge, while in the intervening regions, the current varies with ω but I is not proportional to $\omega^{1/2}$. As ω is increased the plateau is not reached until higher overpotentials, because with the higher rates of mass transport, the range of at least partial kinetic control is extended. Figure 3.8 (a) shows the $|I|^{-1}$ vs $\omega^{1/2}$ plots for some typical overpotentials, while Figure 3.8 (b) shows the Tafel plots which result from the estimation of $\overleftarrow{k}$ and $\overrightarrow{k}$ from the mixed region using equations (3.22) and (3.23).

3.2.6 Coupled Chemical Reactions

The study of homogeneous chemical reactions with the RDE is generally carried out by investigating the variation of the limiting current with rotation rate because it leads to greatly simplified boundary conditions when it is certain that the rates of electron transfer at the disc surface are very fast. The I_L-ω relationship must be dependent on the rate constant of a chemical step; this makes the RDE best suited to the study of CE, ece or catalytic reactions where either (i) the increase in flux of a reactant puts pressure on a chemical reaction forming the electroactive species *e.g.* the CE mechanism, or (ii) the rotation rate affects the residence time of an intermediate in the layer at the electrode surface and hence the extent to which it undergoes a chemical reaction within the influence of the electrode, *e.g.* ece or catalytic mechanisms.

3.3 The Rotating Ring-Disc Electrode

A sketch of the rotating ring-disc electrode (RRDE) is shown in Figure 3.1 and Figure 3.9 shows the essential features. It is a view from below and shows the electrode disc surrounded by the concentric ring electrode with a thin layer of insulating material between.

As the rotation of the electrode causes a particular flow pattern in the solution. The solution is pulled at the centre of the electrode and then thrown out radially across the surface of the disc (Figure 3.3). Hence, intermediates formed at the disc are swept out towards the ring; the ring is therefore effectively downstream of the disc and can

be used to obtain information about intermediates formed at the disc.

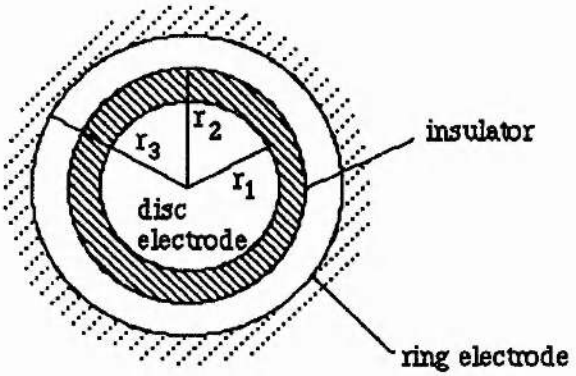

Figure 3.9

Critical dimensions of the rotating ring-disc electrode.

The electrical contacts to the ring and disc electrodes are made so that the two electrodes can be controlled independent of each other. In order to obtain the maximum information from the system a four electrode potentiostat is required. This allows individual control of both the ring and disc electrode. The experiments that can be performed using this system are

(i) the disc electrode is held at a constant potential where the reaction of interest takes place, and an I-E curve is recorded at the ring electrode. In principle, this scheme allows the identification of intermediates formed at the disc.

(ii) an I-E curve is recorded at the disc while the potential at the ring is held constant at a value where the intermediate is oxidised or reduced. This allows the exact potential range for the formation of the intermediate to be determined.

(iii) both the ring and disc electrodes are held at constant potentials. The disc is held at a potential where the intermediate is formed and the ring is held at a potential where it can be detected. This is the standard mode of operation for the determination of quantitative kinetics.

In each of the above experiments, the rotation rate is an independent variable. Increasing ω will decrease the time taken for intermediates to be transported from the disc to the ring. The detection of short-lived intermediates requires the use of high

rotation rates and the construction of an electrode with a thin inter-electrode gap. These experiments give a similar flexibility as cyclic voltammetry for the study of mechanism and kinetics with the additional advantage that solution-free and adsorbed intermediates are directly distinguished (adsorbed species onto the disc are not transported to the ring). The disc and ring do not have to be made from the same material, and often the material is selected to give the best response for detecting the species under investigation.

One disadvantage of the RRDE is that it is both difficult and expensive to make and as such must be handled with caution. The gap between the disc and ring has to be uniform and for the detection of short-lived intermediates the gap has to be thin. There should also be no leakage of the solution between the electrodes and the sheath (usually PTFE or epoxy resin).

3.4 Rotating Disc Electrochemistry of $[Ni(cyclam)]^{2+}$

Various electrodes were tried to find the best system and hence determine a method of comparing different complexes by the analysis of the intercept of the Levich plot. After checking the electrode and cell with a standard 1 mM solution of $Fe(CN)_4^{3-}$ with an GC disc electrode (Area = 0.126 cm^2) and by using equation (3.3) a diffusion coefficient of 1.32 x 10^{-5} cm^2s^{-1} was obtained, this electrode was electroplated with mercury but this only worked for a short time before the mercury surface became unstable and deteriorated. The electrode is always held at negative potentials to avoid the deterioration but over time the surface was still unstable. The alternative solution was to electroplate the mercury onto a copper electrode. This system appeared to work except that upon closer examination the mercury surface had deteriorated and the bare copper surface was acting as the substrate.

Under argon with the copper electrode no current plateaux are observed because of the background hydrogen evolution reaction. However, under carbon dioxide current plateaux are observed that increase with rotation rate (Figure 3.10). To ensure that it was the $[Ni(cyclam)]^{2+}$ species causing the plateau in the experiment

then a blank run was run without the nickel catalyst. Under argon the blank showed no effect but in the presence of carbon dioxide the background current decreased with rotation rate. This is due to the bare copper reducing the carbon dioxide to a species, probably methane,[4] which adsorbs onto the electrode and blocks the subsequent reduction of carbon dioxide.

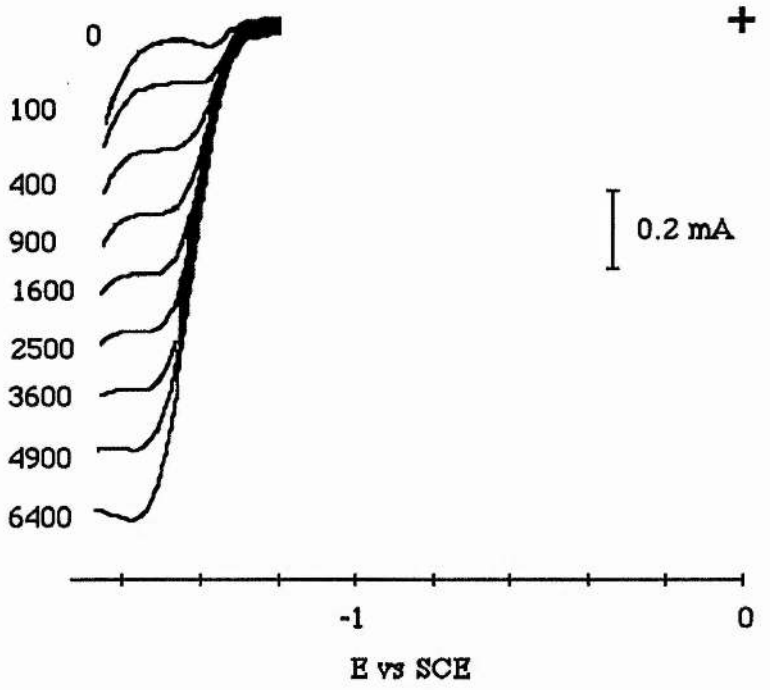

Figure 3.10

A typical RDE plot for $[Ni(cyclam)]^{2+}$ in 0.1 M $NaClO_4$ with a Cu/Pt/SCE electrode system under carbon dioxide. Rotation rates ranging from 100 to 6400 rpm.

A 1 mM solution of $[Ni(cyclam)]^{2+}(ClO_4)_2$ was dissolved in distilled water containing 0.1 M $NaClO_4$ and the solution run with an Cu/Pt/SCE electrode system and the rotation rates varied from 100 to 6400 rpm. As before plateaux were observed under carbon dioxide and this time a plot of current versus $(\text{rotation rate})^{1/2}$ (Levich plot) was recorded (Figure 3.11). This is a linear relationship and from this graph it was thought possible to determine the mechanism and efficiency of the catalysis by comparing Levich plots for different complexes.

The presence of these plateaux under carbon dioxide indicates that catalysis

can be determined by rotating disc electrochemistry. Since earlier work[5] has determined that carbon monoxide is the product of the reduction then the slope of the graph should be equivalent to an n = 2 reduction. This is discussed further in the next section.

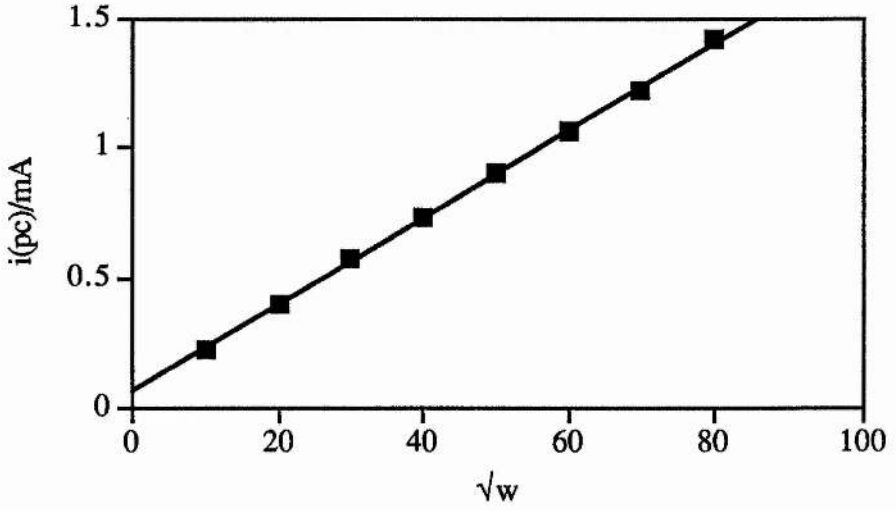

Figure 3.11

A plot of current against (rotation rate)$^{1/2}$ for a 1 mM solution of [Ni(cyclam)]$^{2+}$ in an aqueous solution containing 0.1 M $NaClO_4$ corresponding to Figure 3.10.

A rotating ring disc electrode (GC/Hg disc and Pt ring) was also used in order to determine *in situ* whether carbon monoxide could be identified. This is due to carbon monoxide being adsorbed onto platinum and desorbing at +1.0 V vs SCE. Unfortunately it was not possible to see this because the quantities of carbon monoxide produced were not significant enough to be observed on the ring which has a small surface area.

3.5 Concentration Studies on $[Ni(cyclam)]^{2+}$

Since current plateaux are observed under carbon dioxide the next obvious stage in the investigation was to look into the effect of the concentrations of both catalysts and carbon dioxide on the behaviour of the rotating disc electrode. A detailed study of the relationship between concentration and the Levich plots should lead to an understanding of the mechanism involved in the reduction of carbon dioxide. Each concentration was tested three times and the average value of the slope obtained.

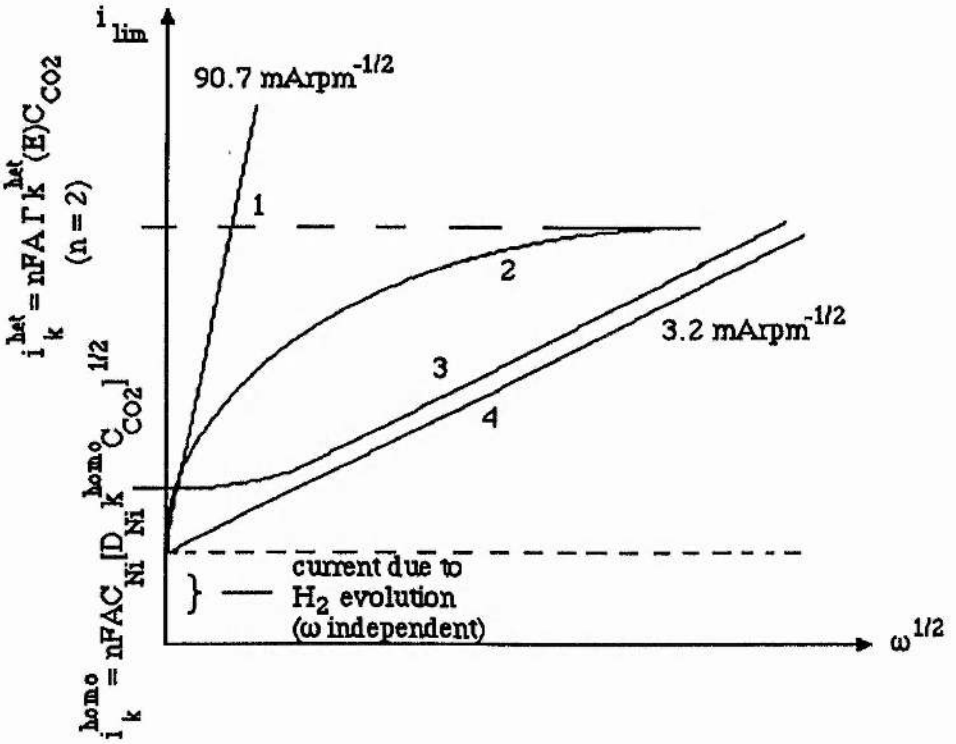

Figure 3.12

Theoretical diagram showing the different possibilities for the system.
For case 1, the slope α 2 $D_{CO2}^{2/3}$ C_{CO2}. For case 4, the slope α $D_{Ni}^{2/3}$ C_{Ni}.

The possibilities that exist for the reduction in the system are shown in Figure 3.12. For convenience the following form of the Levich equation is used

$$i = 41.71nAD^{2/3}C\omega^{1/2}$$

where i is measured in amps, c in mM and $\omega^{1/2}$ in $rpm^{1/2}$. Slope 1 shows the direct two electron reduction of carbon dioxide which gives a theoretical slope of 90.7 $mArpm^{-1/2}$ (using $D_{CO2} = 1 \times 10^{-5}\ cm^2s^{-1}$ and $C_{CO2} = 33$ mM)[6] while slope 2 shows the kinetically limited reduction of carbon dioxide, slope 3 shows the catalytic mechanism which reaches a limiting value at low values of rotation rates and slope 4 shows the Ni(II/I) reduction where n = 1.

To determine the relationship between the slope of the Levich plot and nickel concentration, various solutions of $[Ni(cyclam)]^{2+}$ were tested, the results are summarised in Table 3.1. From the plot of the Levich slope versus nickel concentration there is a clear linear dependence (Figure 3.13).

[Ni] (mM)	Levich Slope ($mArpm^{-1/2}$)
0.1	7.82×10^{-4}
1.0	3.22×10^{-3}
1.77	4.32×10^{-3}
3.69	8.52×10^{-3}
6.59	1.62×10^{-2}
8.03	1.88×10^{-2}
10.0	2.66×10^{-2}

Table 3.1

The effect of nickel concentration on the Levich slope in an aqueous solution containing 0.1 M $NaClO_4$ with $[CO_2] = 0.033$ M.

As there is a linear relationship between the value of the Levich slope and the nickel concentration then for the catalytic mechanism to hold there should also be a dependence on the carbon dioxide concentration.

For a catalytic mechanism occurring at the RDE the Levich plot reaches a limiting value at low values of ω.[7] Since the plateaux are observed in this system only

under carbon dioxide and the nickel catalyst, it seemed a reasonable assumption that it was the catalytic reduction of the carbon dioxide being observed. For the catalytic mechanism involving adsorbed nickel catalyst onto the copper surface (as in the Hg case, see Figure 2.2 and Figure 2.3) a linear relationship of the intercept of the Levich curve with the concentration would be expected for the nickel complex and with the square root of carbon dioxide concentration.

A similar set of experiments were run to find out the dependence on carbon dioxide concentration. A 6.59 mM solution of $[Ni(cyclam)]^{2+}$ was tested with various carbon dioxide concentrations and the results are summarised in Table 3.2. From the plot of the Levich slope against carbon dioxide concentration (Figure 3.14) the reaction is zero order with respect to the carbon dioxide concentration.

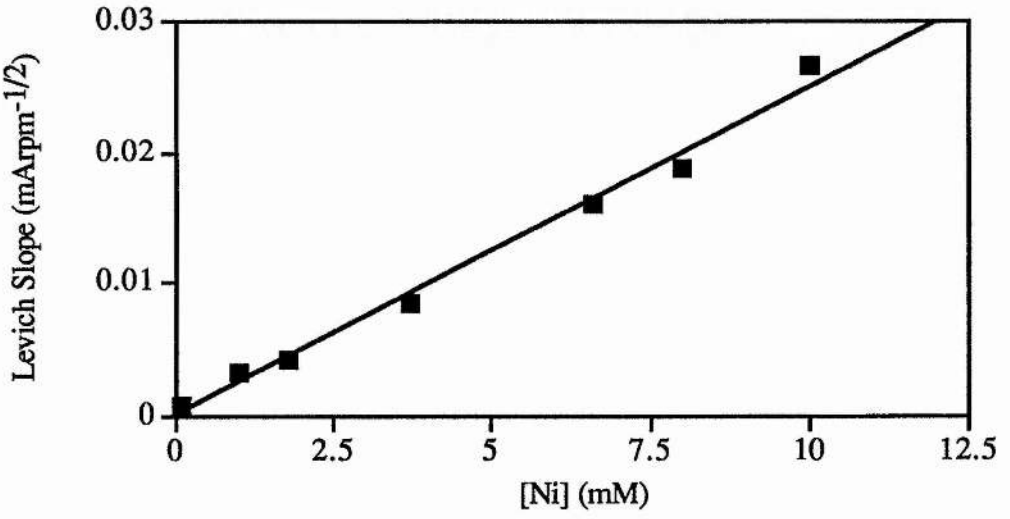

Figure 3.13

A plot of Levich slope as a function of nickel concentration in an aqueous solution containing 0.1 M $NaClO_4$ with $[CO_2] = 0.033$ M.

It is this zero order with respect to the carbon dioxide concentration that leads to the abandonment of the catalytic mechanism and therefore the current plateaux are due to the Ni(II/I) reduction. Another interesting fact to disprove the catalytic mechanism is if the intercept of the Levich plot is taken as a function of concentration

(both nickel and carbon dioxide) then the graphs show a large scatter and there is no relationship obtained.

$[CO_2]$ (M)	Levich Slope ($mAr pm^{-1/2}$)
0.0033	1.63×10^{-2}
0.0066	1.73×10^{-2}
0.0132	1.69×10^{-2}
0.0198	1.63×10^{-2}
0.0264	1.69×10^{-2}
0.033	1.62×10^{-2}

Table 3.2

The effect of the carbon dioxide concentration on the Levich slope in an aqueous solution containing 0.1 M $NaClO_4$ with [Ni] = 6.59 mM.

As seen above, at the copper RDE in the presence of carbon dioxide there is only the Ni(II/I) reduction and no catalytic reduction of carbon dioxide. It is then possible to determine the diffusion coefficient for the complex using the Levich equation, *i.e.* $D = 3.59 \times 10^{-5}$ cm^2s^{-1}. The diffusion coefficient gives information on how the complex moves in the solution and thus how quickly the complex moves towards the electrode surface. This information may gave an insight into the different catalytic behaviour of complexes, if they have widely differing diffusion coefficients. Generally, however, it is more convenient to measure the diffusion coefficient using chronoamperometry or chronocoulometry.

Since no kinetic data on the catalysis can be obtained by this method we can however obtain diffusion coefficients for the various complexes under investigation. This will be discussed later when other complexes are discussed in more detail and also other methods for obtaining diffusion coefficients.

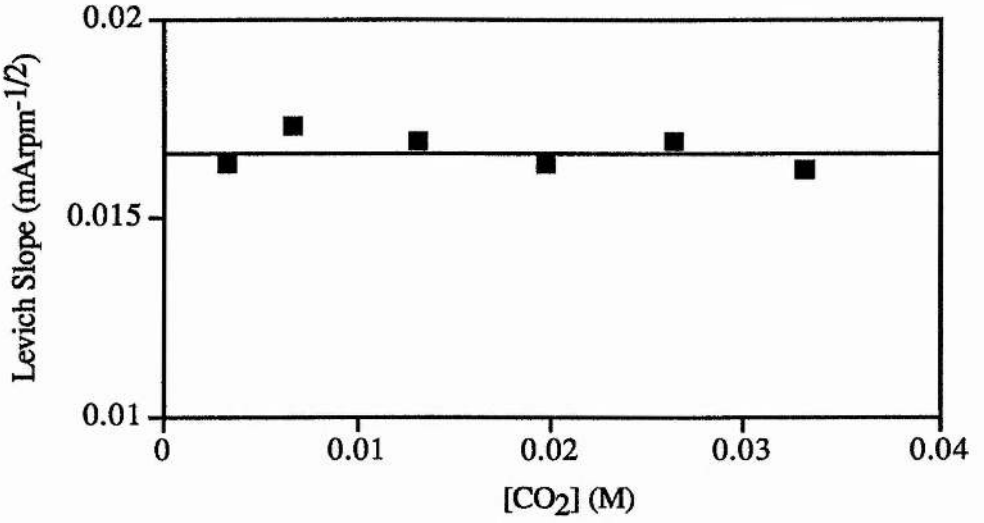

Figure 3.14

A plot of the Levich slope as a function of carbon dioxide concentration in an aqueous solution containing 0.1 M $NaClO_4$ with [Ni] = 6.59 mM.

3.6 The Effect of Macrocycle Ring Size

As discussed above, rotating disc electrochemistry using a mercury coated glassy carbon or copper electrode is unsuitable for determining kinetic data in relation to the catalytic activity of different complexes. However, since a carbon dioxide atmosphere shows the presence of the Ni(II/I) reduction we can obtain a comparison of diffusion coefficients of these complexes from this method. Diffusion coefficients are a measure of the ability of a species to move towards the electrode. The diffusion coefficient varies depending on the solvent, the size of the molecule and the degree of solvation and can be calculated by a variety of methods including RDE, chronocoulometry and cyclic voltammetry.

The complexes investigated were the [n]aneN_4 complexes with values of n ranging from 13 to 16. A 0.5 mM solution of the complex under investigation was tested with the copper electrode system, the current was recorded as a function of the rotation rate and a graph of the plateau current in milliamps against (rotation rate)$^{1/2}$ plotted and from the slope of this graph and the Levich equation (equation (3.3)) the

diffusion coefficient was calculated. The experiment was repeated three times to get an average value and the results are summarised in Table 3.3.

Complex	[Ni] (mM)	Levich Slope ($mAr pm^{-1/2}$)	D ($cm^2 s^{-1}$)
[13]aneN_4	0.5	1.8714×10^{-3}	4.50×10^{-5}
[14]aneN_4	0.9997	3.222×10^{-3}	3.59×10^{-5}
[15]aneN_4	0.5	1.397×10^{-3}	2.90×10^{-5}
[16]aneN_4	0.5	1.000×10^{-3}	1.76×10^{-5}

Table 3.3

A comparison of diffusion coefficients for complexes [n]aneN_4 for n = 13 - 16 obtained in aqueous solution containing 0.1 M $NaClO_4$.

The trend across the series is that the diffusion coefficient decreases with the size of the macrocycle. This is consistent with the Stokes-Einstein equation (equation (3.24) that the diffusion coefficient varies inversely with the hydrodynamic radius, a:

$$D = \frac{RT}{N_a \pi \eta a} \qquad (3.24)$$

where N_a is Avogadros Number, η is the viscosity and a is the hydrodynamic radius.[8] Although $[Ni(cyclam)]^{2+}$ is the best catalyst for carbon dioxide reduction it does not have the highest diffusion coefficient in the series. However as discussed earlier (Section 2.4), the cavity of the [13]aneN_4 is the best fit for the Ni^{2+} ion and hence the reduction is more difficult as the Ni^{+} is forced out the plane of the macrocycle. It is a combination of these conflicting factors that reduce the activity of the [13]aneN_4 complex.

In the case of $[Ni(cyclam)]^{2+}$ the catalysis occurs via an adsorbed catalytic species. However, in concentrated solutions it has been proposed that there may be a contribution from solution catalysis.[9] If there is any solution catalysis then the diffusion coefficient of the complex would play an important part in determining the

catalytic activity.

For a heterogeneous reaction the limiting current is given by

$$i_k^{het} = nFA\Gamma_{Ni}k^{het}(E)C_{CO2} \tag{3.25}$$

and for an EC' reaction in solution the expression is:

$$i_k^{soln} = nFAC_{Ni}[D_{Ni}k^{soln}C_{CO2}]^{1/2} \tag{3.26}$$

Now assuming that $k^{het}(E)$ and k^{soln} may be approximated by the homogeneous rate constant, k a ratio of the contribution from the adsorbed catalyst to the contribution from the soluble catalyst of

$$\frac{i_k^{het}}{i_k^{soln}} = \frac{\Gamma_{Ni}k^{1/2}C_{CO2}^{1/2}}{C_{Ni}D_{Ni}^{1/2}} \tag{3.27}$$

is obtained. If limiting values are substituted into the equation, *i.e.* consider a diffusion controlled reaction with a value of $k = 10^{10}$ $M^{-1}s^{-1}$, $C_{Ni} = 10^{-3}$ M, $D_{Ni} = 3.59 \times 10^{-5}$ cm^2s^{-1}, $C_{CO2} = 0.033$ M and $\Gamma_{Ni} = 1 \times 10^{-10}$ $molcm^{-2}$, a value for the $\frac{i_k^{het}}{i_k^{soln}}$ ratio of 0.959 is obtained which suggests that the currents are almost equal. If the rate constant, k is only 10^6 $M^{-1}s^{-1}$ then the ratio is 0.00959 which would strongly favour the solution contribution, and the diffusion coefficient value would become an important factor.

However, since no catalytic current for carbon dioxide reduction is observed at the copper RDE the model is therefore more complex. The rate constant $k^{het}(E)$ must be specific to the surface species.

There are therefore two important factors in considering the rate of heterogeneous catalysis: 1) If there is a greater coverage on the electrode then the heterogeneous catalytic current increases; and 2) if the value of the rate constant

increases then the heterogeneous catalytic current increases. The coverage, Γ will be dependent on the substrate (better adsorption on mercury than copper), structure and redox potential (since only Ni^{I} adsorbs). The rate constant is probably structure-dependent and potential dependent.

3.7 Comparison of $[Ni(isocyclam)]^{2+}$ with $[Ni(cyclam)]^{2+}$

Since $[Ni(isocyclam)]^{2+}$ is also a catalyst for the reduction of carbon dioxide, rotating disc electrochemistry was attempted originally to find out whether the catalytic rate differed. However, since this is not possible with this system, it is therefore possible to compare the diffusion coefficients of the two isomers, the data is summarised in Table 3.4.

Complex	[Ni] (mM)	Levich Slope ($mAr pm^{-1/2}$)	D ($cm^2 s^{-1}$)
$[Ni(isocyclam)]^{2+}$	1.043	4.738×10^{-3}	6.01×10^{-5}
$[Ni(cyclam)]^{2+}$	0.9997	3.222×10^{-3}	3.59×10^{-5}

Table 3.4

A comparison of diffusion coefficients for $[Ni(isocyclam)]^{2+}$ and $[Ni(cyclam)]^{2+}$ obtained in an aqueous solution containing 0.1 M $NaClO_4$.

The diffusion coefficient for the $[Ni(isocyclam)]^{2+}$ is almost twice that of the $[Ni(cyclam)]^{2+}$, this is unusual as these are isomers of each other, and would therefore be expected to have very similar hydrodynamic radii.

In 0.1 M sodium perchlorate at 21.7°C the planar $[Ni(isocyclam)]^{2+}$ exists in equilibrium with the octahedral $[Ni(isocyclam)]^{2+}(H_2O)_2$.[10] It is this equilibrium which affects the diffusion coefficient of the complex. The extra Ni-O bonds cause a correspondingly decrease in the strength of the Ni-N bonds, the bonds are longer (207 - 210 pm) than those obtained in the planar species (188 - 191 pm). This is in contrast to the $[Ni(cyclam)]^{2+}$ where in 0.1 M sodium perchlorate it exists almost entirely in the planar form and in the trans III conformation. This extra co-ordination

from the axial waters causes an increase in the sphericity of the complex. It is known that a spherical particle has a greater diffusion coefficient than a flattened orange-like molecule (oblate ellipsoid). For example, an oblate ellipsoid of diameter 2a and height $^{a}/_{2}$ has a 15 % smaller diffusion coefficient.[11]

3.8 Conclusions

Originally it was thought that the copper RDE would give information on the kinetic behaviour of the complexes under investigation, and that rate constants for the reduction of carbon dioxide could be obtained. However, careful analysis of the dependence of the Levich slope on the concentration of nickel and carbon dioxide showed that catalysis did not occur on copper after all. There was no dependence on the carbon dioxide concentration but the limiting current varied linearly with the nickel concentration. Therefore currents observed under carbon dioxide were solely due to the one-electron reduction of the nickel complex. The experiments only allowed the diffusion coefficients for the complexes to be determined, and their variation with structure cannot be related to the observed catalytic currents at the mercury electrode.

3.9 Experimental Section

Rotating disc electrochemistry was carried out with a Pine Instruments RDE 4 (EG & G, Wokingham, UK) potentiostat and a Pine Instruments rotator with a Graphtec XY Recorder WX2300. The RDE's were obtained in aqueous solutions with 0.1 M sodium perchlorate as supporting electrolyte. The working electrode was either glassy carbon or copper; the counter electrode was platinum wire and the reference electrode was a SCE. After fabrication solid electrodes were polished firstly with successively finer grades of wet/dry paper (#120, 240, 600, 800). Thereafter polishing with diamond paste (Engis) of grade 6, 1 and 0.25 μm was carried out, with 5 minutes sonication in distilled water between grades. Alternatively, grades alumina 3, 1 and 0.5 μm (Buehler) were used instead of the diamond paste. If necessary, during an experiment the electrode was repolished at the finest grade of alumina.

The copper electrode was fabricated in house by Mr. Jim Rennie and Mr. Robert Cathcart in the Mechanical workshop.

Chapter Three References

1. S. R. Sanchez and D. J. Schiffrin, *Corrosion Science*, 1982, **22**, 585
2. R. W. Zurrilla, R. K. Sen and E. Yeager, *J. Electrochem. Soc.*, 1978, **125**, 1103
3. D. Jahn and W. Vielstich, *J. Electrochem. Soc.*, 1962, **25**, 849
4. B. P. Sullivan, K. Krist and H. E. Guard, "Electrochemical and Electrocatalytic Reactions of Carbon Dioxide", Elsevier, Amsterdam, 1993, Pg. 180
5. M. Beley, J. P. Collin, R. Ruppert and J. P. Sauvage, *J. Am. Chem. Soc.*, 1986, **108**, 7461
6. S. Kapusta and N. Hackerman, *J. Electrochem. Soc.*, 1984, **131**, 1511
7. A. J. Bard and L. R. Faulkner, "Electrochemical Methods, Fundamentals and Applications", Pg. 468
8. Atkins, "Physical Chemistry" 4th Edition, Pg. 765
9. K. Shigehara and F. C. Anson, *J. Phys. Chem.*, 1982, **86**, 2776
10. R. W. Hay, B. Kinsman and C. I. Smith, *Polyhedron*, in press
11. Atkins, "Physical Chemistry" 4th Edition, Pg. 689

Chapter Four

A Study of the Adsorption of $[Ni(cyclam)]^{2+}$

4.0 Introduction

The adsorption of $[Ni(cyclam)]^{2+}$ onto the mercury electrode is an important feature in the electrocatalytic reduction of carbon dioxide. There are two suitable techniques for studying the adsorption of reactants onto the electrode of interest: chronocoulometry and a.c. impedance spectroscopy. The two techniques differ in that chronocoulometry measures the amount of charge on the electrode while a.c. impedance spectroscopy indicates the capacitance of the solution as a function of voltage.

The key step in an electrochemical reaction occurs at the interface of the conducting electrode (usually solid) and the electrolyte solution (usually liquid). Here ionic current is transformed into electronic current by an electrode reaction. The electrode/electrolyte interface in the electrochemical cell often shows chemical properties different from those of the bulk of the electrode and in the electrolyte solution far from the interface. An interesting property of many electrode/electrolyte interfaces is their ability to attract and retain reactants. This is known as "adsorption" of reactants at electrode surfaces. Much research has been done to find a way of measuring the quantity of any reactant that may be adsorbed at the electrode. This is not a trivial problem because the quantity of species adsorbed lies in the range of 10^{-12} to 10^{-10} mole for each cm^2 of interface.

4.1 Chronocoulometry[1]

4.1.1 Electrode Reactions Controlled by the Supply of Reactant to the Electrode Surface

In Figure 4.1 a typical current-potential curve (recorded under steady state conditions *e.g.* using a rotating disc electrode) for the reduction of a reactant at an electrode surface. No current flows until the potential reaches values near the reduction potential of the reactant where there is a sharp increase in current. As the potential is made more negative, the current reaches a limiting value where every reactant molecule that reaches the electrode is immediately reduced.

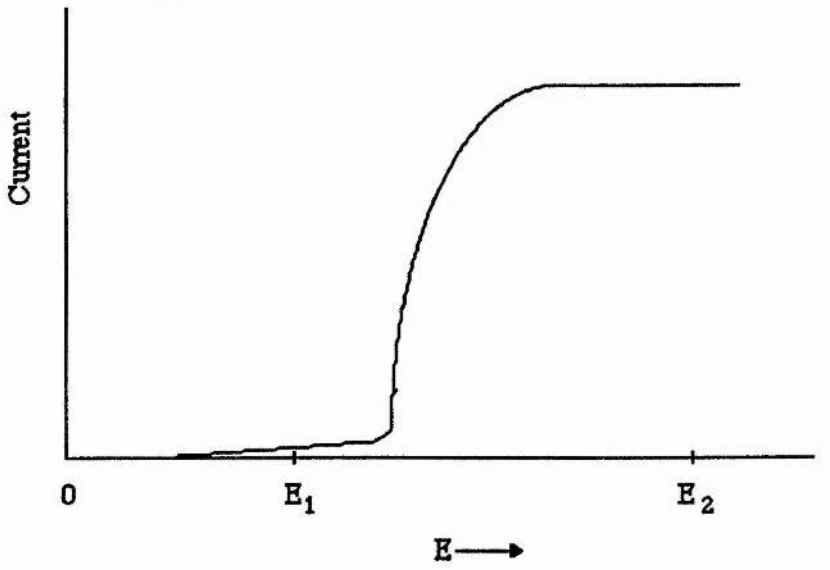

Figure 4.1

Typical steady-state current-potential curve for the reduction of a reactant at an electrode surface. Reduction currents are plotted upward; and the potential becomes more negative to the right.

At potentials in the plateau region the current is limited by the rate at which the reactant is supplied to the electrode surface. If experimental conditions are arranged such that the reactant is transported to the electrode surface by means of linear diffusion (*i.e.* unstirred solution, flat electrode) then an equation which was originally

derived by Cottrell[2] can be used to calculate the current that flows at any time after the application of the potential step as a result of the reduction of the reactant. Suppose the electrode potential is stepped from an original value (*e.g.* E_1 in Figure 4.1) where no reaction is occurring to a value on the limiting current plateau (E_2 in Figure 4.1), then the resulting current is described in equation (4.1):

$$i = FnAC_b(\frac{D}{\pi t})^{1/2} \tag{4.1}$$

where F is Faraday's constant, n is the number of electrons, A is the electrode area (cm^2), C_b is the concentration of the reactant in the bulk solution (mol cm^{-3}), D is the diffusion coefficient (cm^2s^{-1}) and t is the time following the potential step. Figure 4.2 (a) shows the potential step applied to the electrode and (b) shows the resulting current. The current is composed of two components: the Cottrell current given by equation (4.1) plus a "charging current", i_c that flows to charge up the double layer capacitance that is also present in electrode/electrolyte interfaces. The charging current alone can be observed by applying the potential step in the absence of reactant, the dashed line in Figure 4.2 (b). The charging current decays much more rapidly than the Cottrell current and becomes zero once the interfacial capacitance has become fully charged.

The total charge passing through the electrode is the time integral of the two current components:

$$Q = \int FnAC^b(\frac{D}{\pi t})^{1/2}\,dt + \int i_c\,dt \tag{4.2}$$

$$Q = 2FnAC^b(\frac{Dt}{\pi})^{1/2} + Q_c \tag{4.3}$$

where Q_c is the charge flowing into the interfacial capacitance when the electrode potential is stepped from E_1 to E_2. Figure 4.2 (c) shows the charge-time response expected on the basis of equation (4.3). The dashed horizontal line at $Q = Q_c$

represents the response in the absence of reactant.

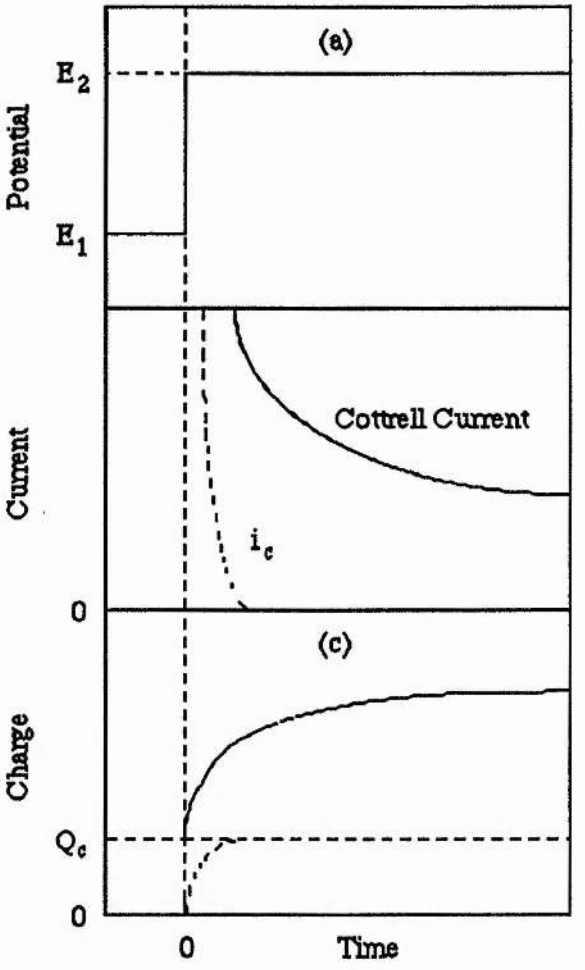

Figure 4.2

Temporal behaviour of the electrode potential, current and charge in chronocoulometric experiments. (a) The electrode potential is stepped from E_1 to E_2 at time = 0; (b) The current that flows in response to the potential step (solid curve). The dashed line is the current obtained when the experiment is repeated in the absence of reactant; (c) The time-integrals of the two curves in (b).

According to equation (4.3), plots of Q versus $t^{1/2}$ should be linear with intercepts of Q_c and slopes proportional to the concentration of the reactant. This behaviour is shown by line 1 of Figure 4.3. The charge increases in chronocoulometric experiments with the square root of time because additional reactant is transported to the electrode surface by diffusion.[3] Suppose that some of the

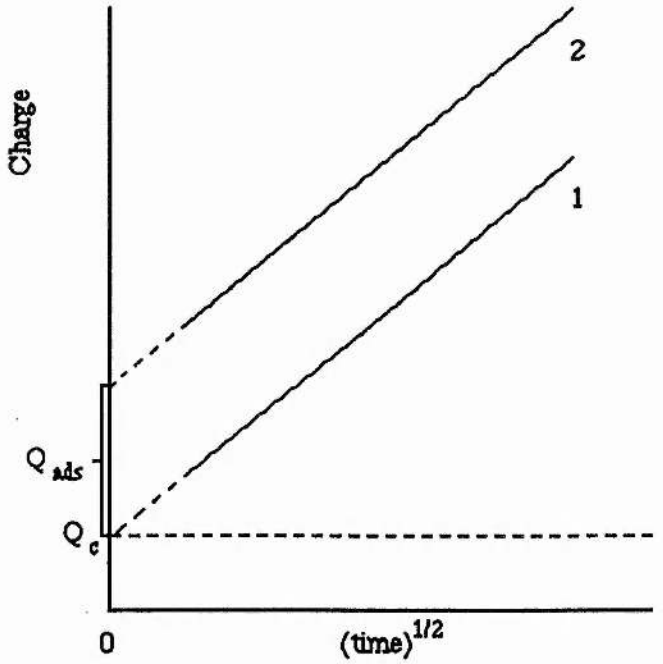

Figure 4.3

Chronocoulometric plots of charge versus (time)$^{1/2}$. The dashed, horizontal line represents the charge response obtained in the absence of reactant. Line 1 results if the reactant is not adsorbed. Line 2 results with the same concentration of adsorbed reactant. The dotted extensions of lines 1 and 2 indicate that the intercepts of chronocoulometric plots are usually obtained by linear extrapolation from the shortest times at which reliable data are available.

reactant is adsorbed at the electrode/electrolyte interface while the electrode is resting at potential E_1 (Figure 4.1). When the potential is stepped to E_2 the adsorbed species will be instantaneously reduced as it is already present on the electrode surface and needs no time to diffuse to the surface. The adsorbed reactant gives rise to an extra burst of charge as soon as the potential is stepped to E_2, but thereafter the response is unaffected by the adsorption. Hence, the total charge when adsorbed reactant is present will obey equation (4.4) instead of equation (4.3).

$$Q = 2FnAC^b\left(\frac{Dt}{\pi}\right)^{1/2} + Q_c + Q_{ads} \qquad (4.4)$$

where Q_{ads} is the extra charge produced by the adsorbed reactant. Under these conditions plots of Q versus (time)$^{1/2}$ will have intercepts that exceed Q_c by an amount of charge equal to Q_{ads}. This behaviour is displayed in line 2 of Figure 4.3. Note that the slope is unaffected by the adsorbed reactant. The values of Q_{ads} are direct measures of the quantity of reactant adsorbed because of Faraday's Law

$$Q_{ads} = FnA\Gamma \tag{4.5}$$

where Γ is the quantity of adsorbed reactant in moles per unit area. This relationship between the experimentally accessible parameter Q_{ads} and the quantity to be measured, Γ, that makes the technique valuable.

4.1.2 Double Potential Step Chronocoulometry[1]

As shown in Figure 4.3, to obtain Q_{ads} from the intercept of a chronocoulometric plot of Q versus $t^{1/2}$ it is necessary to know or measure Q_c. This causes no problem when the reactant adsorption produces little or no change in the interfacial capacitance so that the value of Q_c measured in a "blank" experiment (no reactant present, dashed line in Figure 4.2 (c)) applies to measurements in the presence of the adsorbing reactant. However, adsorption of the reactant often produces significant changes in the interfacial capacitance so that values of Q_c evaluated in the absence of the reactant do not apply when reactant is present.

This problem can be overcome by double potential-step chronocoulometry where the electrode potential is returned to its initial potential before the experiment is finished.[4] However, so far the theory has only been developed for the situation in which only the reactant is adsorbed according to the following scheme where the reactant is in oxidised form and the product R is not adsorbed.

$$O_{(aq)} \rightleftharpoons O_{(ads)} \tag{4.6}$$

$$O_{(ads)} + ne^- \rightleftharpoons R_{(aq)} \qquad (4.7)$$

Figure 4.4 shows the potential-, current- and charge-time responses obtained in such double potential-step experiment for cases where the product of the electrode reaction is re-oxidised when the potential is returned to the original value.

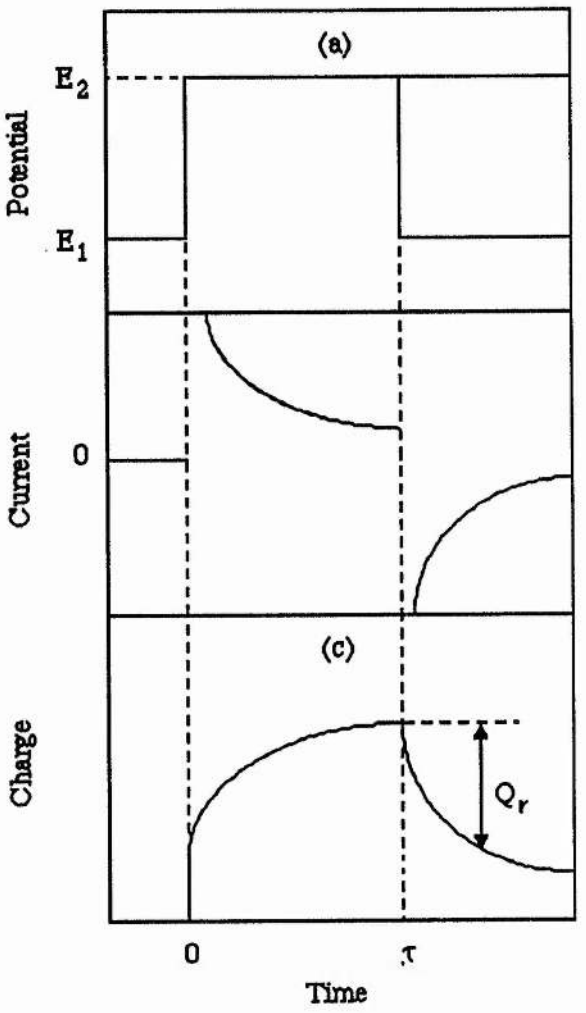

Figure 4.4

Temporal behaviour of: (a) potential, (b) current, and (c) charge in double potential step chronocoulometry.

The charge-(time)$^{1/2}$ plot of the data acquired during the first potential step (Figure 4.5, line 1) is, of course, identical to those obtained in the single-step experiment. So

long as neither the reactant nor the product of the electrode reaction are adsorbed, the charge, Q_r, (Figure 4.4) that passes following the second potential step is a linear function of $[\tau^{1/2} + (t - \tau)^{1/2} - t^{1/2}]$, where τ is the duration of the first step. The corresponding plot for data acquired during the second potential step is shown in line 2 of Figure 4.5. In cases where it is the reactant and not the product of the electrode

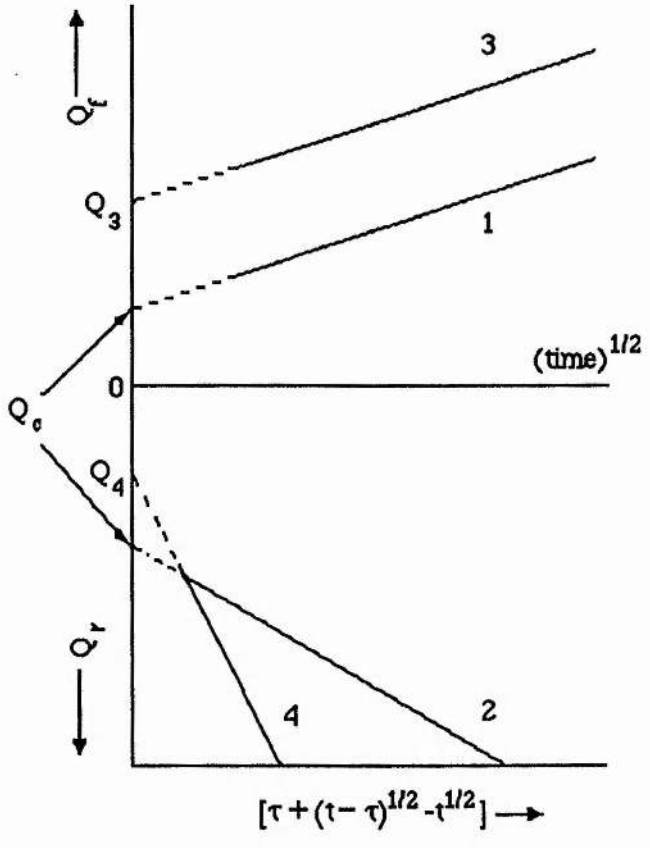

Figure 4.5

Chronocoulometric plots for double potential-step chronocoulometry. Lines 1 and 2 correspond to no adsorption of the reactant or product. Lines 3 and 4 correspond to reactant but not product adsorption.

reaction that is adsorbed, *e.g.* the reduction of a variety of d^{10} metal complexes to metal amalgams at mercury electrodes,[5] lines 3 and 4 are obtained and the intercept of the chronocoulometric plot for the reverse step (after a small correction is applied[6]) provides a direct measure of Q_c in the presence of adsorbed reactant.[6,7] Thus the difference between the two intercepts (Q_1 - Q_2) is directly related to the coverage: *i.e.*

$Q_3 - Q_4 = nFA\Gamma_o$. This feature of double potential-step chronocoulometry makes it useful for measuring the quantities of adsorbed reactants. Conversely, when the two chronocoulometric plots have equal (and opposite) intercepts, this is a good indication of the absence of reactant (or product) adsorption. With favourable experimental conditions the intercepts can be measured with a precision of $\approx \pm 0.5 \times 10^{-6}$ coul cm^{-2} which corresponds to an uncertainty in Γ of $\approx 5 \times 10^{-12}$ mole cm^{-2} (for a one electron reactant).

4.2 A.C. Impedance

4.2.1 Introduction

The excitation of the electrochemical cell by a sinusoidal signal and the analysis of the currents produced were first developed for measuring rate constants of fast electron transfer reactions.[8] In reactions which are fast the information from whatever measurement has to be obtained at short times, otherwise diffusion rather than kinetics becomes the rate determining process. The a.c. bridge was for a time the only instrumental technique available to allow measurements on the millisecond timescale and below, and the basis of present-day a.c. techniques and methods of analysis were worked out using an electrochemical cell at equilibrium as the unknown arm of a Wheatstone Bridge. Modern instrumentation allows a.c. measurements to be made far more expeditiously than with a manually balanced bridge, and so permitting the continuous recording of a.c. parameters under dynamic rather than equilibrium conditions, *e.g.* in cyclic voltammetry or polarographic experiments. At the other end of the timescale, a.c. techniques are now important in corrosion studies, where rapid response is of lesser importance than complete analysis of what are often complicated processes involving surface and solution reactions. Here, the efficient application of a wide spectrum of a.c. frequencies combined with modern computational methods have been essential in the application of a.c. methods.

4.2.2 A.C. Impedance for Measuring Adsorption onto the Electrode

Although a.c. impedance is a widely used technique for most electrochemical systems, the technique is used here to measure adsorption of the electroactive species onto the mercury electrode surface. The experiment is run as a normal a.c. impedance experiment recording Z_{imag} and Z_{real} as a function of frequency. Then the experimental data is converted into a measure of the double layer capacitance. This is done by using equation (4.8) which defines the relationship between double layer capacitance and the experimental factors. If a plot of double layer capacitance against voltage is considered then adsorption can be identified from the almost zero capacitance and spikes, known as pseudo capacitance, on either side of the adsorption.[9]

$$C = \frac{Z''}{\omega(Z'^2 + Z''^2)} \qquad (4.8)$$

where Z' the real impedance is defined as $Z_{real} = \frac{R}{1 + (\omega CR)^2}$, Z'' the imaginary impedance is defined as $Z_{imag} = \frac{\omega CR^2}{1 + (\omega CR)^2}$ and $\omega = 2\pi f$

This ability to detect adsorption makes this an ideal technique to help investigate the mechanism of carbon dioxide reduction where an adsorbed Ni(I) species is proposed as an catalytic species.[10,11]

4.3 A Study of the Adsorption of $[Ni(cyclam)]^{2+}$ onto Mercury

The most important surface for the reduction of carbon dioxide is mercury. The catalytic species is proposed to be an adsorbed Ni^{I} species which reacts with the carbon dioxide and transfers an electron to reduce the molecule. Chronocoulometry is used to determine how the species adsorbs. To determine the adsorption onto the electrode, the potential is stepped from -x V to 0 V (x varying from -0.20 V to -1.70 V vs SCE) and the plot of charge versus $t^{1/2}$ is recorded. To determine the amount of adsorbed charge the intercept of this plot is recorded and this is plotted against the

potential in volts. The data recorded is then corrected for any background adsorption by recording the same potential step with no complex present and subtracting this from the recorded data.

A 4.895 mM solution of $[Ni(cyclam)]^{2+}$ containing 0.1 M $NaClO_4$ was investigated under argon and also carbon dioxide to determine if there is any difference in the adsorption of the catalytic species under a carbon dioxide atmosphere.

4.3.1 Single Potential Step Chronocoulometry under Argon

Since the catalytically active species is proposed to be adsorbed onto the mercury surface then the chronocoulometry technique is ideal. To determine the adsorption of the reduced $[Ni(cyclam)]^{+}$, the potential is stepped from -x V to 0.0 V to generate the $[Ni(cyclam)]^{+}$ species. The charge obtained after subtracting the charge in the absence of complex is shown in Figure 4.6.

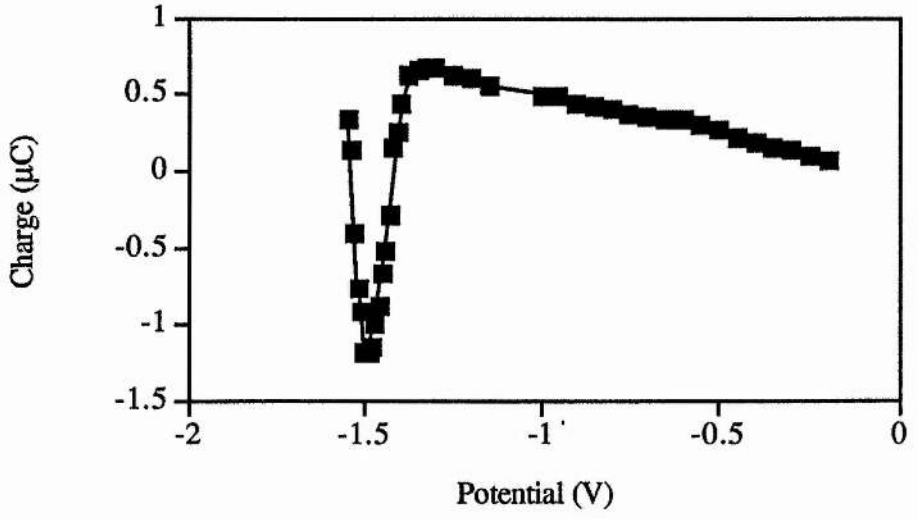

Figure 4.6

Charge versus potential plot for single step chronocoulometry of a 4.895 mM solution of $[Ni(cyclam)]^{2+}$ in 0.1 M $NaClO_4$ with a mercury electrode (area = 0.0139 cm^2) under argon. The potential is stepped from -x V to 0.0 V.

As seen from the graph the charge on the surface increases slowly to a maximum at -1.30 V, after which adsorption of the $[Ni(cyclam)]^+$ is masked by the minimum at -1.50 V. The $[Ni(cyclam)]^+$ can adsorb freely onto the mercury surface and hence become the catalytically active species. These results are very similar to those of Balazs and Anson[11] in the 0 to -1.40 V region, allowing for the difference in electrode area and the higher concentration of metal complex. The greater difference however lies in the region at $E_i < -1.40$ V.

4.3.2 Single Potential Step Chronocoulometry under Carbon Dioxide

Again the single potential step is repeated under carbon dioxide to determine whether there is any change in the adsorption. On stepping from -x V to 0.0 V to see the adsorption of [Ni(cyclam)]+ the major change under carbon dioxide is the increased amount of charge due to adsorbed species on the electrode (Figure 4.7) although the basic shape of the graph is the same. There is a greater amount of charge due to adsorbed electroactive species on the electrode surface at -1.20 V, which is the

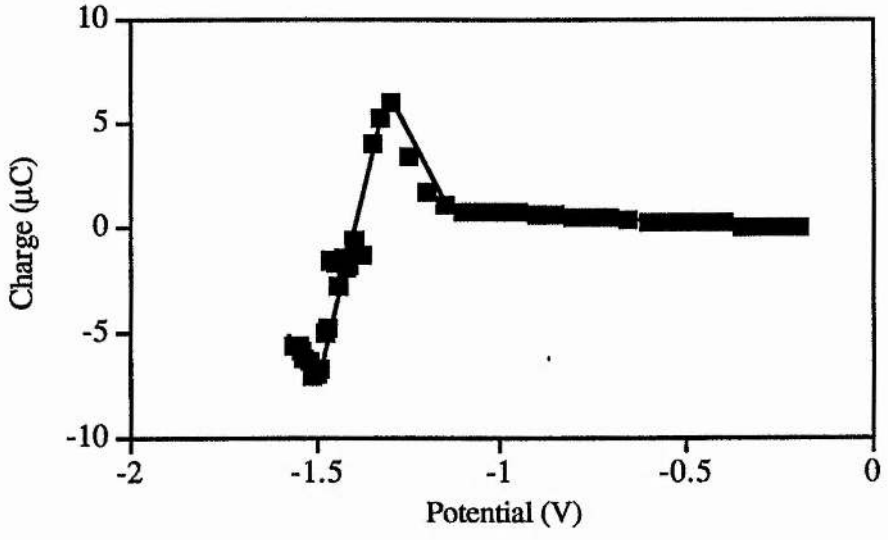

Figure 4.7

Charge versus potential plot for single step chronocoulometry of $[Ni(cyclam)]^{2+}$ with a mercury electrode under carbon dioxide.

The potential is stepped from -x V to 0.0 V. Other conditions as Figure 4.6.

potential at which the complex is thought to adsorb and undergo a rearrangement to give the catalytic species.[11] Our results agree with the adsorption occurring before the redox potential of the complex in solution although the potential is more negative in this work. Another curious feature in the plot is that the amount of charge also increases at -1.5 V.

The overall increased charge observed under carbon dioxide suggests that the carbon dioxide is promoting the adsorption of the $[Ni(cyclam)]^+$ onto the mercury surface. This enhanced adsorption is perhaps indicative of double layer charging effects with more $[Ni(cyclam)]^+$ interacting with the carbon dioxide via hydrogen-bonding, this effect is cancelled out using the double potential step method discussed below. Alternatively, it may be due to the build up of adsorbed $[Ni(cyclam).CO]^+$, which has been proposed as a poisoner of the surface reaction.

4.3.3 Double Potential Step Chronocoulometry under Argon

The double potential step method is used to determine the degree of adsorption of $[Ni(cyclam)]^+$ onto the electrode while correcting for changes which may occur in the double layer capacitance. As seen from Figure 4.8 there is a maximum in the adsorption at -1.40 V which is slightly before the redox potential of the complex. The occurrence of this peak maximum at a potential slightly less negative than the redox potential of the complex suggests that adsorption of the complex does occur at a potential less than the redox potential of the solution species, *i.e.* $[Ni(cyclam)]^+$ adsorbs before the $[Ni(cyclam)]^+$ is formed in solution. However, it is not as far away from the redox potential as suggested by Anson[11] (V) so it is not necessary to invoke the formation of a rearranged complex with an anodically shifted $Ni^{II/I}$ redox potential. Such a rearrangement is impractical since $[Ni(cyclam)]^{2+}$ is one of the most stable macrocycles (half life is 30 years in acidic conditions) and for the conversion to take place the Ni(II) or Ni(I) would have to come out of the plane of the macrocycle ring and allow some of the N-H bonds to interconvert to give one of the other less stable conformers (Figure 2.26).

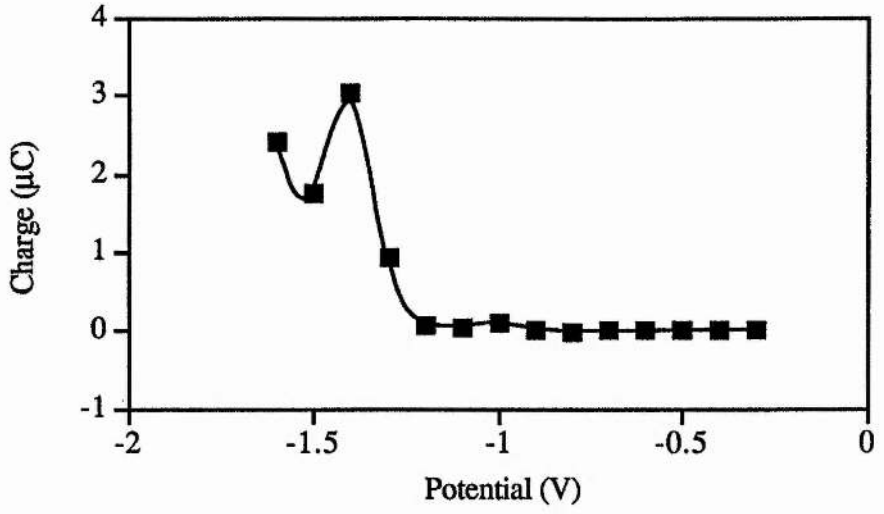

Figure 4.8

Charge versus potential plot for double step chronocoulometry of $[Ni(cyclam)]^+$ with a mercury electrode under argon. The potential is stepped from -x V to 0 V to -x V. Other conditions as in Figure 4.6.

4.3.4 Double Potential Step Chronocoulometry under Carbon Dioxide

As seen from Figure 4.9 there is no major change in the adsorption versus potential characteristics of $[Ni(cyclam)]^+$ under carbon dioxide. This result appears to favour the proposition that the increased charge observed in the single-step experiment (Figure 4.7) is due to changes in the double layer capacitance rather than the build-up of $[Ni(cyclam).CO]^+$. Since the curve closely matches the CV for the catalytic current (the adsorption maximum occurs at same potential as the catalytic current), it may indicate that the variation of Γ_{cat} with potential largely controls the shape of the cyclic voltammogram.

4.3.5 Determination of Diffusion Coefficient

The technique of chronocoulometry is also used to determine diffusion coefficients. The diffusion coefficient is obtained by stepping the potential to beyond the redox potential of the complex and recording the slope on the current versus $t^{1/2}$ graph. The diffusion coefficient is then calculated using the integrated form of

equation (4.1). A diffusion coefficient of 1.75 x 10^{-5} cm^2s^{-1} is obtained for $[Ni^{II}(cyclam)]^{2+}$ while for the reduced complex $[Ni^{I}(cyclam)]^{+}$, D = 7.67 x 10^{-6} cm^2s^{-1}. The diffusion coefficient for $[Ni(cyclam)]^{2+}$ is in fairly good agreement with that obtained by rotating disc electrochemistry (3.59 x 10^{-5} cm^2s^{-1}). The Ni^{I} moves more slowly through the solution although the difference is fairly small. This may indicate a lower degree of axial water co-ordination as discussed in Section 3.7.

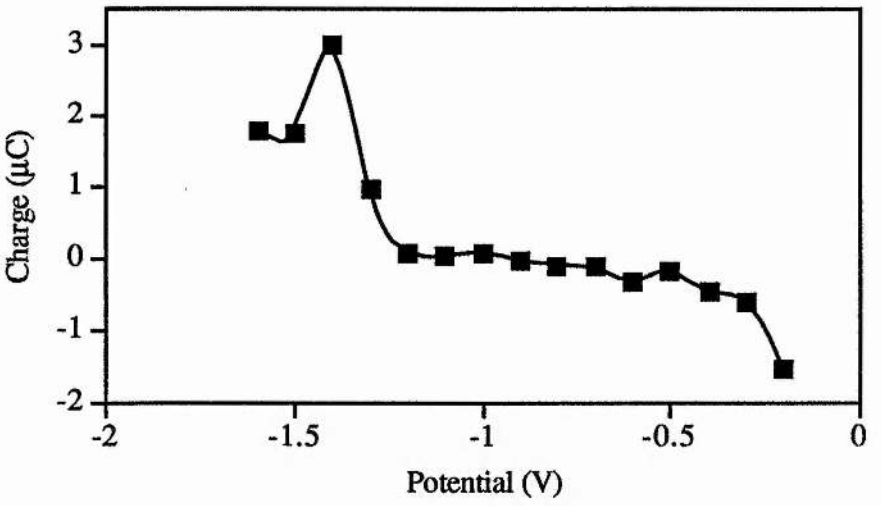

Figure 4.9

Charge versus potential plot for double step chronocoulometry of $[Ni(cyclam)]^{+}$ with a mercury electrode under carbon dioxide. The potential is stepped from -x V to 0 V to -x V. Other conditions as in Figure 4.6.

4.4 A Study of the Adsorption of $[Ni(cyclam)]^{2+}$ onto Copper

Since a copper electrode was found to be an active surface (Chapter Three) for the investigation of the $[Ni(cyclam)]^{2+}$ system, it was necessary to establish whether adsorption onto the surface was occurring as in the case of a mercury electrode. A detailed study of this adsorption is carried out using both the single and double potential step methods of chronocoulometry. A 4.895 mM solution of $[Ni(cyclam)]^{2+}$ containing 0.1 M $NaClO_4$ was investigated under argon and also carbon dioxide to determine if there is any difference in the degree of adsorption of the catalytic species

under a carbon dioxide atmosphere.

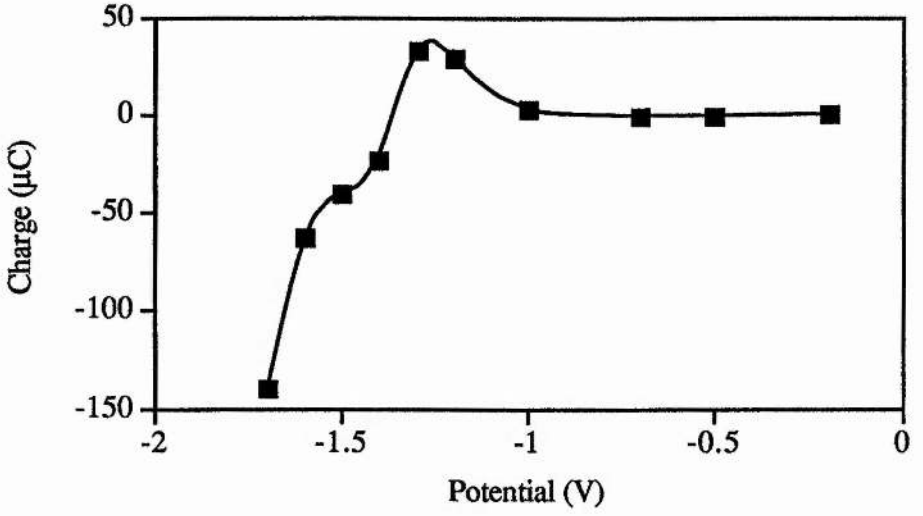

Figure 4.10

Charge versus potential plot for single step chronocoulometry of $[Ni(cyclam)]^{2+}$ with a copper electrode under argon. The potential is stepped from -x V to -0.1 V. Other conditions as in Figure 4.6.

4.4.1 Single Potential Step Chronocoulometry under Argon

The adsorption of the reduced species, $[Ni(cyclam)]^{+}$, onto the electrode surface was investigated. This is done by potential step measurements ranging from -x V to -0.1 V vs SCE, the potential is held at -x V for 30 seconds to allow the $[Ni(cyclam)]^{+}$ to form and to then adsorb onto the surface. The data is then corrected for charge measured in the absence of the nickel complex and is shown in Figure 4.10.

As seen from the graph, there is a large negative charge on the electrode at very negative potentials which is probably due to the reduction of adsorbed hydrogen (bubbles are observed on the electrode surface under these conditions). This adsorption at -1.20 V corresponds to the $[Ni(cyclam)]^{+}$ adsorption. This peak is similar to that obtained on mercury although the charge is much greater even when corrected for electrode area.

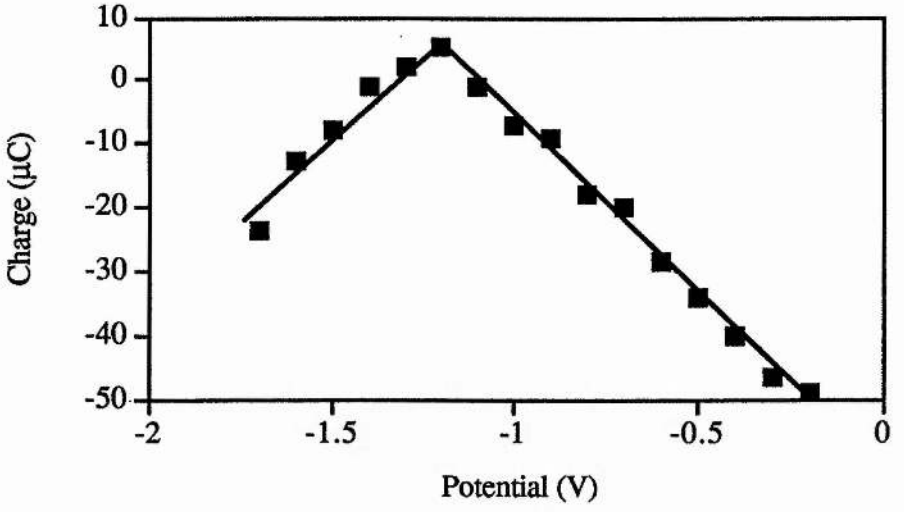

Figure 4.11

Charge versus potential plot for single step chronocoulometry of $[Ni(cyclam)]^{2+}$ with a copper electrode under carbon dioxide. The potential is stepped from -x V to -0.1 V. Other conditions as in Figure 4.6.

4.4.2 Single Potential Step Chronocoulometry under Carbon Dioxide

There is a major change in the charge due to $[Ni(cyclam)]^{+}$ adsorption (Figure 4.11) under carbon dioxide. Although there is still a small peak at -1.20 V there is less charge at more negative potentials, a feature which is more apparent when the graphs are overlaid (Figure 4.12). The reason for the reduction in the amount of adsorbed charge at negative potentials is because the carbon dioxide inhibits the hydrogen evolution reaction and so the charge on the electrode is due solely to the $[Ni(cyclam)]^{+}$ species.

The two small adsorption peaks coincide at -1.20 V, although under carbon dioxide the peak charge is much smaller. This is due to the small amount of adsorption of the $[Ni(cyclam)]^{+}$ species which corresponds to the pre-wave seen on the cyclic voltammogram on mercury. The lower degree of adsorption under carbon dioxide may indicate that the carbon dioxide is competing effectively for adsorption sites. No charge due to adsorbed carbon dioxide is observed as it is not electroactive in the potential range studied.

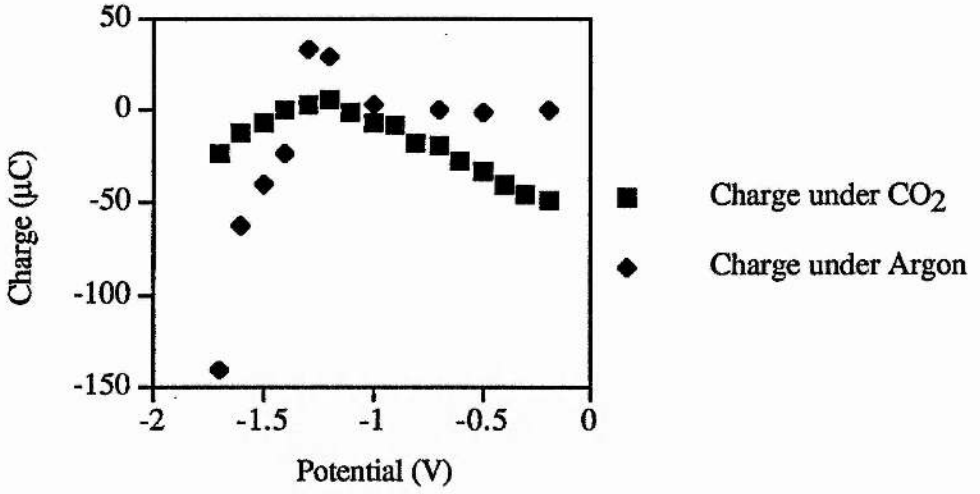

Figure 4.12

Comparison of the charge on the electrode under argon with carbon dioxide.

4.4.3 Double Potential Step Chronocoulometry under Argon

Here the potential is stepped from -x V to -0.1 V and back again to -x V. The charge is recorded for both the forward and backward reactions. The forward reaction is the oxidation of $[Ni(cyclam)]^{+}$ some of which is adsorbed onto the electrode and the backward reaction is the reduction of the $[Ni(cyclam)]^{2+}$ which one expects is not adsorbed significantly onto the electrode. So when the intercept of the chronocoulometric plot of the backward reaction is subtracted from the forward reaction we obtain a measure of the adsorption of the $[Ni(cyclam)]^{+}$ without any interference of the $[Ni(cyclam)]^{2+}$ adsorption. This method is better for studying the adsorption of the reduced species as there is no possible interference from any other species when measuring the charge present on the electrode.

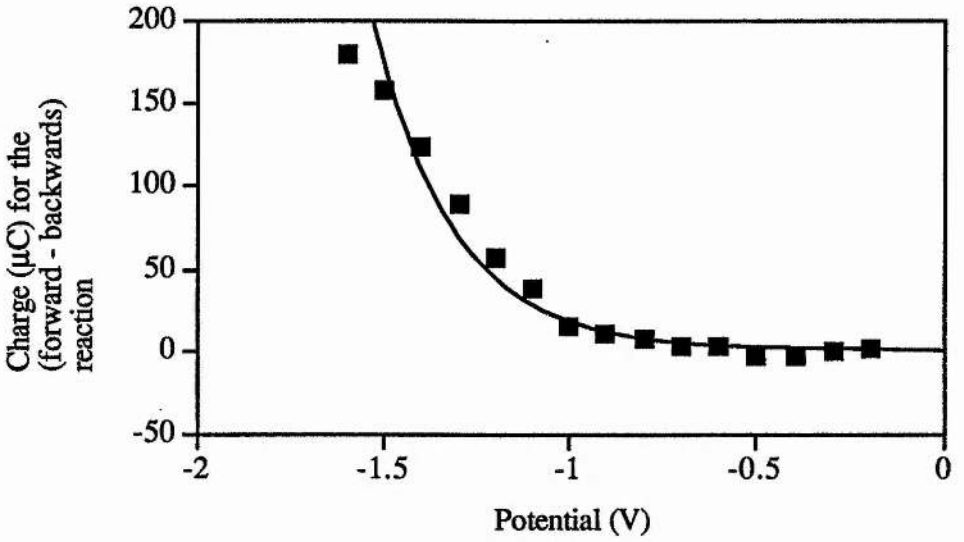

Figure 4.13

Charge versus potential plot for double step chronocoulometry of $[Ni(cyclam)]^{2+}$ with a copper electrode under argon. The potential is stepped from -x V to -0.1 V to -x V. Other conditions as in Figure 4.6.

As seen from Figure 4.13, the charge on the electrode increases dramatically from -1.0 V corresponding to the $[Ni(cyclam)]^{+}$ adsorption. The value of the charge is much higher than expected due to the interference from the hydrogen evolution reaction which leaves adsorbed hydrogen atoms on the copper surface.

4.4.4 Double Potential Step Chronocoulometry under Carbon Dioxide

When the double potential step experiment is repeated under carbon dioxide a decrease in the charge produced at negative potentials was observed (Figure 4.14). This effect is due to the carbon dioxide suppressing the production of hydrogen by the reduction of water at high negative potentials. Again we see a slight adsorption of the $[Ni(cyclam)]^{+}$ species on the copper electrode at -1.20 V.

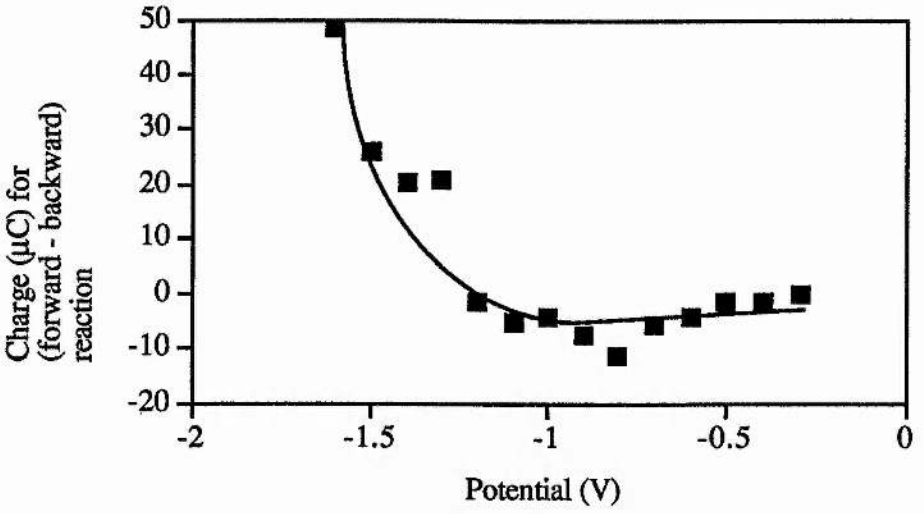

Figure 4.14

Charge versus potential plot for double step chronocoulometry of $[Ni(cyclam)]^{2+}$ with a copper electrode under carbon dioxide. The potential is stepped from -x V to -0.1 V to -x V. Other conditions as in Figure 4.6.

4.5.5 Determination of Diffusion Coefficients

An apparent diffusion coefficient of 2.43 x 10^{-3} cm^2s^{-1} is obtained for $[Ni(cyclam)]^{2+}$ and a diffusion coefficient of 1.09 x 10^{-3} cm^2s^{-1} is obtained for $[Ni(cyclam)]^{+}$. The diffusion coefficient is much higher than that obtained by rotating disc electrochemistry for $[Ni(cyclam)]^{2+}$ and reflects the interference of the hydrogen evolution reaction as well as corrosion of the copper surface.

4.5 A.C. Impedance on $[Ni(cyclam)]^{2+}$

A.C. impedance is another useful technique for determining the adsorption of a complex. Here a 15 mM solution of $[Ni(cyclam)]^{2+}$ was tested for adsorption onto a mercury electrode by running a variety of potentials ranging from -0.20 V to -1.50 V holding the potential while the frequency is changed from 65 kHz to 0.1 Hz. The double layer capacitance was then calculated for each point and a graph of capacitance as a function of potential was plotted (Figure 4.15).

As seen from the graph there are two areas of adsorption occurring over the

potential range of interest. There is an area of adsorption from -0.5 V to -0.9 V. This is the $[Ni(cyclam)]^{2+}$ adsorbing onto the electrode as at these potentials it is the only species present in the solution. The other area of adsorption occurs from -1.20 V to -1.50 V, this adsorption is due to the $[Ni(cyclam)]^{+}$ adsorbing onto the electrode surface. The adsorption occurs at a potential more positive than the redox potential of the $[Ni(cyclam)]^{2+}$ in solution. These results are in agreement with those obtained for chronocoulometry discussed earlier.

4.6 A Study of the Conformations of $[Ni(cyclam)]^{2+}$ by A. C. Impedance

To determine a possibility for the difference in reactivity between the two conformations of $[Ni(cyclam)]^{2+}$ for the reduction of carbon dioxide then the adsorption of both complexes onto the mercury electrode was tested. As the trans V is only stable in acidic conditions the a.c. impedance experiments were carried out in 0.1 M perchloric acid to prevent the isomerization occurring. The trans III isomer is also run in 0.1 M perchloric acid to do a complete comparison. A 1 mM solution of *cis*-$[Ni(II)cyclamBr_2]$ was dissolved up in 0.1 M perchloric acid and left to isomerize for a few days before the experiment was run. The results are shown in Figure 4.16 and Figure 4.17.

As seen from Figure 4.16 there are two regions of adsorption occurring over the potential range of interest. The first adsorption occurs from 0 V to -1.20 V, this corresponds to the adsorption of $[Ni(cyclam)]^{2+}$ onto the electrode, the next area occurs from -1.2 V to -1.6 V which corresponds to the $[Ni(cyclam)]^{+}$ adsorption. This is slightly different to the 15 mM solution run earlier where the $[Ni(cyclam)]^{2+}$ stopped adsorbing at -0.9 V, however there are often differences when concentrations vary. The adsorption effects are more often seen at low concentrations, hence in this system the effect seen is a change in the species being adsorbed at -1.20 V.

Figure 4.17 shows the trans V isomer under the same conditions. The effect here is one area of adsorption from -0.20 V to -1.70 V. This is the $[Ni(cyclam)]^{2+}$

adsorption and there is no adsorption of the $[Ni(cyclam)]^+$ onto the mercury. As the trans V conformation of $[Ni(cyclam)]^{2+}$ does not reduce carbon dioxide then it is this difference in the adsorption of the complex which causes the catalyst not to be active.

4.7 Conclusions

There is no significant adsorption of $[Ni(cyclam)]^{2+}$ onto a copper electrode but adsorption does occur on the mercury electrode. The $[Ni(cyclam)]^+$ adsorbs slightly onto copper but there is interference from hydrogen adsorption which is reduced in the presence of carbon dioxide as this inhibits the reduction. The $[Ni(cyclam)]^+$ adsorbs onto the mercury from -1.20 V, the single step method shows interference. A carbon dioxide atmosphere affects the adsorption of the active species onto the electrode.

A.C. impedance analysis of the complex also shows the adsorption of the $[Ni(cyclam)]^{2+}$ onto the electrode. There are two areas of adsorption on the capacitance versus potential graph indicating the two species, $[Ni(cyclam)]^{2+}$ and $[Ni(cyclam)]^+$, adsorbing. The two methods discussed give similar results for the $[Ni(cyclam)]^{2+}$ complex.

However for the trans V isomer of cyclam there is only one area of adsorption indicating that only the Ni(II) adsorbs and hence the catalytically active species does not adsorb onto the electrode. It is this lack of adsorption that affects the catalytic behaviour of this conformation.

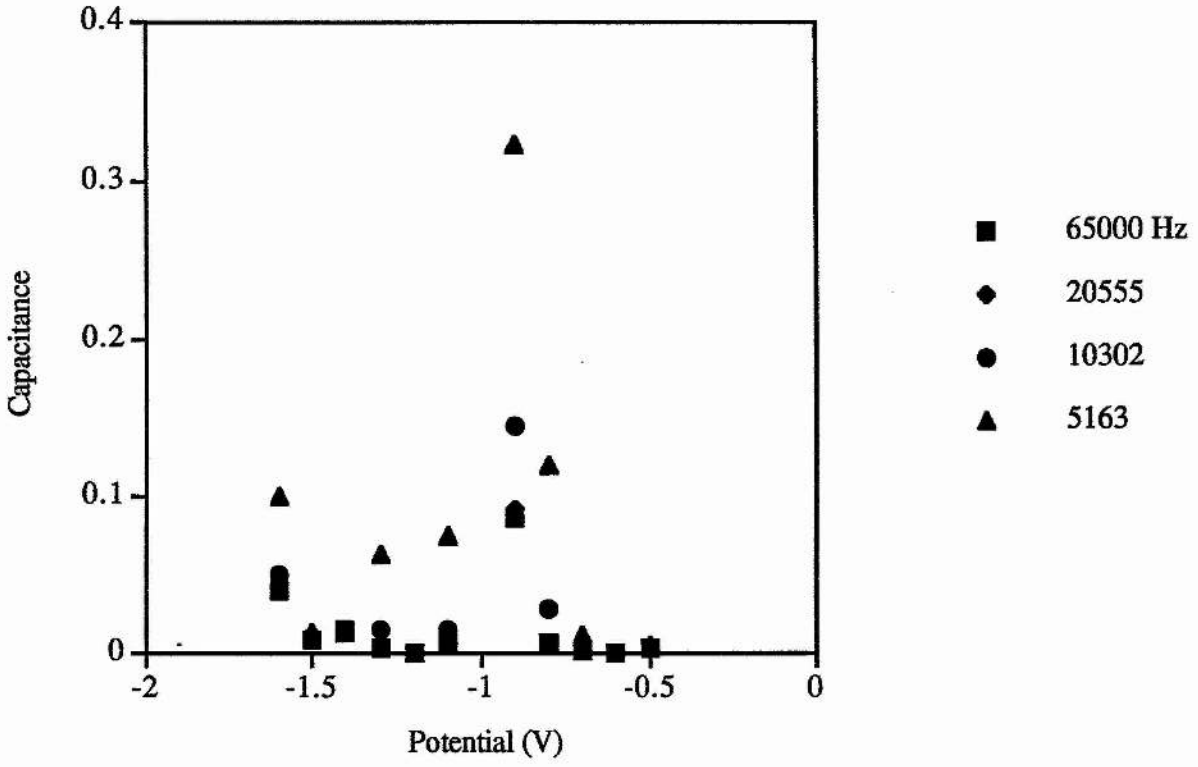

Figure 4.15

A plot of double layer capacitance as a function of potential for a 15 mM aqueous solution of $[Ni(cyclam)]^{2+}$ containing 0.1 M $NaClO_4$ with an mercury working electrode (area = 0.0139 cm^2).

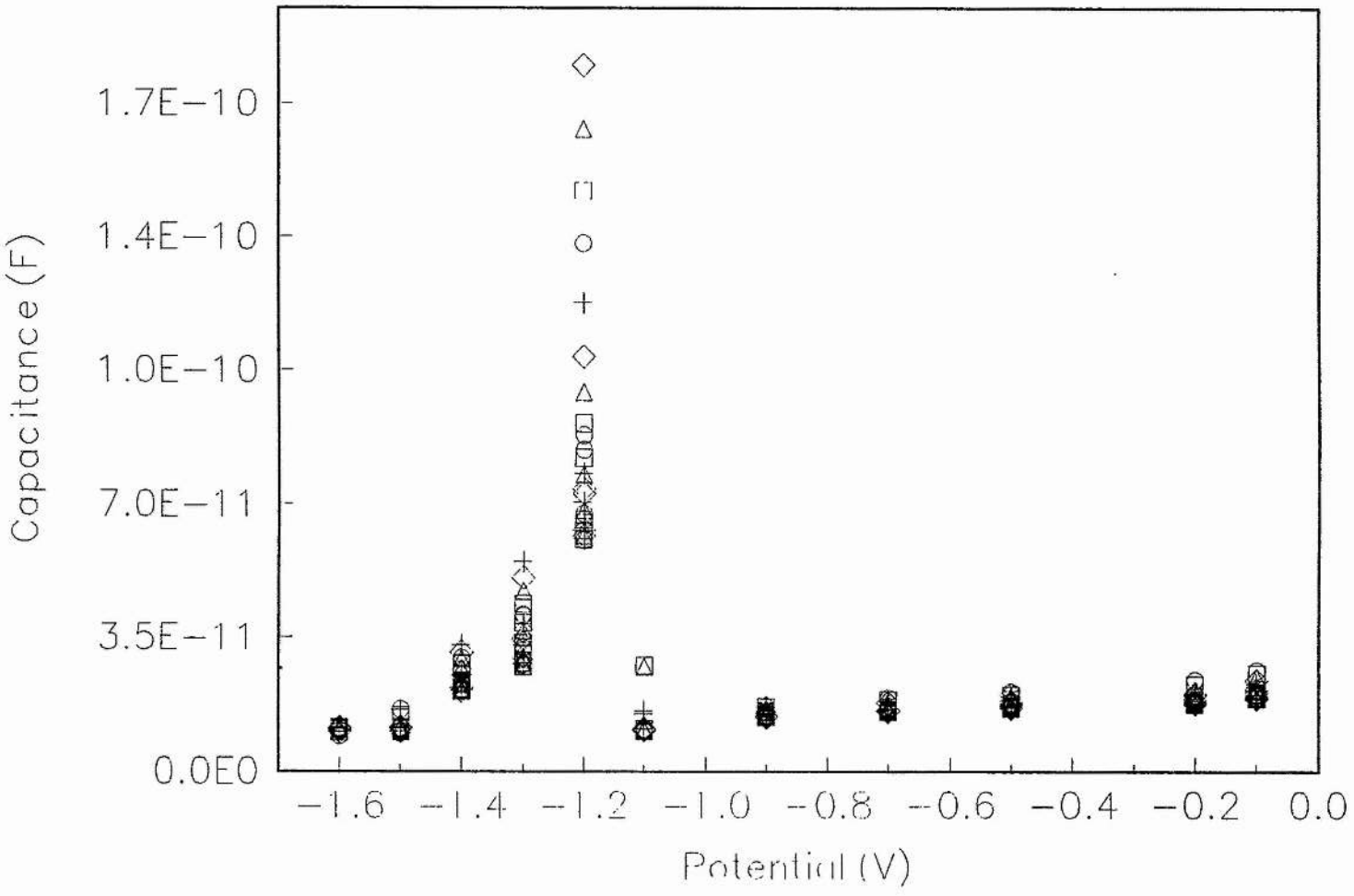

Figure 4.16

A plot of double layer capacitance as a function of potential for the trans III isomer of $[Ni(cyclam)]^{2+}$ in 0.1 M perchloric acid.

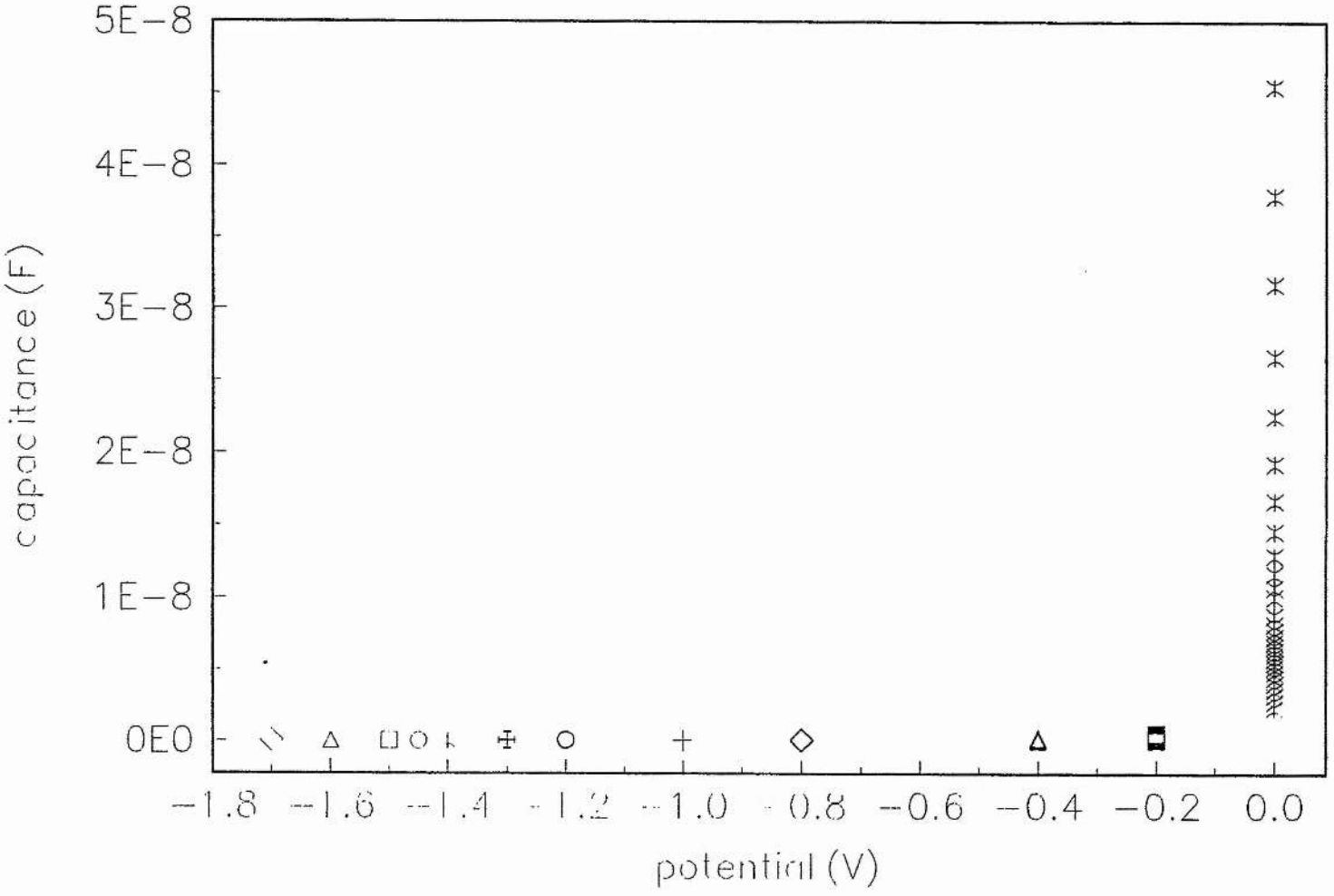

Figure 4.17

A plot of double layer capacitance as a function of potential for the trans V isomer of $[Ni(cyclam)]^{2+}$ in 0.1 M perchloric acid.

4.8 Experimental Section

Chronocoulometry was carried out with a 273 Parr Electrochemical System (EG & G, Wokingham, UK) and analyses of the data was carried out using a 486 Elonex computer. The chronocoulometry was carried out in an aqueous solution of 0.1 M sodium perchlorate as supporting electrolyte. The working electrode was either copper or mercury; the counter electrode was platinum and the reference electrode was a SCE.

A. C. impedance was carried out using an IBM compatible PC connected up to a Schlumberger Solatron 1286 electrochemical interface and a Schlumberger Solatron 1255 high frequency response analyser. The electrodes were connected with grounded coaxial cables to eliminate noise. The results were collected by the Z_{plot}/Z_{view} program from Scribner Association Inc. written by Derek Johnson with a M^{c}Donald fitting program. The graphs were obtained from the axum program.

Chapter Four References

1. F. C. Anson and R. A. Osteryoung, *J. Chem. Ed.*, 1983, 60, 293
2. F. G. Cottrell, *Z. Physik. Chem.*, 1902, **42**, 385
3. A. J. Bard and L. R. Faulkner, "Electrochemical Methods", John Wiley and Sons Inc., New York, 1980, Chapter 5
4. F. C. Anson, *Anal. Chem.*, 1966, **38**, 54
5. F. C. Anson, *Accts. Chem. Res.*, 1975, **8**, 400
6. J. H. Christie, R. A. Osteryoung and F. C. Anson, *J. Electroanal. Chem.*, 1967, **13**, 236
7. J. H. Christie, R. A. Osteryoung and F. C. Anson, *J. Electroanal. Chem.*, 1967, **13**, 343
8. Southampton Electrochemistry Group, "Instrumental Methods in Electrochemistry", Ellis Horwood Limited, Chichester, 1985
9. P. Delahay, "Double Layer and Electrode Kinetics", Interscience Publishers, 1965, Pg. 102
10. (a) M. Beley, J. P. Collin, R. Ruppert and J. P. Sauvage, *J. Am. Chem. Soc.*, 1986, **108**, 7461

    (b) M. Fujihira, Y. Hirata and K. Suga, *J. Electroanal. Chem.*, 1990, **292**, 199
11. G. B. Balazs and F. C. Anson, *J. Electroanal. Chem.*, 1992, **322**, 325

Chapter Five

A Survey of a Variety of Tetradentate Macrocycle and Chelate Complexes for Carbon Dioxide Reduction

5.0 Introduction

The saturated macrocyclic catalysts described in Chapter Two for the reduction of carbon dioxide have similar Ni(II/I) redox potentials but different behaviour towards carbon dioxide. For example, the $[Ni(isocyclam)]^{2+}$ complex[1] has a more positive redox potential for the Ni(II/I) reduction, and reduces carbon dioxide at a more positive potential, although with a reduced catalytic current. To lower the potential of the carbon dioxide reduction, one strategy would be to design a complex with a more positive Ni(II/I) redox potential. There is a usually a positive shift of around 200 mV when the reduction occurs: There are two methods for lowering the redox potential of the Ni(II/I) reduction, double bonds may be introduced into the macrocyclic structure; alternatively the nitrogen atoms may be alkylated (discussed in Chapter Two).

A limited number of [14] membered macrocycles with co-ordinated imine groups were available for investigation. It has been shown electrochemically by Busch *et al*[2] that such complexes are more easily reduced to Ni(I) due to delocalization of the charge onto the ligand. We were interested to find out whether compounds with higher values of E° ($Ni^{II/I}$) were active in carbon dioxide reduction, since less driving force would be required. Similarly, some Schiff base complexes have imino groups conjugated to phenyl rings for the delocalization of added electrons.

5.1 A Comparison of Ring Size on the Trans-[n]-Diene (n = 14 - 16) Complexes

The first macrocyclic complex to be synthesised was [Ni(trans-[14]-diene)]$^{2+}$ which was made by Curtis and Hay[3] in 1960. This was a one-pot ring closure on the $Ni(en)_3^{2+}$ centre. Subsequent papers[4] have dealt with the easier methods of preparation utilised here. Other complexes have since been added to the series, and their structures are shown in Figure 5.1. After preparing and characterising these complexes we carried out cyclic voltammetry experiments in the presence and absence

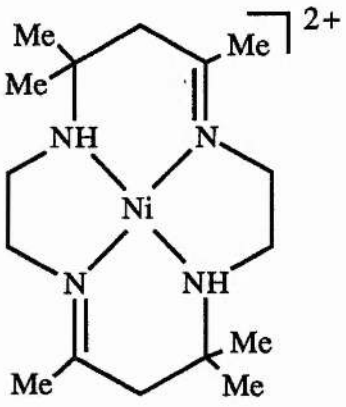

Ni(trans-[14]-diene)

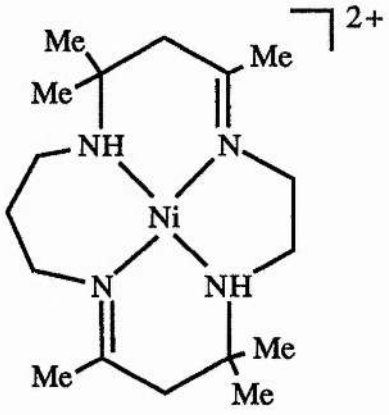

Ni(trans-[15]-diene)

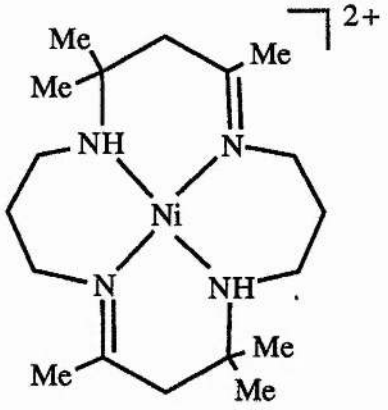

Ni(trans-[16]-diene)

Figure 5.1

Structures of the trans-[n]-diene complexes with n = 14 - 16

of carbon dioxide. The results of the electrochemistry of these complexes are shown

in Table 5.1. For comparison with $[Ni(cyclam)]^{2+}$ catalysis runs were also performed in 9:1 $MeCN/H_2O$ solvent.

As we can see from the table the redox potentials of the Ni(II/I) reduction follow the trend 14<15<16 which is the order expected. As the ring size increases the reduction becomes more facile because it is easier to accommodate the larger Ni^I cation. These results are in agreement with those obtained for the saturated [n]aneN_4 macrocycles discussed in Chapter Two.

					Reaction with CO_2		
Complex	Solvent	Electrode	Ni(II/I) (V)	Ni(III/II) (V)	i_{pa}	Δi_{pc}	E_{pc}
[14]diene	MeCN	Pt	-1.21 (60)	+ 1.32 (440)	-	-	-
	MeCN	GC	-1.19 (140)	+1.38 (360)	-	-	-
	MeCN	HMDE	-1.21 (100)	-	-	-	-
	9:1 $MeCN/H_2O$	GC/Hg	-1.23 (220)	-	0	no change	-1.34 V
	9:1 $MeCN/H_2O$	HMDE	-1.29 (100)	-	0	no change	-
[15]diene	MeCN	Pt	-1.21 (80)	+1.65 (180)	-	-	-
	MeCN	HMDE	-1.05 (420)	-	-	-	-
	9:1 $MeCN/H_2O$	HMDE	-1.40 (160)	-	0	no change	-1.44 V
[16]diene	MeCN	Pt	-1.09 (140)	not seen	-	-	-
	MeCN	HMDE	-1.15 (500)	-	-	-	-
	9:1 $MeCN/H_2O$	HMDE	-1.34 (520)	-	0	no change	-1.22 V

Table 5.1

Comparison of ring size for the trans-[n]-diene complexes for n = 14 to 16.

The figures in brackets denote the peak separation in mV.

The results demonstrate that the $Ni^{II/I}$ $E_{1/2}$ is considerably anodically shifted compared to $[Ni(cyclam)]^{2+}$. On bubbling carbon dioxide through the 9:1 $MeCN/H_2O$ solution the $Ni^{II/I}$ wave from the $[Ni(trans[n]diene)]^{2+}$ loses its reversibility, but there is no catalytic current. This suggests either: (i) the reduced complex irreversibly forms an adduct with carbon dioxide (EC reaction); or (ii) that electron transfer to carbon dioxide to give $CO_2^{\bullet-}$ is occurring; or (iii) that a carbonyl complex is formed. Reaction (ii) is unlikely, considering the difficulty in forming $CO_2^{\bullet-}$ (E° = -2.21 V). Regarding (iii), Gagne *et al*[5] reported that the CO binding constant for $[Ni^{I}(trans[14]diene)]^{+}$ is 4.7 x 10^4 M^{-1} in DMF, he also noted that the smallest K^{CO} corresponds to a more rigid macrocyclic structure and also to the smallest ring.

5.2 Macrocycles Derived from 1,2-diaminocyclohexane

A recent paper reported the synthesis of a variety of macrocycles prepared from 1,2-diaminocyclohexane.[6] Here the electrochemistry of an unsaturated nickel complex and its corresponding saturated complex is investigated. The structures are shown in Figure 5.2 and the results are summarised in Table 5.2.

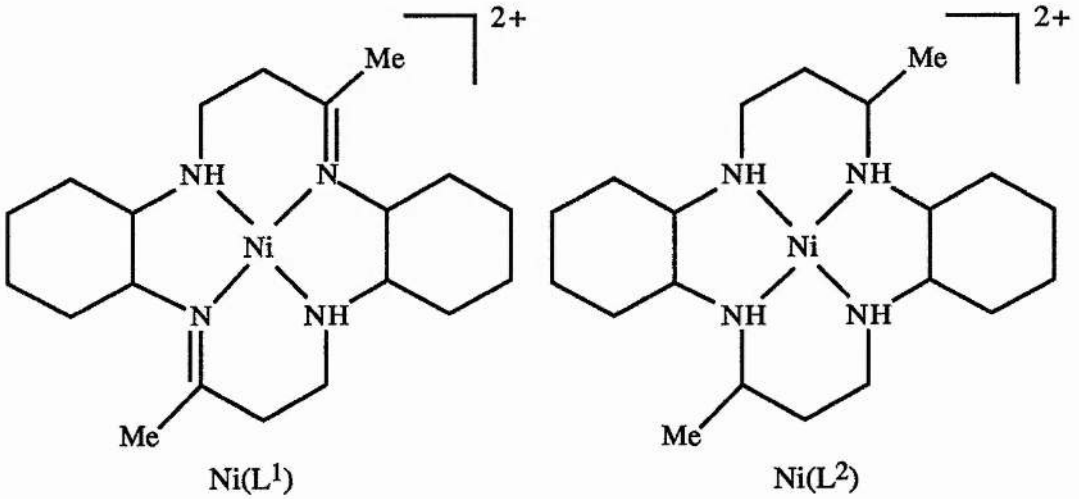

$Ni(L^1)$ $Ni(L^2)$

Figure 5.2

Structures of the macrocycles derived from 1,2-diaminocyclohexane.

Complex	Solvent	Electrode	Ni(II/I) (V)	Ni(III/II) (V)	Reaction with CO_2		
					i_{pa}	Δi_{pc}	E_{pc}
Ni(L^1)	MeCN	Pt	not seen	+0.36 (280)	-	-	-
	MeCN	HMDE	-1.14 (200)	-	0	no change	-1.24 V
	9:1 MeCN/H_2O	Pt	-1.11 (60)	-	-	-	-
	9:1 MeCN/H_2O	HMDE	-1.06 (200)	-	0	no change	-1.16 V
Ni(L^2)	MeCN	Pt	-1.26 (80)	+1.12 (80)	-	-	-
	9:1 MeCN/H_2O	HMDE	-1.34 (240)	-	0	no change	-1.46 V

Table 5.2

Comparison of various macrocycles derived from 1,2-diaminocyclohexane.

The figures in brackets denote the peak separation in mV.

As the complex is hydrogenated the redox potential of the Ni(II/I) reduction becomes more negative. This is due to the loss of the α-imine bonds which facilitate the reduction by lowering the $d_{X^2-Y^2}$ redox orbital, as seen for the other complexes discussed in this chapter. For Ni(L^1) the redox potential for the Ni(II/I) couple is at -1.06 V (200) in 9:1 MeCN/H_2O with a HMDE. When carbon dioxide is bubbled through the solution the reversibility of the peak is lost but there is no increase in the cathodic current. If the potential is taken more negative then a small cathodic current (88 μA) is observed at -1.78 V. However, when an argon atmosphere is allowed back into the cell the reversibility of the couple was not restored. This suggests that the carbon dioxide binds irreversibly to the complex or a carbonyl complex passivates the

electrode surface. As the reduction potential is very positive[5] then the binding constant for carbon monoxide would be quite small and hence the carbonyl formation is likely to be reversible.

For Ni(L^2) the Ni(II/I) reduction occurs at -1.34 V (240) in 9:1 MeCN/H_2O on a HMDE. The hydrogenation of the macrocycle causes a 280 mV lowering of the Ni(II/I) reduction. Consequently the reduction of carbon dioxide would occur at a less negative potential. Like Ni(L^1), when carbon dioxide is bubbled through the solution no catalytic current is observed. However, unlike Ni(L^1) the Ni(II/I) wave is completely restored when argon is allowed back into the cell.

Clearly these complexes do not reduce carbon dioxide catalytically, rather the unsaturated macrocycles undergo EC reactions, probably binding to carbon dioxide or carbon monoxide. In a previous chapter the saturated macrocycles were generally found to reduce carbon dioxide to an extent but in this case the saturated macrocycle Ni(L^2) does not. The unsaturated complex is more flexible than the saturated macrocycle and therefore is likely to have a higher CO binding constant.

5.3 Substituted [14] Dienes

There are a number of unsaturated [14]-membered ring dienes, two of which are shown in Figure 5.3. These complexes are easy to synthesise and as they are unsaturated macrocycles then the reduction potential for the Ni(II/I) reduction should be more positive than the corresponding saturated macrocycle. The results of the electrochemistry are summarised in Table 5.3.

As we can see from the table the presence of the phenyl groups as well as the presence of the α-imine group facilitate the Ni(II/I) reduction. Although the reduction is over 200 mV more positive than that of $[Ni(cyclam)]^{2+}$ there is no catalytic reduction of carbon dioxide. All that happens under carbon dioxide is that the reversibility of the peak is lost but there is no increase in the cathodic current. The reversibility of the wave is restored on returning an argon atmosphere to the cell. This behaviour closely resembles that of the related complex Ni(L^1).

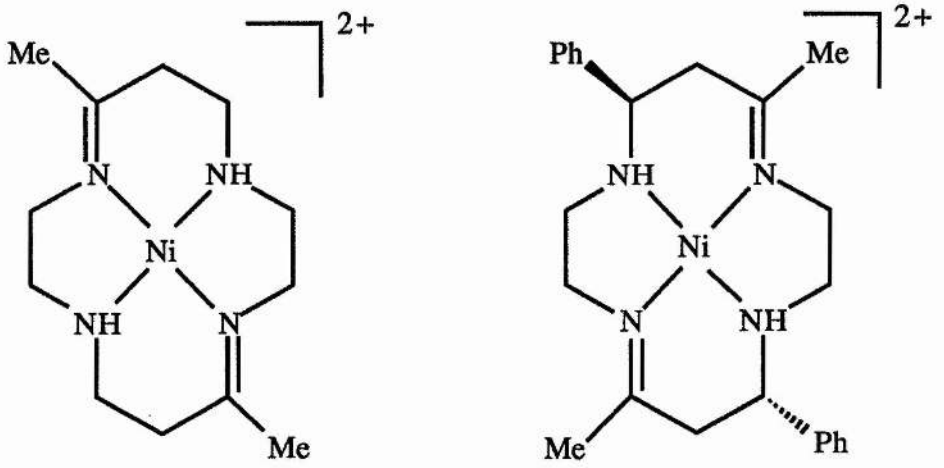

$[Ni(Me_2[14]diene]^{2+}$ $[Ni(Ph_2Me_2[14]diene)]^{2+}$

$Ni(L^3)$ $Ni(L^4)$

Figure 5.3

Structures of two alkyl substituted [14] dienes.

					Reaction with CO_2		
Complex	Solvent	Electrode	Ni(II/I) (V)	Ni(III/II) (V)	i_{pa}	Δi_{pc}	E_{pc}
$Ni(L^3)$	MeCN	Pt	-1.23 (60)	+1.11 (60)	-	no change	-1.28 V
	water	Au/Hg	-1.4 (i)	-	-	-	-
	water	GC/Hg	-1.46 (i)	-			-1.40 V
$Ni(L^4)$	MeCN	Pt	-1.14 (70)	+1.13 (60)	-	-	-
	MeCN	GC/Hg	-1.16 (120)	-	0	no change	-1.24 V
	9:1 MeCN/H_2O	HMDE	-1.15 (140)	-	0	no change	-1.20 V

Table 5.3

A comparison of the electrochemistry of some substituted [14] dienes.

The figures in brackets denote the peak separation in mV.

5.4 Complexes with Unsaturated Ligands Containing Conjugated Diimine Groups

5.4.1 [15]- and [16]-Membered Unsaturated Macrocycles

Here two larger membered rings were investigated to find how this affects the redox potential. The larger ring should have a less negative potential since it will accommodate the larger Ni^{I} cation more easily.

The two complexes discussed first (Figure 5.4) are structurally related to the [15]aneN$_4$ and [16]aneN$_4$ complexes discussed in Chapter Two. The results of the electrochemistry are summarised in Table 5.4. Ni(L^5) has an irreversible Ni(II/I) reduction at -0.86 V but there is no sign of the Ni(III/II) oxidation. The Ni(II/I) reduction is almost 1 V more positive than the saturated form ([15]aneN$_4$). For Ni(L^6) the Ni(II/I) reduction and the Ni(III/II) oxidation are not observed under these experimental conditions, possibly because the extended π-system and planarity causes the complex to adsorb strongly onto the electrode. A more positive redox potential for Ni(L^6) is expected compared to (Ni[16]aneN$_4$)$^{2+}$ because of the presence of the double bonds and the phenyl rings, however, in this case we are unable to observe these redox waves.

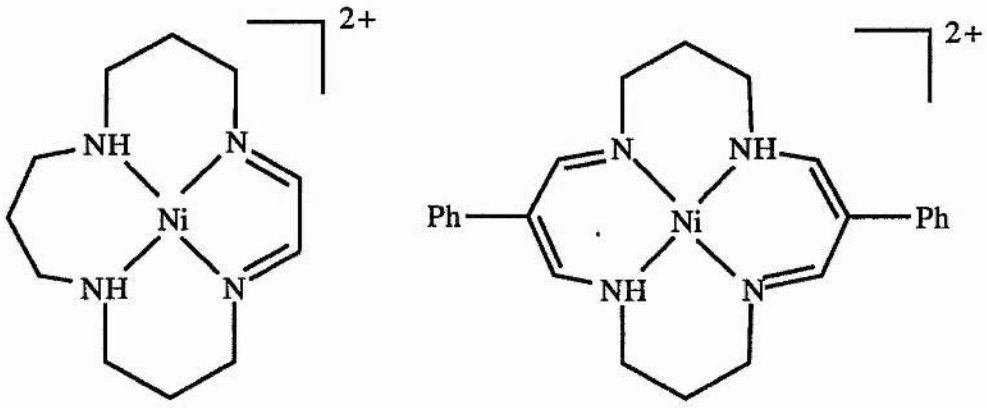

Ni(L^5) Ni(L^6)

Figure 5.4

Structures of the [15]- and [16]-membered unsaturated macrocycles.

					Reaction with CO_2		
Complex	Solvent	Electrode	Ni(II/I) (V)	Ni(III/II) (V)	i_{pa}	Δi_{pc}	E_{pc}
$Ni(L^5)$	DMF	Pt	-0.86 (i)	not seen	0	slight increase	-1.20 V
$Ni(L^6)$	DMF	Pt	not seen	not seen		no change	
	9:1 MeCN/H_2O	GC/Hg	not seen	not seen		no change	

Table 5.4

A comparison of some [15]- and [16]-membered unsaturated macrocycles.

For these complexes there is no reaction with carbon dioxide; although the $Ni(L^5)$ complex shows a small increase in the background current this is negligible in the overall discussion of catalytic carbon dioxide reduction. The lack of straightforward electrochemistry from these complexes suggested that there was strong irreversible adsorption onto mercury which led to partial or complete passivation of the electrode surface.

5.5.2 Electrochemistry of Nickel(II) (2,12-dimethyl-3,7,11,17-tetraazabicyclo [11.3.1] heptadeca-1(17),2,11,13,15-pentaene perchlorate

Nickel(II) (2,12-dimethyl-3,7,11,17-tetraazabicyclo [11.3.1] heptadeca-1(17),2,11,13,15-pentaene perchlorate (structure shown in Figure 5.5) in MeCN using a GC working electrode has a Ni(III/II) redox couple at +1.45 V (220) but the Ni(II/I) wave is not observed. However, using a platinum working electrode the Ni(III/II) couple is at +1.41 (140) and there are two couples in the cathodic region, one at -0.63 V (60), the $L \rightarrow L^-$ reduction, and the other at -1.20 V (40), the $Ni^{II} \rightarrow Ni^{I}$ reduction. Lewis *et al*[7] confirm the assignment of these reductions via ESR

spectroscopy and also showed that in the presence of π-acceptor ligands, e.g. CO, the $E_{1/2}(L^{0/-})$ shifts to positive potentials and the $E_{1/2}(Ni^{II/I})$ shifts to negative potentials. Using a HMDE the two redox waves are at -0.63 V (160) and -1.22 V (120). When carbon dioxide is bubbled into the solution the reversibility of the peaks is lost. Cathodic peaks are observed at -0.46 V, -0.76 V and -1.22 V. There is an increase in the current at -1.22 V (34.5 μA compared to 23.5 μA). Prolonged degassing with argon is required to return to the original voltammogram. Clearly, by analogy with Lewis *et al* the behaviour of the waves at -0.46 V and -1.22 V are consistent with the formation of the carbonyl adduct, which is then strongly adsorbed.

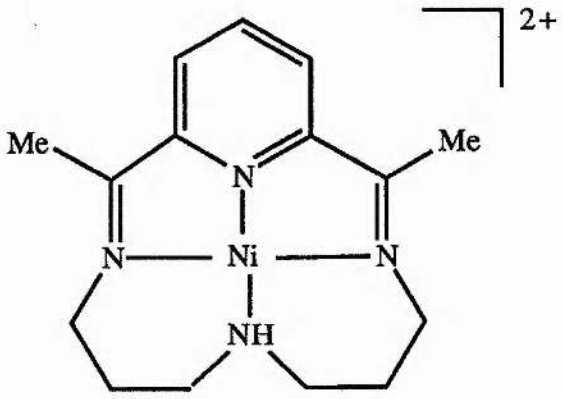

Figure 5.5

Structure of Nickel(II) (2,12-dimethyl-3,7,11,17-tetraazabicyclo [11.3.1] heptadeca-1(17),2,11,13,15-pentaene perchlorate, commonly denoted $[Ni(CR)]^{2+}$.

In 9:1 $MeCN/H_2O$ there are three redox waves, at -0.31 V (60), -0.65 V (60) and -0.98 V (40). When carbon dioxide is bubbled into the solution then the first two redox couples are not much affected at -0.34 V (40) and -0.70 V (0). The latter wave has zero peak separation and must be due to a surface-confined or adsorbed redox couple. However, the wave at -0.98 V is shifted to -1.08 V (i). There is also a large current (40 μA) at -1.34 V.

5.5.3 Electrochemistry of (2,3,9,10-tetramethyl-1,4,8,11-tetraazacyclotetradeca-1,3,8,10-tetraene) Nickel(II) Perchlorate

Nickel(II) (2,3,9,10-tetramethyl-1,4,8,11-tetraazacyclotetradeca-1,3,8,10-tetraene) perchlorate has two redox waves at -0.72 V (i) and -0.94 v (i) in an aqueous solution containing 0.1 M sodium perchlorate. Initially these were assigned to a ligand-based reduction and a metal-based reduction respectively. However, when carbon dioxide is present in solution there is only a slight shift (20 mV) of the redox waves in the positive direction. It is therefore probable that both of the observed waves actually correspond to step-wise reduction of each diimine group. However Busch *et al*[2] propose that the two reversible reductions are formally due to the Ni(I) and Ni(0) state. Upon the addition of carbon monoxide the ESR shows a d^9 metal with axial symmetry. The binding constant for this complex with CO is 1.7×10^2 M^{-1} which suggests that the CO does not bind as strongly to the Ni(I) centre as with other diimine complexes. The binding constant for the cobalt derivative with carbon dioxide is < 4 M^{-1} which indicates no detectable binding.[8] Usually the corresponding nickel complexes have smaller binding constants.

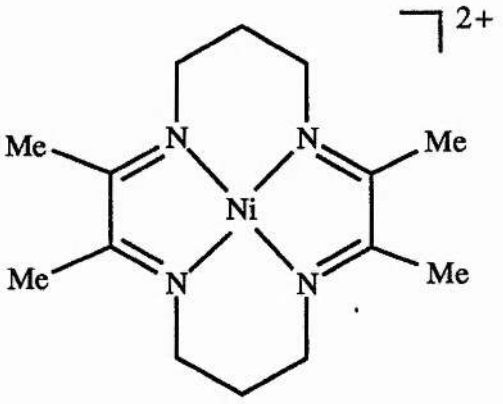

Figure 5.6

The structure of (2,3,9,10-tetramethyl-1,4,8,11-tetraazacyclotetradeca-1,3,8,10-tetraene) Nickel(II) perchlorate, commonly called $[Ni(TIM)]^{2+}$.

This is similar to the tetraaza[14]annulenes which have been studied to a

certain extent although not to the same degree as other complexes for the electrochemical reduction of carbon dioxide. One particular complex is found to be active[9] when polymerised onto the electrode. The catalytic reduction of carbon dioxide occurs at -1.85 V versus SSCE with only formate ion as the product of the electrolysis. Although $[Ni(TIM)]^{2+}$ resembles the tetraaza[14]annulenes there is no apparent catalytic reduction of the carbon dioxide.

A related copper(II) TIM macrocycle was synthesised to determine whether the copper(II) centre would be active for carbon dioxide. The macrocycle copper(II) (structure shown in Figure 5.7) was synthesised and isolated as the chloride, bromide and perchlorate salt. With the chloride and bromide complex there is a ligand based reduction observed at -1.65 V (180, qi) and the Cu(III/II) oxidation is observed at +1.0 V (120), the oxidation of the chloride and bromide ions is also seen at large positive values. There is no Cu(II/I) reduction observed, this is usually a very broad wave at around -0.4 V[10] but in this case it is obscured by the background current.

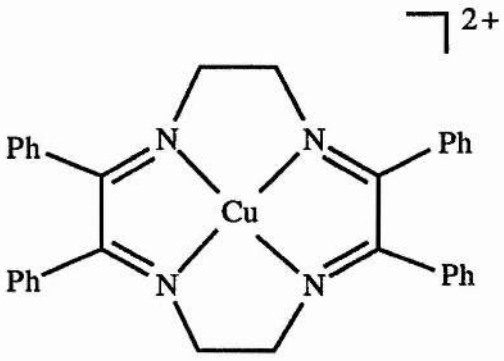

Figure 5.7

Structure of $[Cu(Ph_4[12]TIM)]^{2+}$.

Another feature is the large anodic peak observed at -0.28 V which is due to the Cu(0) plating out onto the electrode. The ease of this plating out is attributed to the Cu sitting atop of the macrocyclic ring. The copper(II) ion is too large to fit in the cavity of the [12]-membered macrocycle and so the ion sits above the cavity. There is also co-ordination of the anion to give a five co-ordinate copper complex (this was

determined by conductivity studies which proves that these complexes are 1:1 electrolytes), this extra co-ordination stabilises the macrocycle. With the perchlorate salt the reduction potentials are the same but there is no corresponding oxidation of the anion.

5.4.4 Electrochemistry of Nickel(II) Tetraphenylporphyrin

Part of the inspiration for our investigation was to find a nickel macrocycle that would mimic the function of the co-factor (F430M) found in methanogenic bacteria. It was of interest therefore to examine a similar type of macrocycle with a [16]-membered unsaturated ring close to that found in the co-factor. One of the closest type to this natural compound is the porphyrin system. The simplest porphyrin to synthesise is tetraphenylporphyrin which is made by a condensation reaction between pyrrole and benzaldehyde.[11] The nickel complex is then made and tested for catalytic activity.

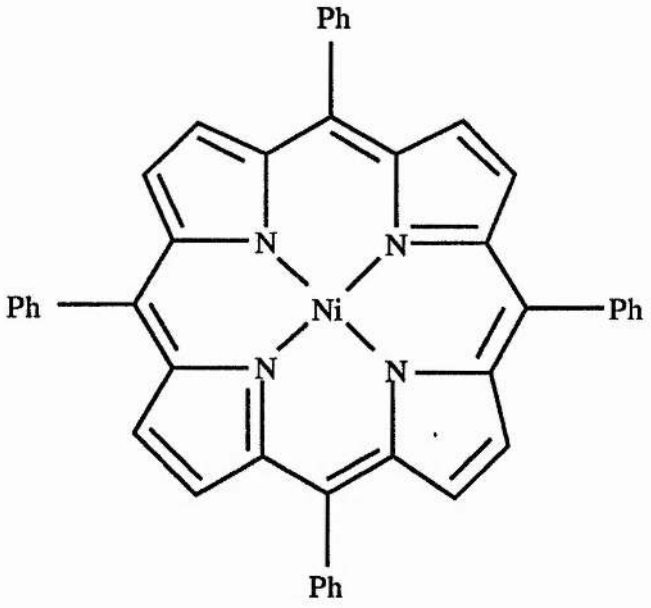

Figure 5.8

The structure of nickel(II) tetraphenylporphyrin

The electrochemistry of this porphyrin was studied to determine the interaction

of the reduced form with carbon dioxide. However, the Ni(II/I) reduction could not be observed, nor were the expected two ligand based reductions at around -1.6 V.[2,12] The nickel(II) tetraphenylporphyrin is insoluble in most common organic solvents apart from DMF. The experiments were run in 9:1 DMF/H_2O but again no reduction of carbon dioxide was observed. Once again it is likely that these unsaturated macrocycles are irreversibly adsorbed onto the electrode.

5.5 Electrochemistry of Schiff Base Complexes

Although schiff base complexes are not macrocycles but anionic complexes there has been a report[13] where the complexes [Co(salen)] and [Co(salophen)] reduce carbon dioxide, but these complexes require the complexation of a lithium or sodium ion in order for the reaction to proceed. The carbon dioxide interacts with the [Co(salophen)Li] to give a head to tail dimer complex which is C-bonded to cobalt and further stabilised by the lithium ion. The electron addition to the latter, followed by elimination of carbonate ion yields a cobalt carbonyl complex which slowly releases carbon monoxide.

5.5.1 Cyclic Voltammetry

Once again some difficulties were encountered in finding a good solvent for these complexes . Ni(salen) and Ni(nitro-salen) were the only complexes studied to show reversible Ni(II/I) waves in acetonitrile so DMF was the preferred solvent for the study.

The reduction of [Ni(salen)] to $[Ni(salen)]^-$ occurs at -1.66 V (280) with a pre-peak at -1.58 V perhaps due to the complex being adsorbed onto the electrode. Under carbon dioxide a cathodic current increase is observed at -1.84 V (E_{pc}). The catalytic current produced is 56 μA. Currents up to 200 μA have been recorded, but they are unreliable. The reason for this variability is unknown at present. An anodic peak is seen at -0.16 V which is assigned to the $[Hg(salen)]^{2+/0}$ couple.

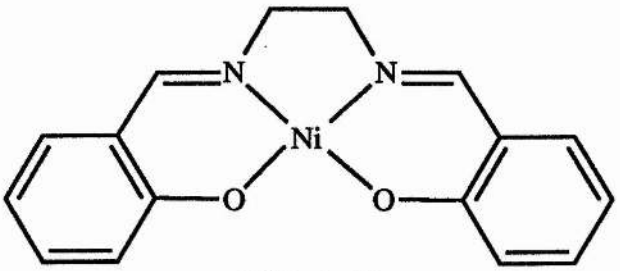

[Ni(salen)]

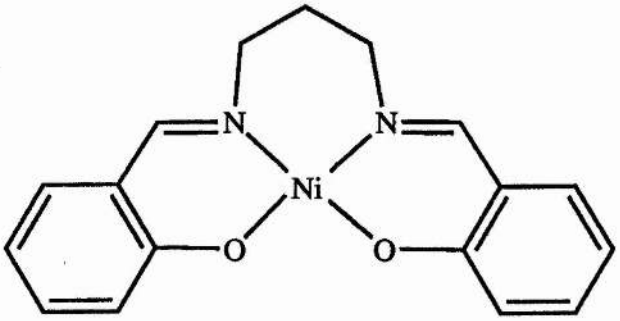

[Ni(salpen)]

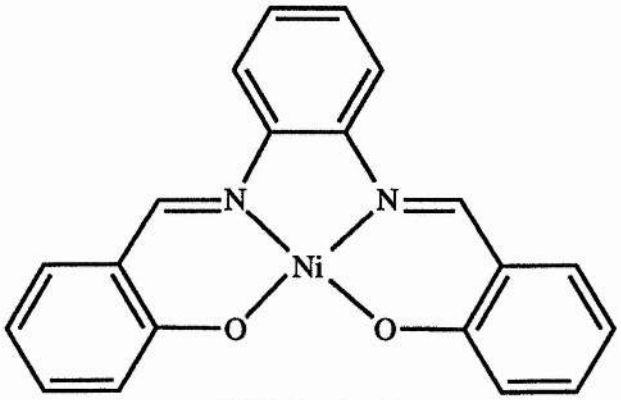

[Ni(salophen)]

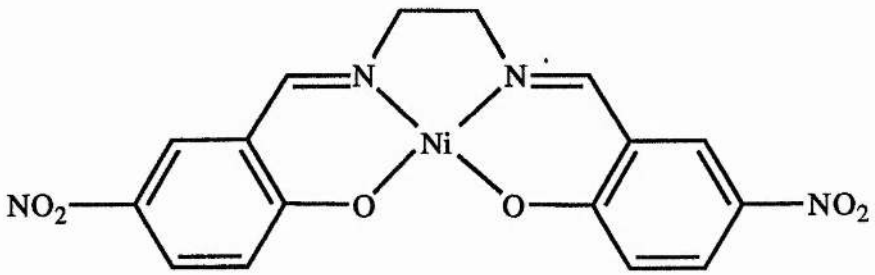

[Ni(nitrosalen)]

Figure 5.9

Structures of a variety of nickel(II) schiff bases.

					Reaction with CO_2		
Complex	Solvent	Electrode	Ni(II/I) (V)	Ni(III/II) (V)	i_{pa}	Δi_{pc}	E_{pc}
Ni(salpen)	9:1 DMF/H_2O	HMDE	-1.38 (i)	-	0	12 μA	-1.68 V
Ni(salophen)	9:1 DMF/H_2O	HMDE	-1.56 (i)	-	0	25 μA	-1.86 V
Ni(salen)	MeCN	Pt	-1.62 (40)	+0.99 (260)	0	-	-
	MeCN	HMDE	-1.67 (340)	-	0	66 μA	-2.02 V
	9:1 DMF/H_2O	HMDE	-2.01 (260)	-	0	74 μA	-1.70 V
Ni(nitro-	MeCN	GC	-	-	-	-	-
salen)	MeCN	HMDE	-1.69 (260)	-	-	-	-
	9:1 DMF/H_2O	HMDE	-2.82 (i)	-	-	-	-

Table 5.5

A comparison of the various nickel(II) schiff base complexes.

The figures in brackets denote the peak separation in mV.

In contrast for [Ni(salophen)] under argon the one-electron reduction of [Ni(salophen)] to [Ni(salophen)]$^-$ occurs at -1.56 V. The anion is known to dimerise to [Ni(salophen)]$_2^{2-}$,[14] which is then oxidised at -0.86 V. This is consistent with the site of the reduction being on the ligand rather than the metal. When carbon dioxide is bubbled through the solution new cathodic peaks are observed at -0.39 V and -1.19 V, possibly due to adsorbed species, while the Ni(II/I) couple is shifted to -1.48 V. The shift represents binding of the carbon dioxide to the Ni(I) species. A large reduction peak is then observed at -1.88 V, which is coupled to an anodic peak at -0.05 V. The latter peak may be associated with a Ni-CO complex or perhaps the [Hg(salophen)[$^{2+/0}$ couple.[15]

[Ni(salpen)] is reduced irreversibly at -1.38 V under argon but there appeared to be no associated dimer product peak. Under carbon dioxide, however, the electrochemistry of this complex is very similar to that of [Ni(salophen)]; the potentials and currents are given in Table 5.5. However, unlike [Ni(salophen)] the peak due to the dimeric species is also observed in the presence of carbon dioxide but not under argon. Like Ni(salophen), the anodic peak near -0.05 V becomes more pronounced when the potential is swept more cathodically than -1.80 V. Therefore, the peak at -1.90 V probably represents a reductive demetallation of the complex, leading to $[Hg(salpen)]^0$ which is then oxidised by two electrons at -0.05 V.

The reduction of [Ni(nitrosalen)] is difficult to observe because of the insolubility of the complex ($\leq$ 1 mM) in all common solvents. The value of $E_{1/2}$ in MeCN was surprisingly close to that of Ni(salen). It was expected that the electron-withdrawing nitro group should permit the easier removal of an electron from the nickel. Despite this similarity Ni(nitro-salen) differed in its lack of reaction with carbon dioxide.

5.5.2 Rotating Disc Electrochemistry

Rotating disc electrochemistry was run in 9:1 DMF/H_2O in order to obtain the diffusion coefficients of the complexes, summarised in Table 5.6. While running these experiments there was a problem with the complexes polymerising onto the electrode. This problem is minimised by keeping the electrode out of the solution as much as possible and polishing the electrode when the background becomes very noisy.

As we can see from the table the diffusion coefficient again follows the size of the molecule. The diffusion coefficients are lower than obtained for $[Ni(cyclam)]^{2+}$ because of the phenyl rings attached to the ring.

Complex	D (cm^2s^{-1})
Ni(salen)	1.08×10^{-5}
Ni(salpen)	8.69×10^{-6}
Ni(salophen)	2.23×10^{-6}

Table 5.6

A comparison of diffusion coefficients for schiff base complexes obtained in 9:1 MeCN/H_2O containing 0.1 M TBAT.

5.5.3 Electropolymerisation of Nickel(II) Salen

In MeCN at a GC electrode the Ni(III/II) redox couple is at +0.98 V (560) and the Ni(II/I) redox couple is at -1.76 V (440). On continual scanning between -2.25 V and +1.5 V (Figure 5.10), the Ni(II/I) couple disappears and the Ni(III/II) redox couple grows (and broadens), while at the same time a new peak grows in at +0.5 V. On removing the electrode from the solution an orange-yellow powdery film was seen on the electrode. By placing the electrode in fresh MeCN a Ni(III/II) couple is seen at +0.95 V (900) but there is no sign of a Ni(II/I) couple. Electropolymerisation has been reported by Bedioui *et al*,[16] but the resulting modified electrode has not been tested for activity towards carbon dioxide reduction.

Instead of scanning over the entire range, polymerisation was carried out between 0 V and +1.1 V (before polymerisation Ni(III/II) = +0.98 V (560) and Ni(II/I) = -1.62 V (240)). After polymerisation there is no Ni(II/I) couple and only a large reversible current at the Ni(III/II) couple. Placing this polymer electrode into fresh MeCN allows the observation of a Ni(III/II) redox couple at +0.86 V (400) and a Ni(II/I) redox couple at -1.82 V (400) (Figure 5.11 (a)). Bubbling carbon dioxide into this solution causes the Ni(II/I) couple's reversibility to be lost but a small catalytic current of 95 μA at -1.82 V (Figure 5.11 (b)). This current is only apparent on the first scan (the current decreases until it reaches background levels). On degassing with argon the original CV returns with the Ni(III/II) at +0.81 V (180) and

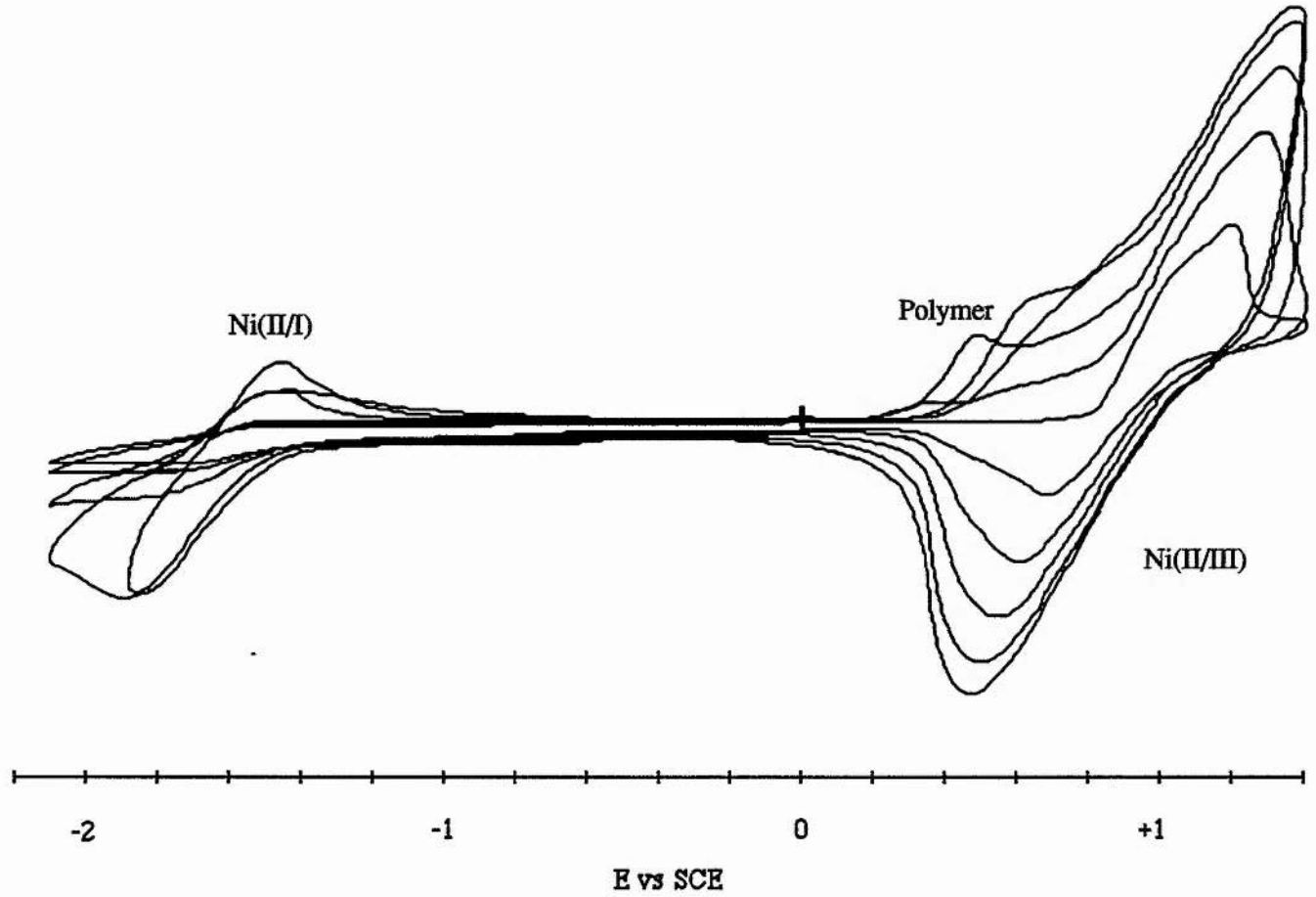

Figure 5.10

Electropolymerisation of [Ni(salen)] in MeCN + 0.1 M TBAT onto a GC electrode. The first five scans are shown only.

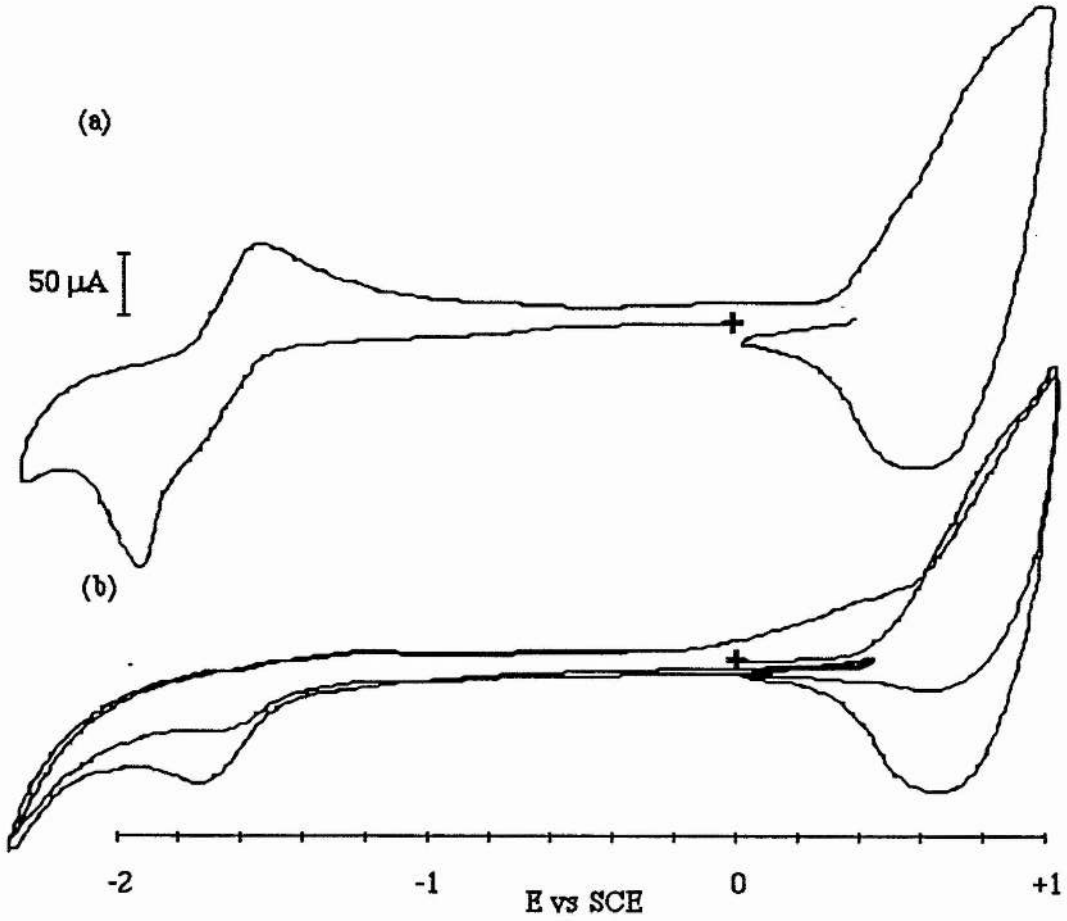

Figure 5.11

A cyclic voltammogram of electropolymerised [Ni(salen)] on GC in MeCN + 0.1 M TBAT (a) under argon and (b) under carbon dioxide.

the Ni(II/I) at -1.68 V (120). If water is added to the solution then the catalytic current, as well as the normal electroactivity of the polymer, is lost. This behaviour suggests that this polymer electrode could be used as a sensor for carbon dioxide, but only in the absence of water *i.e.* in the solid-state or in non-aqueous solution.

5.6 Conclusions

Unsaturated macrocycles have a less negative Ni(II/I) reduction and a more positive Ni(III/II) oxidation. This is caused by delocalization of charge onto the C=N bonds in the macrocycle, so facilitating the reduction. Although the reduction is more positive there is no catalytic reduction of the carbon dioxide. Some complexes do bind carbon dioxide or its reduction product, carbon monoxide, but this is usually irreversible.

The reduced imine groups are highly reactive leading to side reactions such as dimerisation and polymerisation or hydrolysis. Further complications can arise when unsaturated ligands with extensive π-systems are irreversibly adsorbed onto the electrode leading to passivation.

The N_2O_2 chelate complex Ni(salen) and its relatives did show some catalytic activity but in several cases the reduction was complicated by side reactions such as dimerisation. In the future these side-reactions could be minimised by designing such complexes with blocking groups at the coupling sites.

5.7 Experimental Section

Infra-red spectra were recorded as KBr discs on a Perkin Elmer 1710 Infra-red Fourier Transform Spectrometer.

NMR spectra were recorded using a Varian Gemini-200 Spectrometer (200 MHz) and a Bruker AM300 NMR Spectrometer (300 MHz).

Electronic spectra were recorded on a Philips PU8720 scanning spectrometer and a Perkin-Elmer Lamda 5 spectrometer against a background of pure solvent.

Elemental analyses were carried out in house at St. Andrews by Mrs Sylvia Smith.

Cyclic voltammetry was carried out with a Pine Instruments RDE 4 (EG & G, Wokingham, UK) potentiostat with a Graphtec XY Recorder WX2300. The CV's were obtained in high performance liquid chromatography grade (hplc) acetonitrile or dimethylformamide with 0.1 M tetrabutylammonium perchlorate or tetrabutylammonium tetrafluoroborate as supporting electrolyte or in aqueous solutions with 0.1 M sodium perchlorate as supporting electrolyte. The working electrode was either mercury (Metrohm Hanging Mercury Drop Electrode, HMDE with drop surface area 1.39 mm^2), platinum, glassy carbon, glassy carbon-mercury amalgam, copper or a gold-mercury amalgam; the counter electrode was platinum wire and the reference electrode was a SCE. After fabrication solid electrodes were polished firstly with successively finer grades of wet/dry paper (#120, 240, 600, 800). Thereafter polishing with diamond paste (Engis) of grade 6, 1 and 0.25 μm was carried out, with 5 minutes sonication in distilled water between grades. Alternatively, grades alumina 3, 1 and 0.5 μm (Buehler) were used instead of the diamond paste. If necessary, during an experiment the electrode was repolished at the finest grade of alumina.

Rotating disc electrochemistry was carried out with a Pine Instruments RDE 4 (EG & G, Wokingham, UK) potentiostat and a Pine Instruments rotator with a Graphtec XY Recorder WX2300. The RDE's were obtained in high performance liquid chromatography grade (hplc) acetonitrile or dimethylformamide with 0.1 M

tetrabutylammonium perchlorate or tetrabutylammonium tetrafluoroborate as supporting electrolyte or in aqueous solutions with 0.1 M sodium perchlorate as supporting electrolyte. The working electrode was either glassy carbon or copper; the counter electrode was platinum wire and the reference electrode was a SCE.

Carbon dioxide/argon mixtures were prepared by adjusting the flow rates of each gas. Catalytic currents were measured by subtracting the current in the absence of carbon dioxide (presumed to be the hydrogen evolution or the Ni(II/I) couple) from the peak height of the catalytic wave in the presence of carbon dioxide.

Preparation of Trans [14] Diene and the Nickel(II) Complex[3,4]

The ligand was prepared by dissolving 22.2 g of 1,2-diaminoethane dihydrobromide in 200 ml of acetone and then 6.0 g of 1,2-diaminoethane was added. The mixture was heated under reflux on a steam bath for 45 minutes during which time a copious white precipitate of the macrocycle formed. The solution was cooled to room temperature and the solid collected by filtration, washed with ice-cold acetone then ether and dried in a dessicator.

Yield = 28.87 g

m.p. = 105 - 107°C

I.R. Data:- ν(C=N) = 1667 cm^{-1}

Microanalysis:- Calculated for $C_{16}H_{32}N_4.2HBr.2H_2O$

C 40.2% H 8.0% N 11.7%

Found:- C 40.47% H 8.66% N 11.71%

The complex was prepared by making a slurry of 2 g of the ligand in 30 ml of water and adding an excess of basic nickel carbonate. The mixture was heated on a steam bath for ca. 30 minutes until the solution turned yellow. The excess nickel carbonate was filtered off. A saturated solution of sodium perchlorate was added to the filtrate and then cooled in ice. The complex was filtered off and dried in a dessicator.

Yield = 0.5 g

I.R. Data:- ν (N–H) = 3168 cm^{-1}, ν (C=N) = 1668 cm^{-1}, ν (ClO_4^-) = 1079 cm^{-1}, ν (ClO_4^-) = 624 cm^{-1}

Microanalysis:- Calculated for $C_{16}H_{32}N_4NiCl_2O_8$

C 35.56% H 5.93% N 10.37%

Found:- C 35.59% H 6.07% N 10.48%

λ_{max} = 437 nm

Preparation of Tris-(1,3-propanediamine) Nickel(II) Perchlorate[4,17]

18.25 g (0.05 moles) of nickel(II) perchlorate hexahydrate was dissolved in 150 ml of ethanol and added with stirring to a warm solution of 11.1 g (0.15 moles) of 1,3-propanediamine in 150 ml of ethanol. Heat was given out and the solution turned blue. The solution was allowed to cool while stirring continued and mauve crystals formed. The crystals were filtered off and dried *in vacuo*.

Yield = 18.59 g

Preparation of Me_6 [16] Diene Nickel(II) Perchlorate[17]

10 g of tris-(1,3-propanediamine) nickel(II) perchlorate was dissolved in 200 ml of dry acetone and the solution was tightly stopered and allowed to stand at room temperature for ten days. The orange crystals were filtered off and dried *in vacuo*.

Yield = 9.78 g

I. R. Data:- ν (N–H) = 3437 cm^{-1}, ν (C=N) = 1664 cm^{-1}, ν (ClO_4^-) = 1088 cm^{-1}, ν (ClO_4^-) = 628 cm^{-1}

Microanalysis:- Calculated for $C_{18}H_{36}N_4NiCl_2O_8$

C 38.19 % H 6.41 % N 9.90 %

Found C 38.22 % H 6.44 % N 9.99 %

λ_{max} = 429 nm

Preparation of Nickel(II) Salen

2.68 g of salen were dissolved in ethanol and 2.48 g of nickel acetate were dissolved in a mixture of ethanol and water. The two solutions were warmed on a steam bath then added together and allowed to cool. The precipitate was filtered off and air-dried.

Yield = 2.74 g

I. R. Data:- ν (C=N) = 1664 cm^{-1},

Microanalysis:- Calculated for $C_{16}H_{14}N_2NiO_2$

C 59.13 % H 4.34 % N 8.52 %

Found C 56.94 % H 4.72 % N 8.15 %

λ_{max} = 410 nm

Preparation of 3,14-dimethyl-2,6,13,17-tetraazatricyclo [16.4.4.0] docosa-2,12-diene[6] and the Nickel Complex

To a cooled (0 - 4°C) ethanol (200 ml) solution of 1,2-diaminocyclohexane (35 ml) was added dropwise 60 % perchloric acid (25 ml) with stirring. Methyl vinyl ketone (22 ml) was added over a period of one hour to the solutions at 0 - 4°C, and then white precipitates of the product were formed. The resulting suspension was allowed to warm up to ambient temperature and then stored overnight to complete crystallisation. The white product was filtered off, washed with ethanol and dried under vacuum.

Yield = 12.68 g

I.R. Data:- ν (N–H) = 3426 cm^{-1}, ν (C=N) = 1665 cm^{-1}, ν (ClO_4^-) = 1088 cm^{-1},

ν (ClO_4^-) = 629 cm^{-1}

Microanalysis:- Calculated for $C_{20}H_{40}N_4Cl_2O_9$

C 43.6 % H 7.31 % N 10.2 %

Found C 44.42 % H 6.84 % N 10.29 %

The complex was prepared by refluxing 7.5 g of the 3,14-dimethyl-

2,6,13,17-tetraazatricyclo [16.4.4.0] docosa-2,12-diene.2$HClO_4$.H_2O and 3.5 g of nickel(II) acetate in methanol for 30 minutes when yellow solids were precipitated. After it was cooled to room temperature, the yellow product was filtered, washed with methanol, recrystallised from hot acetonitrile-water (3:2) mixture, and air-dried.

Yield = 5.37 g

I.R. Data:- ν (N–H) = 3426 cm^{-1}, ν (C=N) = 1665 cm^{-1}, ν (ClO_4^-) = 1086 cm^{-1}, ν (ClO_4^-) = 625 cm^{-1}

Microanalysis:- Calculated for $C_{20}H_{38}N_4NiCl_2O_8$

C 40.57 % H 6.47 % N 9.46 %

Found C 40.19 % H 6.43 % N 9.48 %

λ_{max} = 454 nm

Preparation of 3,14-dimethyl-2,6,13,17-tetraazatricyclo [16.4.4.0] docosane[6]

To a cooled (0 - 4°C) methanol (50 ml) suspension of 10.7 g of 3,14-dimethyl-2,6,13,17-tetraazatricyclo [16.4.4.0] docosa-2,12-diene.2$HClO_4$.H_2O were slowly added 1.60 g of sodium hydroxide and 1.81 g of sodium borohydride over a period of two hours at room temperature and then heated at reflux for 20 minutes. After cooling, the solution was filtered and 4.8 g of sodium hydroxide in water (100 ml) was added to the filtrate. The solution was stirred until precipitation of the product was complete. The white product was filtered off, washed with water and air dried. The product was recrystallised from hot methanol-water (4:1) mixture.

Yield = 4.09 g

I.R. Data:- ν (N–H) = 3426 cm^{-1}, ν (ClO_4^-) = 1088 cm^{-1}, ν (ClO_4^-) = 629 cm^{-1}

^{13}C NMR:- δ17.4, δ25.1, δ25.8, δ30.7, δ31.3, δ36.6, δ43.2, δ47.1, δ57.7, δ63.8

Microanalysis:- Calculated for $C_{20}H_{40}N_4$

C 71.4 % H 12.0 % N 16.7 %

Found C 69.93 % H 12.86 % N 16.39 %

The complex was prepared by refluxing a solution of 4.7 g of 3,14-dimethyl-2,6,13,17-tetraazatricyclo [16.4.4.0] docosane and 3.5 g of nickel(II) acetate in methanol (50 ml) for 30 minutes and then cooled to room temperature. Excess amount of sodium perchlorate was added to the solution and yellow crystals formed. The yellow product was filtered, washed with methanol, recrystallised from hot acetonitrile-water (3:2) mixture, and air-dried.

Yield = 3.98 g

I.R. Data:- ν (N–H) = 3425 cm^{-1}, ν (ClO_4^-) = 1089 cm^{-1}, ν (ClO_4^-) = 627 cm^{-1}

Microanalysis:- Calculated for $C_{20}H_{40}N_4NiCl_2O_8$

C 39.5 % H 6.25 % N 9.21 %

Found C 41.18 % H 7.38 % N 9.62 %

λ_{max} = 453 nm

Preparation of 5,12-dimethyl-7,14-diphenyl-tetra-azacyclotetradeca-4,11-diene[18] and the Nickel(II) Complex[19]

The ligand was prepared by dissolving molar equivalents of benzylideneacetone (14.6 g) and ethylene diamine (6 g) in 150 ml of 1:2 cyclohexene/ether and heating under reflux with 10 g of anhydrous potassium carbonate present for 3 hours. The potassium carbonate was then filtered off and the solvent evaporated. The residue, which slowly solidified, was suspended in 80 ml of ether and kept overnight in the fridge. The crystals which precipitated were filtered and washed with ether.

Yield = 3.38 g

I.R. Data: - ν (N–H) = 3314 cm^{-1}, ν (C=N) = 1665 cm^{-1}

^1H NMR:- δ1.8 (6H), δ2.5 (8H), δ3.2 (4H), δ4.1 (4H), δ7.3 (10H)

Microanalysis:- Calculated for $C_{24}H_{32}N_4$

C 76.6% H 8.6% N 14.9%

Found:- C 77.32% H 8.91% N 14.73%

The complex was prepared by warming 0.73 g of nickel (II) perchlorate and 0.76 g of the ligand in 30 ml of methanol on a steam bath until all the reactants had completely dissolved (some orange product crystallised out). 10 ml of propan-2-ol were added and the methanol evaporated off. The orange product was filtered from the solution and recrystallised from methanol/propan-2-ol.

Yield = 0.90 g

I.R. Data:- ν (N–H) = 3178 cm^{-1}, ν (C=N) = 1652 cm^{-1}, ν (ClO_4^-) = 1093 cm^{-1}, ν (ClO_4^-) = 622 cm^{-1}

Microanalysis:- Calculated for $C_{24}H_{32}N_4NiCl_2O_8$

C 45.4% H 5.10% N 8.83%

Found:- C 45.14% H 4.91% N 8.78%

Λ_m = 334 Scm^2mol in MeCN ≡ 2:1 electrolyte

λ_{max} = 456 nm

Preparation of N,N'-bis(3-aminopropyl)-1,3-propanediamine (3,3,3-tet)[20]

3.4 g of 1,3-diaminopropane was placed in a 500 ml three-necked flask equipped with a magnetic stirrer bar, a dropping funnel and a thermometer. The diamine was cooled to ice temperature and then 12.12 g of 1,3-dibromopropane was added dropwise with vigorous stirring. After the addition was complete, the mixture was heated on a steam bath for 1 hour and then concentrated to $^1/_3$ of its original volume. This was returned to the original flask and 9.0 g of potassium hydroxide pellets added. The mixture was then heated on a steam bath for 2 hours with efficient stirring. The solids were removed by filtration and washed with several portions of ether to remove any adsorbed product. The filtrate and washings were combined and rotary evaporated to a viscous oil (the oil was separated from any solid that formed by ether extraction and decantation - the decanted ether was evaporated to an oil.) The viscous oil was vacuum distilled, and the tetramine protected from the air as it forms a solid hydrate with moist air.

Yield = 2.86 g

^{1}H NMR:- δ1.6, δ2.6, δ4.8

^{13}C NMR:- δ37.56, δ37.74, δ37.90, δ41.28

Preparation of [15] Diene N_4[21]

3.64 g of nickel chloride was dissolved in 100 ml of water in a 250 ml conical flask. To this was added 2.86 g of 3,3,3-tet with stirring, followed by 3.6 ml of a 30% aqueous glyoxal solution. The resulting blue solution was heated at 60 - 80°C for 3 hours until the colour became red/brown (which indicates the formation of planar nickel). Sodium perchlorate was added to the solution and the resulting crystals were filtered off.

Yield = 0.61 g

The product was insoluble in all common solvents and was thus unable to be recrystallised.

Preparation of 5,10,15,20-tetraphenylporphyrin[10]

11.2 ml of pyrrole and 16.0 ml of benzaldehyde were added to 600 ml of propionic acid and refluxed for 30 minutes. The solution was then cooled to room temperature and filtered. The precipitate was washed thoroughly with methanol and the crystals dried *in vacuo*.

Yield = 4.0 g

Preparation of the Nickel(II) Tetraphenylporphyrin

1 g of meso-tetraphenylporphyrin was dissolved in 100 ml of dimethylformamide and heated to reflux. To this was added 0.34 g (0.0016 moles) of nickel(II) acetate in 2 or 3 portions and the heating was continued for another 15 minutes. The solution was then cooled, first in air then on an ice-bath. 100 ml of cold water were added and the solution filtered. The product was washed with water and dried in air.

Yield = 0.83 g

Preparation of Nickel(II) (2,12-dimethyl-3,7,11,17-tetraazabicyclo [11.3.1] heptadeca-1(17),2,11,13,15-pentaene perchlorate.[22]

1.3 g (0.008 moles) of 2,6-diacetylpyridine was dissolved in 20 ml of ethanol, and 1.9 g of nickel(II) chloride hexahydrate dissolved in 25 ml of water was added. The solution was heated to 65°C and 1.12 ml of 3,3'-diamino-dipropylamine was added. The solution became slightly cloudy on addition of the amine and 0.5 ml of acetic acid was added to clarify the solution. The reaction mixture was held at 65°C for six hours, after which the ethanol was removed, reducing the volume to about 15 ml. After filtering the remaining solution, 5 ml of concentrated aqueous sodium perchlorate was added, precipitating the crude product. The product was collected by filtration, washed with ethanol and recrystallised from 30 - 40 ml of warm (65°C) water. After filtering the warm solution, 3 ml of 70 % perchloric acid was added and the flask containing the acidified filtrate was allowed to cool slowly. Grey-brown needles of the hydrated product were formed. The product was collected by filtration, washed successively with ethanol and ether, and dried in vacuo over P_4O_{10}.

Yield = 1.7 g

I.R. Data:- ν(C=N) = 1654 cm^{-1}, $\nu(ClO_4^-)$ = 1087 cm^{-1}, $\nu(ClO_4^-)$ = 626 cm^{-1}

Microanalysis:- Calculated for $C_{15}H_{26}N_4NiCl_2O_{10}$

C 32.69 % H 4.75 % N 10.15 %

Found C 32.44 % H 4.69 % N 10.18 %

λ_{max} = 468 nm

Preparation of 1,3-Diaminopropane Dihydrochloride[17,23]

71 ml of 1,3-diaminopropane was added to 750 ml of 95% ethanol and cooled in an ice-bath. 150 ml of concentrated hydrochloric acid (12 M) was added dropwise, with stirring, at such a rate that the solution temperature remained below 20°C. The product was collected, washed with ethanol and then ether and dried *in vacuo*.

Yield = 85.87 g

Preparation of (2,3,9,10-Tetramethyl-1,4,8,11-Tetraazacyclotetradeca-1,3,8,10-Tetraene) Nickel(II) Perchlorate[24]

14.7 g of 1,3-diaminopropane dihydrochloride in 500 ml of methanol was cooled to 5°C and 8.61 g of 2,3-butanedione were added. The solution was stirred for 30 minutes and then allowed to stand at room temperature for 20 minutes, and then 12.45 g of nickel(II) acetate were added to the orange solution. The solution darkened to a red/brown colour and was stirred for 4 hours, after which time 9.85 g of hydrochloric acid were added, followed by 6.8 g of zinc chloride. The Ni(Me_4[14]-1,3,8,10-tetraene N_4)[$ZnCl_4$] precipitated out after stirring overnight and the addition of some THF. The product was filtered off, washed with ethanol and then ether and dried *in vacuo*.

2.5 g of the tetrachlorozinate salt were dissolved in 30ml of water and 1.25 g of sodium perchlorate were added. The solution was left in the fridge to allow the complex to form. The crystals were filtered off, washed with ether and dried *in vacuo*.

Yield = 0.25 g

I.R. Data:- ν(C=N) = 1607 cm^{-1}, ν(N=C-C=N) = 1221 cm^{-1}, $\nu(ClO_4^-)$ = 1089 cm^{-1}, $\nu(ClO_4^-)$ = 624 cm^{-1}

Microanalysis:- Calculated for $C_{14}H_{24}N_4NiCl_2O_8$

C 33.23% H 4.75% N 11.07%

Found:- C 32.24% H 4.76% N 10.69%

λ_{max} = 397 nm

Preparation of Ph_4[12]TIM and the Copper Complexes[25]

The ligand was made by dissolving 20.0 g of benzil in 200 ml of ethanol and 10 ml of ethylenediamine was added with stirring, followed by 1.5 ml of concentrated HCl. The resulting solution was refluxed on a steam bath for 4 hours then allowed to stand overnight at room temperature. The yellow crystalline product was filtered off, washed with ethanol, then ether and air dried. The crude product was then recrystallised from the minimum amount of methanol.

Yield = 3.19 g

m.p. = 158 - 160°C

I.R. Data:- ν(C=N) = 1553 cm^{-1}

^1H NMR: δ3.7 (8H), δ7.3 (20H)

Calculated for $C_{32}H_{28}N_4$:- C 82.0% H 6.0% N 11.96%

Found:- C 81.74% H 5.85% N 11.96%

Preparation of the Chloride Complex: 0.14 g of copper(II) chloride was dissolved in ethanol and added to 0.3 g of Ph_4[12]TIM in ethanol. The complex precipitated out of solution and was filtered off.

Yield = 0.27 g

Microanalysis:-Calculated for $C_{32}H_{28}N_4CuCl_2$

C 63.73% H 4.68% N 9.29%

Found:- C 62.55% H 3.37% N 8.77%

Λ_m = 94.2 Scm^2mol in MeCN $\equiv$ 1:1 electrolyte

$\chi_g = 1.956 \times 10^{-6}$, $\chi_M = 1.249 \times 10^{-3}$

$\lambda_{max} > 900$ nm

Preparation of the Bromide Complex: 0.17 g of copper(II) bromide was dissolved in ethanol and added to 0.3 g of Ph_4[12]TIM in ethanol. The complex precipitated out of solution and was filtered off.

Yield = 0.34 g

Microanalysis:-Calculated for $C_{32}H_{28}N_4CuBr_2$

C 55.54% H 4.08% N 8.10%

Found:- C 55.02% H 3.38% N 7.90%

Λ_m = 127.0 Scm^2mol in MeCN ≡ 1:1 electrolyte

$\chi_g = 1.36 \times 10^{-6}$, $\chi_M = 9.05 \times 10^{-4}$

$\lambda_{max} > 900$ nm

Preparation of other nickel complexes.

The rest of the complexes used in this chapter were obtained from Professor R. W. Hay and Professor N. F. Curtis.

Chapter Five References

1. R. W. Hay, B. Kinsman and C. I. Smith, *Polyhedron*, in press
2. F. V. Lovecchio, E. S. Gore and D. H. Busch, *J. Am. Chem. Soc.*, 1974, **96**, 3109
3. (a) N. F. Curtis, *J. Chem. Soc.*, 1960, 4409
   (b) M. Blight and N. F. Curtis, *J. Chem. Soc.*, 1962, 2644
4. R. W. Hay, G. A. Lawrance and N. F. Curtis, *J. Chem. Soc. Perkin I*, 1975, 591
5. R. R. Gagne and D. M. Ingle, *Inorg. Chem.*, 1981, **20**, 420
6. S. G. Kang, J. K. Kweon and S. K. Jung, *Bull. Korean Chem. Soc.*, 1991, 12, 483
7. J. Lewis and M. Schroder, *J. Chem. Soc. Dalton Trans.*, 1982, 1085
8. M. H. Schmidt, G. M. Miskelly and N. S. Lewis, *J. Am. Chem. Soc.*, 1990, **112**, 3420
9. (a) C. L. Bailey, R. D. Bereman, D. P. Rillema and R. Nowak, *Inorg. Chim. Acta*, 1986, **116**, L45
   (b) P. J. Lukes, J. A. Crayston, D. J. Ando, M. E. Harman and M. B. Hursthouse, *J. Chem. Soc. Perkin Trans. 2*, 1991, 1845
10. (a) R. R. Gagne, *J. Am. Chem. Soc.*, 1976, **98**, 6709
    (b) R. R. Gagne, J. L. Allison, R. S. Gall and C. A. Koval, *J. Am. Chem. Soc.*, 1977, **99**, 7170
    (c) R. R. Gagne, J. L. Allison and D. M. Ingle, *Inorg. Chem.*, 1979, **18**, 2767
11. (a) J. Y. Becker, B. Vainas, R. Eger and L. Kaufman, *J. Chem. Soc. Chem. Comm.*, 1985, 1471
    (b) T. Atoguchi, A. Aramata, A. Kazusaka and M. Enyo, *J. Electroanal. Chem.*, 1991, **318**, 309
    (c) R. E. Bozak and C. L. Hill, *J. Chem. Ed.*, 1982, **59**, 36

(d) J. P. Collman, R. R. Gagne, C. A. Reed, T. R. Halbert, G. Lang and W. T. Robinson, *J. Am. Chem. Soc.*, 1975, **97**, 1427

12. K. M. Kadish, *Prog. Inorg. Chem.*, 1986, **34**, 435

13. (a) A. A. Isse, A. Gennaro, E. Vianello and C. Floriani, *J. Mol. Catal.*, 1991, **70**, 197

(b) D. J. Pearce and D. Pletcher, *J. Electroanal. Chem.*, 1986, **197**, 317

14. (a) A. A. Isse, A. Gennaro and E. Vianello, *Electrochim. Acta.*, 1992, **37**, 113

(b) C. Gosden, J. B. Kerr, D. Pletcher and R. Rosas, *J. Electroanal. Chem.*, 1981, **117**, 101

15. G. B. Balazs and F. C. Anson, *J. Electroanal. Chem.*, 1992, **335**, 75

16. (a) F. Bedioui, E. Labbe, S. Gutierrez-Grunados and J. Devynck, *J. Electroanal. Chem.*, 1991, **301**, 267

(b) L. A. Hoferkamp and K. A. Goldsby, *Chem. Mater.*, 1989, **1**, 348

17. D. A. House and N. F. Curtis, *J. Am. Chem. Soc.*, 1964, **86**, 223

18. K. Hideg and D. Lloyd, *J. Chem. Soc. (C)*, 1971, 3441

19. D. F. Cook, N. F. Curtis and R. W. Hay, *J. Chem. Soc. Dalton Trans.*, 1973, 1160

20. E. K. Barefield, F. Wagner, A. W. Herlinger and A. R. Dahl, *Inorg. Syn.*, 1977, **16**, 222

21. E. K. Barefield and G. Freeman, *Inorg. Syn.*, 1981, **20**, 108

22. (a) J. L. Karn and D. H. Busch, *Inorg. Chem.*, 1969, **8**, 1149

(b) L. L. Efros, H. H. Thorp, G. W. Brudvig and R. H. Crabtree, *Inorg. Chem.*, 1992, **31**, 1722

23. J. F. Myers and N. J. Rose, *Inorg. Chem.*, 1973, **12**, 1238

24. (a) A. M. Tait and D. H. Busch, *Inorg. Syn.*, 1979, **18**, 22

(b) S. C. Jackels, K. Farmery, E. K. Barefield, N. J. Rose and D. H. Busch, *Inorg. Chem.*, 1972, 11, 2893

25. R. W. Hay, I. Fraser, V. M. C. Reid and C. I. Smith, *Trans. Met. Chem.*,

1994, **19**, 307

Chapter Six

New Catalysts for Carbon Dioxide Reduction

6.0 Introduction

In this chapter a variety of new catalysts will be discussed in relation the most active catalyst to date, $[Ni(cyclam)]^{2+}$. Most of these complexes are structurally related to cyclam, having saturated ring systems yet have more positive redox potentials than $[Ni(cyclam)]^{2+}$. This will facilitate a useful comparison of how the reduction is affected by redox potential and macrocyclic structure.

Another means of facilitating the Ni(II/I) reduction is to add alkyl substituents to the macrocyclic structure. By making the Ni(II/I) redox potential less negative the driving force for the reduction should be lowered and hence make the reduction of carbon dioxide more favourable. All the complexes discussed are saturated since as shown in Chapter Five the unsaturated macrocycles are not suitable for carbon dioxide reduction.

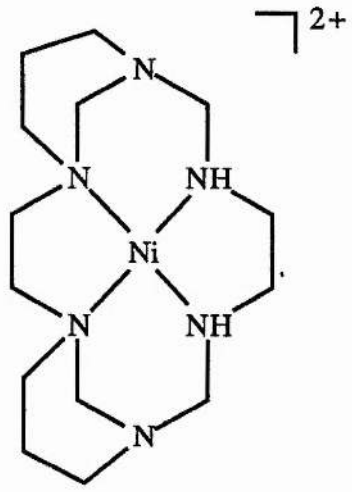

Figure 6.1

Structure of nickel(II) 1,3,6,8,12,15-hexaazatricyclo [13.3.1.1] eicosane perchlorate, commonly called Ni(tricyclo).

6.1 A Study of the Electrochemistry of nickel(II) 1,3,6,8,12,15-hexaazatricyclo [13.3.1.1] eicosane perchlorate

6.1.1 Cyclic Voltammetry

The macrocycle nickel (1,3,6,8,12,15-hexaazatricyclo [13.3.1.1] eicosane) perchlorate (Figure 6.1) in MeCN + 0.1 M TBAT with a Pt electrode has a Ni(III/II) redox couple at + 1.35 V (60) and a Ni(II/I) redox couple at -1.08 V (80). In MeCN using a HMDE the Ni(II/I) redox couple is at -1.12 V (80) which is considerably more positive than $[Ni(cyclam)]^{2+}$ and this shift corresponds to the alkylation of the

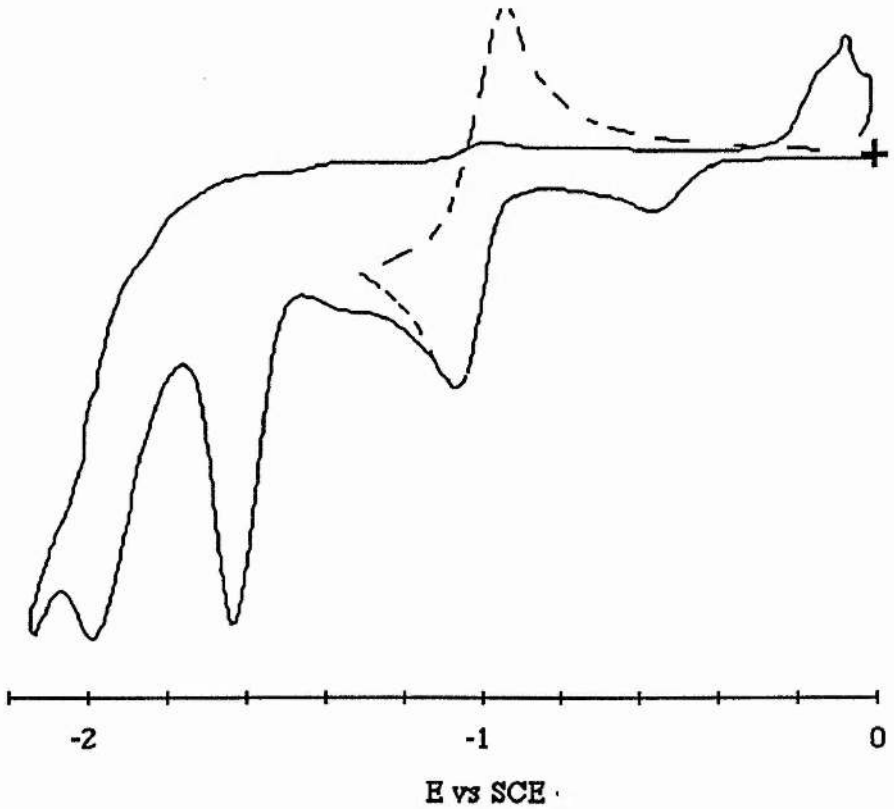

Figure 6.2

A cyclic voltammogram of $[Ni(tricyclo)]^{2+}$ in MeCN + 0.1 M TBAT under CO_2.

The dashed line indicates the second scan which was reversed at -1.40 V.

nitrogen atoms *c.f.* $[Ni(TMC)]^{2+}$ with a Ni(II/I) reduction at -1.03 V (140). These redox waves correspond to those found by Suh *et al.*[1] On reaction with carbon dioxide there is an increase in hydrogen evolution (the sloping background current

increases) but there is no catalytic current for the reduction of carbon dioxide. The Ni(II/I) redox couple is still present at -1.14 V (120, quasi-reversible) but new cathodic peaks appear at -1.80 V and -2.06 V and a new anodic peak appears at -0.12 V (Figure 6.2). Further experiments demonstrate that the Ni(II/I) wave firstly becomes chemically reversible ($i_{pa}/i_{pc} \approx 1$) when the scan is reversed at -1.40 V immediately under the peak. Secondly, the peak at -0.12 V only appears after the scan is allowed to proceed to -2.06 V. Thirdly, the addition of water to the solution does not bring about the expected catalytic carbon dioxide current but the peak at -2.06 V disappears.

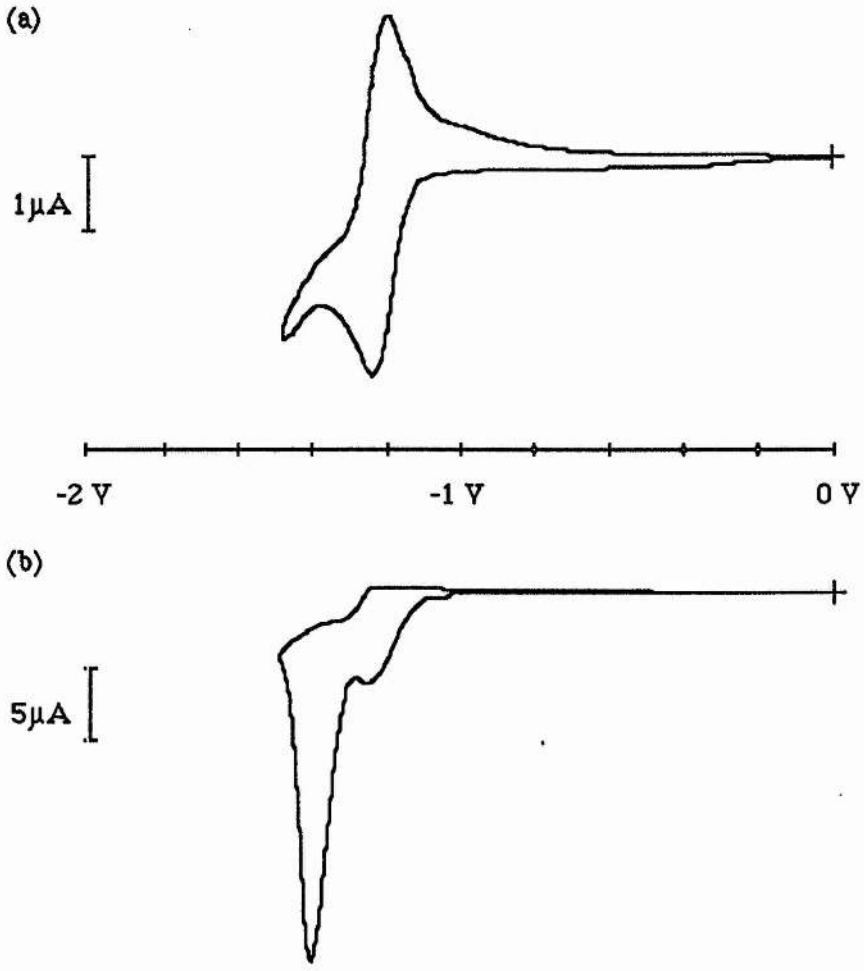

Figure 6.3

A cyclic voltammogram of $[Ni(tricyclo)]^{2+}$ in 9:1 $MeCN/H_2O$ + 0.1 M TBAT

(a) under argon and (b) under carbon dioxide.

When this complex is dissolved up in 9:1 MeCN/H_2O solution a Ni(II/I) redox couple is observed at -1.22 V (80) on a mercury electrode. When carbon dioxide is bubbled through the solution a catalytic current of 25 μA is observed at -1.42 V with a pre-wave at -1.26 V (Figure 6.3).

The reason that this complex is not as efficient as $[Ni(cyclam)]^{2+}$ may be due the molecule being more hindered than $[Ni(cyclam)]^{2+}$ because the conformation of the complex is the same as the trans III isomer of $[Ni(cyclam)]^{2+}$. Finally, the Ni(II/I) couple is more positive than for $[Ni(cyclam)]^{2+}$ and there is thus a lower driving force for carbon dioxide reduction.

6.1.2 Rotating Disc Electrochemistry

Since diffusion coefficients have been discussed as a possible link to catalytic activity rotating disc experiments were attempted on this complex. The results are shown in Table 6.1.

Complex	D (cm^2s^{-1})
$[Ni(tricyclo)]^{2+}$	4.78×10^{-5}
$[Ni(cyclam)]^{2+}$	8.85×10^{-5}

Table 6.1

A comparison of diffusion coefficients for $[Ni(tricyclo)]^{2+}$ and $[Ni(cyclam)]^{2+}$ obtained in 9:1 MeCN/H_2O + 0.1 M TBAT.

As seen from the above Table, the value of the diffusion coefficient of $[Ni(tricyclo)]^{2+}$ is half that of $[Ni(cyclam)]^{2+}$ under the same conditions. The diffusion coefficient of $[Ni(cyclam)]^{2+}$ is greater than obtained in aqueous solution. This is what is expected as a species moves more quickly in acetonitrile than in water. The diffusion coefficient of $[Ni(tricyclo)]^{2+}$ is less than that of $[Ni(cyclam)]^{2+}$ because it is a bulkier molecule (D varies with $a^{-1/2}$ where a is the hydrodynamic radius).

As discussed earlier (Chapter Three) there is be a link between the diffusion coefficient and the catalytic activity of the complex ($i_k = nFAD^{1/2}$). In this case the $[Ni(tricyclo)]^{2+}$ has a lower catalytic current but also a more positive reduction potential. The $[Ni(tricyclo)]^{2+}$ moves more slowly towards the electrode and so is unable to regenerate the Ni^{I} species fast enough for a large catalytic current.

6.2 A Study of the Electrochemistry of the $R_2[14]aneN_6$ Complexes

A variety of $R_2[14]aneN_6$ macrocycles can be synthesised easily and here the first two in the series are discussed to determine how the introduction of the extra nitrogen atoms affects the redox potentials and the reduction of carbon dioxide. The structures of the two complexes investigated are shown in Figure 6.4.

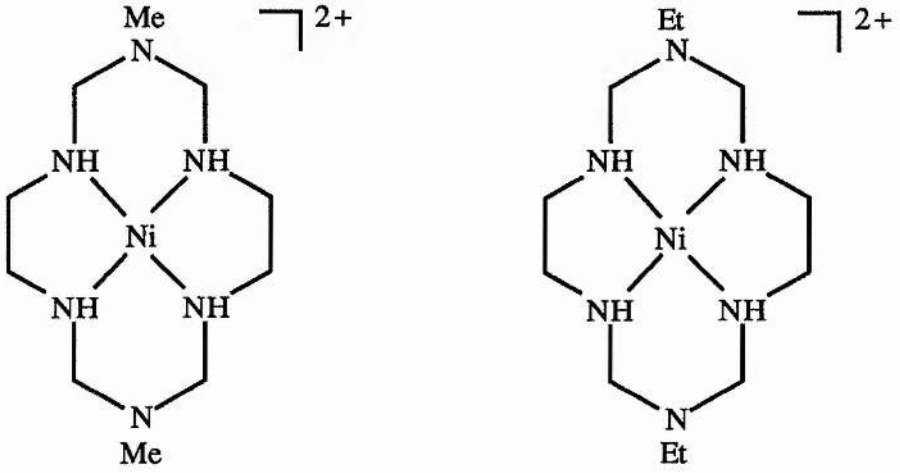

Figure 6.4

Structures of the $R_2[14]aneN_6$ Macrocycles.

6.2.1 Cyclic Voltammetry

$[Ni(Me_2[14]aneN_6)]^{2+}$ in MeCN with a GC working electrode has a Ni(III/II) redox couple at +1.05 V (100) and a Ni(II/I) redox couple at -1.42 V (40), close to that of $[Ni(cyclam)]^{2+}$, and to those found by Jung *et al.*[2] (Table 6.2). Interestingly, using a mercury electrode in MeCN the Ni(II/I) redox couple is absent (this is surprising behaviour as $[Ni(cyclam)]^{2+}$ shows a redox couple under the same

conditions Table 2.3), until water is added (9:1 MeCN/H_2O) and the Ni(II/I) redox couple is then seen at -1.44 V (120). When carbon dioxide is bubbled through this

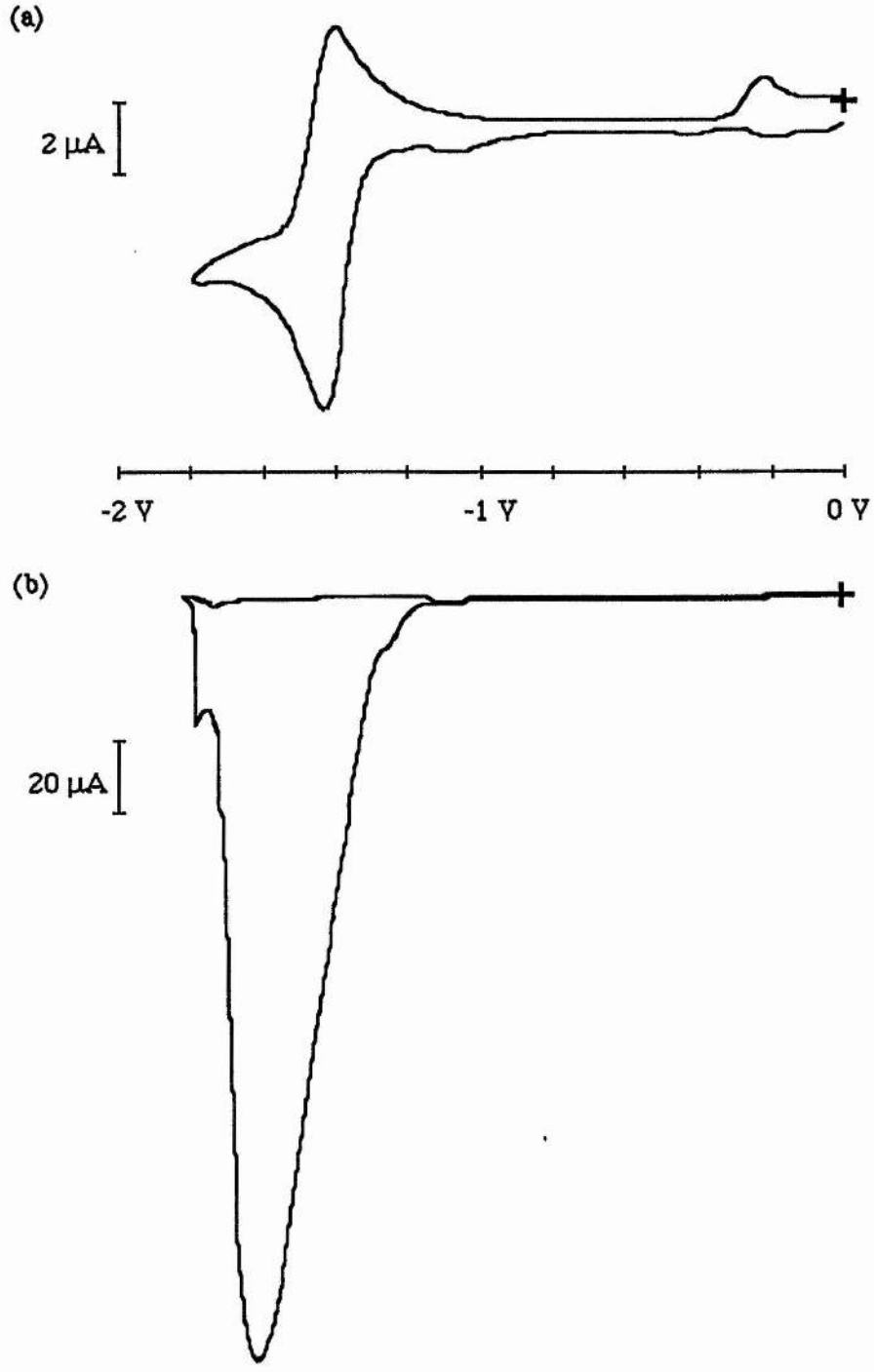

Figure 6.5

A cyclic voltammogram of $[Ni(Me_2[14]aneN_6)]^{2+}$ in 9:1 MeCN/H_2O + 0.1 M TBAT (a) under argon and (b) under carbon dioxide.

solution then there is a large catalytic current of 135 μA at -1.80 V, with pre-waves at -1.50 V and -1.28 V, and an anodic peak appears at -0.18 V. The original cyclic voltammogram is restored only after prolonged degassing with argon to remove all trace of carbon dioxide. Repeating the experiment, we get the same catalytic current but at a slightly different potential (-1.68 V). On allowing carbon dioxide to bubble for longer times the current increases to 216 μA (Figure 6.5). The results for this set of experiments are also summarised in Table 6.2.

			Ni(II/I)	Ni(III/II)	Reaction with CO_2		
Complex	Solvent	Electrode	(V)	(V)	i_{pa}	Δi_{pc}	E_{pc}
$Me_2[14]aneN_6$	MeCN	GC	-1.42 (40)	+1.05 (100)	-	-	-
	9:1 MeCN/H_2O	HMDE	-1.44 (120)	-	0	135 μA	-1.80 V
	water	HMDE	-	-	0	45 μA	-1.40 V
$Et_2[14]aneN_6$	MeCN	Pt	-1.48 (240)	1.04 V (80)			
	9:1 MeCN/H_2O	HMDE	-1.48 (240)	-	0	120 μA	-1.74 V

Table 6.2

A comparison of the $R_2[14]aneN_6$ macrocycles.

The figures in brackets denote the peak separation in mV.

In summary it should be noted that the $[Ni(Me_2[14]aneN_6)]^{2+}$ is more active than $[Ni(cyclam)]^{2+}$ under the same conditions (9:1 MeCN/H_2O with a HMDE). This appears to strengthen the case for the driving force being an important factor since the main difference between the two complexes appears to be the redox potential.

Unfortunately $[Ni(Me_2[14]aneN_6)]^{2+}$ is very insoluble in water (≤ 1 mM) so it is not possible to see the redox waves; however, on bubbling carbon dioxide into

the solution a catalytic current of 45 μA at -1.40 V is seen as well as a anodic peak at -0.14 V. On increasing the carbon dioxide bubbling time the catalytic current is increased to 60 μA. From the scan rate dependence of the catalytic current in this case

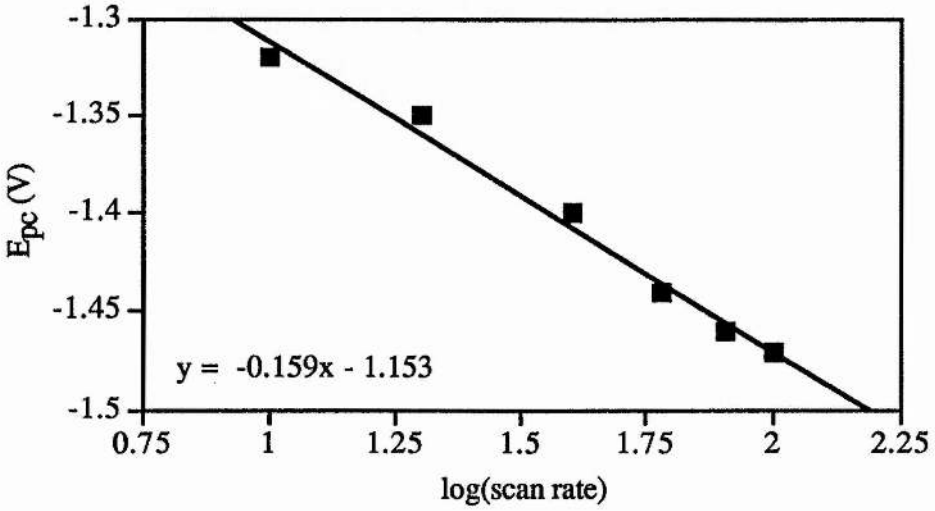

Figure 6.6

A plot of E_{pc} values against log(scan rate) for $[Ni(Me_2[14]aneN_6)]^{2+}$.

a plot of the shift in E_{pc} values as a function of the log(scan rate) is obtained (Figure 6.6). If the catalyst is assumed to be situated on the electrode then the theory for a totally irreversible redox system is applicable.[3,4] Thus $i_{p,cat}$ is proportional to both carbon dioxide concentration and (scan rate)$^{1/2}$ and E_{pc} shifts negative by $\frac{30}{\alpha n_a}$ mV per ten-fold increase in scan rate at 25°C, where α is the transfer coefficient (usually assumed to be 0.5) and n_a is the number of electrons transferred in the rate determining step. A high value of 159 mV is observed, consistent with the low value of α (0.27) observed for the reduction of carbon dioxide at a bare mercury electrode in dimethylformamide,[5] which was shown to be a one-electron process (equation (6.1)). Similar values of the slope were obtained for $[Ni(tricyclo)]^{2+}$ and $[Ni(cyclam)]^{2+}$ under the same conditions. The high value of the slope may also be due to resistance effects arising in the solvent (9:1 $MeCN/H_2O$) at those high catalytic currents. The current is indeed dependent on $v^{1/2}$ and thus diffusion controlled. (It

should be noted that a small correction should be made for the spherical nature of the electrode.[4])

$$CO_2 + H_2O + e^- \longrightarrow HCO_{2(ads)} + OH^- \qquad (6.1)$$

The excellent catalytic activity of the $[Ni(Me_2[14]aneN_6]^{2+}$ may be due to hydrogen-bonding interactions between co-ordinated carbon dioxide and the remote tertiary amine group (Figure 6.7), as proposed from UV-Visible studies on the related 3-methyl-1.3,5,8,12-pentaazacyclotetradecane complex between co-ordinated chlorine and water.[6] On the other hand, the $[Ni(Me_2[14]aneN_6]^{2+}$ is known to stabilise the high-spin state by stabilisation of the axial ligands.

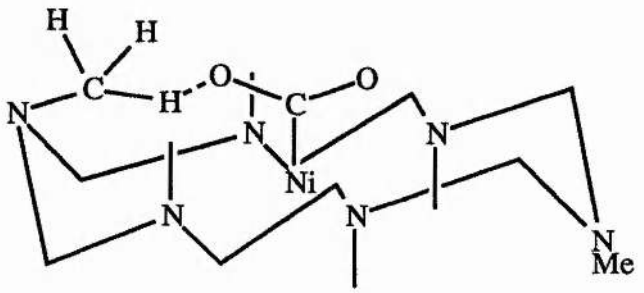

Figure 6.7

Diagram showing the proposed hydrogen-bonding interaction between the co-ordinated carbon dioxide and the tertiary amine.

The $Ni(Et_2[14]aneN_6)]^{2+}$ under an argon atmosphere in MeCN with a platinum electrode has a Ni(III/II) redox couple at +1.04 V (80) and a Ni(II/I) redox couple at -1.48 V (240), which is comparable to the value obtained for the Ni(II/I) reduction of $[Ni(cyclam)]^{2+}$ (-1.45 V (80)) under the same conditions. The results are summarised in Table 6.2.

In 9:1 $MeCN/H_2O$ a Ni(II/I) redox couple is observed at -1.48 V (240) using a HMDE. When carbon dioxide is bubbled through the solution, the i_{pc} for the Ni(II/I) reduction wave increases and the anodic peak is no longer visible. The value

of the current is 120 μA at -1.74 V (shown in Figure 6.8), which is comparable to that of $[Ni(cyclam)]^{2+}$ under the same conditions. The current does not increase as drastically as $[Ni(Me_2[14]aneN_6)]^{2+}$ on giving more bubbling time for carbon dioxide. This suggests that the saturation value for the carbon dioxide is reached more quickly than for $[Ni(Me_2[14]aneN_6)]^{2+}$.

There are other complexes in this series for investigation but as the size of the alkyl group increases then the relative activity of the complex decreases. Hence the complexes from R = Pr will be less active.

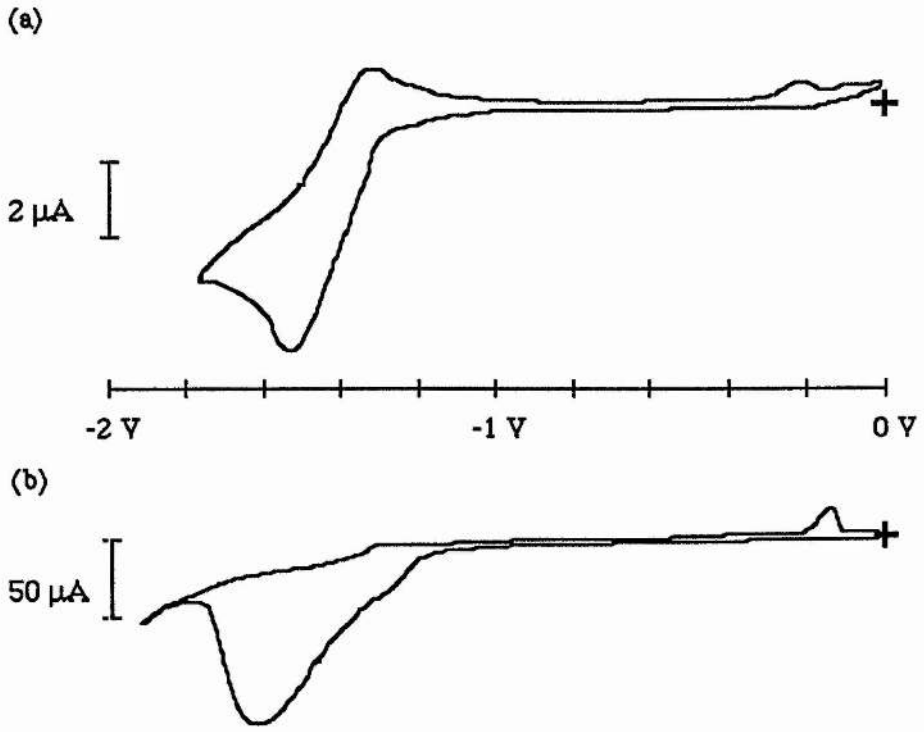

Figure 6.8

A cyclic voltammogram of $[Ni(Et_2[14]aneN_6)]^{2+}$ in 9:1 $MeCN/H_2O$ + 0.1 M TBAT (a) under argon and (b) under carbon dioxide.

6.2.2 Rotating Disc Electrochemistry

Rotating disc experiments were carried out to determine how the diffusion coefficients of these complexes compare to $[Ni(cyclam)]^{2+}$, the results are shown in Table 6.3.

Complex	D (cm^2s^{-1})
$[Ni(Me_2[14]aneN_6)]^{2+}$	4.63×10^{-4}
$[Ni(Et_2[14]aneN_6)]^{2+}$	1.44×10^{-4}
$[Ni(cyclam)]^{2+}$	8.85×10^{-5}

Table 6.3

A comparison of diffusion coefficients for the $R_2[14]aneN_6$ macrocycles obtained in 9:1 $MeCN/H_2O$ + 0.1 M TBAT.

As seen from the above table the two $R_2[14]aneN_6$ complexes have larger diffusion coefficients than $[Ni(cyclam)]^{2+}$, and this would contribute to a less negative potential for carbon dioxide reduction. As the value for the more efficient catalyst, $[Ni(Me_2[14]aneN_6)]^{2+}$, is five times greater, this explains how this catalyst moves to the electrode and regenerates the catalytic species much more quickly than $[Ni(cyclam)]^{2+}$. This seems to confirm the argument that there is a relationship between the catalytic current and the diffusion coefficient of the complex only if there is a significant contribution from solution catalysis. If a series of literature diffusion coefficients of complexes is known then it may be possible to identify possible catalysts from this information.

6.3 A Study of the Electrochemistry of Amino Group Macrocycles

Recently there has been a renewed interest in the reduction of carbon dioxide and how the interaction of amine groups could stabilise the co-ordinated carbon dioxide.[7] To investigate this effect further there were two macrocycles available (Figure 6.9) which have the same basic structure but with one major difference. One macrocycle has a co-ordinated amine group (denoted 4ß $(ClO_4)_2$) and the other which has a protonated amine group (denoted by 4ß $(ClO_4)_3$).

As seen from the results of the electrochemistry, summarised in Table 6.4, there is very little difference in the Ni(III/II) redox potential of the two complexes but

there is 300 mV difference in the Ni(II/I) redox potential. Therefore the co-ordination of the amine group does not affect the oxidation behaviour of the complex but does affect the reduction. However there is a major difference in the reaction with carbon dioxide.

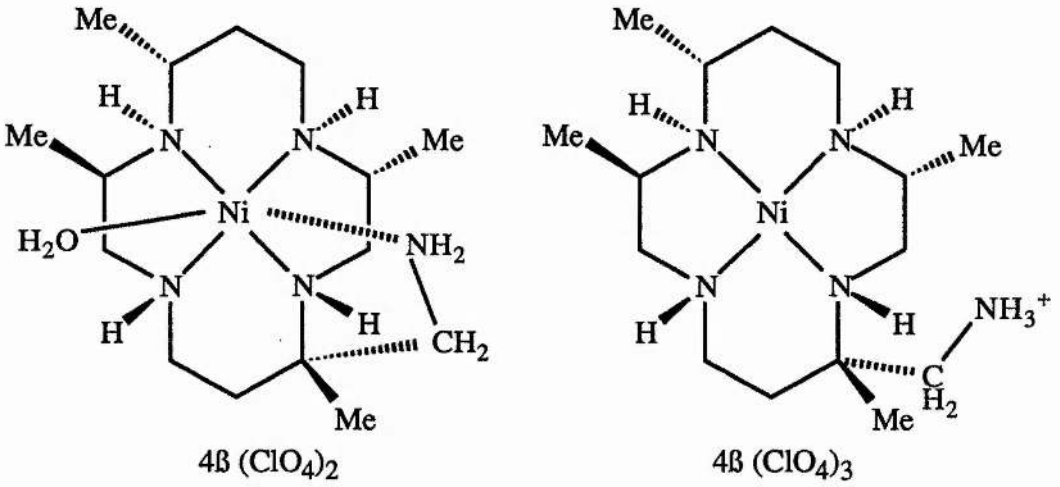

Figure 6.9

Structures of the amino-group complexes.

As we can see the co-ordinated amine group has a higher catalytic current but the potential for the reduction is much more negative than the one electron reduction of the carbon dioxide to the radical anion. On restoring an argon atmosphere the original CV is not returned. With the uncoordinated amine group the catalytic current is much lower and the reduction potential is 800 mV more positive. For this complex also the CV is not restored on returning the argon atmosphere. This suggests that an irreversible adsorption of the nickel carbonyl complex occurs as the CV is not restored even with a new drop. The Ni-CO adsorbs and poisons the electrode surface before the redox potential and hence the electrode becomes passivated (Section 2.1.5 (c)).

6.4 Conclusions

A new improved catalyst for the reduction of carbon dioxide has been identified. These catalysts have peripheral nitrogen atoms on the macrocyclic ring

which has a proposed hydrogen bonded interaction with the co-ordinated carbon dioxide. It is this hydrogen-bonding that stabilises the intermediate Ni^{I}-CO_2 intermediate and hence the current increases and the reduction potential is less negative.

			Ni(II/I)	Ni(III/II)	Reaction with CO_2		
Complex	Solvent	Electrode	(V)	(V)	i_{pa}	Δi_{pc}	E_{pc}
4ß $(ClO_4)_2$	MeCN	Pt	-	+0.98 (120)	-	-	-
	MeCN	GC	-1.73 (140)	+1.34 (i)	-	-	-
	MeCN	HMDE	-1.87 (180)	-	-	-	-
	9:1 MeCN/H_2O	HMDE	-2.00 (i)	-	0	140 µA	-2.70 V
	water	Pt	not seen	+1.10 (i)	-	-	-
	water	HMDE	-1.38 (i)	-		no change	
4ß $(ClO_4)_3$	MeCN	Pt	not seen	+0.98 (90)	-	-	-
	MeCN	GC	not seen	not seen	-	-	-
	MeCN	HMDE	not seen	-	-	-	-
	9:1 MeCN/H_2O	HMDE	-1.72 (80)	-	0	36 µA	-1.90 V

Table 6.4

A comparison of amino-group macrocycles

6.5 Experimental Section

Infra-red spectra were recorded as KBr discs on a Perkin Elmer 1710 Infra-red Fourier Transform Spectrometer.

Electronic spectra were recorded on a Philips PU8720 scanning spectrometer and a Perkin-Elmer Lamda 5 spectrometer against a background of pure solvent.

Elemental analyses were carried out in house at St. Andrews by Mrs Sylvia Smith.

Cyclic voltammetry was carried out with a Pine Instruments RDE 4 (EG & G, Wokingham, UK) potentiostat with a Graphtec XY Recorder WX2300. The CV's were obtained in high performance liquid chromatography grade (hplc) acetonitrile or dimethylformamide with 0.1 M tetrabutylammonium perchlorate or tetrabutylammonium tetrafluoroborate as supporting electrolyte or in aqueous solutions with 0.1 M sodium perchlorate as supporting electrolyte. The working electrode was either mercury (Metrohm Hanging Mercury Drop Electrode, HMDE with drop surface area 1.39 mm^2), platinum, glassy carbon, glassy carbon-mercury amalgam, copper or a gold-mercury amalgam; the counter electrode was platinum wire and the reference electrode was a SCE. After fabrication solid electrodes were polished firstly with successively finer grades of wet/dry paper (#120, 240, 600, 800). Thereafter polishing with diamond paste (Engis) of grade 6, 1 and 0.25 μm was carried out, with 5 minutes sonication in distilled water between grades. Alternatively, grades alumina 3, 1 and 0.5 μm (Buehler) were used instead of the diamond paste. If necessary, during an experiment the electrode was repolished at the finest grade of alumina.

Carbon dioxide/argon mixtures were prepared by adjusting the flow rates of each gas. Catalytic currents were measured by subtracting the current in the absence of carbon dioxide (presumed to be the hydrogen evolution or the Ni(II/I) couple) from the peak height of the catalytic wave in the presence of carbon dioxide.

Preparation of 1,3,6,8,12,15-hexaazatricyclo [13.3.1.1] eicosane and the Nickel Complex[1]

To a stirred methanol solution (50 ml) of 11.9 g nickel(II) chloride were added 8.7 g of N,N'-bis (3-aminopropyl) ethylenediamine (3,2,3-tet), 16.2 ml of 36% aqueous formaldehyde and then 3 g of ethylenediamine. The mixture was refluxed for 6 hours, filtered hot and then allowed to cool to room temperature. A saturated methanol solution of excess sodium perchlorate (~ 2 g) was added and the solution was left in the fridge until orange-red crystals formed. The crystals were filtered off, washed with methanol and air-dried. The crystals were recrystallised from hot water.

Yield = 2.86 g

I.R. Data:- ν (N–H) = 3234 cm^{-1}, ν (ClO_4^-) = 1089 cm^{-1}, ν (ClO_4^-) = 629 cm^{-1}

Microanalysis:- Calculated for $NiC_{14}H_{30}N_6Cl_2O_8(0.5H_2O)$

C 30.63% H 5.69% N 15.31%

Found:- C 30.63% H 5.18% N15.68%

λ_{max} = 482 nm

Preparation of other nickel complexes.

The rest of the complexes used in this chapter were obtained from Professor R. W. Hay.

Chapter Six References

1. M. P. Suh, S. Kang, V. Goedken and S. Park, *Inorg. Chem.*, 1991, **30**, 365
2. S. Jung, K. Kang and M. P. Suh, *Bull. Korean Chem. Soc.*, 1989, **10**, 362
3. Southampton Electrochemistry Group (R. Greef, R. Peat, L. M. Peter, D. Pletcher and J. Robinson), "Instrumental Methods of Electrochemistry", Ellis Horwood, Chichester, 1985, pp 185 - 189
4. A. J. Bard and L. F. Faulkner, "Electrochemical Methods", Wiley, New York, 1980, pp 222 - 224
5. J. Ryu, T. N. Andersen and H. Eyring, *J. Phys. Chem.*, 1972, **76**, 3278
6. L. Fabbrizzi, A. M. Manotti Lanfredi, P. Pallavicini, A. Perotti, A. Taglietti and F. Ugozzoli, *J. Chem. Soc., Dalton Trans., 1991*, 3263
7. E. Kimura, M. Haruta, T. Koike, M. Shionoya, K. Takenouchi and Y. Iitaka, *Inorg. Chem.*, 1993, **32**, 2779

Bibliography

Advances in Inorganic Chemistry, ed. A. G. Sykes, Academic Press Inc, San Diego, 1988, Vol 32

Biocoordination Chemistry: Coordination Equilibria in Biologically Active Systems, ed. K. Burger, Ellis Horwood Limited, New York, 1990

The Bioinorganic Chemistry of Nickel, ed. J. R. Lancaster, Jr., VCH, New York, 1988

Carbon Dioxide Activation by Metal Complexes, A. Behr, VCH, New York, 1988

Electrochemical and Electrocatalytic Reactions of Carbon Dioxide, ed. B. P. Sullivan, K. Kirst and H. E. Guard, Elsevier, Amsterdam, 1993

Electrochemical Methods Fundamentals and Applications, A. J. Bard and L. R. Faulkner, Wiley, New York, 1980

The Global Greenhouse Regime. Who Pays?, ed. P. Hayes and K. Smith, United Nations University Press, New York, 1993

Instrumental Methods in Electrochemistry, Ellis Horwood Limited, Chichester, 1985

Man-Made Carbon Dioxide and Climatic Change. A Review of Scientific Problems, P. S. Liss and A. J. Crane, Geo. Books, Norwich, 1983

Metals in Biological Systems, M. J. Kendrick, M. T. May, M. J. Plishka and K. D. Robinson, Ellis Horwood Limited, New York, 1992

Policy Implications of Greenhouse Warming, National Academy Press, Washington D.C., 1991

"By George she's got it"

Professor Henry Higgins

(My Fair Lady)